JAERI-M
83-129

REACTOR ENGINEERING DEPARTMENT ANNUAL REPORT

(April 1, 1982-March 31, 1983)

September 1983

Department of Reactor Engineering

日本原子力研究所
Japan Atomic Energy Research Institute

JAERI-Mレポートは，日本原子力研究所が不定期に公刊している研究報告書です。
入手の問合わせは，日本原子力研究所技術情報部情報資料課（〒319-11茨城県那珂郡東海村）あて，お申しこしください。なお，このほかに財団法人原子力弘済会資料センター（〒319-11 茨城県那珂郡東海村日本原子力研究所内）で複写による実費頒布をおこなっております。

JAERI-M reports are issued irregularly.
Inquiries about availability of the reports should be addressed to Information Section, Division of Technical Information, Japan Atomic Energy Research Institute, Tokai-mura, Naka-gun, Ibaraki-ken 319-11, Japan.

編集兼発行　日本原子力研究所
印　　刷　いばらき印刷㈱

JAERI-M 83-129

Reactor Engineering Department Annual Report (April 1, 1982 - March 31, 1983)

Department of Reactor Engineering,
Tokai Research Establishment, JAERI

(Received July 25, 1983)

Research and development activities in the Department of Reactor Engineering in fiscal 1982 are described.

The work of the Department is closely related to development of multipurpose Very High Temperature Gas Cooled Reactor and Fusion Reactor, and development of Liquid Metal Fast Breeder Reactor carried out by Power Reactor and Nuclear Fuel Development Corporation. Since fiscal 1982, Systematic research and development work on safeguards technology has been added to the activities of the Department. Contents of the report are achievements in fields such as nuclear data and group constants, theoretical method and code development, integral experiment and analysis, fusion neutronics, shielding, reactor and nuclear instrumentation, reactor control and diagnosis, and safeguards technology, and activities of the Committee on Reactor Physics.

Keywords : Reactor Engineering, Very High Temperature Gas Cooled Reactor, Fusion Reactor Neutronics, Liquid Metal Fast Breeder Reactor, Group Constant, Theoretical Method, Code, Integral Experiment, Analysis, Shielding, Nuclear Instrumentation Reactor Control, Diagnosis, Safeguards

---

JAERI－M 83－129

昭和57年度原子炉工学部年報

日本原子力研究所東海研究所原子炉工学部

（1983年7月25日受理）

昭和57年度における原子炉工学部の研究活動状況をとりまとめた。原子炉工学部の研究は，多目的高温ガス炉の開発，核融合炉の開発，及び動燃事業団による液体金属高速増殖炉の開発に密接に関連するものが多い。さらに昭和57年度から保障措置に関する研究開発が当部において総合的に実施されることとなった。核データと群定数，炉理論とコード開発，積分実験と解析，核融合ニュートロニクス，遮蔽原子炉計装，炉制御と異常診断，保障措置技術，及び炉物理に関する研究委員会活動の各分野にわたり当該年度に得た多くの成果を述べる。

原子炉工学部年報編集委員会

松浦祥次郎（委員長），中原康明（副委員長），高橋秀機，中野正文，秋野藤義，寺田博海，藤沢武夫，伊勢武治，長谷川明，前川洋，吉原文夫．

CONTENTS

Foreword

In the present report is given the annual research activity of Department of Reactor Engineering, Japan Atomic Energy Research Institute, for the period of April 1982 - March 1983. The research activity of the Department extends to a broad area of reactor engineering. The major fields are thermal and fast reactor physics, fusion reactor physics, shielding, reactor instrumentation and control, and safeguards technology.

Total number of people working in the Department at the end of period was 100 in which regular members totalled to 86. Expenditures during the period amounted to about 0.84 billion yen, without including nuclear fuel cost and personnel expenses. In addition, a considerable amount of expenditures was covered under research contracts with outside organizations: Science and Technology Agency (STA) for reactor decommissioning technology and safeguards technology, and Power Reactor and Nuclear Fuel Development Corporation (PNC) for fast reactor physics, instrumentation and control.

The research activities were conducted in 8 Laboratories:

Reactor System Laboratory,
Fast Reactor Physics Laboratory,
Thermal Reactor Physics Laboratory,
Reactor Instrumentation Laboratory,
Reactor Control Laboratory,
Shielding Laboratory,
Fusion Reactor Physics Laboratory and
Safeguards Technology Laboratory,

under the support of the Reactor Physics Facility Operating Division and the Committee on Reactor Physics.

The major research and development projects related closely to research programs in the Department are

(1) Development of multipurpose very high temperature gas-cooled reactor (VHTR),
(2) Engineering research of fusion reactor, and
(3) Development of liquid metal fast breeder reactor (LMFBR).

As concerns the R&D of multipurpose VHTR, measurements were performed on the reactivity worth of control rods and burnable poison

rods at a critical assembly SHE. The reconstruction program for the SHE core has been proceeded, to perform detailed simulation experiments for the Experimental VHTR, by obtaining the official authorization for the reconstruction. For developed high-temperature neutron detectors, a long-term function test has been performed in JRR-4 for more than 3 years to prove the high performance at 600°C. In addition, a high-temperature test was started for a developed fuel failure detection method for coated particle fuels. The development of a dynamic simulation algorithm has been proceeded for the computer aided design to get the good control characteristics of the Experimental VHTR.

Concerning the fusion reactor physics, various reaction rate distributions, including the tritium production rate, were measured in a 40 cm thick lithium oxide slab assembly by using the FNS (Fusion Neutronics Source) facility. In addition, duct streaming experiments were carried out for fast neutrons at the FNS. Furthermore, a blanket engineering benchmark experiment program has been prepared for promoting a cooperative research on the fusion neutronics between JAERI and USDOE by utilizing the FNS facility.

As for the R&D of LMFBR, a series of experiments were performed on the fast critical assembly FCA to measure the Doppler reactivity coefficient and gamma-ray heating, as well as mock-up experiments for the JOYO Mark-II core. Furthermore, a core design study has been proceeded for a helium-cooled actinide burning fast reactor.

As concerns researches other than those related closely to the projects, the development of a shield computer code system BERMUDA has been proceeded for dealing with anisotropic transmission problems in 3-dimensional geometries. In addition, improvements were made on a standard computer code system SRAC for nuclear design calculations of thermal reactors. The development of semiconductor detectors has resulted in various improvements of the characteristics. A study of robotic technology has been performed in connection with the decommissioning of nuclear facilities. Furthermore, discussions were made on various reactor physics problems by the Committee on Reactor Physics.

The Safeguards Technology Laboratory has newly established in the Department for playing the leading role for the R&D of safeguards technology in Japan. Simulation studies were performed for safeguarding various fuel cycle facilities, in addition to the development

of non-destructive and destructive assay techniques. Furthermore, containment and surveillance techniques have been studied for developing a personnel portal monitor as well as remote verification systems RECOVER and TRANSEAVER, under the collaboration with international organizations.

Takumi ASAOKA, Director
Department of Reactor Engineering

1. Nuclear Data and Group Constants

1.1 Thermal Reactor Benchmark Tests of JENDL-2

H. Takano, K. Tsuchihashi, T. Yamane, F. Akino and Y. Ishiguro

The group constant library for the SRAC system[1] has been produced from the JENDL-2 nuclear data file. Using this library, many critical experiments were analyzed and the results were compared with those calculated using the ENDF/B-IV and ENDF/B-V (only U-235) data. The selected experimental cores are summarized in Tables 1.1.1 and 1.1.4. The cell calculations were performed with the ultra-fine group method for calculating numerically the neutron flux distribution. The results calculated by the SRAC system are summarized in Tables 1.1.2, 1.1.3 and 1.1.4. In these tables, J-2/B-5 or B-4/B-5 means that U-235 data of ENDF/B-V is used in place of U-235 of JENDL-2 or ENDF/B-IV.

As for the effective multiplication factors calculated for the U-235 fuel cores, the JENDL-2 gives better results than those of ENDF/B-IV which show underestimate of about 1%. The results for J-2/B-5 or B-4/B-5 show larger values than ones for JENDL-2 or ENDF/B-IV, respectively. Their reasons are mainly due to the differences in the ν-value and fission spectrum of U-235. The ν-values are 2.4367, 2.4286 and 2.4188 for ENDF/B-V, JENDL-2 and ENDF/B-IV, respectively. The fission spectrum of ENDF/B-V is harder than the one of ENDF/B-IV or JENDL-2. On the other hand, for the U-233 fuel cores, the differences between Keff calculated with JENDL-2 and ENDF/B-IV are small.

As for the lattice cell parameters (Table 1.1.3), the δ_{28} values calculated for TRX-1 and TRX-2 are overestimated for JENDL-2, ENDF/B-IV, J-2/B-5 and B-4/B-5. This result is very similar to the one described for the fast reactor benchmark test. The C* value calculated with the JENDL-2 is in good agreement with the experiments. However, the JENDL-2 results in underestimates for ρ_{02} and CR*.

References

1) Tsuchihashi K., Takano H., Horikami K., et al. "SRAC: JAERI Termal Reactor Standard Code System for Reactor Design and Analysis", JAERI 1285 (1983).

Table 1.1.1 Benchmark cores

Assembly	Fuel	Moderator	Mod/Fuel	Comments
TRX1*	U-235	H2O	250	Lattice para. exp.,r=26.2 cm
TRX2*	U-235	H2O	430	Lattice para. exp.,r=27.4 cm
DCA**	U-235	D2O		Lattice para. exp.for ATR
ETA-I***	U-235+Th232	D2O	113	Lattice para. exp.,r=33 cm
SHE- 8****	U-235	C	2316	homogeneous, r=28.7 cm
SHE-13	U-235	C	15724	heterogeneous, r=55.76 cm
SHE-B2	U-235	C		critical assembly for HTGR

* BNL,"Cross Section Evaluation Working Group Benchmark Specifications, ENDF-202 (BNL-19302).

** Hachiya Y., et al. J. Nucl. Sci. Technol., 13(11), 618 (1976).

*** Hardy J., et al., Nucl. Sci. Eng., 55, 401 (1974).

**** Akino F., "Study on Thermal Neutron Spectra in Reactor Moderators by Time-of-Flight Method," JAERI-M 82-207 (1982).

Table 1.1.2 Effective multiplication factors

Assembly	Exp.	Calculation / Experiment			
		JENDL-2	J-2/B-5	ENDF/B-4	B-4/B-5
TRX-1	1.00	0.9934	0.9993	0.9860	0.9916
TRX-2	1.00	0.9945	0.9994	0.9890	0.9942
DCA	1.00	1.0021		0.9948	1.0013
ETA-I	1.00	0.9966	1.004	0.9851	
SHE-8	1.00	0.9949		0.99304	0.99709
SHE-13	1.008	1.0031		1.0006	1.0051
SHE-B2	1.008	0.9850		0.9831	0.9876

Table 1,1.3 Lattice cell parameters

Assembly	parameter	Exp.	Calculation / Experiment JENDL-2	J-2/B-5	ENDF/B-4	B-4/B-5
TRX-1	ρ_{28}	1.311 ± 0.02	1.001	1.004	1.034	1.033
	δ_{25}	0.0981±0.001	0.978	0.981	0.988	0.985
	δ_{28}	0.0914±0.002	1.056	1.094	1.037	1.081
	C*	0.792 ±0.008	0.966	0.993	1.007	1.009
TRX-2	ρ_{28}	0.83 ± 0.015	0.983	0.986	1.016	1.015
	δ_{25}	0.0608±0.0007	0.965	0.969	0.975	0.972
	δ_{28}	0.0667± 0.002	1.032	1.067	1.009	1.051
	C*	0.644 ± 0.002	0.985	0.981	0.992	0.994
DCA	ρ_{28}	0.84	0.94		0.981	0.977
	δ_{25}	0.06	1.00		1.00	1.00
	δ_{28}	0.049	1.00		0.98	1.02
ETA-1	ρ_{02}	10.54 ± 0.15	0.921	0.915	0.981	
	δ_{25}	1.74 ± 0.002	1.012	1.005	1.004	
	δ_{02}	0.0166±0.0009	0.842	0.866	0.778	
	CR*	0.867 ± 0.009	0.896	0.892	0.968	

ρ_{28}, ρ_{02}; ratio of epithermal to thermal U238 or Th232 captures
δ_{25} ; ratio of epithermal to thermal U235 fissions
δ_{28}, δ_{02}; ratio of U238 or Th232 fissions to U235 fissions
C*, CR* ; ratio of U238 or Th232 captures to U235 fissions

Table 1.1.4 Effective multiplication factors for critical experiments*

Assembly	Uncertainty of K-eff	Calculation JENDL-2	ENDF/B-4	Comments Fuel	Mod/Fuel
ORNL- 1	0.9992 to 1.0003	1.003	0.9695 (0.967)	U-233	0.0
ORNL- 4	0.9997 to 1.0003	1.048	1.047 (1.041+0.006)	U-233	73
ORNL- 7	0.9996 to 1.0004	1.003	1.001 (1.003+0.007)	U-233	119
ORNL- 8	0.9973 to 1.0027	1.023	1.021 (1.022+0.007)	U-233	154
ORNL- 9	0.9994 to 1.0006	1.029	1.027 (1.028)	U-233	195
ORNL-10	1.0018 to 1.0054	1.008	1.004 (1.013)	U-233	381
ORNL-11	0.9976 to 1.0027	0.991	(0.996)	U-233+Th-232	1533
ORNL-12	0.9973 to 1.0027	0.992	0.986 (0.991)	U-233+Th-232	1986
ORNL-13	0.9992 to 1.0008	1.0078	1.0062 (1.005)	U-235	0.0
ORNL-14	0.9999 to 1.0001	1.006	1.005 (1.009+0.006)	U-235	50

* McNeany S.R. and Jenkins J.D., Nucl. Sci. Eng., 65, 441 (1978).

1.2 Revision Work for RESENDD Code and its Validation Test through Benchmark-Test of Energy Dependent Point-Wise Cross-Section Generation Codes

A. Hasegawa and T. Narita+

From the study performed for the benchmark test[1] on generating point-wise cross-section codes RESEND[3], RESENDD[2] and RECENT[4], several serious problems have been revealed for RESENDD. We have used RESENDD these several years and this code has already been built in our routinely used code systems. Therefore it is urgently requested to remedy this code to clear off the problems pointed out by the benchmark test. It is our responsibility to correct RESENDD and to perform the validation check of this code.

The problems in RESENDD revealed from the benchmark test performed on major three codes RESENDD, RESEND, RECENT and additional problems revealed through this revision work are the following 6 points, i.e.,

1) process error in the constant background cross-section treatment in the file-3 smooth cross-section part specified by interpolation scheme 1,
2) insufficient data points generated in the resolved resonance range for very narrow resonances,
3) violating the process criteria in the unresolved resonance range. In this range the cross-sections other than the tabulated energies should be defined by interpolating the generated cross-sections,
4) inconsistent cross-section curve generation due to ignoring the definition of the smooth cross-section at the interface energy point between the resonance range and the smooth cross-section range when the cross-section gaps exist at that energy point as observed in the Au-197 (n,γ) case of ENDF/B-V dosimetry file (Vol.531 tape),
5) slightly lower cross-section generation due to coding miss in RESENDD for phase shift calculation of d-wave resonances,

+ Department of Physics, Tokai Research Establishment, JAERI

6) odd cross-section generation at the connecting point of resolved and unresolved range.

For these points we performed revision work of the RESENDD code.

For validation test of the revised code, we performed the same benchmark test as previous one, i.e., the ENDF/B-V dosimetry file (Vol.531 tape) was adopted as the input data file. We calculated the cold (i.e. 0.0 Kelvin) energy dependent point-wise cross-sections and also the unshielded group averages in the 620 group SAND-II structures[6] for convenience of comparisons.

Through the benchmark test of the revised code, we confirmed performance and reliability of the code. All of the fatal errors are now cleared off and the differences in the reference code RECENT are always within 0.5% in all energy ranges and running costs are fairy low comparing with the reference code as seen in Table 1.2.1 and 1.2.2.

All of these results obtained here have contributed to the international comparisons of energy dependent cross-section generation codes[6], organized by Dr. D. E. Cullen of NDS (Nuclear Data Section) IAEA.

References

1) Hasegawa, A., Narita, T.: "Comparisons of Energy Dependent Point-wise Cross-Section Generation Codes: RESEND, RESENDD, RECENT," JAERI-M 82-128 (1982).
2) Nakagawa, T.: RESENDD private communication.
3) Ozar, O.: "RESEND: A Program to Preprocess ENDF/B Materials with Resonance Files into a Pointwise Form," BNL-17134 (1973).
4) Cullen, D. E.: "Program RECENT (Version 79-1): Reconstruction of Energy-Dependent Neutron Cross Sections from Resonance Parameters in the ENDF/B Format," UCRL-50400, vol.17, Part C (1979).
5) Cullen, D. E.: private communication, IAEA NDS (1982).
6) Oster, C. A., McElroy, W. M. and Marr, J. M.: "A Monte Carlo Program for SAND-II Error Analysis," HEDL-TME-73-20 (1973).

Table 1.2.1 Running performance of the processing codes: CPU time and generated data points.

No.	Nuclide	MAT	CPU-time (sec) RECENT	RESENDD (ORIG.)	RESENDD (REV-2)	Generated Points Number RECENT	RESENDD (ORIG.)	RESENDD (REV-2)
1	Na-23	6311	7	10	11	5155	3973	4438
2	Np-237	6337	145	146	141	33066	32308	32897
3	Au-197	6379	601	440	519	106530	54439	71515
4	Th-232	6390	1685	724	938	216435	67167	104116
5	U-235	6395	50	55	48	13000	13422	12982
6	U-238	6398	2353	960	1275	231798	74069	118914
7	Pu-239	6399	110	89	90	33485	23892	25498
8	Sc-45	6426	204	186	200	45462	27573	32146
9	Fe-58	6432	40	32	35	20535	13082	14776
10	Cu-63	6435	8	10	11	5836	5356	5428
11	In-115	6437	201	131	168	62391	34637	44205

Running conditions:
RECENT: LINEAR: 0.1 % ERR: 0.1 %
RESENDD (ORIG.): ERR: 0.1 %, AVERR: 0.0, LSIG: 1.0E-10
RESENDD (REV-2): ERR: 0.1 %, AVERR: 0.0, LSIG: 0.0

Table 1.2.2 Maximum and minimum differences in 620-group averaged cross-sections for RESENDD(ORIGINAL) and RECENT code compared with RESENDD(REV-2) results.

No.	Nuclide	MAT No.		RESENDD(ORIGINAL) minimum	RESENDD(ORIGINAL) maximum	RECENT minimum	RECENT maximum
1	Na-23	6311	(n,g)	-2.2%	+0.2%	-0.1%	+0.2%
2	Np-237	6337	(n,f)	-17.3%	+18.8%	-0.1%	+0.1%
3	Au-197	6379	(n,g)	-0.1%	+2119.8%	-0.1%	+0.1%
4	Th-232	6390	(n,f)	-0.1%	+20.5%	-0.5%	+0.5%
			(n,g)	-0.5%	+11.5%	-0.4%	+0.4%
5	U-235	6395	(n,f)	-1.9%	+2.3%	-0.0%	+0.0%
6	U-238	6398	(n,f)	-0.4%	+5424.5%	-0.3%	+0.3%
			(n,g)	-1.3%	+5627.1%	-0.4%	+0.3%
7	Pu-239	6399	(n,f)	-0.8%	+2.4%	-0.1%	+0.1%
8	Sc-45	6426	(n,g)	-0.1%	+0.1%	-0.4%	+0.1%
9	Fe-58	6432	(n,g)	-0.9%	+226.6%	-0.3%	+0.5%
10	Cu-63	6435	(n,g)	-0.0%	+90.1%	-0.1%	+0.1%
11	In-115	6437	(n,g)	-0.1%	+0.0%	-0.1%	+0.1%

1.3 Development of PROF. GROUCH-G/B, a Processing Code System for Core and Shielding Application

A. Hasegawa

It is very difficult to supply for users a universal group constants set applicable to radiation shielding problems, like the JAERI-Fast Set /1/ which is generally applicable to the reactor core neutronics analysis for fast reactors. Because in core neutronics calculations the resonance peak treatment of neutron cross sections have the primary importance, but for shielding applications this statement is lessened considerably. That is, the dips of cross sections play more important role on shielding applications relatively to the peak of the cross sections. Therefore, for shielding applications users should be very carefull about the position of the resonance windows. Usually this position is completely material-dependent and accordingly we cannot anticipate the position without experiments.

Thus for the preparation of multigroup cross sections in shielding applications, we think it is better for users themselves to decide the group structure considering the materials and their cross section curves. For this purpose, the consolidation of nuclear data retrieval systems and processing systems is very convenient for users. First they look through the cross section curves and identify the windows by using the nuclear data retrieval systems like EDFSRS /2/, next decide the group structures to be taken for their purposes and finally perform production runs to make the group constant library by these processing systems.

From the experiances gained hitherto through the development of processing codes, we propose the following ideas for the processing system:

1. Possessing of our own processing system written by ourselves. This means that all logics taken in the processing code can be completely understood by us and the actions for the user's requests or patch work based on the feed-back information from them should be taken properly and immeadiately. We assert that the logics must not be the black box for us.
2. Increasing the possibility for access to other than the ENDF/B FORMAT /3/ data: In the world there are three major formats, i.e. ENDF/B, UKNDL /4/ and KEDAK /5/. So we want to be free from these

formats dependency for the processing code.

3. Qualification guarantee by code-maintenance: We must always pay attention to the output from the processing codes and carefully watch the code accuracy through benchmark tests or participating in the International Code Comparisons Project /6/.
4. Adopting suitable processing methods for a huge amount of data: There should be no limitation for acceptable data points in using paging method or binary data transfer, because point-wise data exceeds frequently 300000 energy-points in the case of heavy resonant nuclides.

To realize these intentions, we decided to develop a new code system PROF. GROUCH-G/B /7/. This project started in 1982 and will be completed by March 1985 for the first period, i.e. three years project. The schedule is as follows, for the first year, development of one-and two-dimensional neutron nuclear data processing modules, and next year, development of photon production cross section processing module, and final year, development of variance and covariance matrices processing module. Interrelation between this processing code and the environmental systems are shown in Fig. 1.3.1. Up to now we have developed the group constant generation routines for neutron nuclear data. And we also finished the complete revision work for RESENDD (REV-2) based on the benchmark-test of the energy dependent point-wise cross section generation code /8/. The observed maximum differences are within 0.5 % in all energy ranges for all reaction types of the adopted benchmark-test using the ENDF/B-V dosimetry file /9/.

In future, this code system will be directly coupled with EDFSRS (Evaluated Nuclear Data File Storage Retrieval Systems) on TSS (Time Sharing System) basis. It enables users of nuclear data to fetch and manipulate all of the data which they need on their own terminal located at other than JAERI (e.g. KYUSYU, HOKKAIDO area etc.) through a information net work system.

All of the nuclear data stored by EDFSRS and all logics used in this processing code are to be completely and uniquely maintained by us. Therefore users are completely free from the patch work of the code or data updating through the original data change which are frequently taken place.

References

1) Takano H., Hasegawa A., Nakagawa M., Ishiguro Y. and Katsuragi S.: "JAERI Fast Reactor Group Constants Set, Version II," JAERI-1255 (1978).
2) Hasegawa A. and Kaneko K.: to be published.
3) revised by Kinsey R.: "Data Formats and Procedures for the Evaluated Nuclear Data File," BNL-NCS-50496 (ENDF-102) (1975).
4) Parker K.: "The Aldermaston Nuclear Data Library as at May 1963," AWRE/0-70/63 (1963).
5) Woll D.: "Card Image Format of the Karlsruhe Evaluated Nuclear Data File KEDAK," KFK-880 (1968).
6) Cullen D. E.: private communication, IAEA NDS (1982).
7) Hasegawa A., et al.: to be published.
8) Hasegawa A. and Narita T.: "Comparisons of Energy Dependent Point-Wise Cross-Section Generation Codes: RESEND, RESENDD, RECENT," JAERI-M 82-128 (1982).
9) BNL: "ENDF/B Summary Documentation. Third Edition (ENDF/B-V)," BNL-17541 (ENDF-201) (1979).

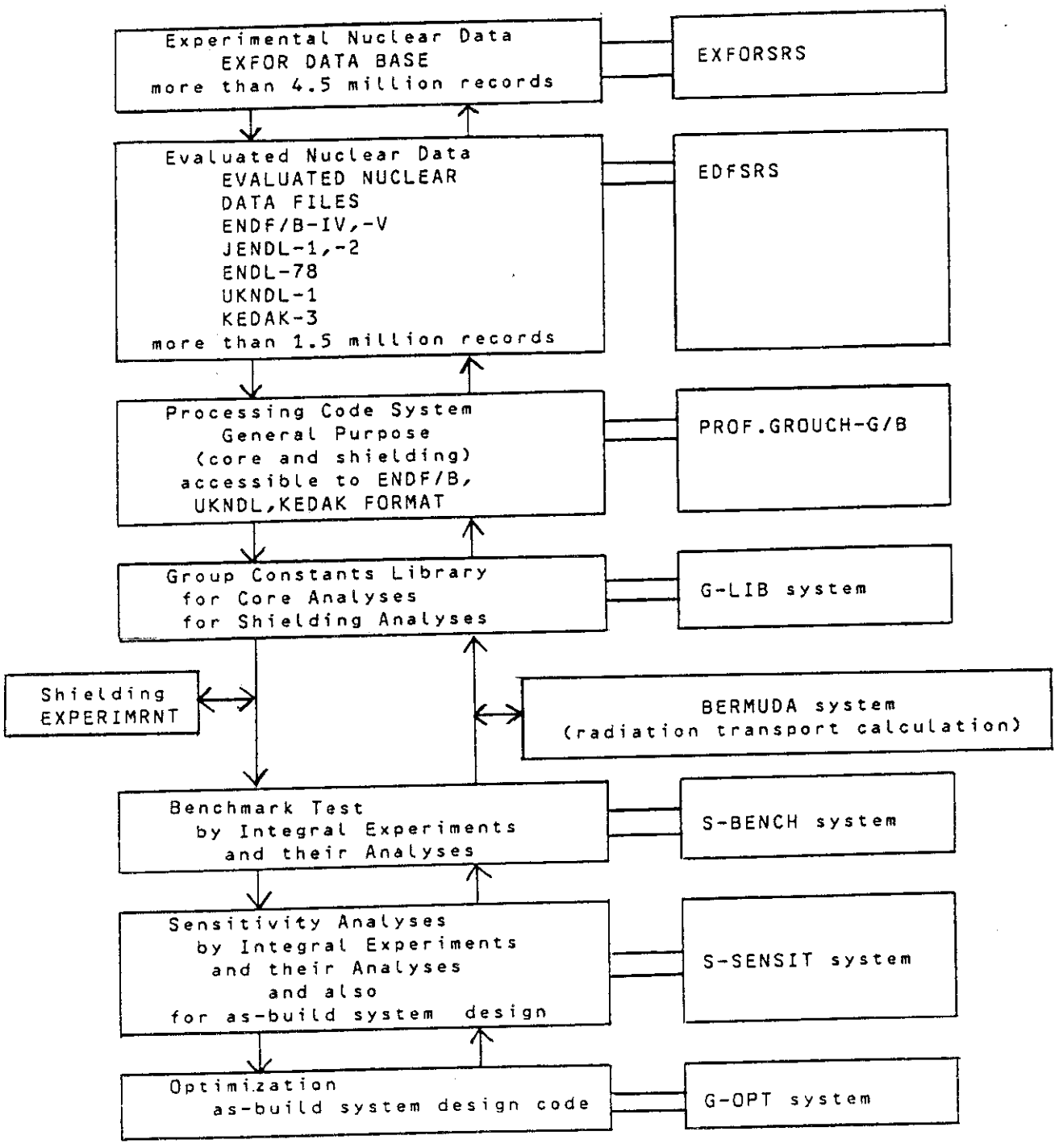

Fig. 1.3.1 Environment of PROF.GROUCH-G/B and nuclear data flow for shielding application

1.4 Development of EDFSRS: Evaluated Data Files Storage Retrieval Systems

A. Hasegawa and K. Kaneko*

Needs for the evaluated nuclear data are increasing more and more continuously in proportion to the spread of application fields of nuclear data. Nowadays even the medical sciences or new material sciences are included in this application fields as well as nuclear sciences for fission or fusion reactors. Thus the population of using those data are definitely increasing.

Access to the evaluated data has been rather difficult up to now for the users not familiar with the evaluated nuclear data files. First such users are requested to learn the complex and complicated format specifications of the individual data format which they want to use. This work is somewhat burdensome and a heavy task for users to simply see the cross section value or some other nuclear quantities. Only experts are able to handle huge amounts of data in the evaluated nuclear data files.

Up to now the evaluated nuclear data files available to us have been only stored in several tens of magnetic tape files separately or stored in disk files independently each other. Total amount of records stored exceeds 1.5 million cards (in 80 bytes records). We cannot treat such a huge amount of data without a computer. It is difficult that users who want to know the available nuclear data for the specified reaction of specified nuclide find out necessary data from such huge data. From these situations, computerization would be necessary for the efficient and economic data retrievals for such a large amount of data using comprehensive data storing technique.

Thus we have developed a complete system: EDFSRS (Evaluated Data File Storage Retrieval Systems) /1/ for general utilities of the evaluated nuclear data files. This system is intended to offer the easy storage and retrievals to the users of evaluated nuclear data file with the best confidences without any extra labors. This system is also designed to work primary on TSS (Time Sharing System) as well as BATCH

---

* Japan Information Service Co. Ltd.

using on-line disk storages.

This system consists of more than 10 independent programs. Those programs are listed in Table 1.4.1. Brief descriptions for key programs are given in the following.

A. Loading of evaluated nuclear data file in ENDF/B /2/, UKNDL /3/, and KEDAK /4/ format data onto physical disks.

1. AKSTREV : Loading program of the major three format data.
2. AKINDXEV: Index table creation program for the physically loaded data by AKSTREV. These index tables are used as key access directory for the retrieval program (see B) and are also used by dictionary (book-style) production program (see C).

B. Retrieval program for evaluated nuclear data files from all loaded evaluated nuclear data files on physical disks.

3. AKRETREVY: Retrieval can be done in any combination of the following items: Evaluated file name, Tape id. number, MAT (material-id.) number, Z (atomic number), A (mass number), MF (file classification -id.) number, MT (reaction-id.) number and Energy-range.
   For each items, the 'inclusive OR' operation is permitted and between items the 'AND' operation will be applied.
   For output, the following materials are available on requests,
   a. Original format output. (in ENDF/B, UKNDL or KEDAK) (on DISK, MT or LIST.)
   b. Computation format output. (on DISK, MT or LIST.)
   c. Cosmetic listing output. (on DISK, MT or LIST.)
   d. Some integral values, using INTER option.
      Thermal cross section value, resonance integral, 14 MeV cross section value, fission spectrum averaged value.

C. Index dictionary (index-book) production program.

The book "Index to Large Evaluated Data Files" /5/ is produced using the programs stated below.

4. AKINDXBKL: Index table listing program for all entries of the evaluated nuclear data files. Materials available are: a) TAPE-id. index, b) MAT-id. index, c) Z-A index and d) MT-id. index.
5. ENDFDATE: Historical status data listing program for ENDF/B-4 and 5.
7. ABBDIC: abbreviated index listing program for all of the TAPE-id., MAT and Z-A entries.

D. Index information retrieval program.

9. PAGEOUT: Retrieval program for information in the INDEX listing.

Materials available are: a) TAPE index, b) MAT index, c) Z-A index, d) MT (reaction) full index and e) MT condensed index.

All of the developed program are written by FORTRAN-77 and the disk organization adopted for storing of evaluated data is FORTRAN direct access files.

From now on, all the evaluated nuclear data received by JAERI Nuclear Data Center will be immediately loaded and routinely maintained by our system. Up to now, the following files have been loaded: ENDF/B-4 /6/, ENDF/B-5 (partial files) /7/, JENDL-1 /8/, JENDL-2 /9/, UKNDL-1 /10/, KEDAK-3 /11/ and ENDL-78 /12/.

In future, this system will be linked to the PROF. GROUCH-G/B: a processing code system for core and shielding application /13/, for more elaborate and flexible manipulation of these data.

References

1) Hasegawa A. and Kaneko K.: to be published.
2) revised by Kinsey R.: "Data Formats and Procedures for the Evaluated Nuclear Data File," BNL-NCS-50496 (ENDF-102) (1975).
3) Woll D.: "Card Image Format of the Karlsruhe Evaluated Nuclear Data File KEDAK," KFK-880 (1968).
4) Parker K.: "The Aldermaston Nuclear Data Library as at May 1963," AWRE/O-70/63 (1963).
5) OECD NEA DATA BANK: "INDEX TO LARGE EVALUATED DATA FILES" (1981).
6) BNL: "ENDF/B-IV: Evaluated Nuclear Data File, Version-IV" (1975).
7) BNL: "ENDF/B-V : Evaluated Nuclear Data File, Version-V" (1979), and its documentation, "ENDF/B Summary-Documentation. Third edition (ENDF/B-V)," BNL-17541 (ENDF-201) (1979).
8) JAERI: "JENDL-1: Japanese Evaluated Nuclear Data Library, Version-1" (1979), and its documentations, JAERI-1261 (1979) & -1268 (1981).
9) JAERI: "JENDL-2: Japanese Evaluated Nuclear Data Library, Version-2" (1983), and its documentation, to be published.
10) AWRE: "UKNDL-1: the UKAEA Nuclear Data Library" (1980).
11) KFK : "KEDAK-3: the Karlsruhe Evaluated Nuclear Data Library" (1977), and its documentation, KFK-2386 (1977).
12) LLL : "ENDL-78: the Livermore (LLL) Evaluated Nuclear Data Library" (1978), and its documentation, UCRL-5400 vol 15 (1978).
13) Hasegawa A., et al.: to be published.

Table 1.4.1 Developed programs and its category of EDFSRS

* user category * program	A) loading of data file	B) evaluated data file retrieve	C) index book production	D) information retrieve
1 AKSTREV	******			
2 AKINDXEV	******			
3 AKRETREVY		******		
4 AKINDXBKL			******	
5 ENDFDATE			******	
6 FORPR			******	
7 ABBDIC			******	
8 PRTOUT				******
9 PAGEOUT				******
10 MTTAB				******
11 MFID				******
12 NUCLID				******

1.5 Lumped Group Constants of Fission Products

H. Takano and W. Sato*

To advance the JFS-3-J2 set[1] for application to design study of large fast breeder reactor, the lumped group constants of fission product nuclides were generated by calculating the group constants for 193 nuclides of fission products. The 28 important nuclides recommended in Ref. (2) were selected from the JENDL-1 and they were Sr-90, Zr-93, Mo-90, Mo-97, Tc-99, Ru-101, Ru-102, Ru-104, Ru-106, Rh-103, Rd-105, Pd-107, Ag-109, I-129, Xe-131, Cs-133, Cs-135, Cs-137, Ce-144, Nd-143, Nd-144, Nd-145, Pm-147, Sm-147, Sm-149, Sm-151, Eu-153 and Eu-155. The others were selected from the ENDF/B-IV file.

The lumped cross sections were calculated by using the weight of the concentration of each fission product nuclides which was calculated at 360 days of burn-up[2]:

$$\sigma_{x,g}^{LFP} = \sum_{i=1}^{I} C_i \sigma_{x,g}^{i} \quad ,$$

$$\mu_{g}^{LFP} = \sum_{i=1}^{I} C_i \mu_{g}^{i} \sigma_{n,g}^{i} \Big/ \sum_{i=1}^{I} C_i \sigma_{n,g}^{i} \quad ,$$

where C_i is the concentration and μ_g^i the average cosine of the angle in elastic scattering for the nuclide i and the energy group g respectively, and the others are the conventional notations used commonly.

The lumped group constants for the mother nuclides of Pu-239, U-235 and U-238 were produced and were stored on the master library of JFS-3-J2. Figures 1.6.1 and 1.6.2 show the comparison of the lumped capture cross sections with those of the JFS-2 set[3] respectively.

References

1) Takano H. and Ishiguro Y.: "Production and Benchmark Tests of Fast Reactor Group Constant Set JFS-3-J2," JAERI-M 82-135 (1982).

2) Kikuchi Y., Hasegawa A., Nishimura H., et al.: "Fission Product Fast Reactor Constants System of JNDC," JAERI 1248 (1976).

3) Takano H., Hasegawa A., Nakagawa M., et al.: "JAERI Fast Group Constants Set, Version-II," JAERI 1255 (1978).

---

* Japan Information Service Co. Ltd.

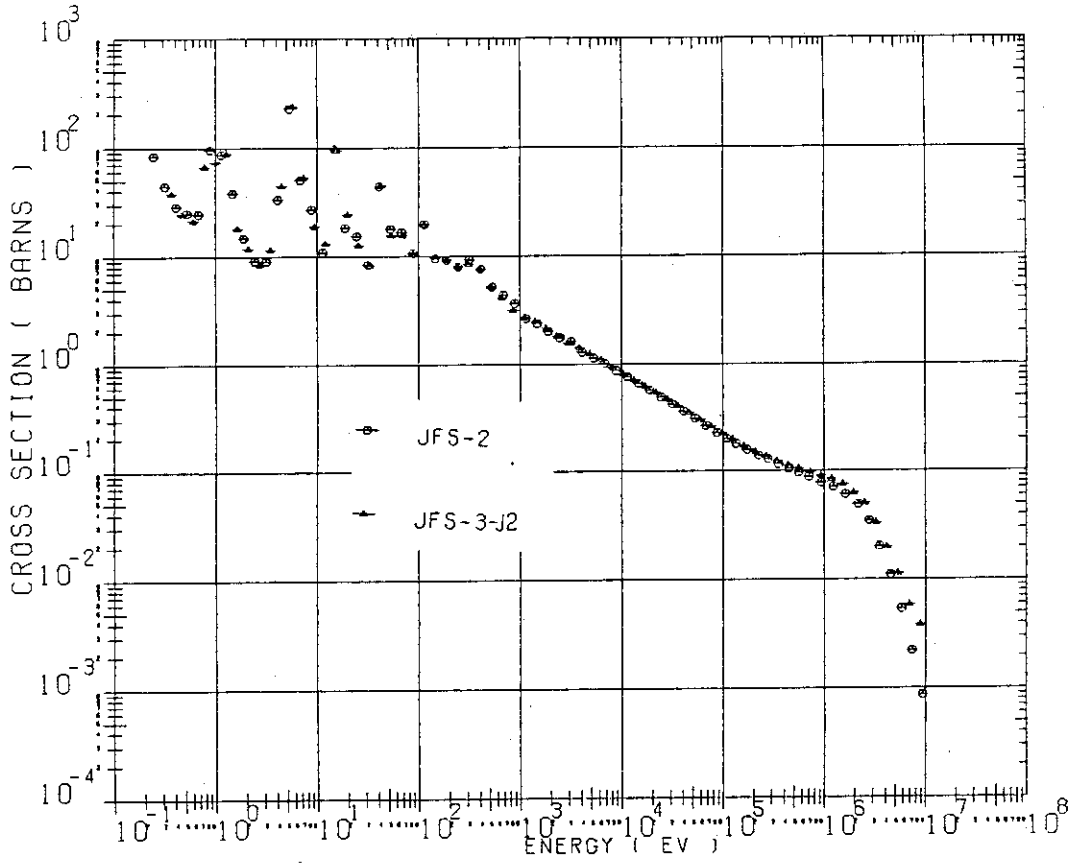

Fig.1.5.1 Comparison of the lumped capture cross sections for U-235

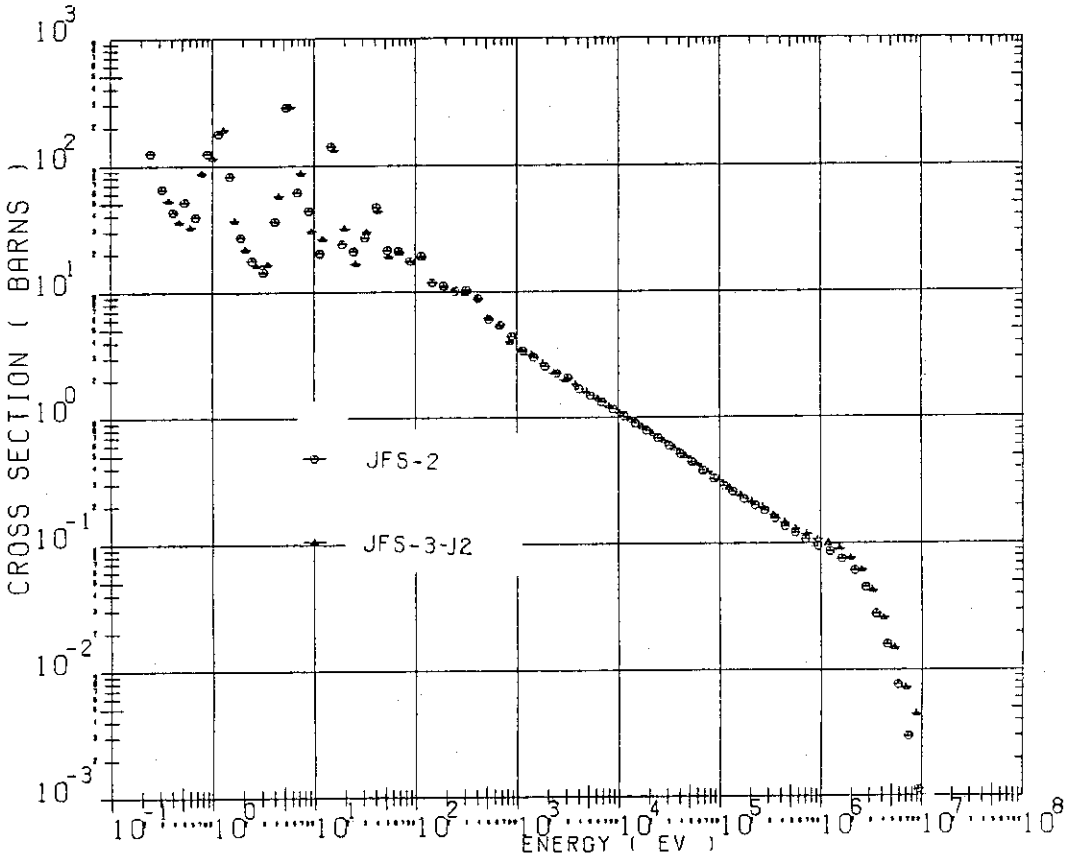

Fig.1.5.2 Comparison of the lumped capture cross sectionsfor Pu-239

1.6 The Effect of Fission Cross Section of Pu-239 on Nuclear Characteristics in Fast Reactors

H. Takano and W. Sato*

The benchmark tests of the JFS-3-J2 set[1] showed several problems such as the noticeable overestimate for sodium void reactivity. To investigate the causes, a sensitivity study of the fission and capture cross sections for important nuclides Pu-239, U-238 and Pu-240 on nuclear characteristics was examined using the two-dimensional benchmark calculation system. The change of Pu-239 fission cross section in the energy range from 600 eV to 2.6 KeV showed very interesting effects on nuclear characteristics. This energy range belongs to the unresolved region which is called the high-α value region. In this region, the group fission cross sections were changed as shown in Fig. 1.7.1. The effect of this changed cross sections on nuclear characteristics are summarized as follows.

The sodium void reactivity calculated for the FCA-VI-2 assembly become small by about 10%. However, the strong dependence[1] of the C/E values for the sodium void reactivity on the voided region was not removed by this change of Pu-239 fission cross sections. The calculated results for the K_{eff}, central reaction rate ratios of U-238 capture to Pu-239 fission and of Pu-239 fission to U-235 fission and the reaction rate distribution of Pu-239 are shown in Figs. 1.7.2 - 1.7.5. For these nuclear characteristics, the change of Pu-239 fission cross section produced much better results than those calculated for the original cross section.

Thus, we will require strongly the accurate measurement and evaluation for the cross sections of Pu-239 in the energy range of the high-α value.

References

1) Takano H. and Ishiguro Y.: "Production and Benchmark Tests of Fast Reactor Group Constant Set JFS-3-J2," JAERI-M 83-135 (1982)

---

* Japan Information Service Co. Ltd.

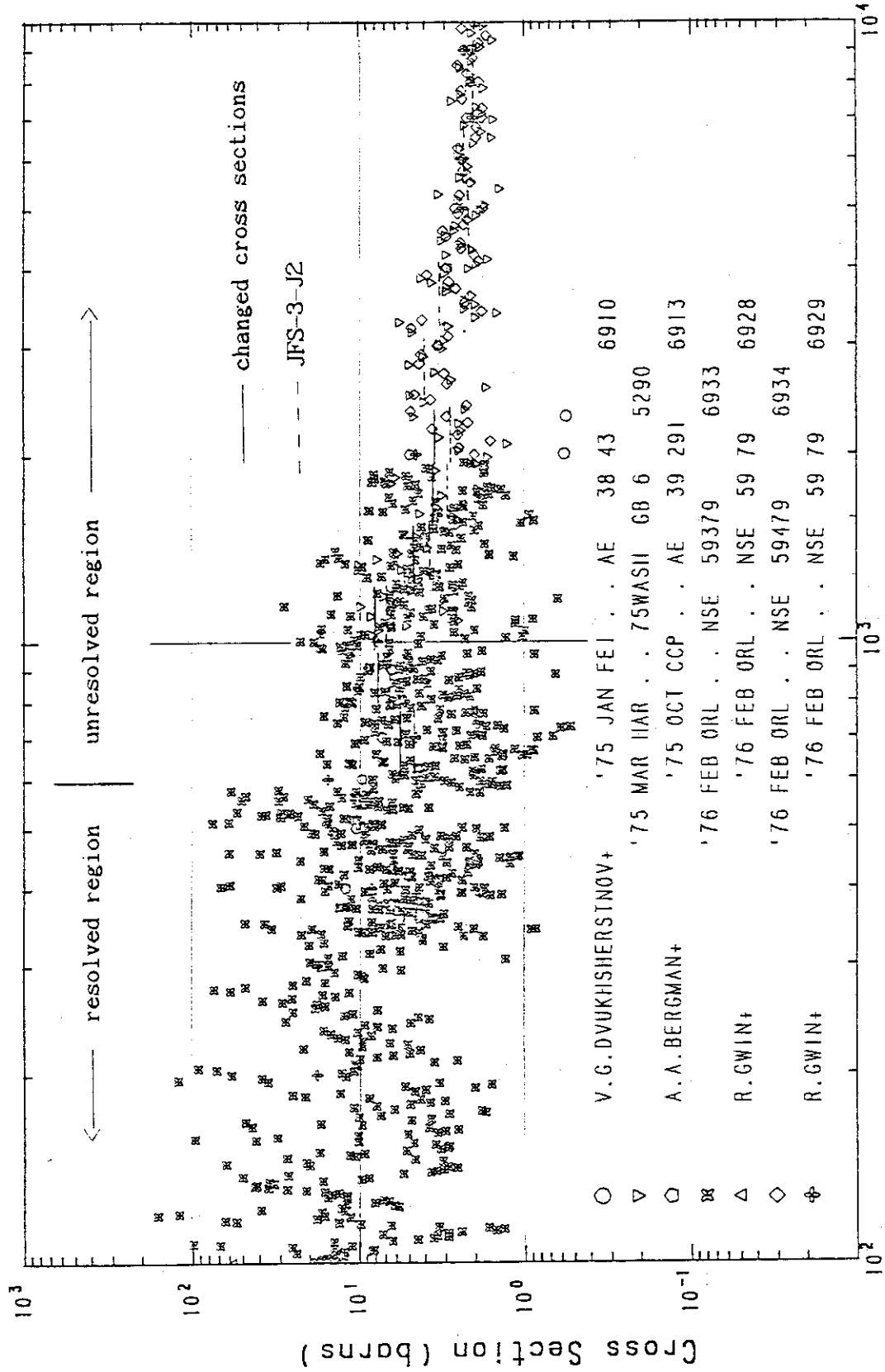

Fig.1.6.1 Comparison of fission cross sections of Pu-239

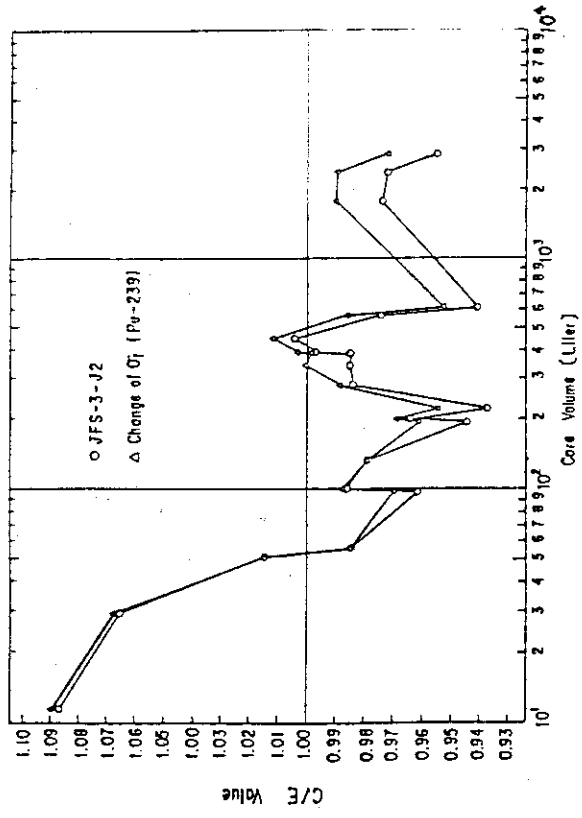

Fig.1.6.2 Comparison of effective multiplication factors

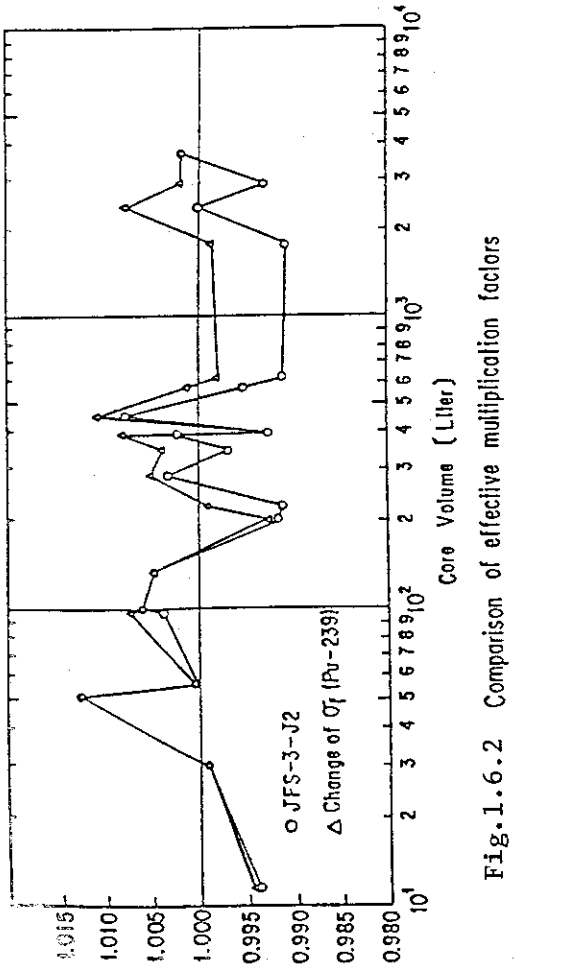

Fig.1.6.3 Comparison of the central reaction rate ratio of ^{238}U capture to ^{239}Pu fission.

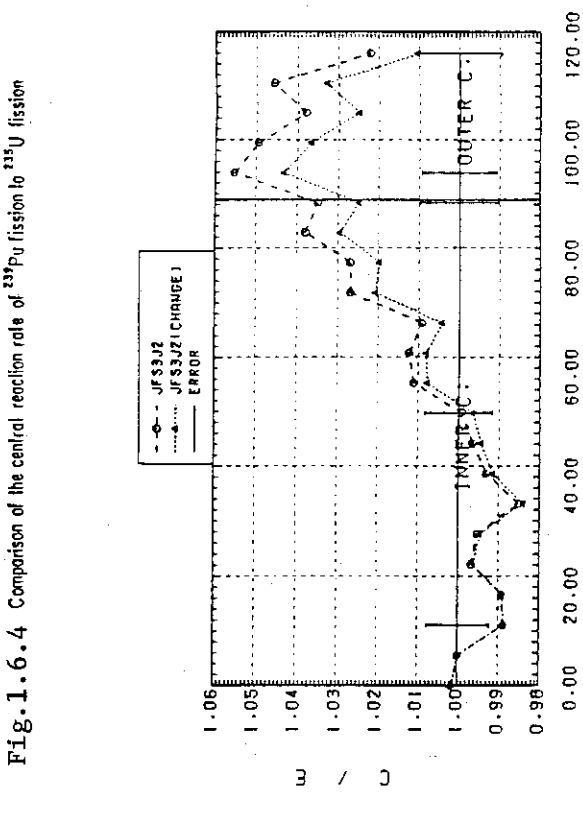

Fig.1.6.4 Comparison of the central reaction rate of ^{239}Pu fission to ^{235}U fission

Fig.1.6.5 Comparison of ZPPR-9 fission rate distributions

2. Theoretical Method and Code Development

2.1 Development of the SRAC Code System for Design and Analysis of a Thermal Reactor and its Application

K. Tsuchihashi, H. Takano and Y. Ishiguro

The development of the SRAC code system has attained the first goal by the publication of its manual[1]. Further efforts have been continued. The functions which have been added in the fiscal year of 1982 are as follows:

Compilation of alternative libraries

Considering several benchmark calculations on the fast reactor physics, the neutron cross sections compiled in JENDL-II seem to give better predictions to the fast neutronic performance than those in ENDF-B/IV. It was discussed at the seminar entitled "Thermal Reactor Benchmark Calculations Results and Applications" held at BNL, May, 1982 [2] that the data in ENDF-B/V gave better predictions to the criticalities of light water moderated reactors than those in ENDF-B/IV. The new libraries based mainly on JENDL-II have been produced, where only the U-235 data in ENDF-B/V have been compiled because the available data for us have been limited to those for U-235. A series of their benchmark calculations have been done[3].

Safety related parameters Λ and β_{eff} in nonuniform core

The calculation of the safety related parameters, the neutron generation time Λ (the life time l) and the effective delayed neutron fraction β_{eff} of the reactor in which the fissile nuclides are nonuniformly loaded has been established. The basic data such as the delayed neutron fractions by family, their neutron spectra, and the effective 1/v cross sections as well as the prompt neutron spectrum are averaged by mixture, then fed into the CITATION routine which is modified to be able to accept those data by mixture. The safety parameters Λ and β_{eff} are obtained by the perturbation theory.

Irradiation Data and Spectral Parameters

The space dependent irradiation fluence can be obtained after calculating the neutron flux distribution by any of transport or diffusion routines installed in the SRAC. Since the macroscopic cross sections are fed for the irradiated material, the self-shielding effect can be taken into account.

The spectral parameters such as $\rho_{28}, \delta_{25}, \delta_{28}$ and C^* or corresponding values for the combination of TH-232 and U-233 can be calculated.

Core Burn-up and Fuel Management

The information for a particular fuel element such as MWD (and % U-235 burnt), nuclide concentrations, and the operation history are stored into the management file. The axial distribution of the above information can be processed only if a three dimensional calculation is indicated. The change of control rod disposition by the burn-up step in an operation cycle can be reflected on the above information through

the distortion of flux distribution. The transient Xenon concentration is not considered. The spatial temperature distribution which is closely related to the power distribution must be specified in the input.

Applications

A series of analyses [4) 5)] have been made for the critical experiments of the MEU core of the KUCA (Kyoto University Critical Assembly). The satisfactory results were obtained for the predictions of the critical masses, the worth of the burnable boron plates, the worth of void tubes of various diameters inserted in the central water island, and the radial distribution of thermal flux across the voided central region, the inner core, the water region for control rods, the outer core, the water gap, and the heavy water reflector. However some underestimations were found in the physical quantities related to the flux peakings appearing at the boundaries of light water regions like the mass coefficient.

Another analysis has been made for the critical experiments of the LEU core of the Ford Nuclear Reactor aiming to check the validity of the prediction by the SRAC for the LEU core of the JRR-4. The prediction to the critical mass was satisfactory while the control rod worth estimated by the average of unshielded cross section failed to be predicted. Further analysis will be made for the control rod of solid stainless steel using the logarithmic differential condition obtained from a transport theory calculation.

References

1) Tsuchihashi K. et al. "SRAC: JAERI Thermal Reactor Standard Code System for Reactor Design and Analysis," JAERI 1285, (1983)
2) Proceedings of "Thermal Reactor Benchmark Calculations Results Technics and Applications" held at BNL, May, 1982, to be published
3) Takano H. et al., unpublished
4) Proceedings of "International Meeting on Reduced Enrichment of Rearch and Test Reactors" held at ANL, Nov, 1982, to be published
5) IAEA Guidebook for "Research Reactor Core Conversion from the Use of Highly Enriched Uranium to Low Enriched Uranium Fuels – Safety and Licensing Issues," Vol 1, to be published

2.2 An Improvement in the Calculation Method of Double Heterogeneity Effect in HTGR

Y. Ishiguro, K. Tsuchihashi and K. Kaneko*

A HTGR design requires the consideration of double heterogeneity; the fuel-grain/moderator heterogeneity and the rod/moderator one. Here, it is known that the double heterogeneity comes mostly from the spatial shielding of resonance cross section. Much works have been done for the self-shielded cross sections in such doubly heterogeneous systems [1)~8)]. Most efforts have been devoted to develope an efficient but approximate method of calculation, since the problem seems to be almost unyielding to a direct numerical method because of the complexity caused by the superposition of internal and external geometries.

The JAERI Standard Reactor Analysis Code(SRAC) System [9)] has incorporated two homogenization procedures for the double heterogeneity treatment. The first one is based on the ultrafine spectrum code PEACO [10)] using the collision probability method. The second one uses an analytical method based on the intermediate resonance approximation (IRA), by which an equivalence principle is derived for the table-look-up-method of a cross section set with resonance shielding. Both the procedures are composed of the two-step calculation. At the first step, the primary grain cell is spatially smeared so as to give a representative for the homogenized mixture. Secondly, the homogenization procedure is executed for the secondary rod/moderator cell with gross heterogeneity.

The two-step calculation in which the first step is executed whithout considering the gross heterogeneity does not always give a higher accuracy, because the effect of moderator regions upon the primary cell is estimated to be not so small due to the shorter diameter of fuel rods. In order to give a better prediction to the double heterogeneity, an approximate expression has been derived for the collision probability calculation by using Leslie's analytical approach [11),12)]. That is, the method developed for an isolated system of clustered fuel rods have been extended to the infinite number of the lattice cells. The present approach is straightforwardly applicable to the LWR and/or LMFBR lattice cells with double heterogeneity. The PEACO code in the SRAC System is being modified by use of the derived method. The details will be published in near future. Here, we will briefly touch upon the procedures used for the derivation and the resulting expressions for the collsion probabilities as follows:

We assume that the fuel rods(F) which are built up of a number of tiny 'particle cells' are imbeded in moderator(M) to constitute the lattice cell with gross heterogeneity. For simplicity, moreover, we assume that there is no distinction among the fuel rods in each lattice . This assumption can be approximately attained by using an average collision probability under a flat flux assumption. The neutron slowing down equation in the M-region is treated by the narrow resonance approximation(NRA). Hence, the neutron balance can be described by a coupled set of equations in the spherical primary cell with an additional slowing down source due to the outer M-region. Here, the primary cell consists of a kernel of UO_2 (f) and a homogeneneous carbon region(m).

---

* Japan Information Service Co. Ltd.(Tokyo)

The collision probability $P_F(i,j)$ that a neutron scattered isotropically in the region i of the F-region will have its first collision in region j(j = f, m, or M) can be shown to be expressed by

$$P_F(i,j) = Q(i,j) - \frac{\alpha_i \alpha_j}{\Sigma_i V_i} T_F \qquad (i,j = f,m) \tag{1}$$

$$P_F(i,j) = \frac{\Sigma_M V_M}{\Sigma_i V_i} P_{FM}(i) \qquad (i = f \text{ or } m;\ j = M) \tag{2}$$

with $$P_{FM}(i) = \frac{\alpha_i}{\Sigma_M V_M} T_F \ , \tag{3}$$

$$T_F = \bar{\Sigma}_F \bar{V}_F \{1 - \bar{P}_{FF}\} \ , \cdot \quad \bar{\Sigma}_F \bar{V}_F = \Sigma_f V_f + \Sigma_m V_m \ , \tag{4}$$

and $$\bar{V}_F = V_f + V_m$$

Here, the quantity $\bar{P}_{FF}$ is the first collision probability for the secondary cell with the homogenized cross section $\bar{\Sigma}_F$, for which the Wigner rational expression can be used. The quantity Q(i,j) corresponds to the collision probability in the infinite array of the particle cells.

The quantities α_f and α_m can be calculated by the method suggested by Leslie et al. [11] and satisfy the relation

$$\alpha_f + \alpha_m = 1 \tag{5}$$

The collision probalility given by Eqs.(1) and (2) can be readily shown to satisfy the two important relations, that is, the conservation law and the reciprocity relation.

References

1) Lane, R.A., Connolly, T.J.: Nucl. Sci. Eng., 24, 18(1962)
2) Askew, J.r., Fayers, F.J., Kemshell, P.B.: J. British Nucl. Soc., 5, 564(1966).
3) Lewis, R.A., Connolly, T.J.: Nucl. Sci. Eng., 24, 18 (1966).
4) Walti, P.: Nucl. Sci. Eng., 45, 321(1971).
5) Jonas, H., Hecker, R., Kolch, M.: Nucl. Sci. Eng., 58, 89(1975).
6) Stamatelatos, M. G.: Nucl. Sci. Eng., 61, 543(1976).
7) Tsuchihashi, k., Ishiguro, Y., Kaneko, K.: Nucl. Sci. Eng., 73, 16(1980).
8) Segev, M.: Nucl. Sci. Eng., 81, 151(1982).
9) Tsuchihashi, K. et al.: "SRAC: JAERI Thermal Reactor Standard Code System for Reactor Design and Analysis," JAERI 1285(1983).
10) Ishiguro, Y.: "PEACO-II : A Code for Calculation of Effective Cross Sections in Heterogeneous Systems," JAERI -M 5527(1974).
11) Leslie, D. C., Hill, J. G., and Jonsson, A.: Nucl. Sci. Eng.,22, 78(1965).
12) Leslie, D. C., and Jonsson, A.: Nucl. Sci. Eng., 23, 82(1965).

2.3 NEA Benchmark Calculations for Pin-Plate Cell Heterogeneity

M. Nakagawa

The NEACRP has proposed to analyse the ZEBRA CADENZA assemblies as an international benchmark problem at the meeting in 1981. This problem will provide an important comparison of the calculational methods used for treating the heterogeneities in pin and plate geometry. It is very important to accurately predict the heterogeneity effect in plate and pin geometry in order to extrapolate the results of measurements made in experimental assemblies to the prediction for the power reactors. Some experiments have been carried out in the critical assemblies using mini-calandrias holding 16 pins in a square box, but they have used it only in small zones within large plate geometry cores. In the CADENZA series of ZEBRA assemblies, the cores are completely fuelled with plates and with pins whose compositions are very similar.

The calculational method performed at JAERI and the results are briefly described in the following.

Calculation Model

Standard 1-D plate cell model: This is a one dimensional model used at Winfrith. The densities of plutonium and UO_2 metal are reduced in the ratio of the pitch area (5.42544 cm * 5.42544 cm) to the actual region area and are diluted with the side walls of the cans and the sheath wall. The top and bottom of cans of plutonium and UO_2 are diluted into the neighbouring sodium and steel regions. Thus, the standard plate cell is divided into seven slab regions with a total thickness 3.748082 cm, and has reflecting top and bottom boundaries. The end cell consists of six regions and a cell thickness is 3.431082 cm.

Modified 1-D plate cell model: In this model, the treatment of the side walls of cans and the sheath wall for plutonium and UO_2 is different from the standard 1-D model described above. The side walls of cans and the sheath wall are smeared into the sodium and SUS regions. This model will be more accurate than the standard model in the calculation of the resonance self-shielding effect of plutonium and uranium isotopes.

Pin cell model: The cell calculations of the pin elements are performed for the cluster models for both of a uniform and mixed pin cells. For mixed pin elements, the cell arrangements are explicitly taken into account. Hence, the cell averaged cross sections are obtained for all the types of the cell. Each fuel pin consists of the fuel pellet, and the cladding and the inner mini-calandria tube. The mini-calandria wall and the sheath wall are treated as the one outermost region with a thickness of 2.6172 mm.

Reactor model: The eigenvalues of cores are calculated in full plane, half-height xyz geometry. The core configurations are based on the standard loading of core 22 for plate elements and on the extrapolated pin arrangement core 23. In order to estimate the mesh size effect, the xy mesh effect is calculated in xy geometry and z mesh effect in rz geometry by using the reference mesh size and the half mesh size. The corrected eigenvalue is obtained by extrapolating these values to the zero mesh size.

The transport correction is obtained from the difference of eigenvalues by the diffusion and the S_8 transport calculations in rz geometry. These corrections are obtained for both of the plate and the pin assemblies. In the pin assembly, all eight pin cells are considered.

Calculation Method

The multi-group cross section library used for calculations is the JFS-3-J2[1] with the 70 group structure. Most of the basic nuclear data are based on the Japan Evaluated Nuclear Data Library Version 2 (JENDL-2)[2] and partially the JENDL-1 and the ENDF/B-IV are used.

The calculations for plate and pin geometries have been carried out by using the SLAROM code[3] which solves the integral transport equations basing on the collision probability method. The heterogeneity effect on the resonance self-shielding for heavy elements is taken into account by using the rational approximation for the resonance integral.

The buckling value of $B^2=2.0*10^{-3}$ cm is used for all the cells in the form of psuedo-absorption term DB^2, where D is an isotropic diffusion coefficient. The pin cell calculations have been made for a square array cluster geometry of 4*4 pins with the white boundary condition.

The in-cell reaction rate distribution has been calculated by using region dependent effective cross sections of U235, U238, Pu239 and Pu240. The neutron balances by material are also obtained from the solution by the collision probability calculations. For a mixed pin 3C, the reaction rate distribution has been calculated for all the pin rods.

The reactor calculations have been performed with the 27 group structure which is recommended in the problem specifications (NEACRP-L-243, ANL-80-78). The cell homogenized cross sections with 70 groups are collapsed by weighting with the neutron flux obtained in the diffusion calculations for the one dimensional spherical model. The reactor eigenvalues, k_{eff}, have been obtained by using the CITATION code[4] and corrected by using the S_8 transport calculation.

The results of the calculations outlined above are given in the Table 2.3.1. The discrepancy of C/E between plate and pin geometry is about 0.5%.

References

1) Takano H. and Ishiguro Y., "Production and Benchmark Tests of Fast Reactor Group Constant Set JFS-3-J2," JAERI-M 82-135 (1982)
2) Kikuch Y. et al., Paper presented at Int. Conf. on Nuclear Data for Science and Technol., Antwarp (1982)
3) Nakagawa M. and Tsuchihasi K., "SLAROM," JAERI-M 5916 (1974)
4) Fowler T. B., et al., "CITATION," ORNL-TM-2496 Rev. 1 (1969)

Table 2.3.1 Whole reactor multiplication factors

	Plate	Pin
Homogeneous xyz	0.9899	1.0048
Heterogeneous xyz		
Standard model	1.0017	1.0065
Modified 1 D model	1.0020	
Mesh correction	-0.0057	-0.0052
Transport correction	0.0029	0.0025
Corrected K_{eff}		
Standard model	0.9989	1.0038
Modified 1 D model	0.9992	
Exp.	1.002	1.001

2.4 Analysis of Heterogeneity Effect in FCA-VI-2 by the Continuous Energy Monte Carlo Code VIM

H. Takano, Y. Ishiguro and S. Mashimo*

The analysis of the heterogeneity effect for pin and plate cell in FCA-VI-2 has been performed with the continuous energy Monte Carlo code VIM[1] and the results are compared with those calculated by the SRAC code[3] in which the collision probability method is used.

Several models for the plate and pin cells of FCA-VI-2[2] were considered to estimate the amount of the resonance shielding and to calculate the spatial fine flux structure. The geometric modelings for the plate cell of T1 drawer of the test region in the FCA assembly VI-2 are shown in Fig. 2.4.1. In the present calculations, three modelings are considered as follows.

Model 1: The whole can which covers Na or Pu plate is smeared into the corresponding plate, which is scaled up by the can width. The upper and lower parts of the drawer and matrix are also smeared uniformly into all the remaining plate region while the total cell height is preserved for atomic density calculation.

Model 1': The composition of the DUO plates is taken to be the real physical composition in order to conserve the background cross section. The top and bottom of the matrix and drawer are distributed only to the remaining regions.

Model 2: This model differs from Model 1 only in the smearing way of the side walls of the cans, excluding their upper and lower walls. Each side of the Na plates is regarded as an isolated region.

The modelings for the pin-calandria geometry are shown in Fig. 2.4.2. Here, two modelings are considered.

Model 1 (Cylindrical geometry): The pin of physical radius and composition is surrounded by an annular diluent region, which has a volume equivalent to 1/16 the total non fuel region, including matrix, drawer and gap, and has a composition which corresponds to the homogenized mixture of the non-fuel regions.

---

* ISL Co. Ltd.

Model 2 (Square assembly with four pin rods): The structural material region consisting of matrix tube, draw and gap are uniformly homogenized without changing its outer boundaries, hence its total volume.

The cross section libraries used for SRAC and VIM were produced by using the ENDF/B-IV nuclear data, respectively. The results calculated with the VIM and SRAC codes are shown in Tables 2.4.1 and 2.4.2. These results show that the heterogeneity effects calculated with the two codes are in good agreement with each other in the range of the standard deviations for Monte Carlo calculations.

References

1) Milton L. J.: "VIM Users' Guide," ANL, Private communication.
2) Iijima T., Hirota J. and Mizoo N.: "FCA Assembly VI-2 Critical Experiment," JAERI-M 7888 (1978).
3) Tsuchihashi K., Takano H., Horikami K. et al.: "SRAC: JAERI Thermal Reactor Standard Code System for Reactor Design and Analysis," JAERI 1285 (1983).

Table 2.4.1 Comparison of heterogeneity effects calculated with the VIM and SRAC codes

	Homogeneous Model	Heterogeneous					
		Model 1		Model 1'		Model 2	
	k_∞	k_∞	Δk_∞	k_∞	Δk_∞	k_∞	Δk_∞
SRAC	1.2152	1.2276	0.0124	1.2289	0.0137	1.2299	0.0147
1	1.2242±0.061	1.2436 ±0.0053	0.0194	1.2373 ±0.0063	0.0131	1.2526 ±0.0070	0.0284
2	1.2351±0.0052	1.2399 ±0.0047	0.0048	1.2543 ±0.0048	0.0191	1.2449 ±0.0058	0.0098
3	1.2351±0.0052	1.2385 ±0.0046	0.0034	1.2480 ±0.0042	0.0129	1.2459 ±0.0053	0.0108
4	1.2303±0.0033	1.2416 ±0.0031	0.0113	1.2476 ±0.0033	0.0173	1.2482 ±0.0035	0.0179
VIM 5	1.2303±0.0033	1.2407 ±0.0036	0.0104	1.2447 ±0.0035	0.0144	1.2484 ±0.0041	0.0181
6	1.2352±0.0052	1.2391 ±0.0042	0.0039	1.2498 ±0.0041	0.0146	1.2457 ±0.0053	0.0105
7	1.2297±0.0034	1.2418 ±0.0031	0.0119	1.2458 ±0.0034	0.0161	1.2487 ±0.0036	0.0190
8	1.2297±0.0034	1.2411 ±0.0036	0.0114	1.2427 ±0.0038	0.0130	1.2492 ±0.0042	0.0195
9	1.2351±0.0052	1.2392 ±0.0042	0.0041	1.2511 ±0.0042	0.0160	1.2452 ±0.0054	0.0103
10	1.2315±0.0034	1.2407 ±0.0032	0.0092	1.2465 ±0.0032	0.0150	1.2478 ±0.0038	0.0163

1: Analog, 2: Track length, 3: Collision length,
4: Analog-Track combine, 5: Analog-Collision combine,
6: Track-Collision combine, 7: Average of Analog-Track,
8: Average of Analog-Collision, 9: Average of Collision-Track,
10: Average of Analog-Track-Collision

$\Delta k_\infty = k_\infty(\text{hetero}) - k_\infty(\text{homo})$

Table 2.4.2 Comparison of heterogeneity effects for pin cell calculated by absorption weighting

	Homogeneous	Heterogeneous			
		Model 1		Model 2	
	k_∞	k_∞	Δk_∞	k_∞	Δk_∞
SRAC	1.2801	1.2892	0.0091	1.2893	0.0107
VIM 1	1.2884 ±0.0032	1.2972 ±0.0027	0.0088	1.3012 ±0.0028	0.0128
VIM 2	1.2917 ±0.0016	1.2999 ±0.0022	0.0082	1.2992 ±0.0035	0.0075
VIM 4	1.2910 ±0.0014	1.2987 ±0.0014	0.0077	1.3004 ±0.0016	0.0094
VIM 7	1.2901 ±0.0018	1.2986 ±0.0014	0.0085	1.3002 ±0.0097	0.0101
VIM 10	1.2906 ±0.0015	1.2990 ±0.0012	0.0084	1.3013 ±0.0017	0.0107

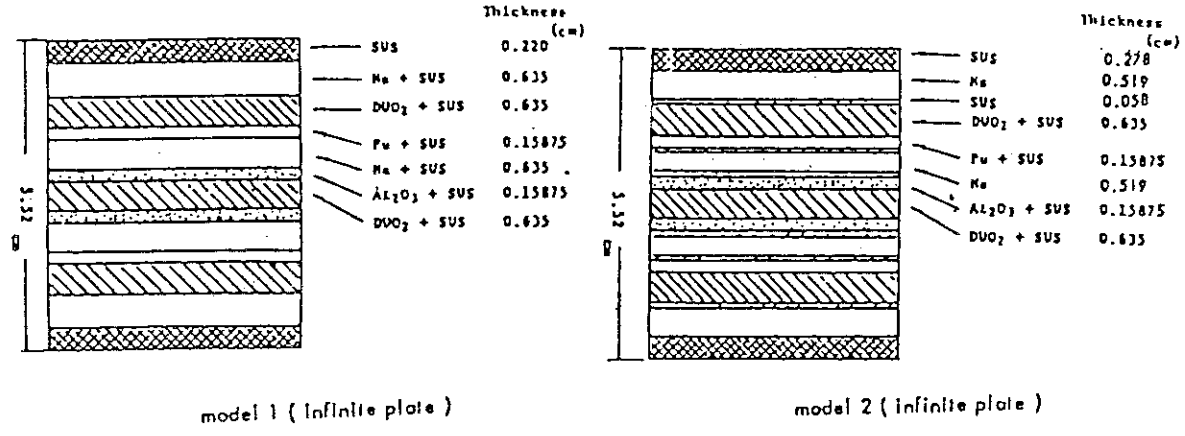

Fig.2.4.1 Cell calculation models of T_1 drawer

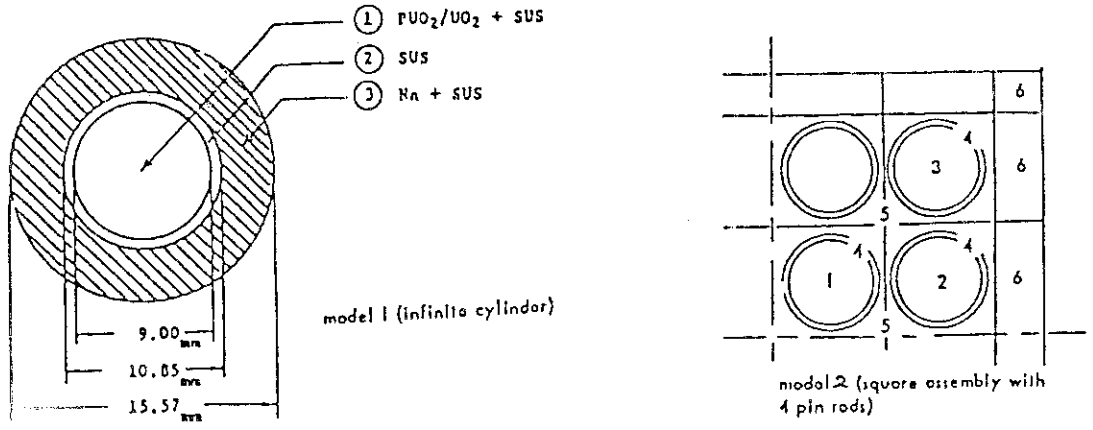

Fig.2.4.2 Cell calculation models of matrix tube, drawer and pin calandria

2.5 Development of a Monte Carlo Code Using Multi-Group Double-Differential Cross Section Library

T. Mori, M. Nakagawa and Y. Ishiguro

The Monte Carlo method is frequently used in the shielding and blanket neutronics calculations for the complex geometry in a fusion reactor. The general purpose Monte Carlo code, MORSE[1], uses the P_l expansion method to describe the angular distribution for a group-to-group scattering event. The conventional multi-group method using the P_l expansion for anisotropic scattering sometimes misdescribes considerably the neutron transport phenomena in the materials with highly anisotropic scattering cross sections. The use of the lower order P_l expansion of the angular distribution leads to negative energy transfer matrices, hence sometimes to the negative flux. Moreover, the conventional multi-group method can not accurately take account of the energy-angular correlated kinematics. In order to overcome such problems, the use of the double-differential form of scattering cross sections (DDX) was proposed for the accurate treatment of the energy-angle correlated kinematics by Takahashi *et al.*[2]. The transport codes using this type of cross section can treat accurately the strong anisotropic scattering observed in the fusion blanket and shielding materials. In the MORSE code, the scattering angle is allowed only for discrete values. Therefore, this code has some disadvantages[3] such as the ray effect and the negative flux. These problems can be solved by using the multi-group DDX.

Investigations have been made for producing the multi-group DDX library and applying it to the Monte Carlo code. The PROF-DDX code has been developed for production of a neutron DDX library from the ENDF/B

type nuclear data file[4] . This code produces partial cross sections $\sigma_{x,g'}$, neutron production cross sections, $\sigma_{pr,g'}$, and energy-angle correlated scattering probability matrix, $I(\mu_k, g' \rightarrow g)$. The anisotropy of scattering is taken into account for both elastic and discrete inelastic scatterings. At the present stage, the multi-group DDX library has been prepared for the fusion neutronics from ENDF/B-IV with 100 energy groups, 20 and 40 angular meshes of equal cosine width.

The MORSE-CG code has been modified to be able to use this library. In the random walk routine, at first, a slowing down group g is sampled at a collision point, and then cosine of scattering angle is determined from the composition dependent scattering probability table $\overline{I}$, which is obtained by mixing I for each constituent i with the weight of $N_i \cdot \sigma_{pr,g'}$. Since $\overline{I}$ is a step function existing between μ_{gmin} and μ_{gmax} , the present method does not suffer from a ray effect, as seen in Fig. 2.5.1, which shows an example of the neutron flux of group 2 penetrating through an iron plate with two mean free path thickness. The original MORSE method using P_8 cross section shows the ray effect at two discrete angles, while both DDX methods give smooth angular distributions. The difference between the results obtained from the DDX's with angular meshes 20 and 40 is small. In this code appropriate flux estimators can be selected among the point, track length, surface crossing and collision density estimators.

In order to examine the adequacy of the present method and the DDX library, the angular neutron spectra from a cylindrical slab of Li_2O and the reaction rates in a Li_2O-C assembly measured at the FNS facility[5),6)] have been analysed and comparisons have been made with the experiments and also with the results obtained from the conventional P_l expansion method. One of the results is shown in Fig. 2.5.2. The result by DDX agrees fairly well with the measurement. The analyses

have been also carried out for neutron leakage spectra from several materials measured by Hansen *et al.*[7] . The present method shows significant improvements for ^{7}Li , graphite and oxygen, as shown in Fig. 2.5.3 for graphite, though the difference between two methods is not so large for heavy materials such as iron and lead. In the case of reaction rates such as tritium production rate, the difference between the two methods is rather small.

References

1) Emmett, E.B.: "The MORSE Monte Carlo Radiation Transport Code System," ORNL-4972(1975).

2) Takahashi, A. and Rusch, D.: "Fast Rigorous Numerical Method for the Solution of the Anisotropic Neutron Transport Problem and the NITRUN System for Fusion Neutronics Applications," KfK 2832/1,2 (1979).

3) Carter, L.L. and Forest, C.A.: Nucl.Sci.Eng., 59, 27(1976).

4) Y.Ishiguro: "A code Development for Calculating Double Differential Cross section," "Reactor Engineering Division Annual Report," p.42, JAERI-M 9672 (1981).

5) Oyama, Y., et al.: "Analysis of Angle-Dependent Fast Neutron Spectra from Lithium-Oxide Cylindrical Slab Assemblies by DOT3.5," to be published in JAERI report,JAERI(1983).

6) Maekawa, H., et al.: J.Nucl.Sci.Technol., 16, 377(1979).

7) Hansen, L.F., et al.: Nucl.Sci.Eng., 60, 27(1976).

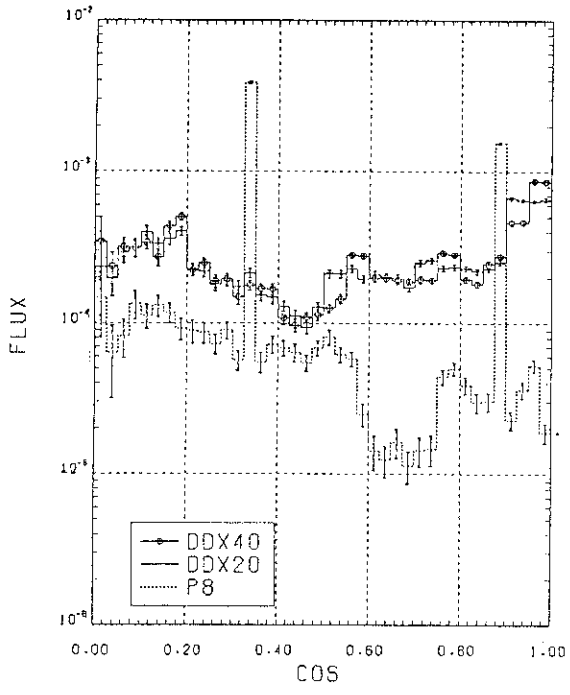

Fig.2.5.1 Neutron flux from 2 mfp thick iron plate calculated by DDX 20, DDX 40 and P_8 .

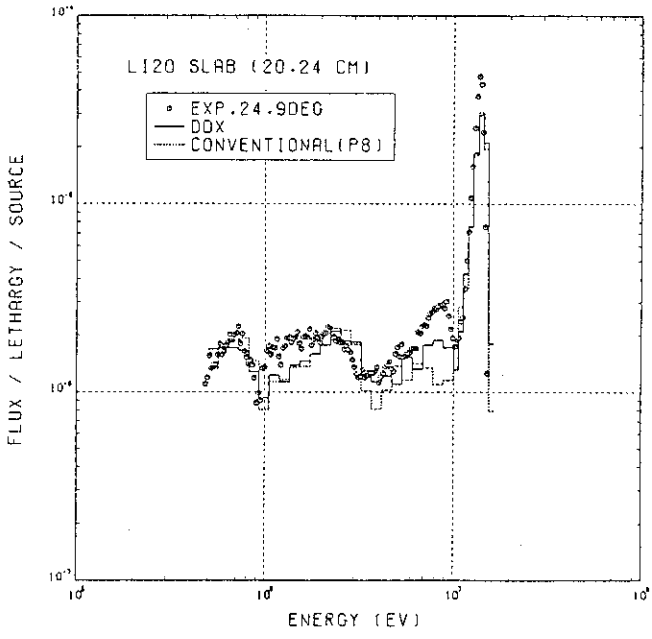

Fig.2.5.2 Comparison of angular neutron spectra from Li_2O slab of 20 cm thickness.

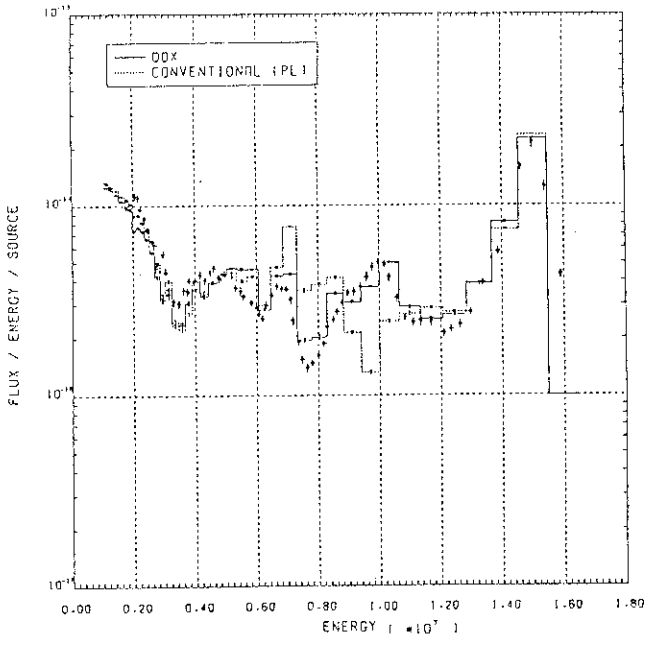

Fig.2.5.3 Comparison of leakage neutron spectra from graphite sphere.

2.6 Variational Solution Scheme by the Double Finite Element Method of the Three-Dimensional Neutron Transport Equation

T. Fujimura, Y. Nakahara and M. Matsumura*

A double finite element method (DFEM), in which both the space-and-angle finite elements are employed, has been formulated and computer codes have been developed to solve the static multi-group neutron transport problems. In addition to the Galerkin method,[1] the variational one[2] is used to apply the DFEM to the three-dimensional geometry.

Variational Scheme

The g-th group flux ψ^g is approximated by

$$\psi^g(r,\Omega) = \sum_{i=1}^{I} \sum_{j=1}^{6} c_{ij}^g \phi_i(r) \chi_j(\Omega)$$

where $\phi_i(r)$ and $\chi_j(\Omega)$ are spatial and angular base functions, respectively. The parity functions are then defined as:

$$\psi^e(\Omega) = \{\psi(\Omega) + \psi(-\Omega)\}/2, \qquad \psi^o(\Omega) = \{\psi(\Omega) - \psi(-\Omega)\}/2,$$

where $\psi(\Omega) = \psi^g(r,\Omega)$. Let us make a similar definitions:

$$c_{i1}^e = (c_{i1} + c_{i6})/2, \quad c_{i2}^e = (c_{i2} + c_{i4})/2, \quad c_{i3}^e = (c_{i3} + c_{i5})/2,$$

$$c_{i1}^o = (c_{i1} - c_{i6})/2, \quad c_{i2}^o = (c_{i2} - c_{i4})/2, \quad c_{i3}^o = (c_{i3} - c_{i5})/2.$$

Since $\psi^e = \sum_{i=1}^{I} \sum_{j=1}^{3} c_{ij}^e \phi_i \chi_j$ and $\psi^o = \sum_{i=1}^{I} \sum_{j=1}^{3} c_{ij}^o \phi_i \chi_j$, we propose a new semi-iteration designed as follows,

$$c_{ij}^e(n') \ (j=1\sim3) \longrightarrow c_{ij}(n) \ (j=1\sim3) \longrightarrow c_{ij}^o(n') \ (j=1\sim3)$$

$$\longrightarrow c_{ij}^e(n) \ (j=1\sim3) \longrightarrow c_{ij}(n) \ (j=4\sim6) \longrightarrow c_{ij}^o(n) \ (j=1\sim3)$$

where n' and n are the inner iteration indices.

Now let $c_{ij} = 1$ $(i=1\sim I,\ j=1\sim6)$ be the initial guess. Then

---

* I.S.L. Co. Ltd., Tokyo

$c^e_{ij}(0) = 1$ and $c^o_{ij}(0) = 0$ for $j = 1 \sim 3$. The new values for c^e_{ij}'s are obtained from the stationary point of the functional for ψ^e by solving the linear equation:

$$A^e c^e = b^e$$

where A^e is a symmetric matrix.

Since a whole reactor domain is divided by a number of (x,y) planar layers, we can solve the g-th group equation applying the SSOR method successively to the planes. The SSOR iteration is accelerated efficiently by an adaptive method.[3] We also use the coarse mesh rebalancing technique to improve the guess flux and the extrapolation method to accelerate the outer iteration.[1]

Sample Calculations

Numerical studies of the scheme have been done in comparison with the Galerkin method and also with the CITATION.[4] and TWOTRAN-II[5] results.

Sample 1. Boundary fluxes A cubic homogeneous reactor shown in Fig. 2.6.1 is chosen for simplicity. As seen in Fig. 2.6.2, the Galerkin and variational methods give the reasonable flux distribution in spite of fewer meshes than the CITATION.

Sample 2. External source problem This is a modification of one of the Lathrop's constant source problems,[6] as shown in Fig. 2.6.3. As seen in Fig. 2.6.4, the DFEM codes have acceptable solutions even for meshes so coarse that the S_n code has only the unphysical solutions. The mitigation of ray effects[6] is clearly seen in the DFEM solutions.

References

1) Fujimura T., Nakahara Y. and Matsumura M.: "Improvements of a Double Finite Element Program for Solving Three-Dimensional Multi-Group Neutron Transport Equation," Reactor Engineering Division Annual Report, p 28, JAERI-M 82-114 (1982).
2) Tomlinson E. T. and Robinson J. C.: Nucl. Sci. Eng., 63, 167 (1977).
3) Fujimura T. and Matsui Y.: Nucl. Sci. Eng., 77, 360 (1981).
4) Fowler T. B., Vondy D. R. and Cunningham G. W.: "Nuclear Reactor Core Analysis Code: CITATION," ORNL-TM-2496 (Rev. 2), (1969).
5) Lathrop K. D. and Brinkley F. W.: "TWOTRAN-II: An Interfaced,

Exportable Version of the TWOTRAN Code for Two-Dimensional Transport," LA-4848-MS, (1973).

6) Lathrop K. D.: Nucl. Sci. Eng., 45, 255 (1971).

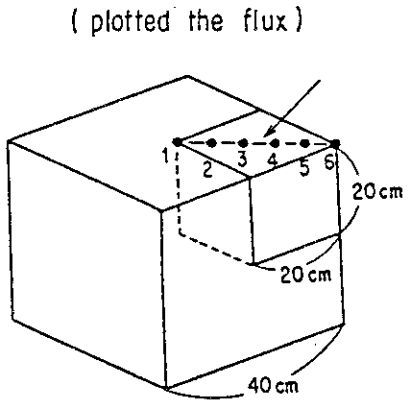

Fig. 2.6.1 A cubic homogeneous reactor used in Sample 1 calculation

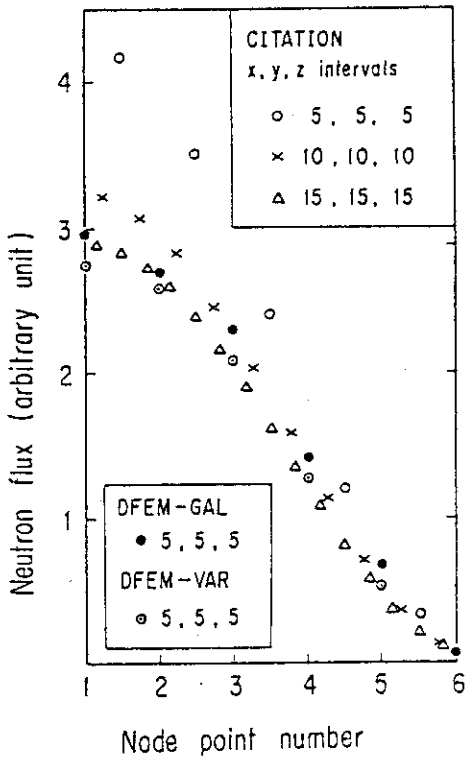

Fig. 2.6.2 Comparison of the first group fluxes along a line as shown in Fig. 2.6.1

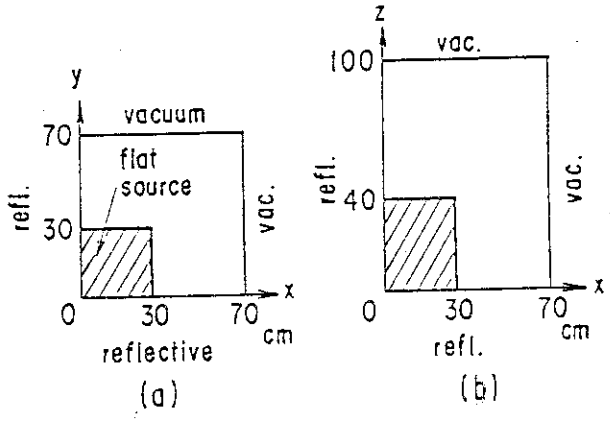

Fig. 2.6.3 A modified Lathrop's constant source problem[6]

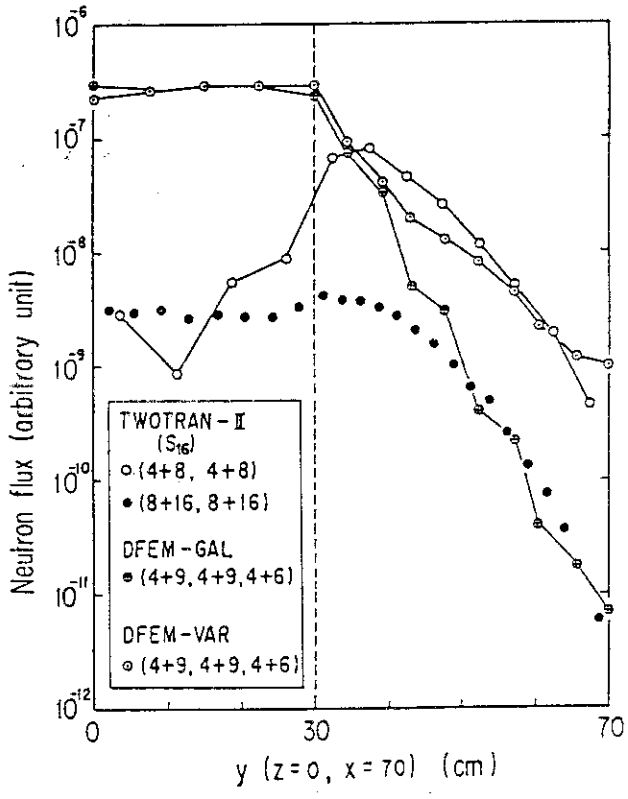

Fig. 2.6.4 Comparison of the fluxes in a source problem along a line (x=70, z=0)

2.7 Vector Processing of the Neutron Transport Codes

M. Ishiguro+ and T. Tsutsui

One of the large scale computations in JAERI is the neutron transport ones used in reactor shielding and criticality analyses. The adaptability of vector processing has been investigated on the neutron transport codes under the assumption of the use of a supper-computer in the near future.

Five codes have been tested. They are DOT3.5[1], TWOTRAN[2] and ANISN[3] based on the finite difference method, and PALLAS-2DCY[4] and BERMUDA[5] on the direct integration method.

It has been found that the gain from vectorization depends upon the numerical method, geometries, and problem types to be solved. That is, the direct integration is rather suited for the vector processing. But in the conventional finite difference method, the difference equation has an unvectorizable recurrence form in (r,z) and (r,θ)-geometries. But by altering the iterative process, the equation can be vectorized and some gains have been found to be achieved in a criticality problem. The results are summarized in Table 2.7.1.

References

1) Mynatt, F. R.: "Development of Two-Dimensional Discrete Ordinates Transport Theory for Radiation Shielding," PHD Thesis of Univ. Tennessee (1969).
2) Lathrop, K. D. et al.: "TWOTRAN II: An interfaced, Exportable Version of the TWOTRAN Code for Two-Dimensional Transport," LA-4848-MS (1973).
3) Engle, W. W. et al.: "DTF-II, A One-Dimensional, Multigroup Neutron Transport Program," NAA-SR-10951 (1966).
4) Takeuchi, K.: "PALLAS-2DCY-FC, A Calculational Method and Radiation Transport Code in Two-Dimensional (R,Z) Geometry," Papers of Ship Research Institute, No. 57 (1979).
5) Suzuki T., et al.: "BERMUDA-2DN: A two-Dimensional Neutron Transport Code," 6-th Inf. Conf. on Rad. Shieldings, Tokyo, May 16-20 (1983).

+ Computing Center, JAERI

Table 2.7.1 Summary of vectorization effect on the neutron transport codes

Code name	Problem	Numerical method	Number of source statements	Vectorized ratio (%)	Speed-up ratio	Vector length	I/O access counts
TWOTRAN	2-Dimension (x,y), S-16	Difference	7000	83	4.5	48	500 ∿ 1000
TWOTRAN	2-Dimension (r,z), S-18	"	"	20	1.1	-	"
TWOTRAN	2-Dimension (x,y), S-8	"	"	75	2.0	10	"
ANISN	1-Dimension	"	3000	21	1.2	-	-
DOT 3.5 (Shielding)	2-Dimension (x,y)	"	6500	80	1.4	96	5600
DOT 3.5 (Shielding)	2-Dimension (r,θ) or (r,z)	"	"	20	1.1	-	-
DOT 3.5 (Critical)	2-Dimension (x,y)	"	"	78	2.0	16	-
DOT 3.5 (Critical)	2-Dimension (r,θ) or (r,z)	"	"	"	2.0	40	500
BERMUDA-2DN	2-Dimension (r,z)	Direct integration	5000	90	3.0	40	500 ∿ 1000
PALLAS-2DCY	2-Dimension (r,z)	"	3800	80	2.6	60	1000 ∿ 3000

2.8 Analysis of Spectra of Spallation Neutrons from a Lead Target Bombarded by High Energy Protons

Y. Nakahara, T. Tsutsui and K. Tsukada*

Measurements of the yield and energy spectrum of spallation neutrons are quite important not only for clarifying the physical processes involved in the neutron production but for performing the reliable feasibility studies of accelerator driven nuclear fuel producers, radioactive waste transmuters and also the efficient designs of intense neutron sources. Recently, the KFK and LANL groups have performed extensive measurements of the spectra of neutrons at several angles from various targets.[1),2)] A remarkable feature seen in their results is the existence of a shoulder around 100 MeV in the neutron spectra.

Concerning the theoretical works, computational analyses of the experiments are performed usually by using a nucleon-meson transport code system NMTC[3)] or its extended version HETC.[4)] The improvements of NMTC have been done to incorporate the high energy fission into the reaction processes.[5)] In constrast to the measured results, no shoulders are seen in the calculated neutron spectra obtained by NMTC or HETC and their improved versions. The calculations give considerably smaller values than the experiments around 100 MeV.[1)]

In trying to reproduce the measured spectral shape by the calculation, we have changed the magnitude of the effective nucleon-nucleon interactions inside a nucleus in order to enhance the leakage of high energy nucleons from the nucleus. In computer code cross sections of the nucleon-nucleon collisions in a free space are used for the intranuclear cascade calculation, although the Pauli-blocking effect is taken into consideration. Recently, an anomalous behavior of the mean free path of a nucleon inside the nucleus has been found and its values are remarkably larger than those expected from the free space nucleon-nucleon cross sections in the energy range from 100 to 500 MeV.[6)] As a preliminary analysis, we multiplied a constant factor(>1) to the nucleon mean free path in the intranuclear cascade calculations by the use of the NMTC/JAERI code.

We performed calculations for a Pb rod target of 10 cm ϕ and 60 cm

* Nihon University

length. The diameter of the proton beam incident on the bottom of the cylinder is 2 cm. Neutron fluxes have been obtained by making integration over angle and taking average on the rod surface. The neutron yield is the total number of neutrons created in the target per one incident proton. As seen in Fig.2.8.1 for the 590 MeV proton beam, the high energy part of the spectrum is increased and the shoulder appears in the calculated spectrum obtained with the multiplication factor of 1.1 ～ 1.5. With the increase of the factor, however, the neutron yield decreases rapidly, as seen in Fig.2.8.2. The increase of neutrons emitted from the nuclei during the cascade process reduces the excitation energies of the residual nuclei, which results in the decrease of evaporation neutrons. With consideration for the balance between the cascade and evaporation contributions, it can be said that the optimum value of the multiplying factor is about 1.1.

It has been shown that the shoulder of the neutron spectrum can be reproduced by the calculation using the stretched mean free path. Extensive calculations are required to get a quantitatively good agreement between experimental and calculated values.

References

1) Cierjacks S.,et al.: " High Energy Particle Spectra from Spallation Target," ICANS-V, Jülich, p.215, Jül-Conf-45(1981).
2) Russel G.J., et al.: "Measurement of Spallation-Target-Moderator Neutronics at the WNR Facility," ICANS-IV, Tsukuba, p.210, KENS Report-II(1981).
3) Coleman W.A., Armstrong T.W.: "NMTC Monte Carlo Nucleon-Meson Transport Code," RSIC CCC-161.
4) Chandler K.C., Armstrong T.W.: "HETC Monte Carlo High-Energy Nucleon-Meson Transport Code," RSIC CCC-178.
5) Nakahara Y., Tsutsui T.: "NMTC/JAERI A Simulation Code System for High Energy Nclear Reactions and Nucleon-Meson Transport Processes," JAERI-M 82-198(1982)(in Japanese).
6) Tsukada K., Arazeki H., Nakahara Y.: "Determination of the Neutron Mean Free Paths and the Optical Potential In the Medium Energy Region," 2.9 in the present report.

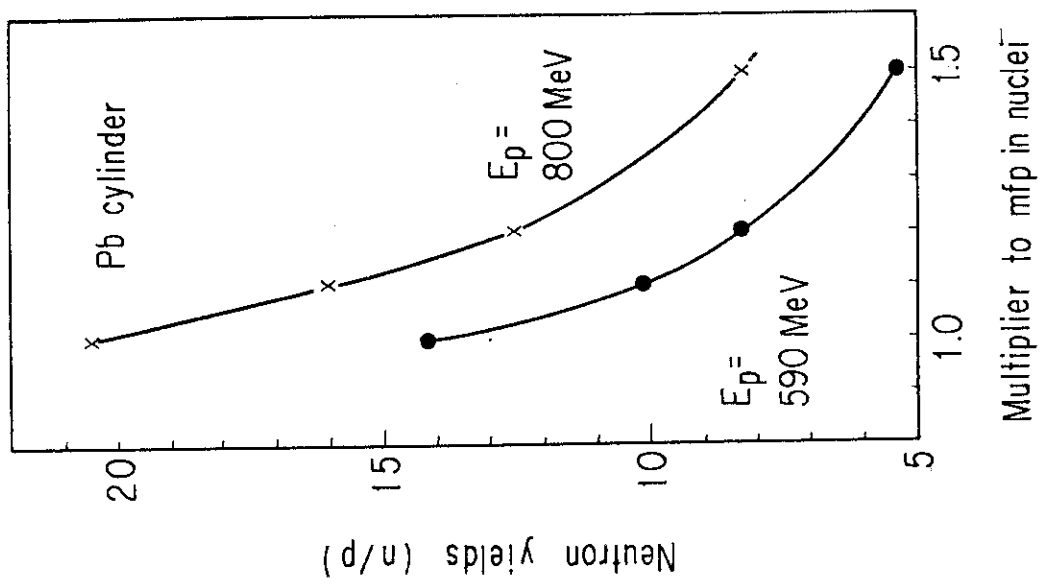

Fig.2.8.2
Influence of the stretched mean free path on the neutron yield

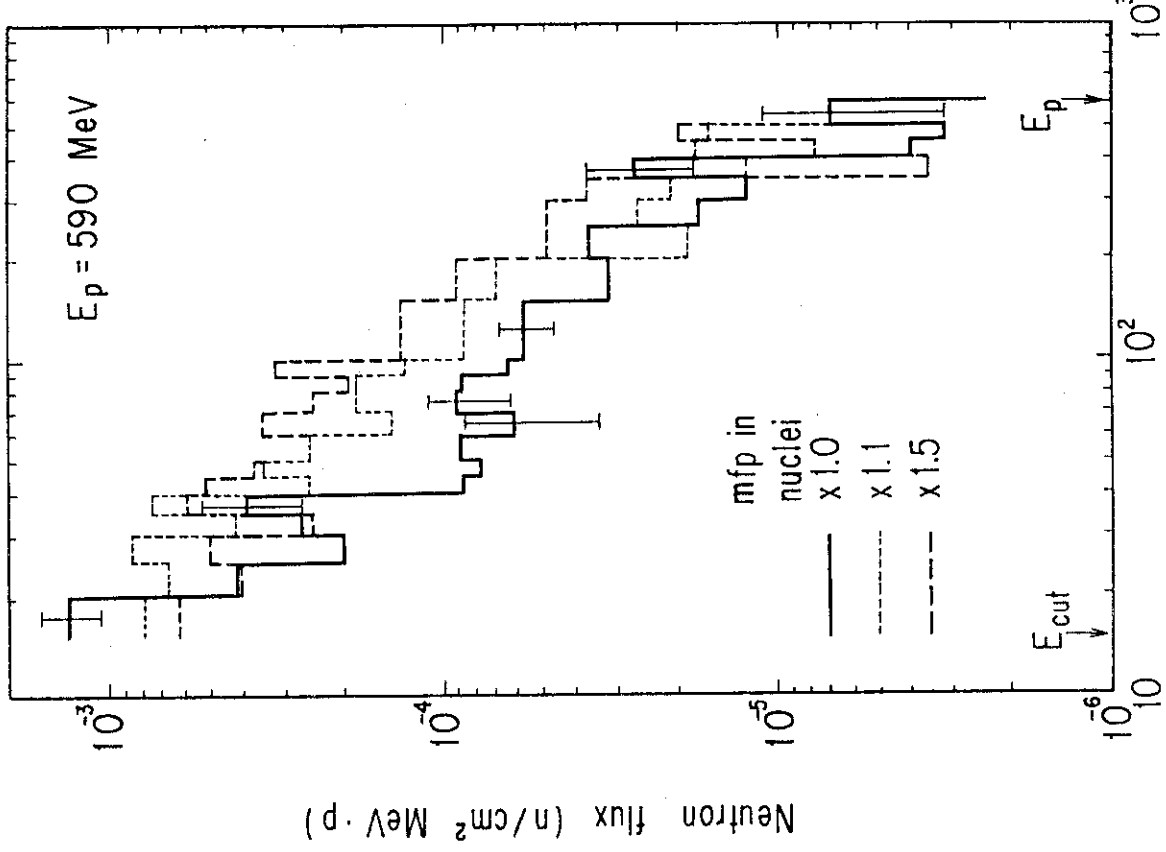

Fig.2.8.1
Effect of the stretched mean free path on the spallation spectrum at the side boundary of the Pb cylinder

2.9 Determination of the Neutron Mean Free Paths in Nuclei and the Optical Potential in the Medium Energy Region

K. Tsukada*, H. Arazeki* and Y. Nakahara

Values of the neutron mean free paths inside nuclei and the related optical potential parameters in an energy range from 100 MeV to 5 GeV have been determined by fitting the semi-classical formulas of the neutron elastic and non-elastic cross sections due to Fernbach et al.[1] to the experimental data.[2]

If the propagation wave vector of the incident neutron is k, the one inside the nucleus is $(k' + i\frac{1}{2}K)$ and $k_1 = k - k'$, we have the following fomulas for the nucleus of mass A, i.e.,

$$\sigma_{non} = \pi R^2(1 - A_0), \tag{1}$$

$$\sigma_{el} = \pi R^2(1 + A_0 - B_0), \tag{2}$$

where

$$A_0 = \{1 - (1 + 2KR)\exp(-2KR)\}/2(KR)^2$$

$$B_0 = (1/D^2)[C - \exp(-KR)\{C + (KR)D\}\cos 2(k_1R) + \exp(-KR)\{2D + (KR)\}(k_1R)\sin 2(k_1R)],$$

$$C = 1/\{4(KR)^2 - (k_1R)^2\}, \text{ and}$$

$$D = 1/\{4(KR)^2 + (k_1R)^2\}.$$

$R = r_0A^{1/3}$: nuclear radius, r_0 being the nuclear radius parameter.

Using the experimental data for σ_{non} and σ_{el} and solving Eqs.(1) and (2), which are now to be treated as a system of nonlinear equations for k_1 and K, we can obtain the values of k_1 and K. The mean free path λ in the nucleus is given by the reciprocal of K, which is a half of the imaginary part of the propagation wave vector inside the nucleus. The sign of k_1 cannot be determined in these calculations. So we have to use another relation. If an optical potential with a simple square well structure, $-(V + iW)$, is assumed, k_1 is given by the relation

$$k_1 = k(\tfrac{1}{2}V/E_n - (V^2 - W^2)/(8E_n^2)), \tag{3}$$

* Nihon University

where E_n is the incident neutron energy. We have also the following relation

$$K^2 = \frac{2m}{\hbar^2} \frac{W^2}{E_n+V+1/4(W^2/E_n)} \qquad (4)$$

where m is the neutron mass.

In Fig.2.9.1 the calculated values of the mean free paths are plotted as the function of E_n. The unexpectedly strong peaks appear in the energy region from 200 to 300 MeV for all the investigated nuclei. The peak values range from 7 fm for Cu to 8 fm for U, but for C the peak is not so steep. In the region above 500 MeV the values are seen between 2 and 4 fm. One of the reasons why the values are so dispersed even at the same energy is the large experimental errors in σ_{non}. As seen in Fig.2.9.1, a minor change of the r_o values also gives a large effect on the calculated values.

The relations of V and W with E_n are shown in Figs.2.9.2 and 2.9.3, respectively. Since some of the values of V's are found to be zero at the energy between 500 and 1,000 MeV, the sign of V's in the higher energy region is taken to be negative. On the other hand, the values of W's increase rapidly with E_n in the region above 500 MeV.

References

1) Fernbach S., et al.: Phys. Rev., 75, 1352(1949).
2) Garber D,I., Kinsey R.R.: BNL-325, 3rd ed., Vol.2(1976).
Schimmerling W.,et al.: Phys. Lett., 15, 177(1971),
Phys. Rev., C7, 248(1973).
Ashmore A., et al.: Proc. Phys. Soc., LXX, 10-A, 51(1957).
Goldanski V.I., et al.: Sov. Phys. DOKLADY, I, 16(1956).

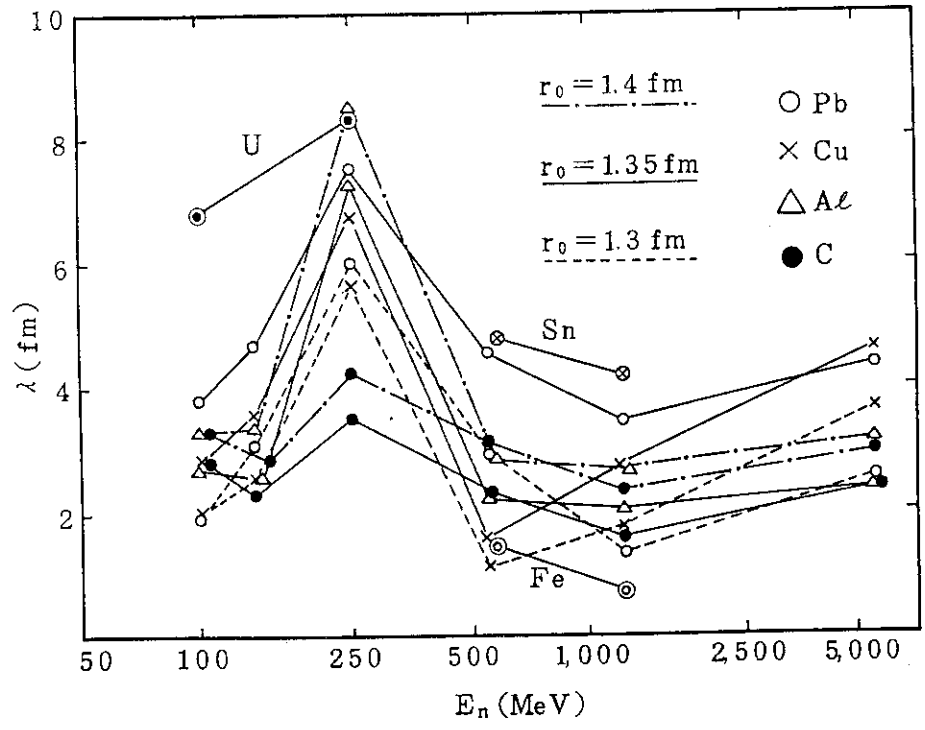

Fig.2.9.1 The neutron mean free path inside the nucleus versus the neutron energy

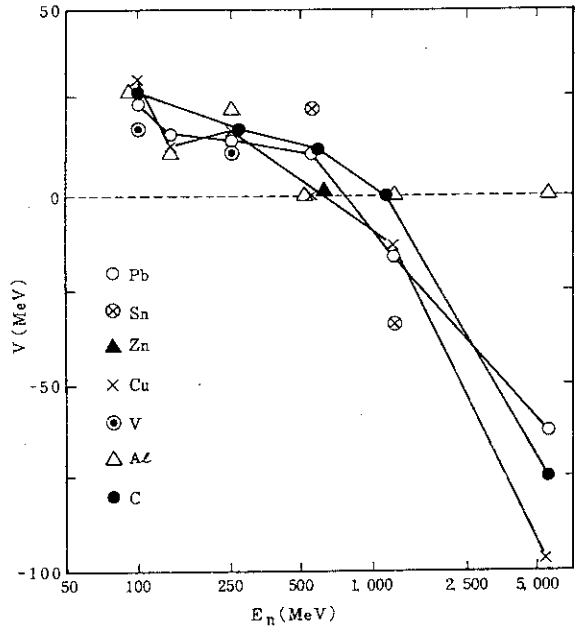

Fig.2.9.2

The real part of the optical potential versus the neutron energy

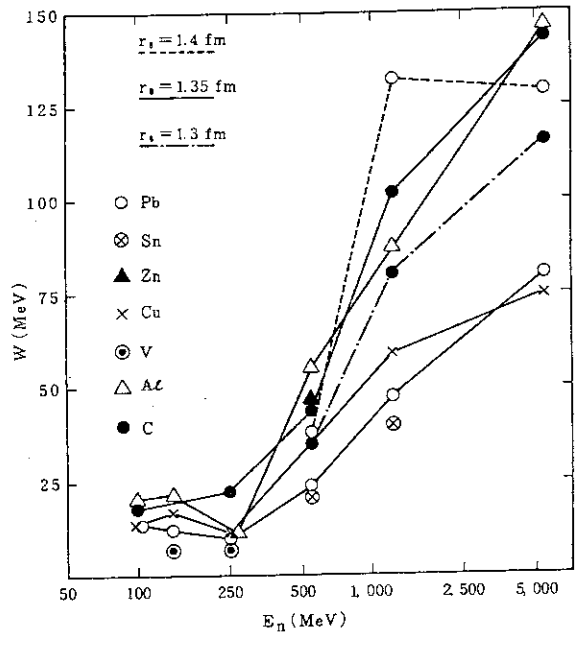

Fig.2.9.3

The imaginary part of the optical potential versus the neutron energy

2.10 Calculations of the Structure Images of Atomic Defect Clusters in Some F.F.C. Metals

T. Nishida and K. Izui[+]

Direct observation of an atomic lattice imperfection can provide a powerful means for visual determination of the precise atom positions and this approach will be applicable to a wide research region of material science. In our works a lot of computer simulations on the high resolution electron microscope image has been performed[1),2)] for some models of small point defect clusters to obtain the basic data for analyzing the observed images.

In the present calculation the multi slice theory[3)] was applied to the computation on the extended unit cell, assuming the periodic continuation,[4)] equal to (4 x 4) times the conventional unit cell of a F.C.C. crystal oriented in (110) in the lateral dimensions. Figure 2.10.1 illustrates the projection of a structural model of an interstitial cluster, which is used in our calculations, onto this superlattice cell. The defect model is composed of some slices each of which contains three interstitial pairs in an asymmetric array with slight outward relaxation of lattice atoms around them. This extension of a unit cell generates a set of diffuse scatterings which should be sampled at finner intervals than those for Bragg reflections in the corresponding reciprocal space. For the defect imaging calculation, it is also necessary to adjust the electron optical parameters such as defocus and the aperture radius in order to bring in the constant phase shift to all the relevant waves passing through the objective lens and contributing to the image formation. From this point of view, authors selected four values of defocusing Δf, i.e., Δf = (a) 407 Å (nearly equal to Scherzer focus), (b) 550 Å, (c) 215 Å and (d) 790 Å with the spherical aberration coefficient C_s = 1 mm at 500 KV, as seen in Fig. 2.10.2, in which the curve representing an imaginary or a real part of lens transfer function looks like almost flat for both (2,1) and (0,2) Bragg reflections and the diffuse scatterings around them,

+ Department of Chemistry, JAERI

although their phase shifts against the transmitted wave (0,0) are different in each case.

At first, the effect of the defect or crystal thickness on its images in an Al metal was examined under the ideal lens condition (Δf = 0 Å, C_s = 0 mm) at 500 KV. These results showed that the high resolution image, in which three atom pairs and the slight relaxation pattern are well reproduced, is obtained in the wide range of thickness less than ~150 Å because the image intensity in Al oscillates relatively slowly in the thickness direction. As well known, a clear fine structure of a crystal lattice or a crystal defect often appears in the image that is calculated at the thickness where the transmitted wave intensity becomes minimum, so-called "a valley", and scattered waves, conversely, have maximum intensities. In Fig. 2.10.3 image intensities under the optimum real lens conditions as described above are shown for Al, Au and Cu for the defect structure at the thickness of the first valley (~110 Å in Al, ~17 Å in Au, ~36 Å in Cu) and compared with the ideal lens image in each metal. These real lens images also well reproduce interstitial and the relaxation patterns although the atoms appear in different aspects in each case. Under the ideal lens condition, an atom image of Al is a white spot surrounded by a dark ring but ones of Au and Cu are small black circles and these are in a good agreement with images formed under the focus conditions (c) and (d) respectively. For imaging under the conditions (a) and (b), the atom positions are found to appear as white spots in all the metals. It may be considered that the difference among the atom images is due to the phase shift of the transmitted wave between the two lens conditions. Additionally, we have confirmed the fact that the thinner becomes the cluster thickness in the crystal, the more obscure becomes the defect pattern.

References

1) Nishida T., Izui K.: "Identification of Small Point Defect Clusters by High Resolution Electron Microscopy," Proc. 5th Yamada Conf., Kyoto, 1981.
2) Nishida T., Izui K.: "Effects of Chromatic Aberration of Objective Lens and Misorientation of a Crystal on High Resolution Images of

Simple Defects in Silicon," JAERI-M 82-114, 37 (1982).

3) Cowley J. M., Moodie A. F., Acta Cryst. 10, 609 (1957).

4) Field P. M., Cowley J. M.: "Computed Electron Microscope Images of Atomic Defects in F.F.C. Metals," Acta Cryst., A34, 103 (1978).

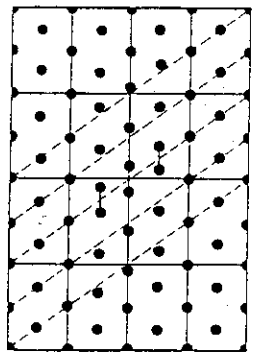

Fig. 2.10.1 A model of defect slice on the (110) superlattice cell.
Three interstitials are at the center with slight outward relaxation which appears as the displacement of atom rows from dashed lines representing an atom plane.

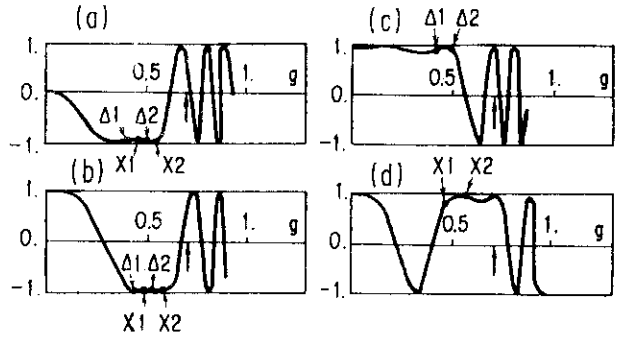

Fig. 2.10.2 Profiles of an imaginary or a real part of lens transfer function for the scattered waves in each metal.
The focus conditions are (a) 407 Å, (b) 550 Å, (c) 215Å and (d) 790 Å with C_s = 1 mm at 500 KV, where symbols of $\Delta 1$ and $\Delta 2$ represent (2,1) and (0,2) reflections in Al and Au, and ones of X1 and X2 those in Cu. The arrow denotes the radius of objective lens.

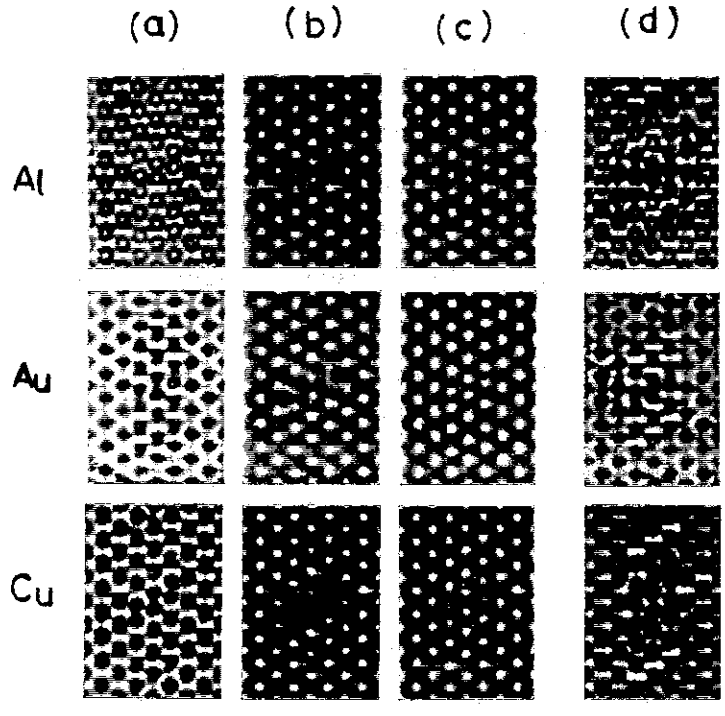

Fig. 2.10.3 Comparisons of the simulated images of the interstitial cluster among Al, Au and Cu metals.
Thicknesses of Al, Au and Cu metals are 111 Å, 17 Å and 36 Å respectively. The imaging conditions are (a) Δf = 0 Å, C_s = 0 mm(ideal lens), (b) Δf = 407 Å, C_s = 1 mm(nearly Scherzer focus), (c) Δf = 550 Å, C_s = 1 mm and (d) Δf = 215 Å for Al & Au or 790 Å for Cu, C_s = 1 mm with the aperture radius ~ 0.01 rad at 500 KV.

2.11 Computer Simulation of Radiation Damages

Y. Taji and T. Yokota+

We have performed studies on the computer simulation of radiation damages concerning the following three items: a) calculation of anisotropic displacement threshold energies in molybdenum[1] by making use of the GRAPE code, b) simulation of the atomic-displacement cascades in stainless steel due to energetic ion injection and c) development of a molecular dynamical code taking account of the effect of noncentral intermolecular forces for simulating radiation damages in the body centered cubic (b.c.c.) crystals and the graphite crystals.

We will here explain about only the item (a). Though the molybdenum is an important structural material for the fusion reactors fundamental surveys of radiation damages have not performed so fully. We dared to calculate displacement threshold energies in every directions of the primary knockon atom (PKA) with respect to the axes of crystals. We have used a pair potential function made by Johnson and Wilson. The size of lattice has been set as 20x20x20 in the half-lattice unit. Three kinds of surface forces, the constant force, the spring force and the viscous force have been set for the lattice to be stable. Then the fundamental triangle bounded by the axes [100], [110] and [111] has been divided into 34 zones (or directions), in each of which the PKA with various energies has been started. We have obtained the contours of constant displacement threshold energy in the fundamental triangle as Fig. 2.11.1. The triangle has been divided into two kinds of zones, i.e., the simple and the complex zone. In the simple zone around the axes [100] and [111] the so-called focusing collisions are dominant so that the Frenkel pair is created easily without dispersing energies to other atoms. On the other hand, in the complex zone other than the simple zone mentioned above the energy of PKA is transferred to the atoms in various directions so that the threshold energy becomes large. The stability of the Frenkel pairs has been checked to obtain a spontaneous recombination domain as shown in Table 2.11.1, which becomes slightly narrower than the domain for iron.

+ Department of Physics, JAERI

Reference

1) Yokota T., Taji Y. and Iwata T.: "Computer Simulation of Anisotropy of Displacement Threshold Energies," Proc. Spring Meet. Phys. Soc. Jpn., 27aH12 (1982).

Table 2.11.1 Stability of the Frenkel pairs.
The interstitial in the dumb-bell type is located at (0,0,0) in the direction <101>, for which the locations of vacancies are tabulated.

loc. of vac.	distance		loc. of vac.	distance	
(1,1,1)	$\sqrt{3}$	unstable	(3,1,-1)	11	stable
(1,1,-1)	$\sqrt{3}$	stable	(2,2,2)	$2\sqrt{3}$	unstable
(2,0,0)	2	unstable	(2,2,-2)	$2\sqrt{3}$	stable
(0,2,0)	2	stable	(4,0,0)	4	stable
(2,2,0)	$2\sqrt{2}$	unstable	(4,0,2)	$2\sqrt{5}$	stable
(2,0,2)	$2\sqrt{2}$	stable	(4,0,-2)	$2\sqrt{5}$	stable
(2,0,-2)	$2\sqrt{2}$	stable	(3,3,3)	$3\sqrt{3}$	unstable
(1,3,1)	$\sqrt{11}$	stable	(0,6,0)	6	stable
(3,1,1)	$\sqrt{11}$	stable	(4,4,4)	$4\sqrt{3}$	stable

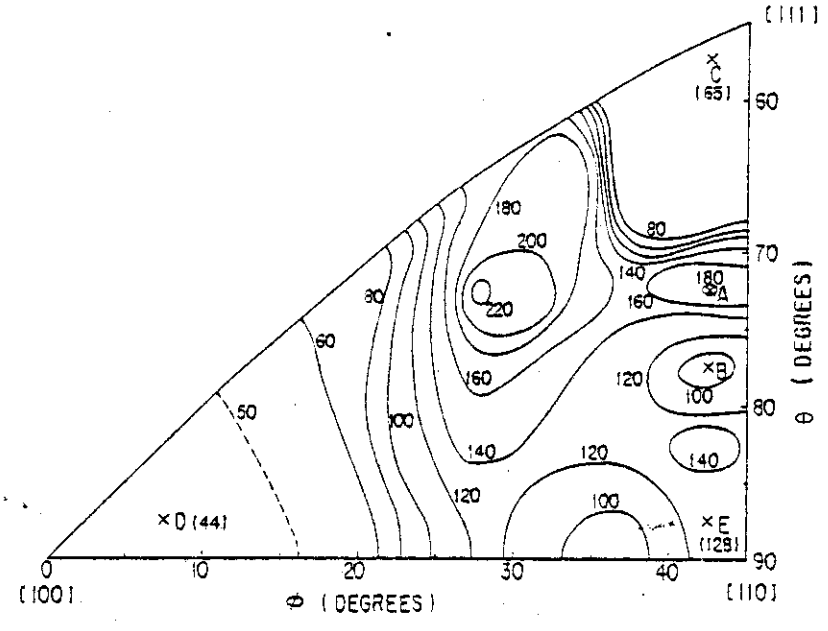

Fig. 2.11.1 Contours of constant displacement threshold energy for Mo

2.12 Investigation of Space-dependent Neutron Flux Fluctuation Excited by Strong Absorber

Y.Gotoh and H.Yasuda

The response of neutron flux to the sudden displacement of absorber plate has been formulated as an initial-value problem[1)3)], by using the inverse Laplace transform method, and it has been applied to a numerical example[2)]. The movement of the neutron flux depression near the absorber was found to be so rapid that the movement should be taken into account in the analysis of the neutron flux response to the vibrating absorber, but there is some time-delay to reach the steady flux in a reactor except the region around absorber. It has been found that this calculational method is useful for the analysis of the neutron flux response to the sudden withdrawal and to the sudden insertion of the absorber.

As an example, we consider a rather large water reactor of width 300 cm. For the kinetic parameters the values ρ =1.0$, $l=7\times10^{-5}$sec , $\lambda=0.1sec^{-1}$, $\beta=0.007$, and for the diffusion length L = 5.8 cm are assumed. The neutron flux response to the displacement of strong absorber ($\gamma=0.07$) from the center(150 cm) to 149 cm, is shown in Fig. 2.12.1 where the difference of fluxes around absorber is very small. To see the details of the response, the local neutron flux responses to the displacement of absorber plate are enlarged in Fig. 2.12.2 .

A formulation which treats the neutron flux response excited by the vibrating strong absorber plate , has been introduced by considering movement of the flux depression caused by the absorber. The singular derivatives of neutron flux and of Green function at the both sides of absorber are divided into a symmetric and an asymmetric parts, unambiguously. It has been shown that the bi-frequency term is proportional to the difference between the static and the frequency dependent asymmetric derivative of Green function at the absorber position, but the term in the first order of displacement vanishes exactly not only in the one group theory but also in the two group theory, because of the frequency- independence of the asymmetric derivative, which is the characteristic of Green function.

The absorber plate vibration induced by coolant flow, for example, is equivalent to the Brownian motion of simple harmonic oscillation. The amplitude of peak in the power spectral density of neutron flux fluctuation shows the strong space dependence which is determined by the relative position between detector and vibrating absorber. For the strong absorber the correction to the amplitude of the peak has been given by the mean value of the derivative of Green function at the position of absorber.

References

1) Gotoh Y. "Study of Stochastic Reactor Kinetics Equation," Prog. Nucl. Energy, 9, 303 (1982).

2) Gotoh Y., Yasuda H.: Fall Meeting of the Atomic Energy Society of Japan (1982).

3) Gotoh Y., Yasuda H. " Investigation of Space-dependent Neutron Flux Fluctuation Excited by Strong Absorber," to be published in Ann. Nucl. Energy.

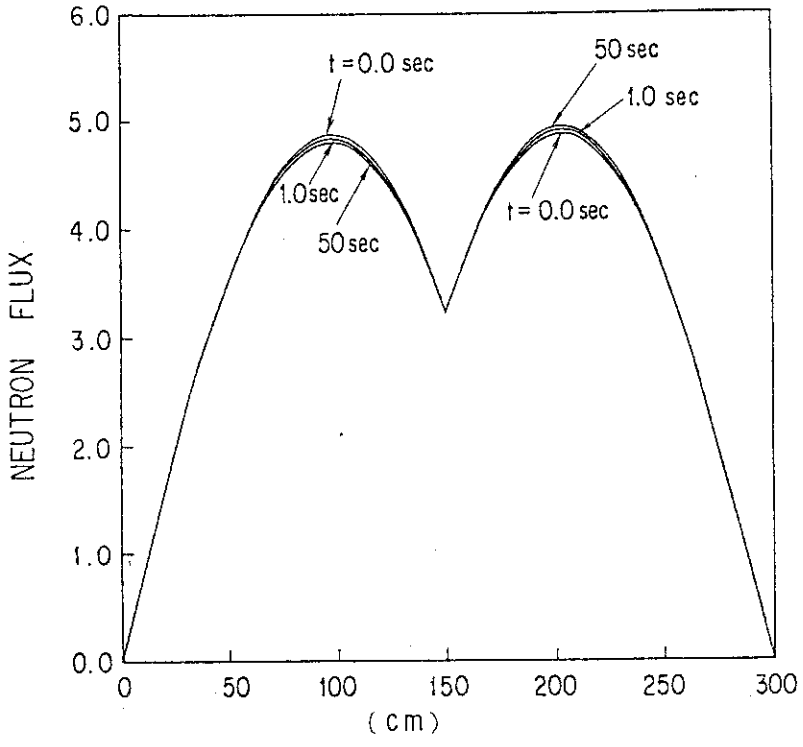

Fig. 2.12.1 Time response of neutron flux to displacement of absorber plate from the center, 150 cm, to 149 cm

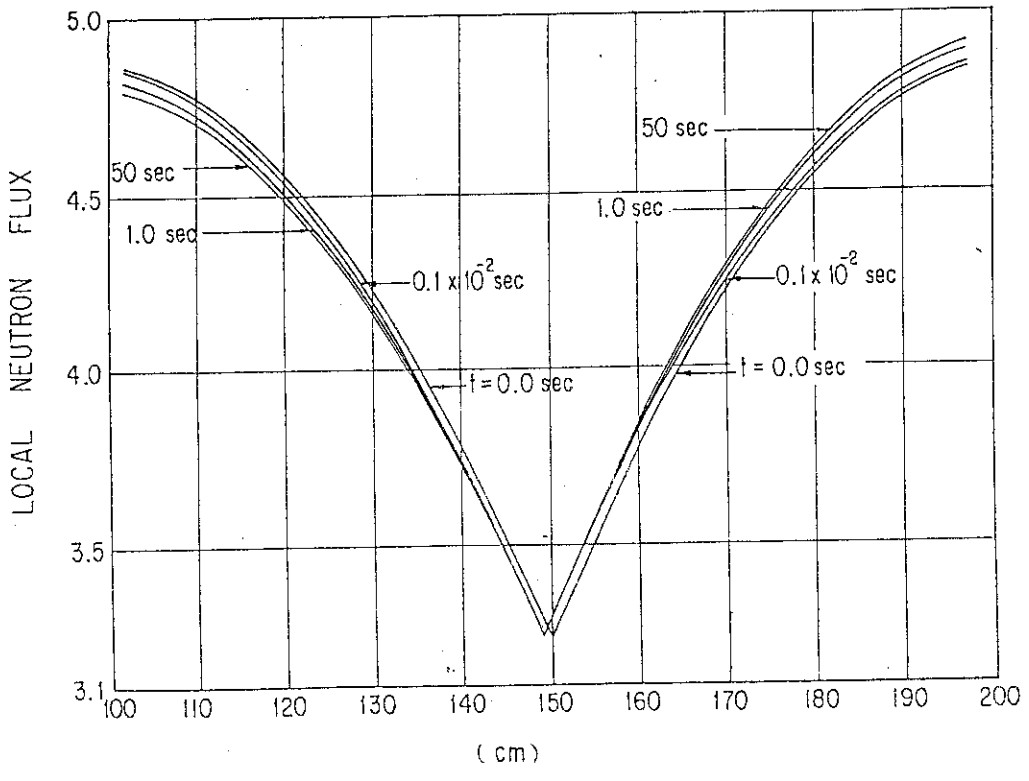

Fig. 2.12.2 Time response of flux dip around absorber plate displaced from the center, 150 cm, to 149 cm

2.13 Conceptual Design Study on Actinide Burning Fast Reactor

T. Osugi, H. Yoshida and R. Tanaka*

A conceptual design study on 850 MWt helium-cooled ABFR (He-ABFR) has been made, since helium cooling provides much harder neutron spectrum than sodium cooling and hence permits the more efficient transmutation of waste actinides because of higher fission to capture ratio.

An extensive parametric study on the He-ABFR has been made to minimize the initial inventory of actinides under the following thermo-hydraulic constraints; (1) the nominal peak fuel temperature be lower than 1950°C, (2) the nominal peak cladding temperature be lower than 650°C, (3) the maximum coolant velocity be lower than 100 m/sec and (4) the pressure drop between upper and lower plenums be lower than 3.0 kg/cm^2.

The He-ABFR plant is similar to the helium-cooled PuO_2-UO_2 fueled fast reactor plant designed so far[1] as seen in Fig. 2.13.1. The equivalent diameter and active height of the reactor core are 244 cm and 100 cm respectively. The fuel of the He-ABR is the waste actinide mixed oxide and magnesium oxide is blended as a diluent material as recommended by E. Zamorani, et al.[2] The helium coolant, at a pressure of 80 atm, flows upward through the core, as is the case of all the gas-cooled fast reactor designs, and is heated up to 500°C from 250°C.

The reactor core performances of the He-ABFR have been evaluated using the currently available neutron cross-section data and material data of actinides, although these data have significantly large uncertainties at present. Detailed neutronic calculations have been carried out using the three dimensional diffusion-burnup code BURN3D[3] coupled with so-called Bateman's formula[4] which is able to treat decay chains of many kinds of actinide nuclides. A set of 25 group cross-sections has also been generated for the neutronic calculations from the JAERI-Fast cross section set V-2[5], and ENDF/B-IV and V.

Thermo-hydraulic calculations have been made in detail, using the

---

* Kawasaki Heavy Industry Ltd.

multichannel thermo-hydraulic analysis code MR.X[6] which is developed for the helium-cooled fast reactor designing, combined with three dimensional power distributions calculated by BURN3D.

The detailed calculation confirms that the total amount of annually transmuted actinides is 265 kg/yr. Fig. 2.13.2 shows irradiation time dependence of alpha-activities from the total actinides and from the actinides with half-lives of more than 1000 years, and of beta-activities from ^{241}Pu. Alpha-activities from the total actinides reach the maximum in one year irradiation and then monotonously decrease with irradiation time. The slight increase during initial irradiation period is mainly due to build up of ^{242}Cm through neutron capture of ^{241}Am. ^{242}Cm with short half-life of 163 days is the dominant nuclide in the total alpha-activities during the whole period considered, and its contribution is 94.5% at the beginning of irradiation and 68.5% after 15 years irradiation. As far as the transmutation of extremely long-lived actinides is concerned alpha-activities monotonously decrease during the irradiation and 60% reduction of the activities from the initial activities is achieved by 15 years irradiation in the 850 MWt He-ABFR.

The neutronic and thermo-hydraulic investigations indicate the feasibility of He-ABFR to transmute the waste actinides.

References

1) Chermanne J., Simon R., Scoville J.: "GCFR Development Status and Introduction," OECD/NEA GCFR Coordinating Group Report (1981)
2) Zamorani E., et al.: European Appl. Res. Rept-Nucl. Sci. Technol. 2 (1980) 681-812
3) Osugi T.: to be published
4) Tasaka K.: "Dchain: Code for Analysis of Build-up and Decay of Nuclides," JAERI 1250 (1977)
5) Takano H., et al.: "JAERI Fast Reactor Group Constants Set, Version-II," JAERI 1255 (1978)
6) Kobayashi K., et al.: "A Thermo-Hydraulics-Nutronics Code Mr. X for Gas-Cooled Fast Reactors," Proc. of GCFR Specialist Meeting (Brussele, 1979)

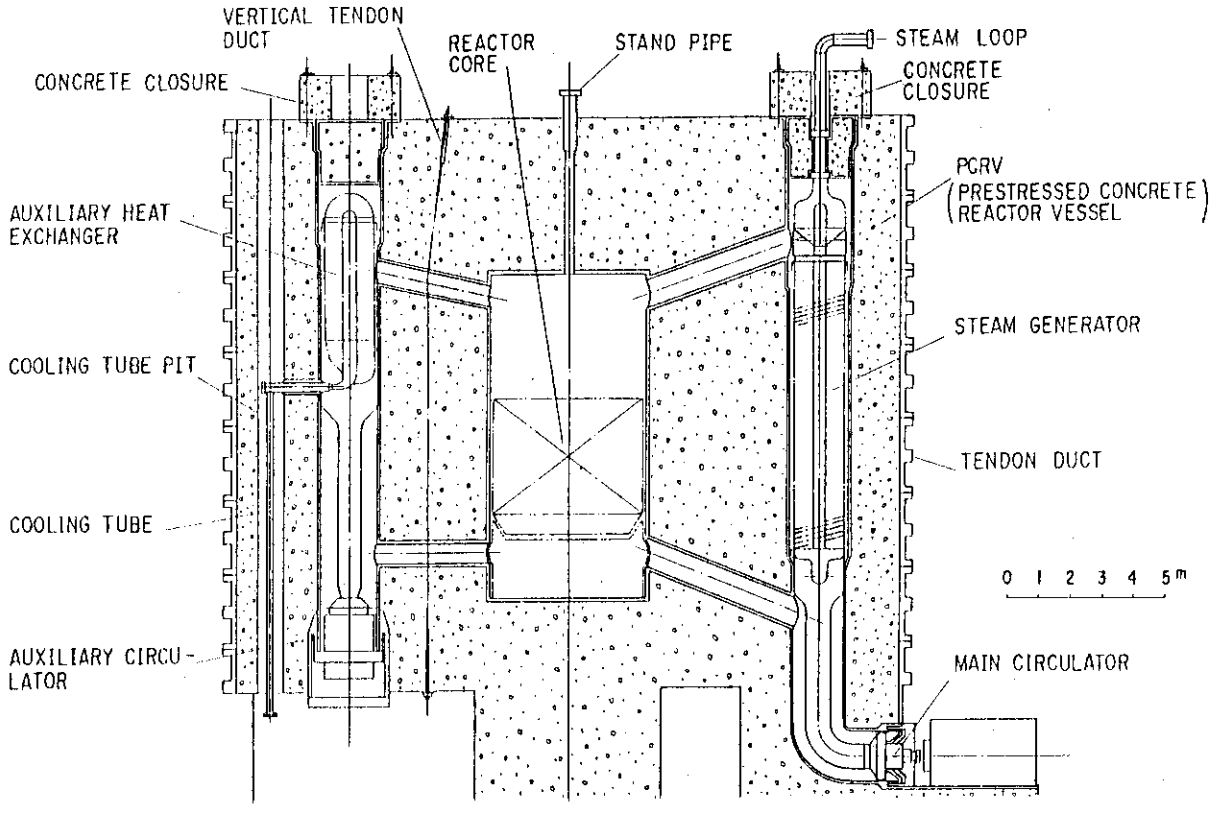

Fig. 2.13.1 Reactor elevation of 850 MWt ABFR

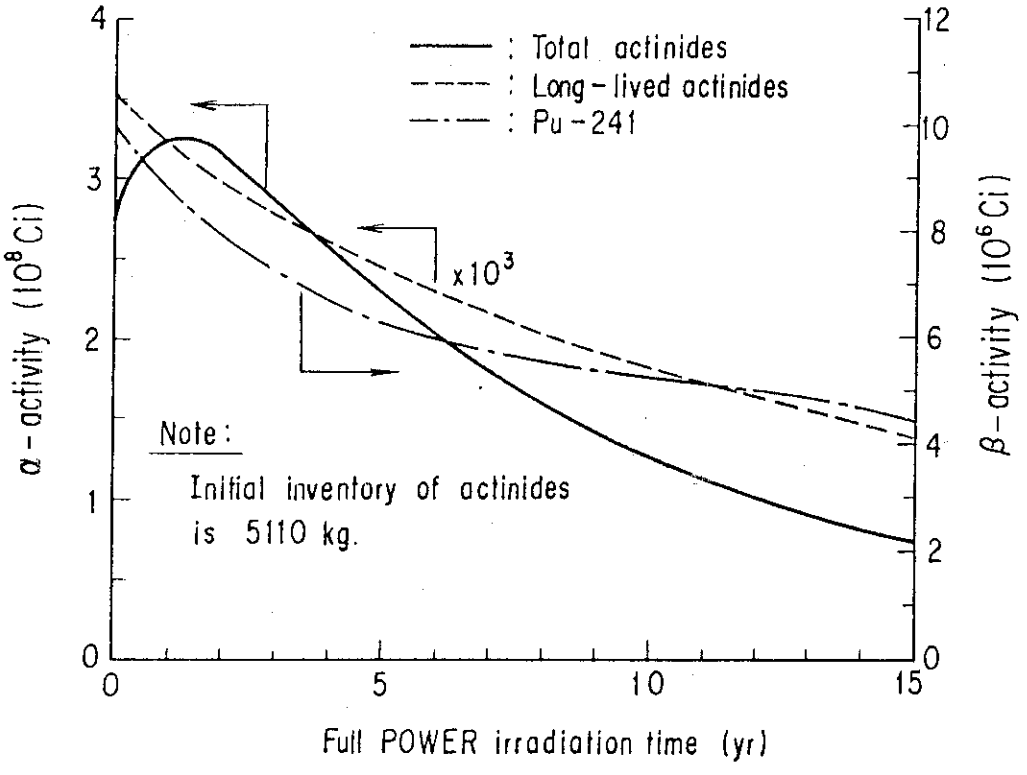

Fig. 2.13.2 Irradiation dependence on alpha-activities of all of the actinides and of extremely long-lived actinides and on beta-activity of Pu-241, in 850 MWt He-ABFR

2.14 A Strategic Investigation on the GCFR-VHTR Symbiotic Energy System and a Design of Gas-Cooled Fast Breeder Reactor

S. Iijima, H. Yoshida and R. Tanaka*

A symbiotic energy system between a gas-cooled fast breeder reactor (GCFR) and a very high temperature reactor (VHTR) appears to be promising as an energy production system self-sufficient in fuel. A strategic investigation on the GCFR-VHTR symbiotic energy system has been performed on the basis of a presumption of relatively moderate growth forecast in nuclear energy demand in Japan for the period 1977-2076. This investigation has been made from the view point of assuring the nuclear energy supply and reducing the amount of uranium ore consumption.

The GCFR, which has been designed in the course of the study, has excellent breeding performance and produces enough fuels for VHTR and GCFR itself. The nuclear and thermo-hydrauric characteristics evaluations and transient analyses have been made in the design of GCFR.

The VHTR used in the investigation has reactor characteristics and nuclear performance similar to ^{233}U-Th fuelled HTGR with improved conversion ratio.

Symbiotic Energy System[1)]

The symbiotic energy system, which is shown in Fig. 2.14.1, is constructed with one 1000 MW (Electric power) GCFR and two 3000 MW (thermal power) VHTRs. Plutonium and uranium mixed oxid fuels are used in the core and the axial blanket of GCFR. Thorium fuel is loaded in the radial blanket of GCFR and ^{233}U is produced in the radial blanket. ^{233}U fuel from the radial blanket is utilized as the VHTR's fuel. VHTR generates both electricity and thermal energy for process heat.

Design of GCFR[2),3),4)]

Fundamental nuclear characteristics were evaluated on breeding performances and reactivity effects of the reference GCFR. The reactivity effects discussed in this design are, (1) reactivity worth for the fuel and structure materials, (2) Doppler reactivity worth, (3) fuel

* Kawakaki Heavy Industries, Ltd.

expansion, (4) helium coolant loss, (5) reactivity requirements for the control rod system, (6) steam entry reactivity worths and (7) kinetic parameters.

Thermo-hydraulic characteristics were evaluated based on the results of nuclear characteristic calculations. The thermo-hydraulic calculations were made taking account of the power distribution distortion caused by control rods insertion in the core at the beginning of the equilibrium cycle (BOEC). The hot spot temperature and maximum fuel and cladding temperature were calculated at BOEC.

The safety performance were evaluated by analyzing two typical transient phenomenon of GCFR. The transient phenomenon discussed in this design are, (1) coolant depressurization accident and (2) reactivity insertion accident.

Conclusion

1000 MW GCFR has been designed as the standard fast breeder reactor on the GCFR-VHTR symbiotic energy system. It was clear that the GCFR had excellent breeding performance and that hot spot temperature and maximum fuel and cladding temperature could satisfy their design constrains. And it was shown from the transient analyses that cold shutdown could be achieved well before leading to core damage or severe fuel and cladding failures.

In the strategic investigations, it was shown that the GCFR-VHTR symbiotic energy system based on the uranium-thorium mixed fuel cycle could assure the nuclear energy supply in Japan for 100 years and could reduce the amount of uranium ore consumption.

References

1) Yoshida H., et al.: "Evaluation of Symbiotic Energy System between Gas-Cooled Fast Breeder Reactor (GCFR) and Multi-Purpose Very High Temperature Reactor (VHTR) (I) - An Investigation GCFR concept -," JAERI-M 9544 (1981).
2) Iijima S., et al.: "Evaluation of Symbiotic Energy System between Gas-Cooled Fast Breeder Reactor (GCFR) and Multi-Purpose Very High Temperature Reactor (VHTR) (II) - Nuclear Characteristics of Reference GCFR Core -," JAERI-M 82-182 (1982)
3) Yoshida H., et al.: "Evaluation of Symbiotic Energy System between

Gas-Cooled Fast Breeder Reactor (GCFR) and Multi-Purpose Very High Temperature Reactor (VHTR) (III) - Reference GCFR Core Configuration and it's Thermo-hydraulic Characteristics -," JAERI-M 82-183 (1982).

4) Iijima S., et al.: "Evaluation of Symbiotic Energy System between Gas-Cooled Fast Breeder Reactor (GCFR) and Multi-Purpose Very High Temperature Reactor (VHTR) (IV) - GCFR Trangient Analysis and Safety Performance Evaluation -," JAERI-M 82-184 (1982).

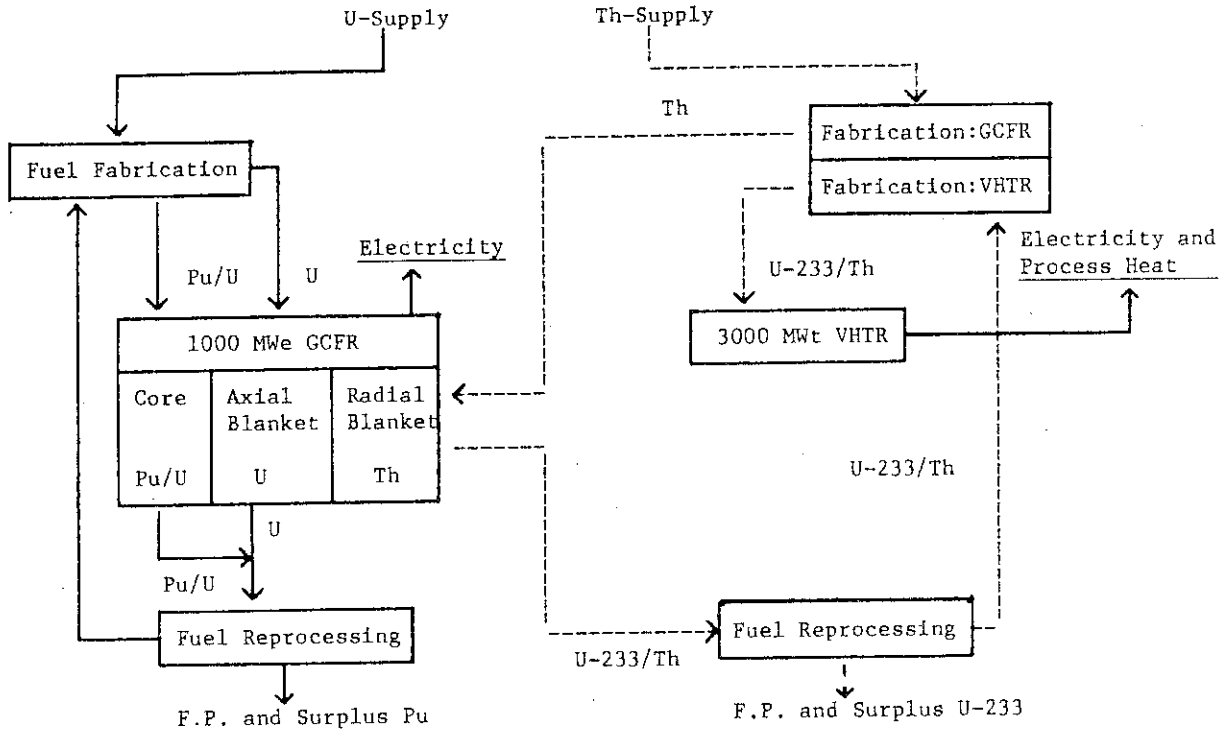

Fig.2.14.1 Schematic diagram of fuel flow in the symbiotic energy system

2.15 Development of a General Purpose Line Plotting Code : GPLP

H. Ihara

A general purpose line plotting code GPLP[1] has been developed so as to satisfy the need of plotting calculated values and measured values together with their confidence intervals in an arbitrary scale on a sheet in a way of multiple plotting in order to evaluate the results of analytical calculations or to prepare a report. GPLP has various functions and characteristics in response to the users' requests, that is:

a) With regard to the data input for plotting
 (1) a function to process the file on which time-dependent data are stored.
 (2) a function to process the file on which static data are stored.
 (3) a function to process the input by cards with free format.
 (4) a function to process the input data given in a mathematical formula with one variable on one card.
 (5) input data can be read in from any logical unit.
 (6) a function to divide a set of input data by another set of data, if so designated by input, for plotting C/E values for example.
 (7) a function to modify the input data by changing their scale factor or multiplying them with the variable on which they depend, e.g., time t.

b) With regard to the display of a figure
 (1) a function to enlarge, reduce, rotate and transfer a figure as a whole or to enlarge and reduce the figure with regard to the coordinates x or y.
 (2) a function to arrange many figures on one sheet.
 (3) a function to handle multiple lines in one figure and, if desired, to display each line separately as a different figure on the same sheet with changing the scale factor of x and y axes.
 (4) a function to smooth the curve by the use of the third order spline interpolation technique or the parabolic blending method.
 (5) a function to display the data stepwise.
 (6) a function to plot the error bars in a scale of relative or absolute values.
 (7) a linear or a logarithmic scaling can be applied to the indication of x and y axes with the scaling values of round number which increase the visibility of the figure.

(8) display of the mesh on the figure is optional, i.e., coarse mesh, fine mesh or no mesh with additional option to the scaling chicks, i.e., some chicks or no chicks, except for the case of fine mesh in which no chicks are plotted.

(9) any size of the characters can be selected to the titles for vertical axis, horizontal axis and the figure itself, to the comments and to the values for scaling.

(10) thickness of a line in the figure, including a character of the title, a lattice and a symbol, can be selected in case of NLP and COM, and its colour is optional in case of Plotter and D-SCAN.

(11) comments can be put into any places in the figure with masking other lines.

c) With regard to the programming techniques

(1) any variables used in the code have variable dimensions and quite a lot of data can be plotted only by properly selecting the memory option in JCL (C.n in FACOM).

(2) the logical unit, from which the data are read in for plotting, is designated by input and a number of data files can be handled at one run.

(3) if the same type of figures should be produced repeatedly, only the different data can be supplied as an input from the second case afterwards.

Major graphic patterns which can be generated by the GPLP programme are shown in Fig. 2.15.1.

Reference

1) Ihara H.: "GPLP: General Purpose Line Plotting Programme," JAERI-M 82-197 (1982) (in Japanese).

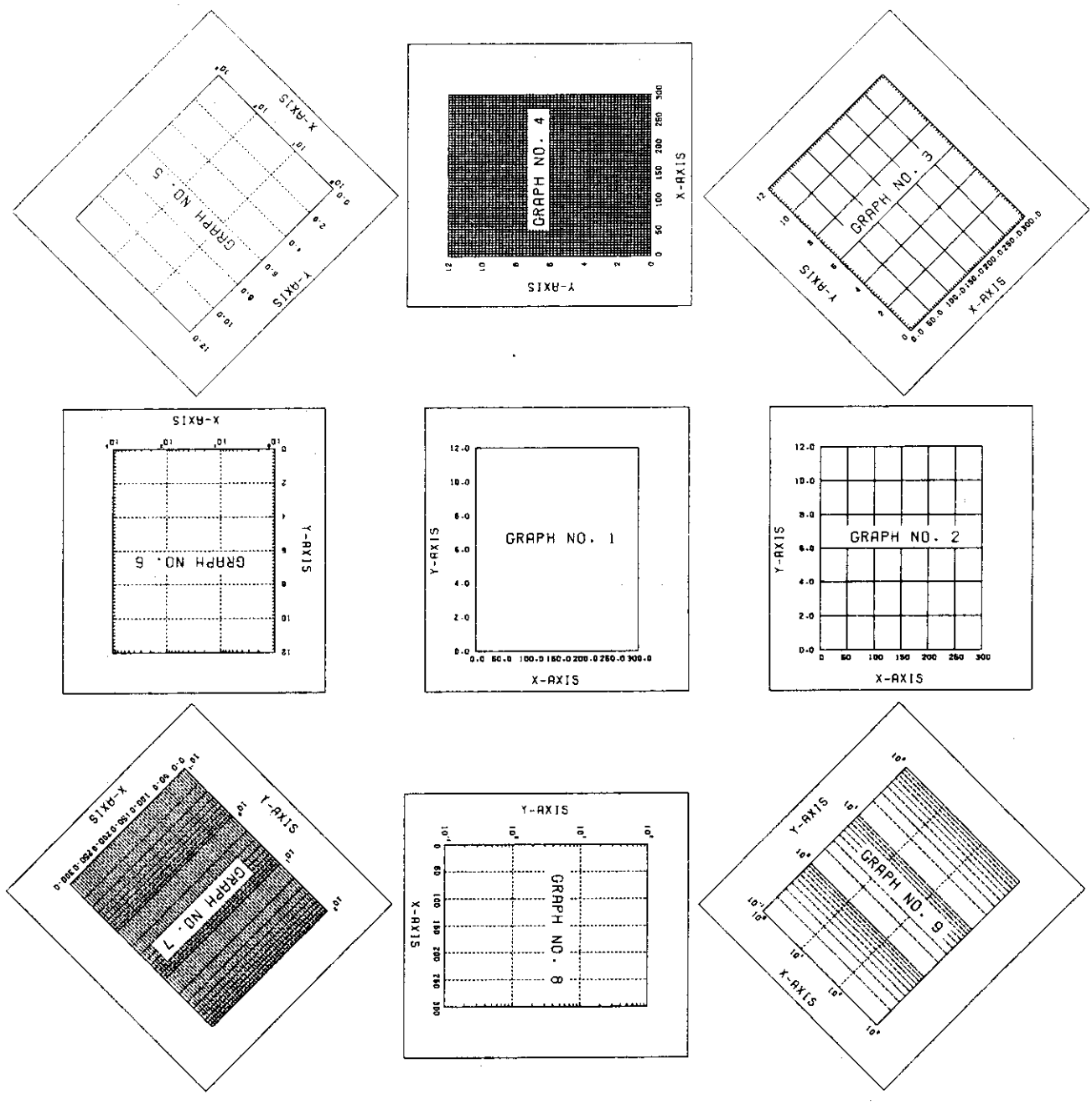

Fig. 2.15.1 Major graphic patterns which can be generated by GPLP programme

2.16 Development of a General Purpose Flow Diagram Processing Code : GPF2

H. Ihara, N. Nirazuka*, K. Ikawa and H. Nishimura

Preparation of input data is one of the most problematic areas for the process of a diagram if a usual line plotting code is used. For example, the drawing of a building or a system diagram requires quite a lot of information as an input and these data have to be modified if a part of the drawing should be changed or some should be added to the original one. Since supplying or changing the data are to be done by hand, it results in a low efficiency of work because of a lot of time consumed. Another problem is how to control these drawings or diagrams. If a diagram is stored in a form of input data, a lot of disk capacity is needed as well as the processing code should be run for the display of the diagram each time. The code GPF2 has been developed for solving these problems as a general purpose diagram processing code.

In this code, it is supposed that a colour graphic display, D-SCAN, and a laser printer for the Japanese language, NLP, are used as the output devices, and a keyboard and a tablet are used as the input devices. Essential features of these devices for displaying diagrams are as follows:
(1) D-SCAN uses the raster scanning method of the reflesh type, and its effective figure display surface is 275 mm x 275 mm, the number of rasters on this surface is 1024, the number of controllable colours for display is 7, the display speed is 400 ns/pixel and the segment buffer is 32 KBytes. Using D-SCAN, a circle, arc, rectangle and a polygon can be generated, the segments are controllable, a fundamental transformation of the coordinates (enlargement, reduction, rotation and parallel transfer) can be performed, a window viewport are changed from place to place with the clipping function, a hatching and a painting are made, and the figure can be drawn in an interactive manner using the firmware[1].
(2) The tablet has a range of effective readout of 380 mm x 380 mm, an accuracy of readout of 0.1 mm, and a stylus pen for input.

A schematic description of GPF2 system is given in Fig. 2.16.3. For the use of this system, a rough sketch of a building or a system diagram, etc., should be prepared beforehand. Then this sketch is to be put on the tablet, the coordinates are to be read in using the stylus pen, and the figure is to be completed in an interactive manner with the computer.

* ISL Co. Ltd.

GPF2 stores the fundamental figures, which can be retrieved and used for drawing by the segment control function of D-SCAN. With one of these figures called, the figure can be set up at an arbitrary position in any scale with a rotation of given angle using the coordinates transformation function. It is possible to write the data, which are obtained from various computer codes as an output, into the fundamental figure in displaying the result. The figure displayed on the screen can be stored on a disk of the host computer (FACOM-M-380) as a data set in the command level[2] using the data transformation programme of GPF2, which makes it possible to directly transfer the figure to D-SCAN without use of a diagram processing code. Correction of a figure can be done in a similar manner. The figure is called from the figure data pool on the disk, displayed on the CRT, and changed in an interactive manner using the tablet.

Such procedure results in a speedup of drawing and makes it possible to reduce the processing time of the host computer as well as the time of work itself, and using these functions, it has become much easier to make a layout of a building or to draw a system flow diagram for a simulation study. The figure produced by this code can be used to rapidly draft a report and efficiently analyze the result of a simulation for its evaluation.

Examples of the output from GPF2 are shown in Figs. 2.16.1 and 2.16.2.

References

1) "Explanation on Software package for D-SCAN : GCSP-II," DaiNiSeikousha Co. (in Japanese).

2) "Explanation on Commands used in D-SCAN," DaiNiSeikousha Co. (in Japanese).

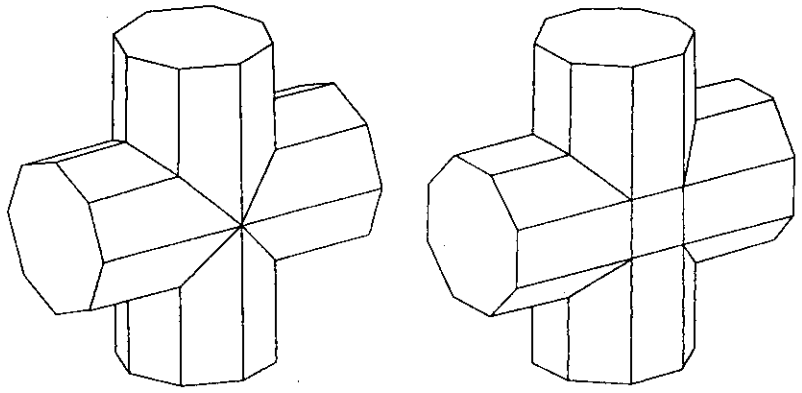

2.16.1 An output example of graphs generated by GPF2

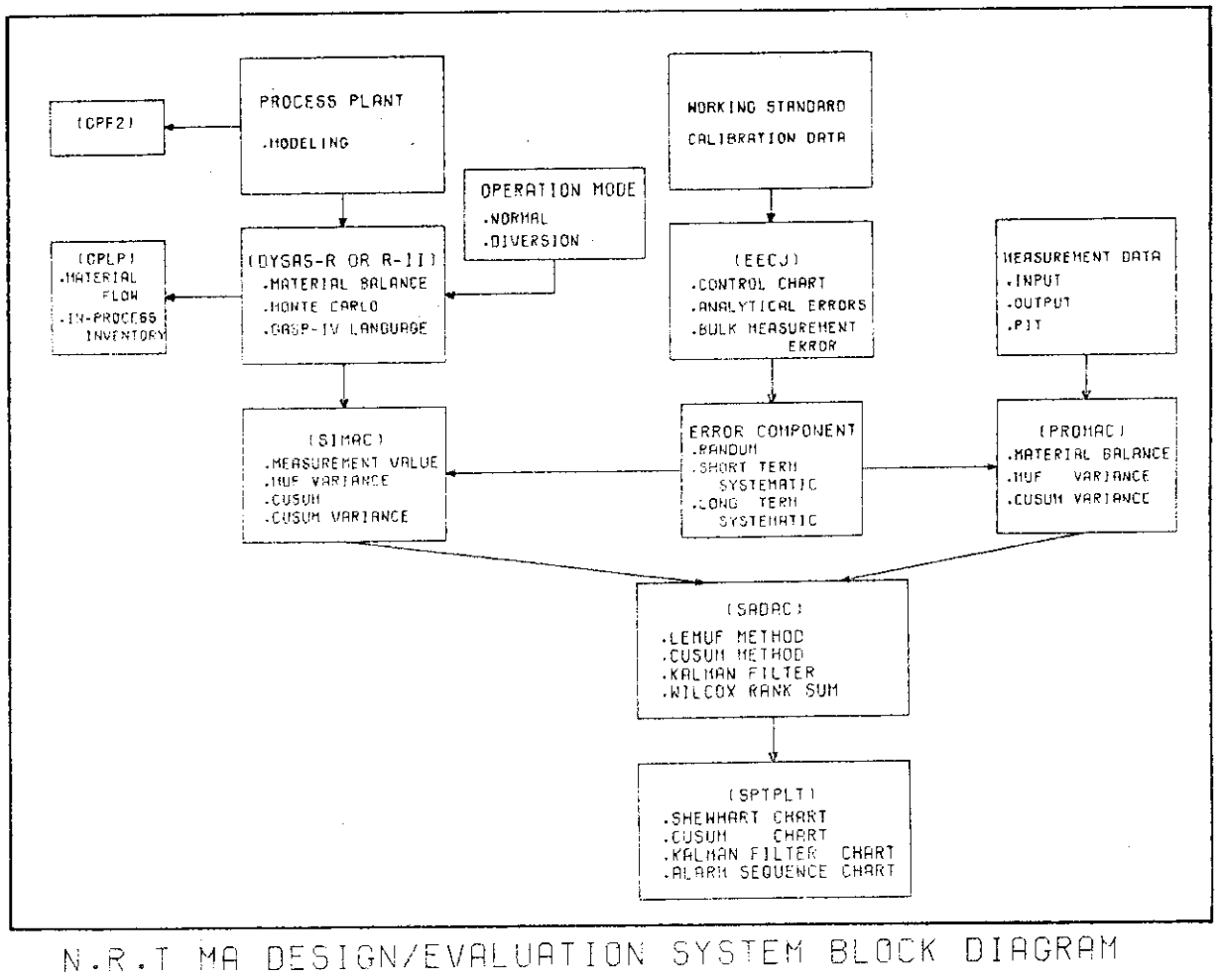

N.R.T MA DESIGN/EVALUATION SYSTEM BLOCK DIAGRAM

2.16.2 Another output example of graphs generated by GPF2

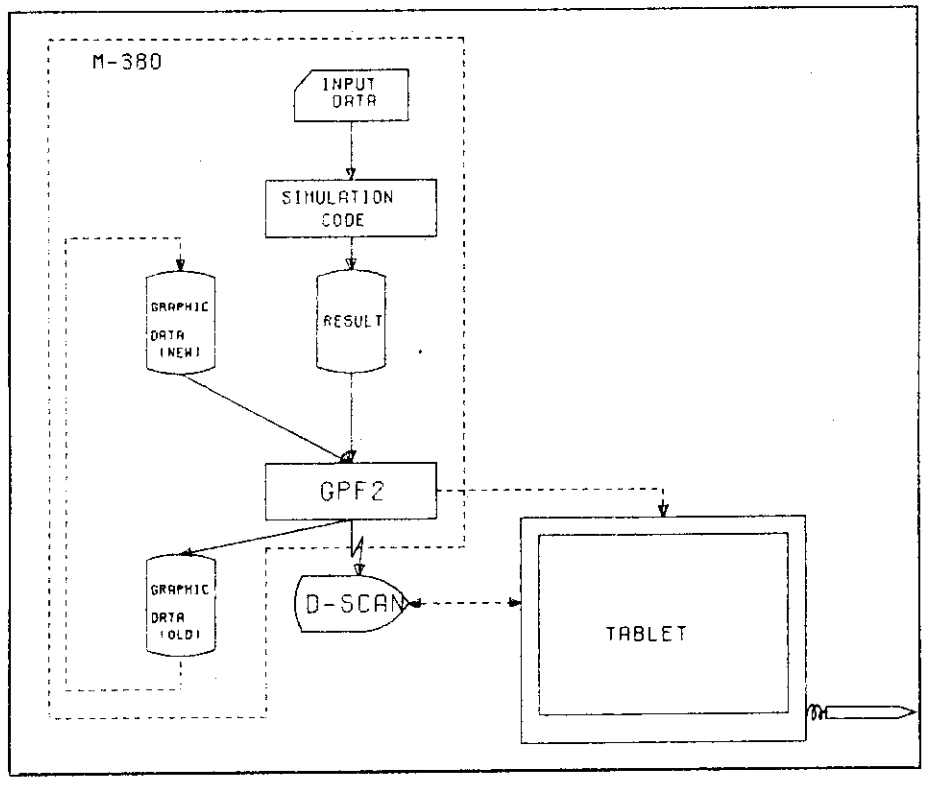

2.16.3 GPF2 system diagram

2.17 Development of the JAERI Scientific Subroutine Library (JSSL)

S. Inoue, T. Fujimura, T. Tsutsui and T. Nishida

The manual for JSSL has been revised[1]. Many subroutines have been added to the library and some ones have been deleted during the conversion for the system FACOM M200 or M380. The main progress in this version is in the fields of mathematical programming and statistical functions which were vacant. The library is now a comprehensive compilation of scientific subroutines covering almost all the important fields. The extention of the library is described respectively in the following categories.

(A) Mathematical Programming

Forty subroutines for optimizing the objective functions under some conditional functions are supplied;

1. Five fundamental programs of the linear programming method, one program based on the decomposition principle and two of the quadratic programming method.
2. Thirty two subroutines of the nonlinear programming method.

(B) Statistical Functions

Fifteen subroutines for upper side probability or percentile of main probability distributions such as Normal, Chi-square, F, t, Beta, Noncentral Chi-square, Noncentral F, Noncentral t distribution and three related special functions are supplied. The mixed logarithmic normal distribution is also added.

(C) Plotter Routines

A new plotter subroutine package UPLOT is supplied with capacities; i) permission to use two different pairs of axes on a same plane, ii) function of automatic scaling, and iii) permission to use many parameters easily. The package consists of 14 subroutines.

References

1) Inoue, S., et al.: "Manual for JSSL (JAERI Scientific Subroutine Library), (3rd Edition)," JAERI-M 82-095 (1982) (in Japanese).

2.18 Extension of the Boltzmann Equation for Anisotropic Transport

Y. Taji

An extension of the neutron transport equation has been already proposed[1] from the intuitive considerations as follows: By rewriting the integration with respect to the directional variables as $\int dE' \int d\Omega' f(,E',\Omega') \sum_s (\Omega' \cdot \Omega, E' \to E) = \int dE' \int d(\Omega' \cdot \Omega) \int d\psi f(,E',\Omega' \cdot \Omega, \psi) \sum_s (\Omega' \cdot \Omega, E' \to E)$ (ψ denotes the azimuth around Ω.) It is seen that the anisotropy in f decays out within a mean free time (or path) because the scattering law in $\sum_s$ is defined as a function of only $\Omega' \cdot \Omega$. Then an average force field has been introduced in the transport equation for the absolute direction to be conserved. Through some preliminary analyses taking account of the average force field, the differences found between conventional analyses and experiments have been explained in quality. However, the force field has been needed to be proved from the first principle of the Liouville equation. We have then found that the absolute direction is already ambiguous in the definition of the closed system, from which the Liouville equation is derived. Then we have developed a kinetic theory for open subsystems.

A closed self-consistent kinetic equation for open subsystems is derived in the place of the Liouville equation for closed systems, from which an extended Boltzmann equation for dealing with anisotropic transport is derived. The present theory starts from the open subsystems directly which are assumed at first to be isolated from the mother systems. The distinction of the isolated subsystem from the closed system is that coordinates of center-of-mass appear explicitly to determine the absolute motion of subsystems. The absolute motion to be wrapped in a time average becomes the condition for kinetic equation to be closed. This condition is also applicable to the subsystems interacting with the mother systems under the adiabatic condition. Under these conditions it is possible to apply the law of action and reaction to the interactions. Then the interactions are expressible as a self-consistent force field independent of characteristic of the mother systems so that the absolute motion wrapped is complemented.

Reference

1) Taji Y.: Phys. Soc. Jpn., 41, 2020 (1976); Proc. Fall Meet. of Phys. Soc. Jpn., 30PSB28 (1982).

3. Integral Experiment and Analysis

3.1 Critical Experiments on Enriched Uranium Graphite Moderated Cores Related to VHTR

F.Akino, K.Kitadate, M.Takeuchi, T.Ono, T.Yamane and Y.Kaneko

In a core design for the Experimental High-Temperature Gas Cooled Reactor (VHTR) progresses[1], evaluation of design precision has become increasingly important. For a high precision design, adequate group constants and a calculation method accurately describing transport of neutrons are required.

The VHTR is designed to accommodate burnable poison rods for reactivity compensation. Accordingly, experimental burnable poison rods equivalent to those designed for the experimental reactor core were prepared. Then, we assembled homogeneous loading core SHE-8 using a graphite-moderated 20% enriched uranium Semi-Homogeneous Experimental Critical Facility (SHE)[2], and obtained experimental data for reactivity worths of experimental burnable poison rods inserted into core center of SHE-8. The reactivity worths were measured by the period and fuel rod substitution methods.

The experimental burnable poison rods[3] were made by inserting 114 absorbing pellets in a hollow graphite rod of 1180 mm in length. The absorbing pellets with 8 mm diameter and 10 mm height were prepared by dispersing B_4C particles in graphite powder. Specifications of B_4C particle diameter and boron content are as follows;

B_4C particle diameter ; 3μm , 270μm , 560μm and 810μm
Boron content ; 2.25w/o, 4.5w/o and 9.0w/o

The result of measurement was shown in Fig.3.1.1. It is clearly shown that due to the self-shielding effect of B4C particles the reactivity worth decreases as the particle diameter increases. For each particle diameter, the reactivity worth is found to increase linearly with the logarithm of boron content.

Furthermore, we assembled the SHE-16 core with radial and end reflectors for the evaluation of a 3-dimensional calculation method. Following experimental data were obtained at SHE-16 core;

Critical mass in U-235,
Reactivity worths of experimental burnable poison rods,
Kinetic parameter (β eff/l),
Reactivity worths of experimental control rods.

Theoretical analysis for critical mass of SHE-16 was performed by the 3-dimensional 10 group diffusion theory, using SRAC code[4] system. Thermal groups were divided into 4 groups in the range from 0.0 to 1.1245eV and fast groups were divided into 6 groups in the range from 1.1245eV to 10MeV.

Agreement between experiment and calculation was within 1% for the effective multiplication factor. Calculation of reactivity worths of burnable poison rods and kinetic paramter is in progress using the SRAC code system.

References

1) Aochi T.,et al.: JAERI-M 6895(1976).
2) Kaneko Y.,et al.: JAERI-1257(1978).
3) Akino F.,et al.: JAERI-M 9223(1980).
4) Tsuchihashi K.,et al.: JAERI-1285(1983).

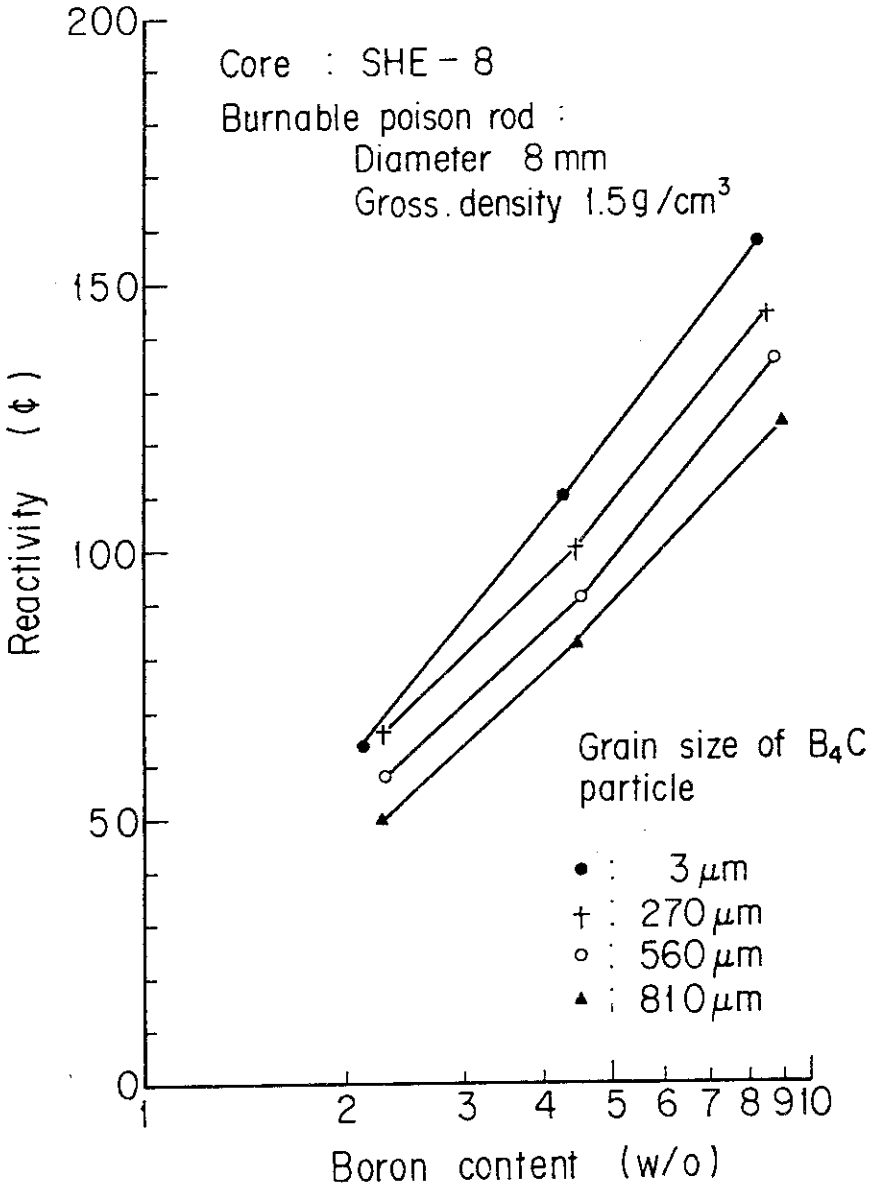

Fig.3.1.1 Measured values of reactivity worth of experimental burnable poison rods at core center in SHE-8 core

3.2 Reconstruction Program of SHE for Experimental VHTR

Y. Kaneko, F. Yoshihara, H. Yasuda, F. Akino, T. Yamane,
H. Yoshifuji, K. Kitadate. M. Takeuchi and T. Ono

Present status

Reconstruction program of SHE, Semi-Homogeneous Experimental Critical Facility, was approved by Japanese government early in 1981. The object of the program is to obtain experimental verification for the design accuracy of the Experimental VHTR fueled with low enriched uranium. Detailed reconstruction design of the SHE facility was accomplished as illustrated in Fig. 3.2.1. Safety examination by the government was completed in May 1983 after full deliberation on the following major aspects;

(1) Design basis accident
(2) Aseismic design
(3) Core heating by use of electric heaters

Then, reconstruction work was started.

Specification of reconstruction

Core geometry	: horizontal half machine type, hexagonal prism, in shape, height and length, 2.4m each.
Core lattice	: pin in block type like the Experimental VHTR.
Core temperature	: room temperature to 200°C throughout the whole core including the reflector, A single fuel rod will be heated up to 800°C.
Fuel	: 2,4 and 6w/o enriched uranium, 260kgU in total coated particle fuel compacts of the same size as the Experimental VHTR BISO or TRISO

Schedule

Reconstructed core will be made critical in 1985.

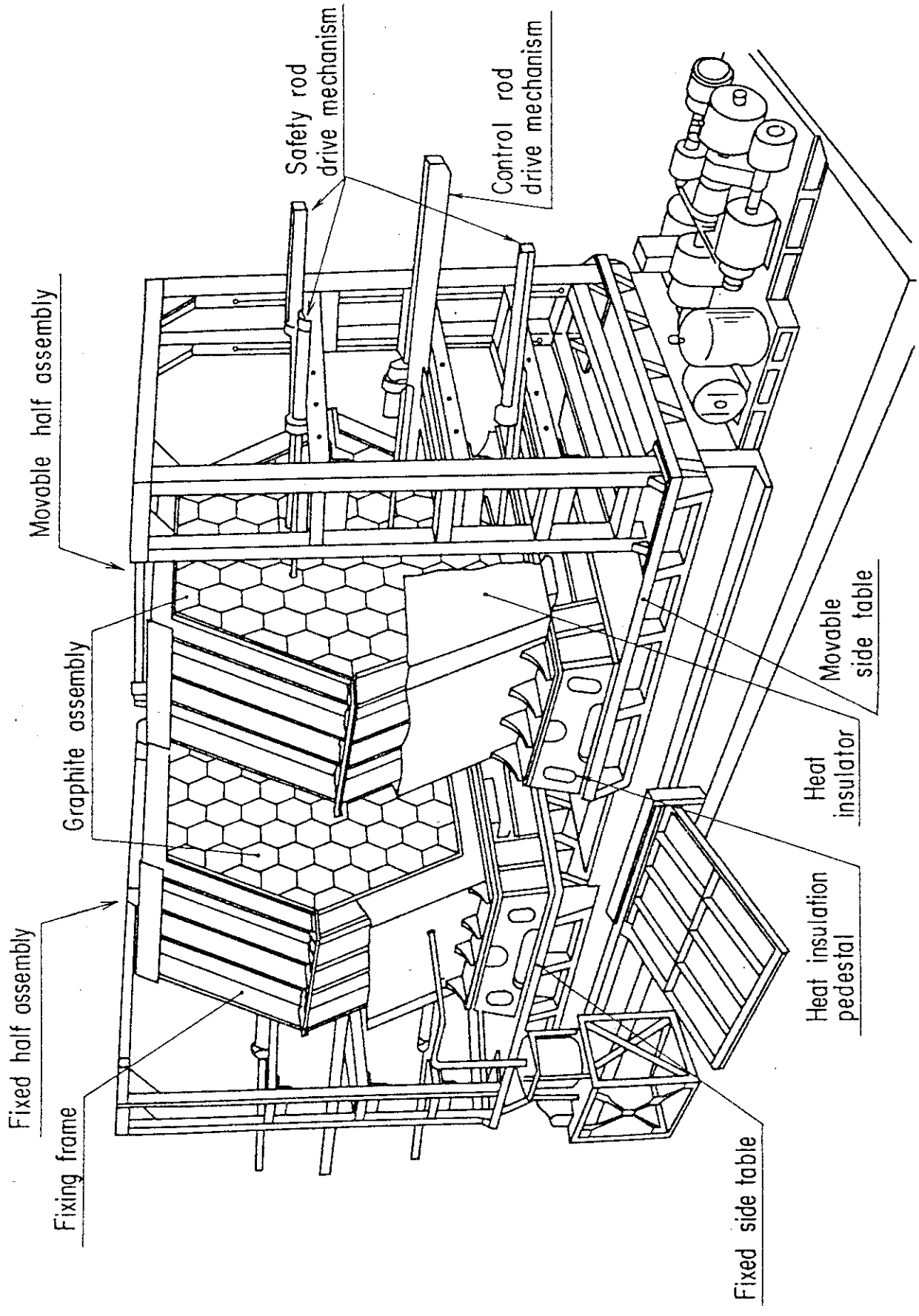

Fig. 3.2.1 Concept of reconstruction of SHE

3.3 Mockup Experiment of "JOYO" MK-II Core on FCA Assembly X

M. Nakano, T. Kawahara*, T. Koakutsu, M. Ōbu, S. Iijima,
T. Osugi and S. Okajima

Mockup experiments of the Fast Experimental Reactor "JOYO" MK-II core have been carried out on FCA Assembly X. In the conversion of "JOYO" to MK-II core, the following changes are made to increase neutron flux in the core:

- Increase of Pu content in fuel material,
- Replacement of the uranium blanket by the stainless steel reflector.

FCA X consists of three different versions of Assembly X-1, X-2 and X-3. The first two assemblies are clean cylindrical cores with no control rod positions, constructed for a physics mockup study. To clarify the effect of the stainless steel reflector, systematic experiments were made in the clean core with a uranium blanket (Assembly X-1) as well as that with a simulated reflector (Assembly X-2). The third assembly is an engineering mockup core of hexagonal cross section which includes six sodium channels simulating control rod positions in the core region. The plate arrangement of the core drawer used in Assembly X-2 and Assembly X-3 is shown in Fig. 3.3.1. The core composition was determined so that the atomic densities of Pu fissile, ^{235}U, ^{238}U and Na were close to those of the MK-II core. To allow axially symmetric loading into the FCA half assemblies, the core height of 50.8 cm (2" x 10) was selected instead of 55 cm of the MK-II core. The core region is followed by the axial reflector of about 35 cm thick.

The vertical cross section of Assembly X-2 is shown in Fig. 3.3.2. The cylindrical core of $L/D \simeq 1$ is surrounded by the reflector composed of stainless steel (SS) plates and Na plates of 1/4" thick. Due to the shortage of SS plates, stainless steel blocks were used in the outer region of the radial reflector of about 17 cm thick. Fissile material loaded in Assembly X-2 is about 100 kg of Pu fissile and about 44 kg of ^{235}U. Measurements were made for criticality, central fission rate ratios, fission rate distributions, sample reactivity worths and B_4C rod worths both in Assembly X-2 and in Assembly X-1.

---

* On leave from MAPI Inc.

The critical mass was decreased by about 3% from Assembly X-1 to Assembly X-2. No difference was observed in the central fission rate ratios of F28/F25, F37/F25 and F49/F25 between the two assemblies. It is observed, however, in the radial ^{239}Pu and ^{235}U fission rate distributions of Assembly X-2 that there is a valley near the core boundary and a peak in the reflector as shown in Fig. 3.3.3. The ratio of the maximum to the minimum ^{239}Pu fission rates in the core is about 1.7, which is compared with the ratio of about 2.2 in Assembly X-1.

In Assembly X-3, the reactivity worth of simulating B_4C rod and the distortion of neutron flux distribution due to insertion of a Na channel and the B_4C rods were studied mainly. Fission rate distributions were measured in the core with a central Na channel (5.5 cm square) and that with three B_4C rods (about 10 cm insertion into the core). At the center of the Na channel, the depressions of about 11% and about 5% were observed for ^{237}Np and ^{239}Pu fission rates, respectively, but there was no significant effect beyond the radius of 15 cm in the radial distributions.

The present work was performed under the contract between Power Reactor and Nuclear Fuel Development Corporation and Japan Atomic Energy Research Institute. The analysis is under way using the JFS-3-J2 group constants.

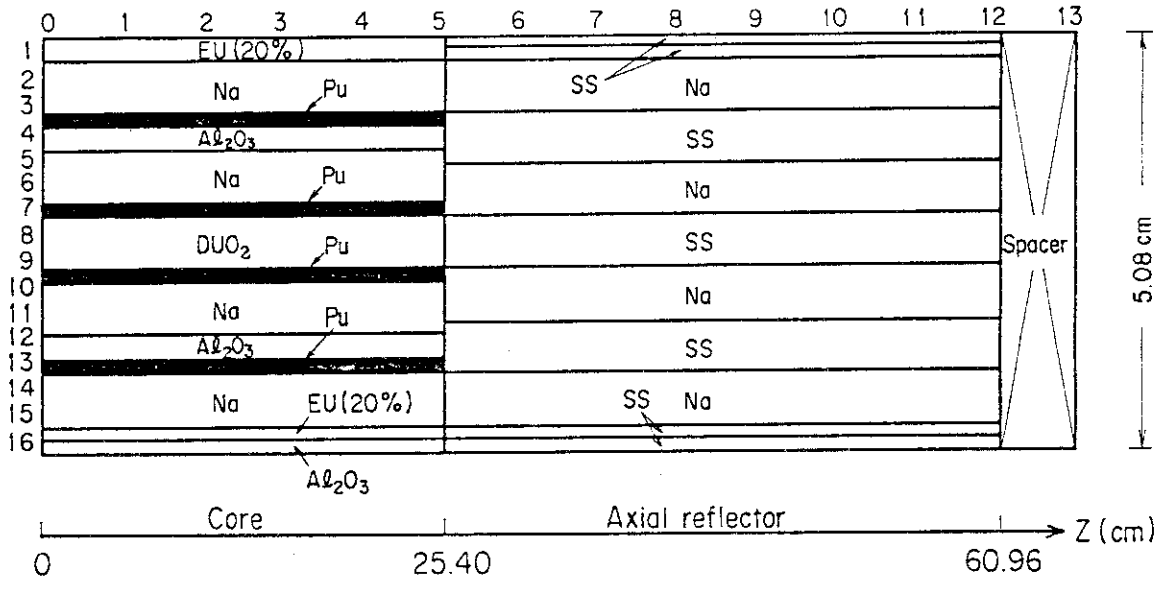

Fig.3.3.1 Core drawer pattern of FCA Assembly X-2

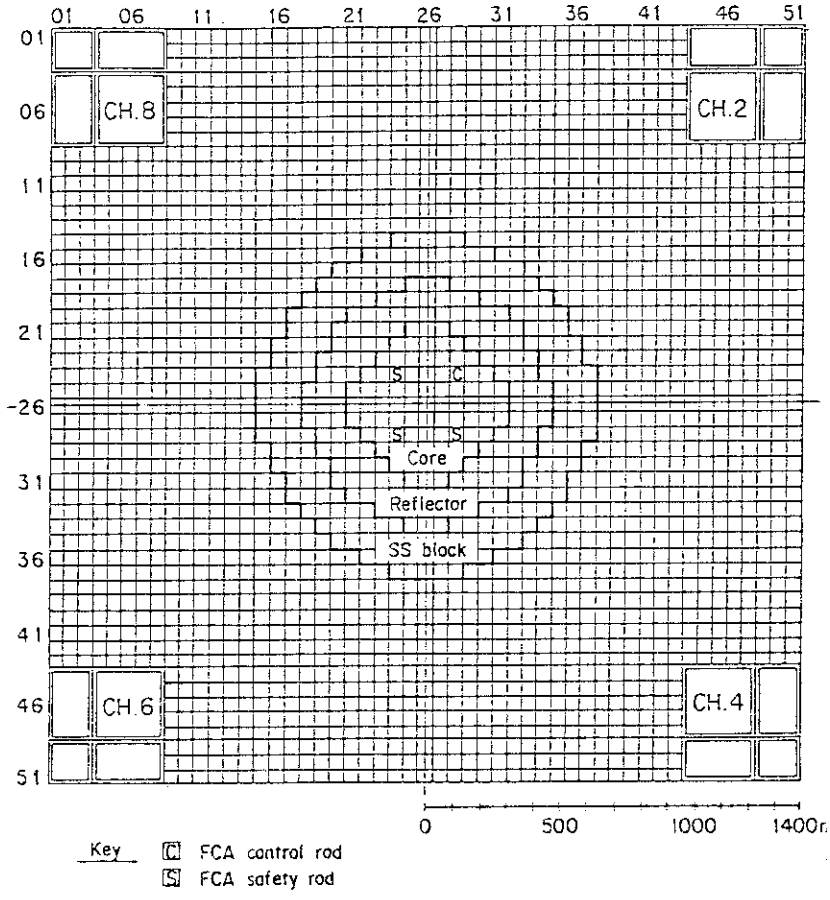

Fig.3.3.2 Vertical cross section of FCA assembly X-2

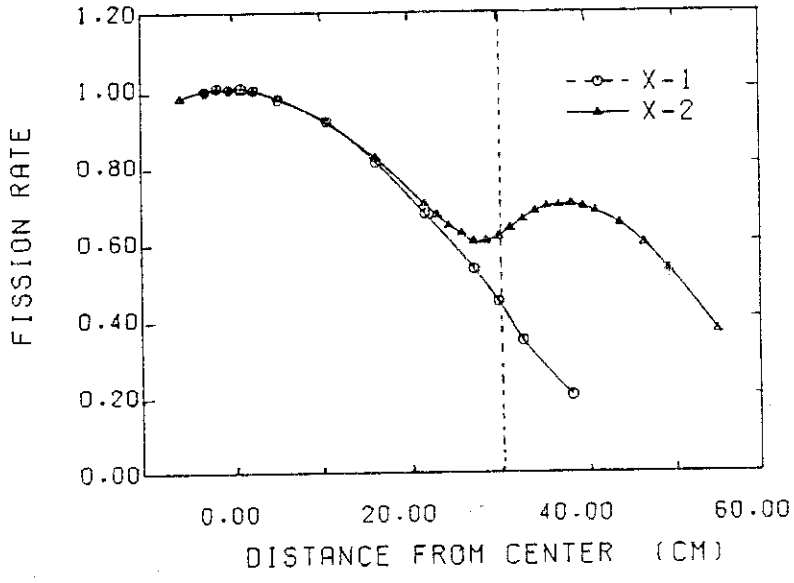

Fig.3.3.3 Radial ^{239}Pu fission rate distributions in Assembly X-1 and Assembly X-2

3.4 Measurement of Gamma-Ray Heating by the Use of TLDs at FCA Assembly X-2

S. Okajima and T. Osugi

Reliable data on gamma-ray heating is one of the important requirements from fast reactor design and engineering viewpoints. The TLD technique provides detailed informations for this purpose.

The gamma-ray heating has been measured using several different types of TLD's at FCA Assembly X-2[1], consisting of the core and the surrounding stainless-steel reflector. Once the absorbed energy is quantitatively related to thermal energy, the gamma-ray heating may be represented by the absorbed dose. The absorbed dose of the concerned medium, such as the core and the reflector, was determined using the method proposed by Tanaka et al.[2]. According to the method, the absorbed dose of the concerned medium can be determined by simple interpolation or extrapolation procedure using measured ones for TLD's with different effective atomic numbers (Z_{eff}), since it can be obtained as a function of the medium dependent Z_{eff}'s which are 73.7 for the core, 22.5 for the reflector and 25.9 for the SS block in FCA Assembly X-2. For this purpose, three kinds of TLD's, ^{7}LiF (Z_{eff} = 7.2), $CaSO_4$ + ^{7}LiF (Z_{eff} = 12.7) and BaSO (Z_{eff} = 45.5), were used in this experiment.

The amount of thermoluminescence of each TLD due to radiation exposure was calibrated by a known ^{60}Co gamma-ray field in the air. Three TLD's of each kind were put into a stainless-steel capsule. This capsule was mounted in each drawer, illustrated in Fig. 3.4.1 and was irradiated for 1 hour at the power level of 0.5 W. The measured absorbed doses shown in Fig. 3.4.2 are represented in unit of erg per gram normalized to the measured fission rate of ^{237}Np at the core center and are determined within the accuracy of +50% and -30% in the core and within ±20% in the reflector and SS block regions.

The calculation was made using the RADHEAT-V3 code system[3]. The coupled 100-neutron and 20-gamma-ray group constants of each medium were generated by RADHEAT-V3 using the basic data. The radial distribution of gamma-ray absorbed dose was calculated by the one-dimensional discrete ordinate transport code ANISN-JR with the P_3-S_4 approximation in the cylindrical geometry. The calculated results are also shown in Fig.

3.4.2. The calculation predicts well the trends of the measured distributions, but underestimates them by 70% in the core and by 30 - 40% in the reflector.

From this experiment, two important things are pointed out in order to improve the accuracy of gamma-ray heating measurement. The first is that the development of new TLDs with larger Z_{eff} should be needed to determine the gamma-ray heating particularly in the core of fast reactors. The other is to evaluate the neutron-induced contribution to the thermoluminescent signal.

References

1) Nakano M., et al.: "Mockup Experiment of "JOYO" MK-II Core on FCA Assembly X," Section 3.3 in this report.
2) Tanaka S., Takeuchi K., Furuta Y.: Proceeding of the 1st ASTM-EURATOMS Symposium on Reactor Dosimetry, Petten (1975) 599.
3) Koyama K., et al.: "RADHEAT-V3," JAERI-M 7155 (1977).

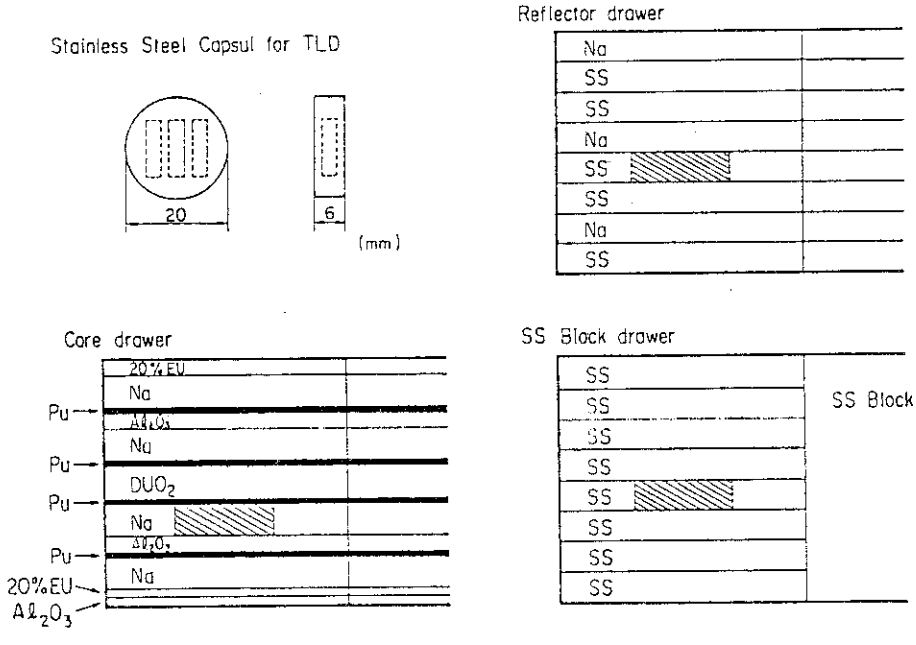

Fig.3.4.1 TLD setting position in the drawer

3.5 Doppler Reactivity Coefficient Measurements in FCA Assembly X-3

T. Mukaiyama and S. Okajima

Doppler reactivity coefficients were measured in the assembly X-3 on FCA for U-238, iron, nickel and stainless steel samples. For these measurements, the sample oscillation technique was used[1]. The dimension and weight of samples used were; (1) for natural uranium oxide (NUO_2) sample, 25,0 mmϕ or 20.0 mmϕ x 150 mmL, uranium weight 686 g or 427 g, respectively, (2) for Fe sample, 25.7 mmϕ x 150 mmL, Fe weight 648 g, (3) for Ni sample, 26.1 mmϕ x 158 mmL, Ni weight 755 g and (4) for stainless steel sample, 26.2 mmϕ x 158 mmL, S.S. weight 688 g.

Doppler reactivity coefficient measurements at FCA had not been carried out since 1973. Therefore, it took a little while to set up the equipment for measurements. Several improvements were incorporated into the system of Doppler experiments. These are, 1) new system of dehumidification for cooling air and 2) microcomputor control of measurements.

A fine control rod was installed to measure the small reactivity change. The reactivity change per unit displacement of the fine control rod was about 0.003 ρ_o/mm (ρ_o = 0.0394 %Δk/k) which was about 1/7 of normal control rod.

Sample materials mentioned above are encapsulated into a stainless steel inner capsule which is connected to a vacuume system together with a heater, a thermocouple, a sample holder and a thermal shielding tube made of nickel and this inner capsule is placed into an outer capsule. The gap between the inner and the outer capsule is used for air flow to remove heat from the heated sample material.

The details of measurement procedures are described in the reference 1). The measurements were carried out at the room temperature, 550°C and 800°C and also during the sample cooling period from 800°C down to 300°C.

Results of measurements

After the correction of reactivity contribution other than from the sample material, the results of measurements are summarized in Fig. 3.5.1.

Comparison of Calculation and Measurement

The 70-group JFS-3-J2[2] data set was used for the calculation. The

effective cross sections of the Doppler sample material and of the plate-cell of the assembly X-3 were obtained using the collision-probability code SLAROM[3]. The fluxes were calculated using CITATION. The temperature coefficients were calculated by perturbation code combining above fluxes and sample effective cross sections.

The calculated Doppler reactivity coefficients are compared with the presently-measured values in Table 3.5.1. The quoted errors are 1 σ due to the uncertainty of control rod position. The uncertainty of sample temperature or other sources of error are presently not taken into account.

The change in size of NUO_2 sample from 25 ϕ to 20 ϕ gives the different tendency of changes in the Doppler reactivity coefficient between calculations and experiments. The weight ratio of 20 ϕ sample to 25 ϕ sample is 0.623. The ratios of the calculated Doppler coefficient for 20 ϕ sample to that for 25 ϕ sample are 0.606 for both temperature change (293 → 823 K and 293 → 1073 K). The ratios for experimental value are 0.650 and 0.674 for temperature change of 293 → 823 K and 293 → 1073 K, respectively. Further study is required to explain this discrepancy.

The good agreement between calculated and experimental values for Fe and S.S. samples is likely by chance.

Errors quoted reflect, as is mentioned before, only the uncertainties of control rod position and further study is under way to evaluate the experimental errors.

References

1) Yasuno T., Nakano M., Mukaiyama T., Iijima T. and Hirota J.: J. Nucl. Sci. & Technol., 7, 271 (1970).
2) Takano H. and Ishiguro Y.: "Production and Benchmark Tests of Fast Reactor Group Constant Set JFS-3-J2," JAERI-M 82-135 (1982).
3) Nakagawa M. and Tsuchihashi K.: "SLAROM, A code for calculation of a heterogeneous core in fast reactor," JAERI-M 5916 (1974).

Table 3.5.1 Comparison of calculated and experimental values of the Doppler Reactivity coefficient in the assembly X-3 on FCA

Sample	Temperature (K)	Reactivity change ($10^{-6}\Delta k/k$)		C/E
		Experimental	Calculated	
NUO_2 25φ	293 → 823	-7.02 ± 0.13*	-6.55	0.933
(686.3g)	293 → 1073	-8.57 ± 0.13	-8.24	0.961
NUO_2 20φ	293 → 823	-4.56 ± 0.15	-3.97	0.871
(427.4g)	293 → 1073	-5.78 ± 0.15	-4.99	0.863
Fe 25φ	293 → 823	—	—	—
(647.5g)	293 → 1073	-2.12 ± 0.13	-2.18	1.03
S.S. 25φ	293 → 823	-1.70 ± 0.17	-1.72	1.01
(667.5g)	293 → 1073	-2.11 ± 0.17	-2.24	1.06
NI 25φ	293 → 823	-2.84 ± 0.11	-3.35	1.18
(754.6g)	293 → 1073	-3.58 ± 0.12	-4.32	1.21

* Quoted error is 1σ and reflects only the error in control rod position

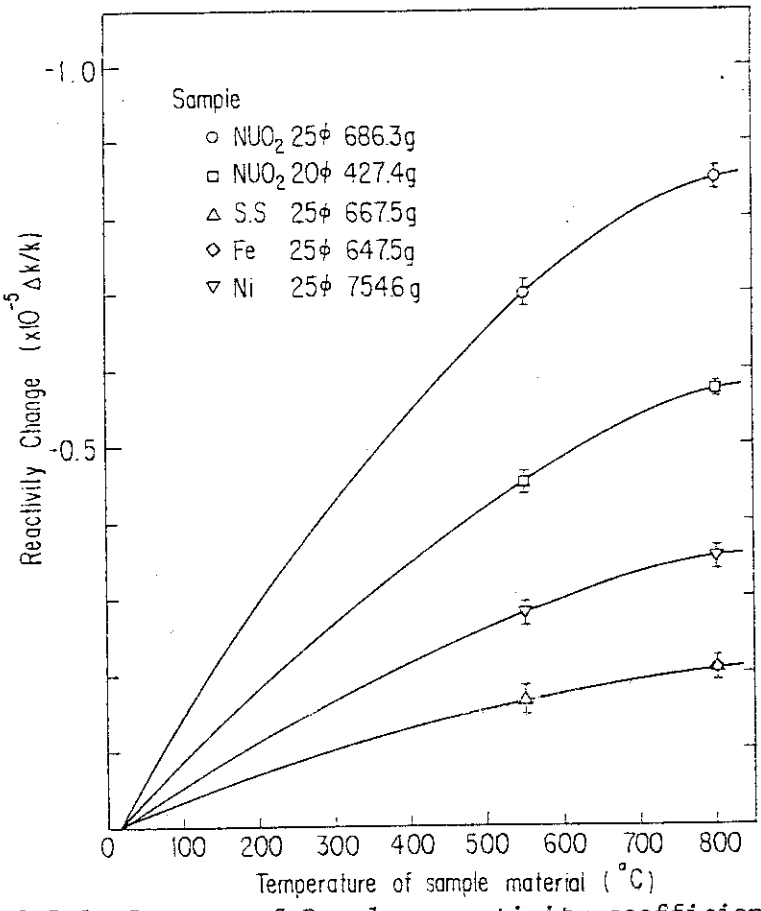

Fig. 3.5.1 Summary of Doppler reactivity coefficient measurements in the assembly X-3 on FCA

3.6 Analysis of ZPPR-9 and ZPPR-10A Experiments Using the JFS-3-J2 Cross Section Set

S. Iijima, H. Shukuya* and H. Yoshida

The JUPITER program was planned to provide integral data for conventional two-zone LMFBR cores in the 700 MWe to 900 MWe range in cooperation between Japan and the United States. The critical experiments were performed in ZPPR Assembly 9 and Assembly 10 at Argonne National Laboratory from 1978 to 1979.

The analysis of ZPPR-9 and -10A experiments have been performed using the JFS-3-J2 cross section set and the standard design calculation method of JAERI. The JFS-3-J2 cross section set was produced from the nuclear data compilation JENDL-2. Some advanced methods were adopted in the generation process of group constant in the JFS-3-J2 set. The one of advanced methods, called "REMO correction", is thought to have more influence than other things on nuclear calculations of a large scale LMFBR. The effects of the adopted REMO correction appears remarkably in the group constants for elastic removal.

The purpose of this study is to investigate the effects caused by the REMO correction on the analysis of the ZPPR-9 and -10A experiments. The effects were evaluated by comparing the results of JFS-3-J2 with those of the conventional group constant set produced from JENDL-2 using conventional generation process.

The analysis has been performed for the criticality, reaction rate distributions, reaction rate ratios, sodium void worth, sample worth, Doppler worth and B4C control rod worth.

Calculation Method

The calculation procedure are as follows:

(1) Cell averaged effective cross sections with 70-group energy structure were generated from the JFS-3-J2 set using the code SLAROM, and directional diffusion coefficients were prepared using the Benoist's formula.

(2) These cross sections were collapsed to the broad group structure

---

* On leave from JAIS, Ltd.

using region average neutron spectrum.

(3) Diffusion calculations were made in the three dimensional X-Y-Z geometry using the code CITATION-FBR.

(4) Reaction rates were calculated using the code RBP and the reactivity worth was calculated using the perturbation calculation code PERKY.

The calculation based on the diffusion theory was mainly used in the analysis and the Sn calculation was used to evaluate a transport correction factor.

Calculation Result

Comparison of neutron spectra calculated at the core center of ZPPR-9 was shown in Fig. 3.6.1. A solid line represents the result of JFS-3-J2 and a dotted line represents that of conventional cross section set. The difference appears at energy range lower than 5 keV. On the other hand, the difference of adjoint fluxes was small through the whole energy range. The fairly large differences appear in the results of Doppler reactivity worths, as shown in Table 3.6.1. The differences also appear in the ^{240}Pu and ^{10}B sample worths, but do not remarkably in the ^{239}Pu and ^{238}U sample worths. Clear differences did not appear in the prediction of k_{eff}, reaction rate distributions, reaction rate ratios, sodium void worths and control rod worths.

Table 3.6.1 Comparison of Doppler reactivity worths in ZPPR-9

(¢/Kg)

Temperature (°K)	JFS-3-J2	JFS-E	δ (%)
487.5	-0.0248	-0.0272	9.73
644.4	-0.0397	-0.0436	9.90
794.0	-0.0512	-0.0564	10.06
935.4	-0.0604	-0.0666	10.27
1087.0	-0.0690	-0.0762	10.42

β = 0.003436 Δk/k/$

Sample Weight 1.08615 Kg

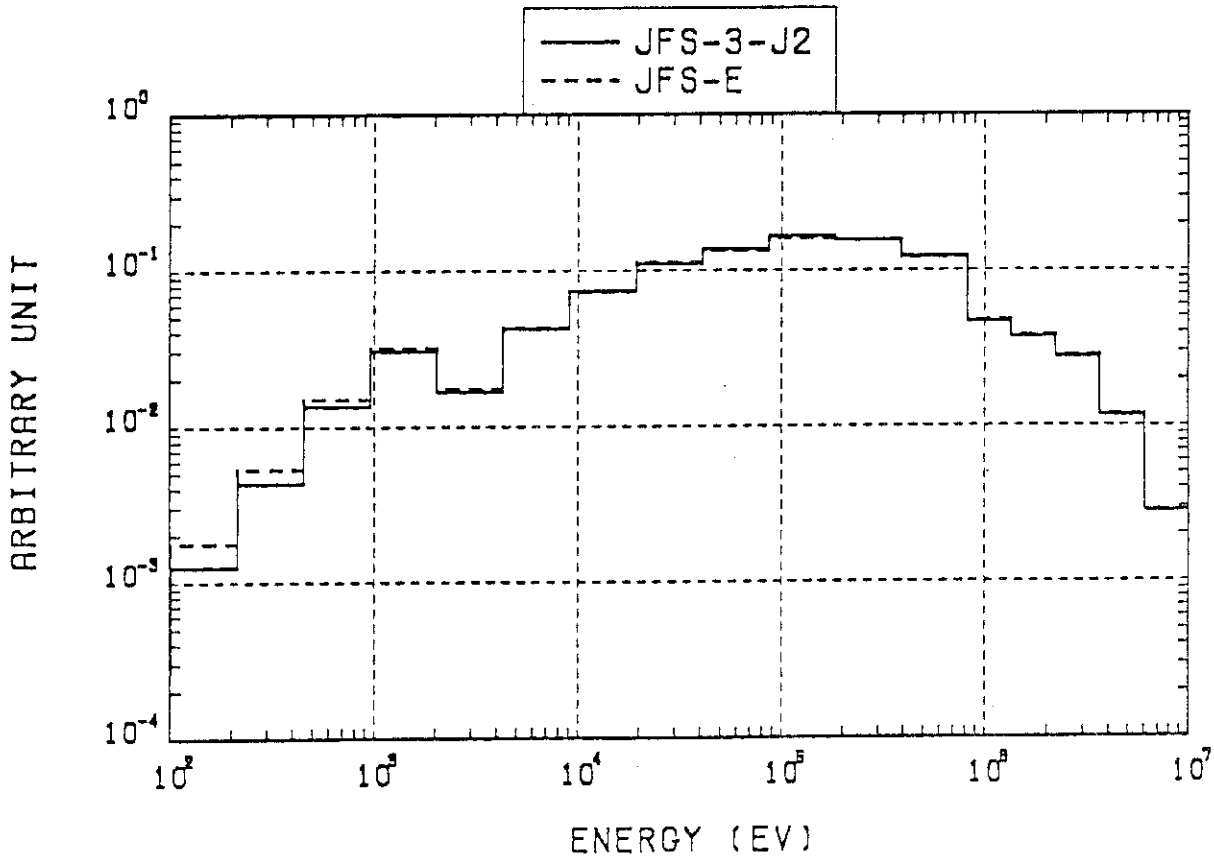

Fig. 3.6.1 Comparison of neutron spectrum at the core center of ZPPR-9

3.7 Effects of Cell Models on Nuclear Physics Characteristics of a Heterogeneous Fast Reactor

H. Yoshida, T. Osugi, S. Iijima and H. Shukuya*

The heterogeneous LMFBR core has more complicated arrangement of fuel assemblies than the homogeneous one, since substantial number of blanket assemblies are introduced into the core region. For this complexity, careful considerations have to be paid to analysing physics performances measured at fast critical assemblies. In this context, applicability of the conventional cell model has been investigated by calculating physics performances of a heterogeneous core, ZPPR-7A[1], shown in Fig. 3.7.1.

Three kinds of cell models are considered for this purpose to represent the core and inner-blanket drawers of ZPPR-7A. The plate arrangements in the drawers are shown in Fig. 3.7.2. The first cell model (CELL-1) is a conventional one often used for homogeneous core analyses, in which the core and inner-blanket drawers are treated separately. The second (CELL-2) is composed of a core drawer followed by an inner-blanket drawer and the third (CELL-3) is composed of two core drawers followed by two inner-blanket drawers. The last two cell models take account of the interaction effects between adjacent core and inner blanket drawers and hence give an improved treatment of the flux fine structures in the cells.

The effective cell averaged cross-sections are generated from each of the cell models, using the integral transport code SLAROM[2] and JFS-3-J2 70 group constants set[3] under the repeated boundary condition. Each cell has its own transverse buckling to keep it critical. Nuclear calculations are made with the diffusion code CITATION-FBR in R-Z geometry.

Table 3.7.1 summarises the effects of cell models on criticality and sodium-void reactivity effects of ZPPR-7A. As for criticality, the conventional cell model (CELL-1) gives K_{eff} lower by 0.49%Δk/kk' and 0.35%Δk/kk' than CELL-2 and CELL-3, respectively, Perturbation

---

* On leave from Japan Information Service Co. Ltd.

analysis indicates that these differences come from lower cell-averaged fission cross-sections for CELL-1. As for sodium-void reactivity effect, the conventional cell model gives the positive reactivity higher by 17% than the other cell models. The perturbation analysis again indicates that the difference is mainly due to that in the fission reaction components in the perturbation formula obtained for the cell models. In addition, the conventional cell model also gives the $^{238}U(n,f)$ reaction rate lower by 7% in the inner-blanket drawers.

From the present study, it should be important to find an adequate cell model for physics analyses of heterogeneous LMFBRs.

References

(1) Lineberry M. J., et al.: Nuc. Technol. Vol. 44, P21-43 (1979).
(2) Nakagawa M., and Tuchihashi K.: "SLAROM: A Code for Calculation of a Heterogeneous Core in Fast Reactors," JAERI-M 5916 (1974).
(3) Takano H., and Ishiguro Y.: "Production and Benchmark Tests of Group Constant Set JFS-3-J2," JAERI-M 82-135 (1982).

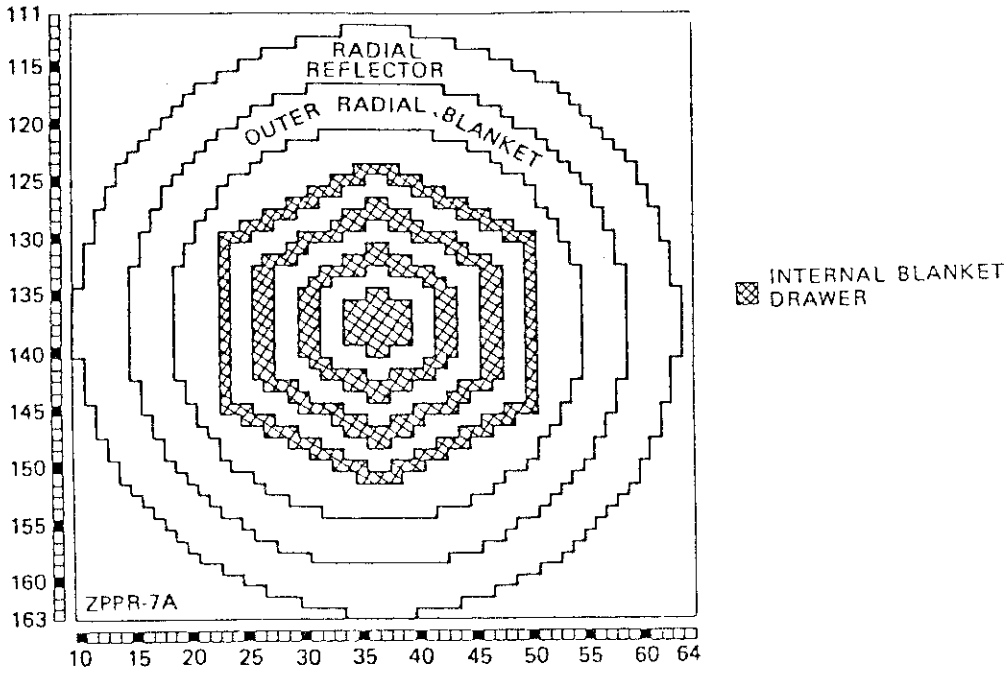

Fig.3.7.1 Cross-sectional view of ZPPR-7A

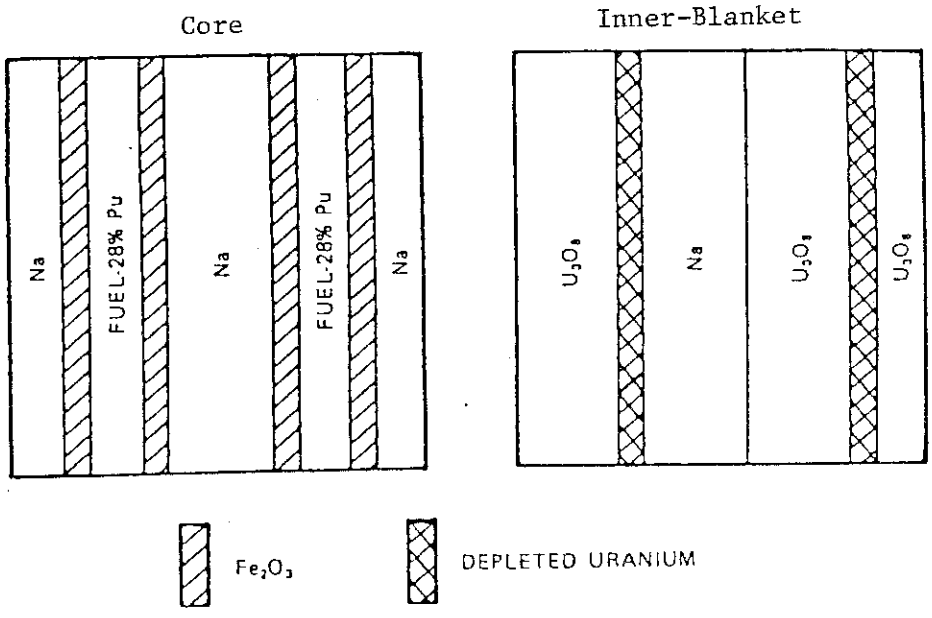

Fig.3.7.2 Plate arrangement in core and inner-blanket drawers of ZPPR-7A

Table 3.7.1 Effects of cell models on criticality and sodium-void reactivity of ZPPR-7A

	Cell-1	Cell-2	Cell-3
K-effective	0.99058	0.99545	0.99403
Dif. in K_{eff} (%Δk/kk')	-	0.49	0.35
Na-void reactivity (%Δk/kk')			
Na-void from Fuel Ring-1*	0.142	0.121	0.118
Na-void from Fuel Ring-1&2*	0.506	0.428	0.427
Dif. in Na-void reactivity (%)			
Na-void from Fuel Ring-1*	-	- 14.8	- 16.9
Na-void from Fuel Ring-1&2*	-	- 15.4	- 15.6

* See Fig.3.7.1, height of voided core is 61.0cm.

3.8 Analysis of the SEFOR Assembly by Using the JFS-3-J2 Cross Section Set

H. Takano and T. Mitsunari*

The application of a cross section set to the calculation of the Doppler reactivity effect is commenly studied by analyzing the sample Doppler experiment. However, the experiments are usually performed at the center of core. In the SEFOR assembly[1], on the other hand, the isothermal Doppler coefficient of the whole core was measured to evaluate the Doppler effect in the operating reactor. Hence, the analysis of the SEFOR assembly is very important to test the temperature dependence of the cross section set. Here, the Doppler coefficient is calculated by using the JFS-3-J2 set.[2] The cell average cross sections were calculated with the SLAROM code[3] in which the cell analysis was performed with the use of the collision probability calculation code LAMP-B.[4] The used super cell model for SEFOR is shown in Fig. 3.8.1. The results calculated with the two-dimensional cylindrical model are shown in Table 3.8.1.

The heterogeneity effect for the Doppler coefficient is -0.00054 Δ(TdK/dT) and in good agreement with that in Ref. (1). The ratio of the calculational and experimental values is 1.11 and hence, the calculation gives overestimate, though this is comparable with the experimental error of 12%.

References

1) Harris R. A.: "Analysis of Doppler Constants of Cores I and II of SEFOR," HEDL-TME 72-78 (1972).
2) Takano H. and Ishiguro Y.: "Production and Benchmark Tests of Fast Reactor Group Constant Set JFS-3-J2," JAERI-M 82-135 (1982).
3) Nakagawa M., et al.: private communication.
4) Tsuchihashi K.: "LAMP-B: A Fortran Program Set for the Lattice Cell Analysis by Collision Probability Method," JAERI 1259 (1972).

---

* Japan Information Service Co. Ltd.

Table 3.8.1 Heterogeneity effect for Doppler coefficient

	Doppler reactivity Δk/k(300°K)		$\frac{\Delta k(1365) - \Delta k(677)}{k(300)}$	$T\frac{\partial k}{\partial T}$
	T = 677°K	T = 1365°K		
Hetero	-0.007329	-0.013995	-0.006666	-0.009515
Homo	-0.006901	-0.013191	-0.006290	-0.008978
Het-effect	6.21%	6.10%	5.9%	6.0%
Ref	-0.006503	-0.01244	-0.00594	-0.008479
Corrected				-0.008988
Exp				-0.0081±0.001
C/E				1.11

SUPER CELL MODELLING FOR "PATH"

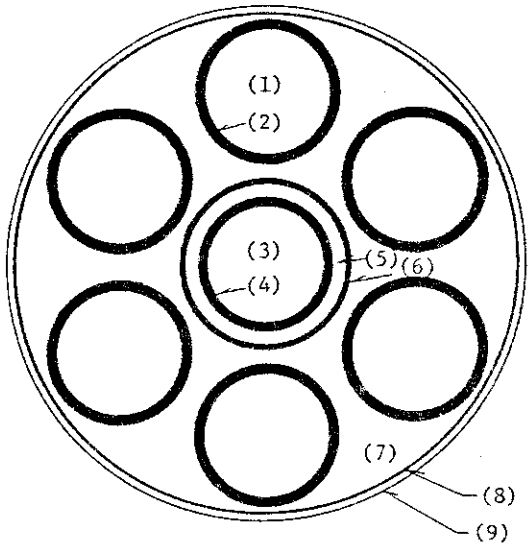

material	radius (cm)	
(1) fuel	1.11125	radial pos.
(2) SUS316 + void	1.23190	2.7813
(3) BeO	0.98679	
(4) SUS316 + void	1.11125	
(5) Na	1.28025	
(6) SUS304	1.37360	
(7) Na + SUS304	4.04079	
(8) SUS304	4.20083	
(9) Na	4.21416	

Fig.3.8.1 Lattice cell model used in the heterogeneity calculation

3.9 Comparison of Calculated and Experimental Decay Heat from Products of U-233, U-235 and Pu-239 Thermal Fissions

T. Osugi, H. Yoshida and M. Hotta*

Experimental data of decay heat measured at Oak Ridge National Laboratory[1] , Los Alamos Scientific Laboratory[2] and Intelcom Radiation Technology[3] were compared with the summation calculations using the updated nuclear data libraries for fission products. Since the different experiments represent varying irradiation and cooling times, it is necessary to use some means to compare the various results on a common basis. For this purpose the least-squares method was applied to the data from the decay heat experiments mentioned above presented in Table 3.9.1.

Table 3.9.1 Measured data of decay-heat

Organisation	Nuclide	Irradiation Time [sec]	Cooling Time [sec]
ORNL	U-235	1, 10, 100	$2.2 \sim 1.2 \times 10^4$
	Pu-239	1, 5, 100	$2.2 \sim 1.2 \times 10^4$
LASL	U-235	2.0×10^4	$10.0 \sim 1.0 \times 10^5$
	U-233	2.0×10^4	$20.0 \sim 1.0 \times 10^5$
	Pu-239	2.0×10^4	$20.0 \sim 1.0 \times 10^5$
IRT	U-235	8.64×10^4	$0.75 \sim 1.5 \times 10^5$

Least-Squares Fitting of Decay Heat Data

In the absence of neutron capture, the decay energy rate at time t following T seconds with a constant fission rate, denoted by F(t,T), can be related to a pulse function, f(t) for which we assumed a simple analytical form, a sum of exponentials:

$$F(t,T) = \int_t^{t+T} f(t')dt' = \sum_i a_i \frac{e^{-\lambda_i t}}{\lambda_i}(1-e^{-\lambda_i T}).$$

Due to the lack of the experimental data for longer cooling times, $t > 10^5$ seconds, the decay heat values based on the summation calcula-

---

* On leave from Information System Laboratory Ltd.

tion were also used as the fitting data. Uncertainties for the fitted decay heat curves were estimated using the experimental uncertainties reported with the measured data.

The least-squares' results for the pulse function of U-235 thermal fission were compared with the measured decay curve processed by Dickens et al.[1] and shown in Fig. 3.9.1. Our fitted curve well agreed with the Dickens' curve including the range of uncertainties.

Comparisons of Fitted and Calculated Decay Heat Curves

Now it has become easy to compare all experiments presented in Table 3.9.1 on a common irradiation basis. Comparisons were made by reducing all results to a pulse function f(t) and also by extrapolation to the infinite function $F(t,\infty)$, with the summation calculations using the one-point depletion code DCHAIN[4] based on the Bateman's formula and the updated nuclear data libraries, "JNDC"[5] and "Rider-Meek"[6]. The typical results were presented in Fig. 3.9.2 for the pulse function of total decay heat (beta plus gamma decay) from products of the U-235 thermal fission. The JNDC library well predicts the ORNL's decay heat curve for a wide range of cooling times.

Conclusion

The decay-heat comparisons, combined with the other comparisons we have made of between calculations and experimental data, indicate that the JNDC library is adequate for many applications to predict the decay-heat power from products of thermal fissions.

References

1) Dickens J. K., et al.: N.S.E., 74, 106 - 129 (1980) and Dickens J. K., et al.: N.S.E., 78, 126 - 146 (1981).
2) Yarnell J. L., Bendt P. J.: "Decay Heat from Products of ^{235}U Thermal Fission by Fast-Response Boil-Off Calorimetry," LA-NUREG-6713, Los Alamos Scientific Laboratory (1977).
3) Frisenhahn S. J., et al.: "U-235 Fission Product Decay Heat from 1 to 10^5 Seconds, "EPRI NP-180, Project 392-1, prepared for Electric Power Research Institute by Intelcom Radiation Technology Corporation (1976).
4) Tasaka K.: "DCHAIN: Code for Analysis of Build-up and Decay of Nuclides," JAERI 1250 (1977).

5) Ihara H., et al.: "JNDC FP Decay and Yield Data," JAERI-M 9715 (1981).

6) Rider B. F., Meek M. E.: "Compilation of Fission Product Yields, Vallections Nuclear Center," NEDO-1254-2(D).

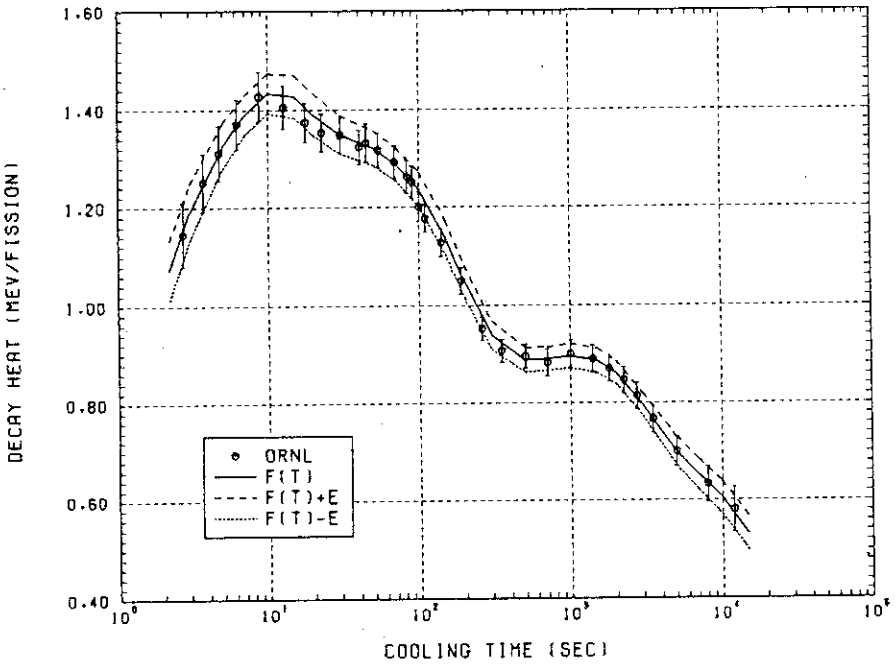

Fig. 3.9.1 Comparison of the pulse functions of total decay heat for U-235 thermal fission between the least-squares results (F(t), F(t)+E, F(t)-E) and measured decay curve at ORNL

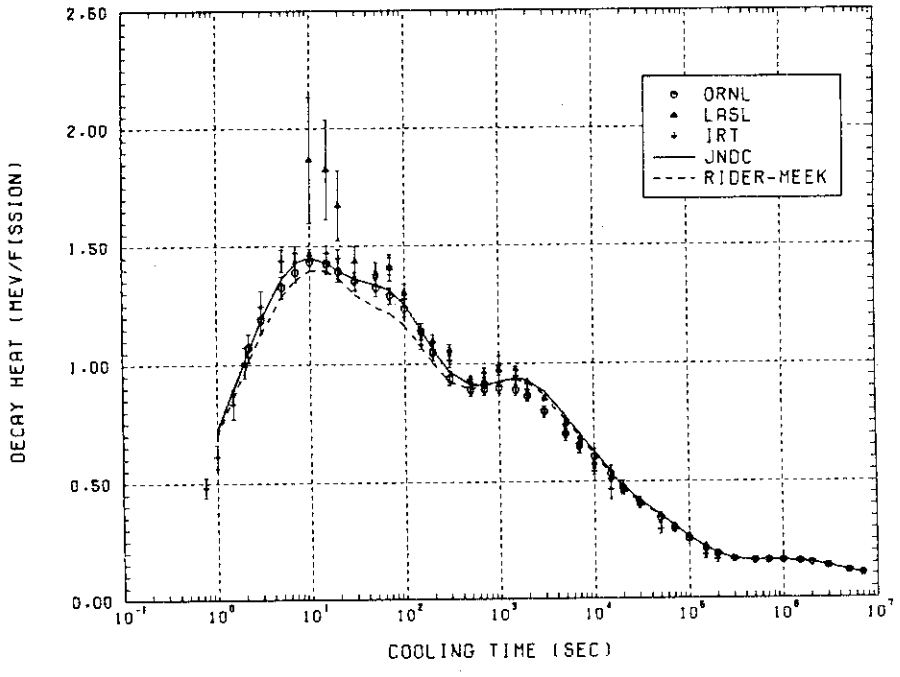

Fig. 3.9.2 Comparison of the pulse functions of total decay heat for U-235 thermal fission between the fitted results of the data measured at ORNL, LASL and IRT and the calculational results using JNDC and RIDER-MEEK libraries

3.10 Operation Report of SHE

F. Yoshihara, K. Kitadate, M. Takeuchi, T. Ono and
H. Yoshifuji

During the first half period of the present fiscal year, SHE was made critical 180 times and recorded operation time of 265 hours and integrated power out put of 53 watt-hours. In the period, four different types of the core, SHE-B2-2, SHE-14R, SHE-16 and SHE-8-2 were assembled for the purpose of measuring the integral quantities as follows;

(1) Reactivity temperature coefficient of a single fuel rod composed of the coated particle uranium fuel compacts
(2) End reflector effect
(3) Reactivity worth of burnable poison rods

and

(4) Reactivity worth of control rods

As for the maintenance, a DC motor for use of the emergency separation of the movable half of the assembly from the fixed one was renewed under the permission of the Science and Technology Agency.

Operation of SHE since the initial critical in 1961 was suspended on October 15, 1982. Fuels in the core were all taken out and disassembled to sheath and disk. Then, fuel disks were encased in alminium cans and stored in birdcages on November 19, 1982. From the initial critical, SHE was made critical 2000 times and recorded operation time of 7833.5 hours and integrated power out put of 5605 watt-hours.

SHE is now under reconstruction aiming at a criticality experiment for the Experimental Very High Temperature Reactor, VHTR.

3.11 Report on Operation and Management of FCA

H. Watanabe, H. Ogawa, S. Fujisaki, K. Yamagishi and A. Ohno

In fiscal 1982, much labor was expended in activities concerning operations and maintenance of the Fast Critical Assembly (FCA), and consequent performance of the operation was achieved in success. FCA-X-1,2,3 and -XI-1 cores were assembled to characterize the "JOYO MK-II" core and to obtain benchmark data on heterogeneity of a large core, respectively. Operations for the above purposes completed as scheduled, without any major problem disturbing the execution of the experiment.

Operations of 147 times were carried out in 124 days to perform the experiment. Among them 6 were scrammed due to noise signals. The operating time was 789 hours and the integrated power 5,011 Wh. The total run of 3426 criticality operations has been recorded at the end of this fiscal year since the first achievement of criticality on 29 April 1967. According to the regulation of operations, at FCA 2 days were devoted to the monthly inspection and about 4 weeks to the annual inspection in November. Normal maintenance activity was done in these days to provide maximum operations for the experiments. The other major works relating to the maintenance activity were carried out. First, the control system in the fuel transfer equipment was renewed in this year. A great consideration was paid on simplification of the control system, easiness in use, smoothness in movement of the fuel drawer carrier, and articulation of the position indication of the fuel drawer carrier in the span between the working and the reactor room. Second, the defects of coating on the surfaces of 93% enriched uranium fuels were repaired for about 3000 coupons by spraying colloidal solution of fluorocarbon. This repair required about 80 man-days. Third, specification of the start-up channel (CH.1 and 2) was determined in cooperation with the Electronics Division of JAERI. To process the operating data of the reactor, the output signal level of the start-up channel was adjusted so as to transfer data to the computer. Design and fabrication shall finish in the next year.

In connection with safeguards, IAEA and NSB carried out every two week inspection under the international treaty. The Physical Inventory Taking (PIT) of the fuels was performed from Feb. 14 to March 18 by means of item counting, weighing and nondestructive assay. IAEA and NSB enforced the Physical Inventory Verification (PIV) from March 7 to 18. No anomaly was confirmed. The computer code which have been developed last year was improved

greatly, and provided quickly the required information on fuels during the PIT and normal inspections.

The activities were also made on the Physical Protection (PP). The major task was the annual inspection of the PP system and the automatic gate drive mechanism under the inspection. A microwave sensor among 8 was renewed because of frequent occurences of misalarms. The cause of the misalarms was the deterioration of the microwave sensor due to sea breezes. 4274 persons accessed to the guarding area and the authorized licenses to the strategic area were issued for 308 persons (exclusive IAEA and NSB inspectors).

With respect to developmental tasks, the SUS tube for the B_4C control rod was designed and fabricated. The control rod can be assembled in the fuel drawer. Then the high accuracy is maintained in positioning the control rod in the core. The other remodeling was done on the sample cooling system in the Doppler equipment. By this equipment, Doppler reactivity is given as a function of the sample temperature and its amount is about $10^{-6}\Delta k/k$. It is very difficult to measure such a small reactivity. The measurement system is required to be highly stable. Cooling of the equipment is made by air. Since the fluctuation of moisture in air brings about reactivity changes, removal of the moisture is indispensable. In this remodeling, the removal of 99.99% moisture was achieved. The computer system was developed to process timely the operating data of the reactor and experimental data. This system consisted of a microcomputer, a CRT display, a lineprinter and a X-Y plotter. Great hopes are expected on the system to save much time in data processing.

4. Fusion Neutronics

4.1 Operation Report of the Fusion Neutronics Source

J. Kusano, C. Kutsukake and S. Tanaka

Operation activities for FNS including operation and maintenance of the facility, tritium target treatment were continued following a schedule of fusion neutronics experiments.

A most intensive neutron generation at FNS using a rotating target (RNT) was started since July 1982.

The stability and the reliability of the accelerator were increased by maintenance performance. Integrated operation time of the accelerator was 420 hours. The consumption of target disk was as follows; two pieces of LLL type 1,000 Ci target, two pieces of water cool type 25 Ci target and four pieces of air cool type 10 Ci target.

0° Line Operation

The first D-T neutron generation on the 0° beam line was performed using the 1,000 Ci tritiated RNT under the 20 mA operation of FNS. Maximum neutron yield of 3.2×10^{12} n/s was confirmed by the calibrated Thorium fission counters and foil activation method. The characteristics tests on the RNT assembly for the neutron generation were carried out. (See 4.3) Typical operation for a heavy irradiation experiment was done continuously for 20 hours under the condition of 310 keV and 20 mA for beam energy and current, respectively. In that operation, an accident of the swing mechanism in the RNT assembly happened. In spite of the trouble, total neutron generation was achieved to be 1.17×10^{16} n.

80° Line Operation

The operations on the low current beam line for the fusion blanket neutronics experiments were made routinely in this fiscal year. The experience from these operations revealed that some improvements were required for the target assemblies i.e., it was desirable to make both the air cooled type and the high speed water cooled type assemblies simpler and lighter structure. After some examinations, a modified air cooled type target assembly has been manufactured. In order to achieve the stable operation of the beam pulsing system, the diverter amplifier was replaced and additional optical fiber cables were built between the console and the high voltage terminal.

The relations between the temperature of a metal target and the release rate of tritium gas from a Scandium tritied and Titanium tritied targets were examined by taking into consideration of the deutrium gas release phenomenon observed previously. The mechanism of the relations could not be elucidated from present examinations. Further investigation should be successively performed during routine operations.

Tritium Handling

A total amount of 52 Ci tritium in the exhaust gas from the vacuum system of FNS was trapped with the Tritium Adsorption Plant (TAP) through the first D-T operations of the 0° beam line by the use of the 1,000 Ci target.

Tritium target disk exchanges on the 80° beam line were performed frequently. In these works, air contamination and radiation exposure for personnels were minimized by the use of a local ventilation system.

A shipping container for over the 1,000 Ci tritium target, that called 20WC-1 in U.S.A (B type), was obtained to make an application for a Japanese certification.

4.2 Time-of-Flight Spectral Analysis of Associated Particles from a Tritium Target Bombarded by Deuterons

Y. Oyama, T. Nakamura and H. Maekawa

The absolute yield of D-T neutrons at FNS is estimated by using the associated particle method. The associated particles are detected by a silicon surface barrier detector (SSD) positioned at the distance of 1.578 m from the tritium target making an angle of 179 degree to the incident deuteron beam. The associated particle of interest is ^{4}He which is produced by $^{3}T(d,n)^{4}He$ reaction, but the unwanted particles are produced at the same time by parasitic reactions, i.e., $^{3}He(d,p)^{4}He$, $^{2}D(d,n)^{3}He$ and $^{2}D(d,p)^{3}T$. Helium-3 is accumulated by the decay of tritium and deuterium is implanted by an accelerated beam.

A thin aluminum foil of 0.14 mg/cm^2 is placed in front of SSD to eliminate the back-scattered deuterons. The detector bias is adjusted to separate the pulse height peaks of particles by using the difference of energy deposit in the depletion layer. The ^{4}He produced by d-^{3}He reaction, however, has almost the same energy as the ^{4}He by d-^{3}T reaction and the pulse height spectrum has a tail to lower energy due to struggling in the foil. Thus the correct spectrum of ^{4}He particles should be examined in order to determine the absolute neutron yield.

The pulse height spectrum of SSD was analyzed by using the time-of-flight method to identify the peaks in the spectrum. The spectrum was measured by gating the pulse height analyzer corresponding to the interval of arrival time for each particle. Associated particle reactions, their energy and flight time are summarized in Table 4.2.1. Figs. 4.2.1 and 4.2.2 show pulse height spectrum and arrival time spectrum of associated particles, respectively. The correspondence of pulse height spectrum for each time region is shown in Fig. 4.2.3.

The component of ^{4}He slowed down to lower energy was separated successfully by this measurement. The contamination in the ^{4}He peak by d-^{3}He reaction can be estimated by its associated proton peak and was about 2.6% of whole ^{4}He counts in this case, this quantity being dependent on the history of the target used. The component of lower tail was estimated to be 5.4% of the whole ^{4}He counts. The absolute ^{4}He counts of interest can be obtained from the ^{4}He peak area determined by using this results.

Table 4.2.1 Associated particle reactions

Reaction type	Q value (MeV)	Particle	Energy (MeV) (θ = 179°)	Flight time (ns) (ℓ = 1.578 m)
$^{3}T(d,n)^{4}He$	17.6	n	13.32	31.8
		^{4}He	2.74	137.8
$^{3}He(d,p)^{4}He$	18.35	p	13.90	30.6
		^{4}He	2.87	134.7
$^{2}D(d,n)^{3}He$	3.27	n	2.08	79.0
		^{3}He	0.45	294.9
$^{2}D(d,p)^{3}T$	4.03	p	2.61	70.6
		^{3}T	0.59	257.0

* Incident deuteron energy is 160 keV which is mean reaction energy for the 310 keV acceleration.

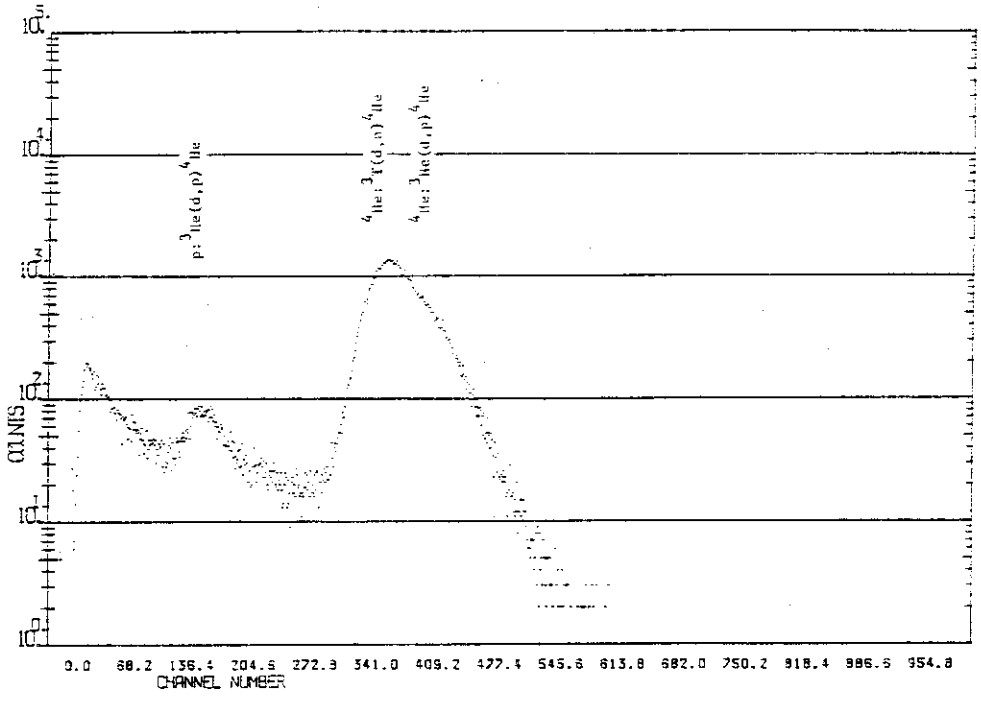

Fig.4.2.1 Pulse height spectrum by associated particles

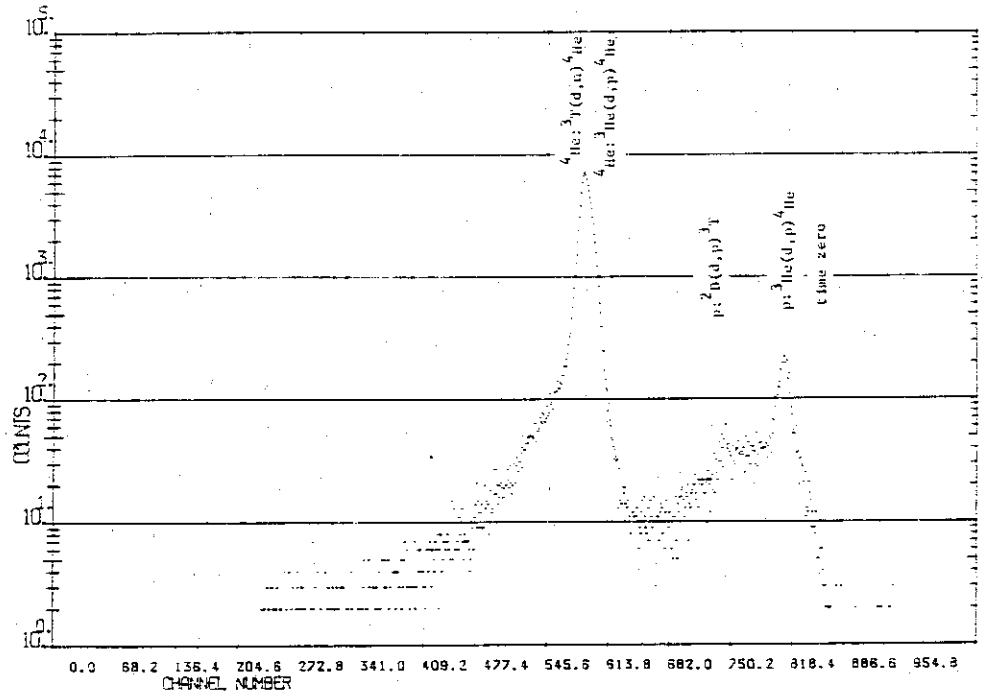

Fig.4.2.2 Arrival time spectrum by associated particles

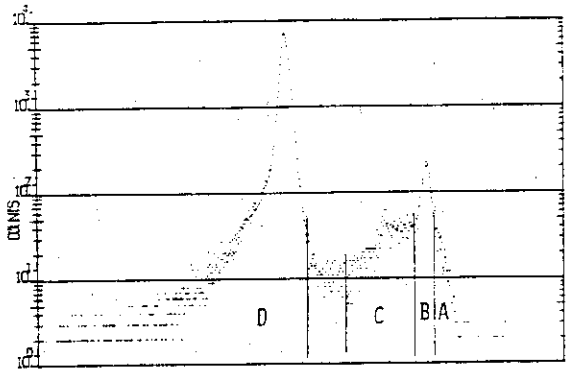

(a) time intervals for gating

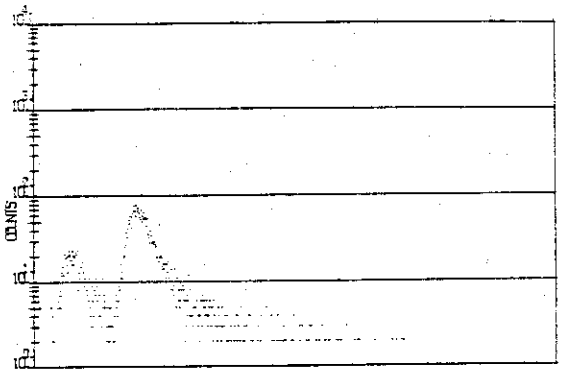

(b) pulse height spectrum gated by interval A+B

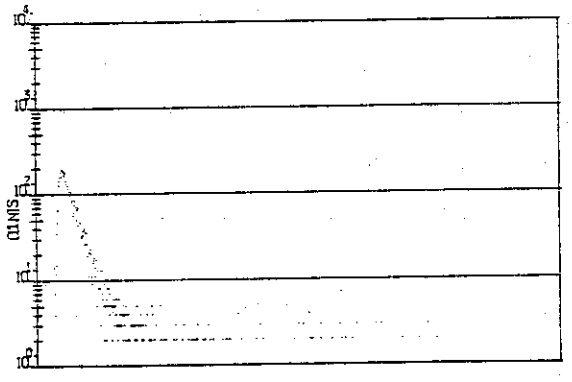

(c) pulse height spectrum gated by interval C

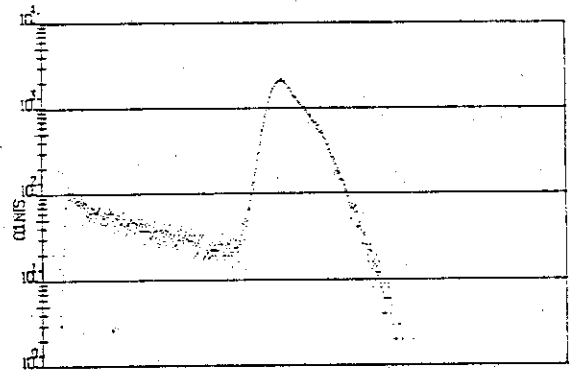

(d) pulse height spectrum gated by interval D

Fig.4.2.3 Time gated pulse height spectrum for various time intervals

4.3 Characteristics Studies of D-T Neutron Production by Using Rotating Target at the 2nd Target Room of FNS

Y. Ikeda, H. Maekawa, S. Tanaka, Y. Oyama, T. Iguchi* and T. Nakamura

After several performance tests of the FNS accelerator on high current deuteron beam with dummy and Ti-D rotating targets (RNT), D-T operations using a 1000 Ci tritium target was started in July 1982.

The monitoring method for intense neutron yield had to be established to obtain absolute experimental values. In the case of the high current beam operation, the usual associated α-particle method using a silicon surface barrior detector (SSD) cannot be applied because the pulse height distribution of SSD is distorted by the pile-up phenomena and the damage of the detector. A fission chamber of ^{232}Th is useful because of its high threshold energy of fission if it can be normalized to the ordinary method. The conversion coefficient between the α-counter and the ^{232}Th fission chamber was obtained at rather low neutron fluxes. The foil activation technique was applied to confirm the reliability of the coefficient. Five threshold reactions, ^{56}Fe(n,p)^{56}Mn, ^{27}Al(n,α)^{24}Na, ^{58}Ni(n,2n)^{57}Ni, ^{93}Nb(n,2n)^{92m}Nb and ^{197}Au(n,2n)^{196}Au, were used to determine the D-T neutron production rate. In Table 4.3.1, the estimated neutron yields are shown in comparison with the value of ^{232}Th counter. It can be seen that the agreements between the ^{232}Th monitor and the activations are good within experimental errors and uncertainties of the cross sections. Standing on this results, we decided to use the ^{232}Th fission chamber as the neutron yield monitor.

The angular dependency of emitted neutrons around the RNT was measured by using fission chambers of ^{232}Th and ^{235}U, an NE213 liquid scintillator and the foil activations in which ^{197}Au(n,γ)^{198}Au reaction was added to those mentioned above. Counters were set at 1.5 m radius from the target center. The angular interval was 30° except in the directions of 70° to 90°, where it was 10°. Foil sets were placed in three-dimensional circumferences having 30 cm radius with its center at the target. After an irradiation by D-T neutrons for 5 hours, distributions of each reaction rate and angular flux were determined. In

* Faculty of Engineering, The University of Tokyo

Fig. 4.3.1, results on horizontal plane were shown with those taken from the counter method. There are significant dips at about 90° in these distributions corresponding to the $^{232}Th(n,f)$ reaction rate, NE213 counts and threshold reaction rates. On the contrary, in the cases of $^{235}U(n,f)$ and $^{197}Au(n,\gamma)^{198}Au$, which have high sensitivities for low energy neutrons, distributions are rather flat. From the results, it can be seen that the direct D-T neutron components are strongly affected by the structural materials of the rotating target assembly. Therefore, when experiments are going to be done around directions of 90°, the emitted neutron distribution should be taken into account in the source determination.

In order to investigate the neutron spectral distribution in the target room which is considered to be a large cavity of 5 x 5 x 4.5 (m^3) surrounded by thick concrete, several reaction rate distributions from target to the room wall were measured. Used reactions were $^{27}Al(n,\alpha)^{24}Na$, $^{58}Ni(n,2n)^{57}Ni$, $^{115}In(n,n')^{115m}In$, $^{115}In(n,\gamma)^{116m}In$ and $^{197}Au(n,\gamma)^{198}Au$. Measured reaction rate distributions are shown in Fig. 4.3.2, together with calculated ones by using reaction cross sections and calculated neutron fluxes by ANISN with a simple calculational model of the target room. From this figure. it is clearly seen that the direct D-T neutron components decrease with radial distances as the inverse of r-square. In contrast to that, reaction rate distributions of $^{115}In(n,\gamma)^{116m}In$ and $^{197}Au(n,\gamma)^{198}Au$ are almost constant. Then, it can be said that the slow neutron components, mainly due to room returned neutrons, distributed uniformly in the target room.

Further analytical studies of the neutron field in the target room will be performed by the Monte Carlo method.

Table 4.3.1 Neutron production rate of RNT

(x 10^{12} n/sec)

position (cm)	$^{56}Fe(n,p)^{56}Mn$	$^{27}Al(n,\alpha)^{24}Na$	$^{58}Ni(n,2n)^{57}Ni$	$^{93}Nb(n,2n)^{92m}Nb$	$^{197}Au(n,2n)^{198}Au$
10.7	2.23	2.16	2.02	1.90	1.89
20.7	2.18	2.10	1.92	1.95	1.64
30.7	2.25	2.13	1.88	2.05	1.88
60.7	2.24	2.18	2.01	1.61	1.80

The yield obtained by ^{232}Th fission chamber was 2.15 x 10^{12} n/sec.

** Experimental errors are estimated to be 6% mainly due to positioning.

** Cross section uncertainties are about 5% for $^{56}Fe(n,p)^{56}Mn$ and $^{27}Al(n,\alpha)^{24}Na$ and 7% for other reactions.

** Total errors are about 7% to 11%.

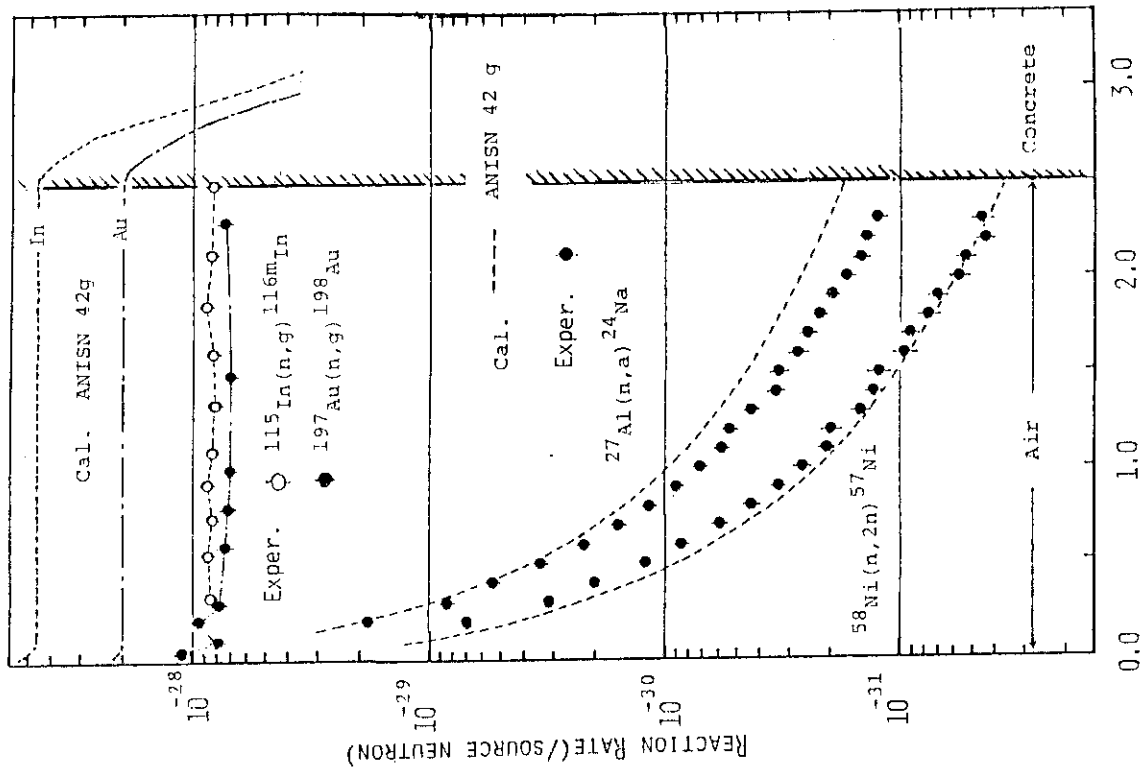

Fig.4.3.2 Radial distribution of the reaction rate in the target room

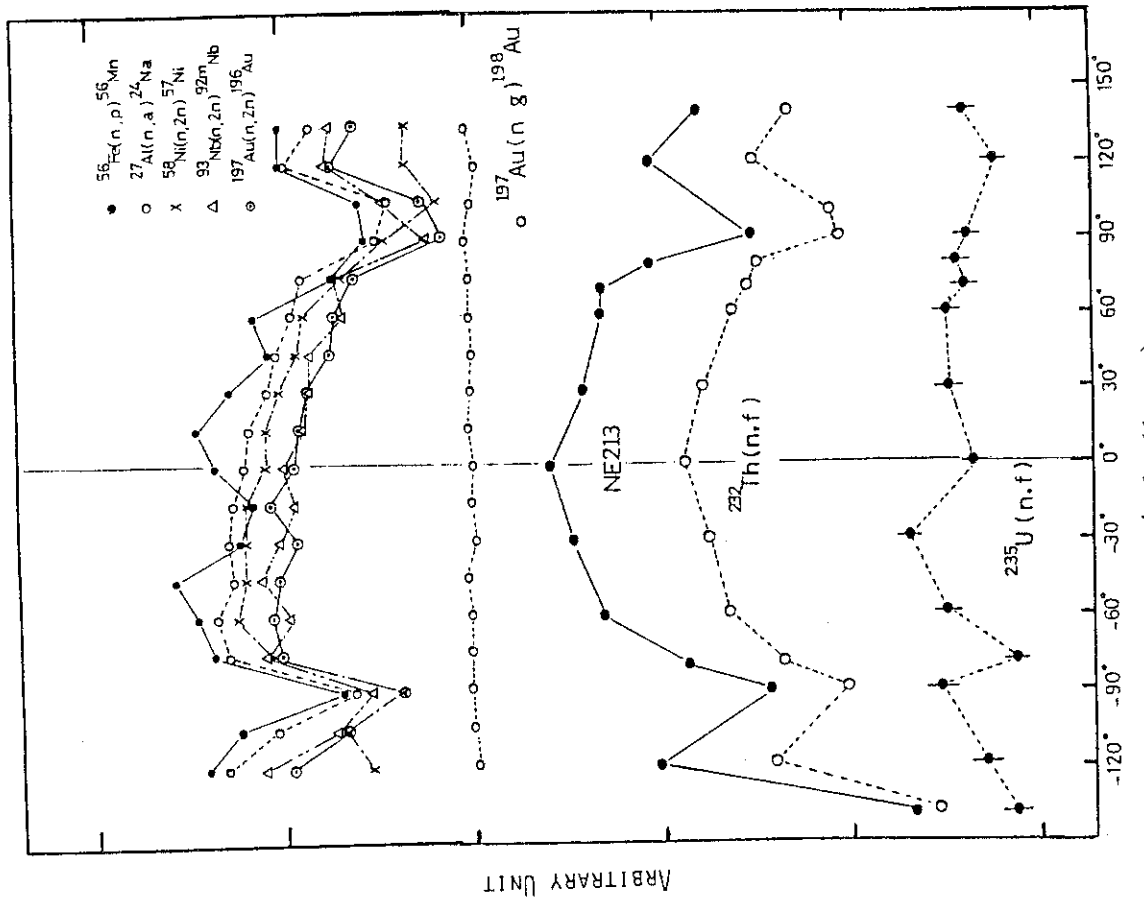

Fig.4.3.1 Angular distribution of the reaction rates on the horizontal plane around the RNT.

4.4 Feasibility Test of a Silicon PIN Diode Neutron Dosimeter for Applications in Fusion Neutronics Experiments

Y. Ikeda, S. Yamaguchi, H. Maekawa, Y. Oyama and T. Nakamura

As a personnel accidental neutron dosimeter, a silicon diode has been used in many reactor plant environments. Although it is rather sensitive to temperature during measurements of its forward voltage drops, it has several excellent features; (1) high sensitivity for fast neutrons, (2) low sensitivity for gamma-rays against to neutrons by magnitude of 10^{-4}, (3) small size (3 mm^3), (4) easiness of handling, (5) low threshold energy of about 150 keV. From the consideration of the features, it can be expected that the PIN diode possesses a possibility to be applied in fusion neutronics experiments, especially in integral experiments, as a spectral index detector.

In order to use it as a spectral index detector, its precise response for the fast neutron should be investigated preceding to the experiments. The relative response curve of a typical PIN diode was calculated by Consnac[1] on the basis of the damage process induced by fast neutrons. Absolute neutron sensitivities of a PIN diode, namely Stusvik Type 5430, were measured by D-D and D-T neutron irradiations using the FNS facility. Thereafter, absolute response curve was obtained by fitting the calculated relative response curve to the measured sensitivities. In Fig. 4.4.1, the fitted curve is shown.

To test the feasibility of the response, some integral response measurements were performed in three different neutron fields. The integral response means the difference of forward voltage drop between before and after irradiations. The PIN diodes were exposed for a day in ^{252}Cf fission neutron field. The source intensity of ^{252}Cf was 2.7×10^7 n/s. After the irradiation, integral responses were compared with the calculated ones obtained by using the fitted response curve and neutron spectrum of ^{252}Cf. In Table 4.4.1, both measured and calculated values are listed. Though errors in positioning are rather large, agreements are not so bad. A radial distribution of the integral responses in the 2nd target room of FNS was measured by an irradiation of D-T neutrons using a rotating target. The result is shown in Fig. 4.4.2, comparing with the distribution of $^{115}In(n,n')^{115m}In$ reaction rate of which the threshold energy is comparable to that of the PIN diode. The

distribution calculated by ANISN using the present response curve is shown simultaneously in Fig. 4.4.2. Both distributions of PIN diode and $^{115}In(n,n')^{115m}In$ show the same tendency and similar overestimations in the calculations can be seen near the room wall. The integral response distribution was measured also in a Li_2O slab assembly. The measured integral responses are shown in Fig. 4.4.3 with those calculated by DOT3.5 in the same manner as that mentioned above. In this figure, it can be seen that the measured PIN diode response distribution agrees with the calculated one in spite of rather large errors.

From considerations of these results, it has been demonstrated that the PIN diode is applicable in fusion neutronics integral experiments as a spectral index detector.

Reference

1) De Cosnac B., Dulieu P., Le Rallie J. C.: "Measure Des Flux de Neutron Rapides au Moyen de Diodes en Silicium Sensibles aux Dommages," CEA-CONF-1067

Table 4.4.1 Integral response of PIN diode for ^{252}Cf

position	Cal.	Exper.(ave.)	C/E
2.0±0.5 cm	$0.70^{+0.54}_{-0.25}$ V	0.44 V	$1.6^{\pm 1.2}_{-0.6}$
8.0±0.5	$0.044^{+0.005}_{-0.006}$	0.037	$1.2^{+0.1}_{-0.2}$
10.3±0.7	$0.026^{+0.004}_{-0.003}$	0.032	$0.8^{+0.1}_{-0.1}$

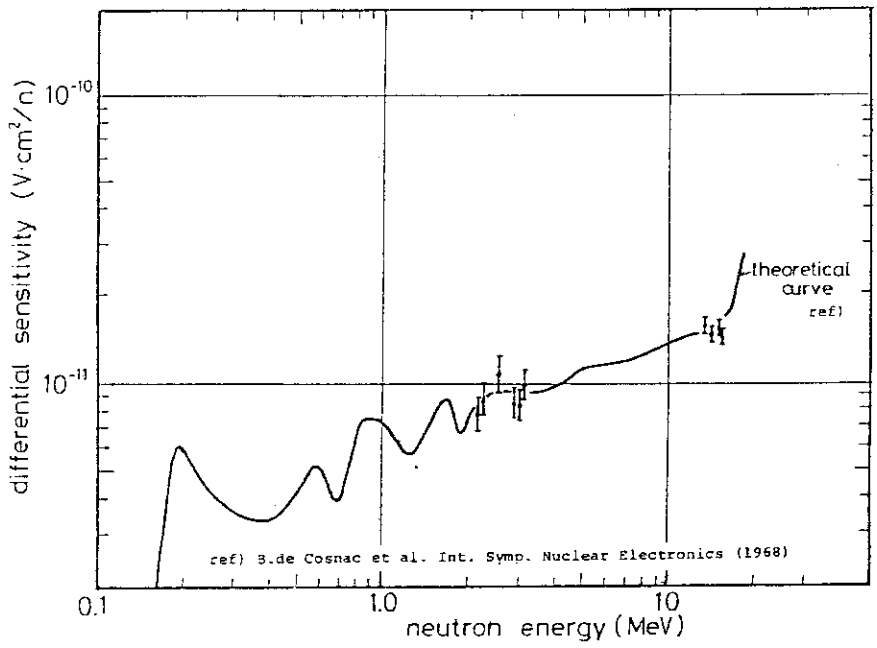

Fig. 4.4.1 Response curve of PIN diode.

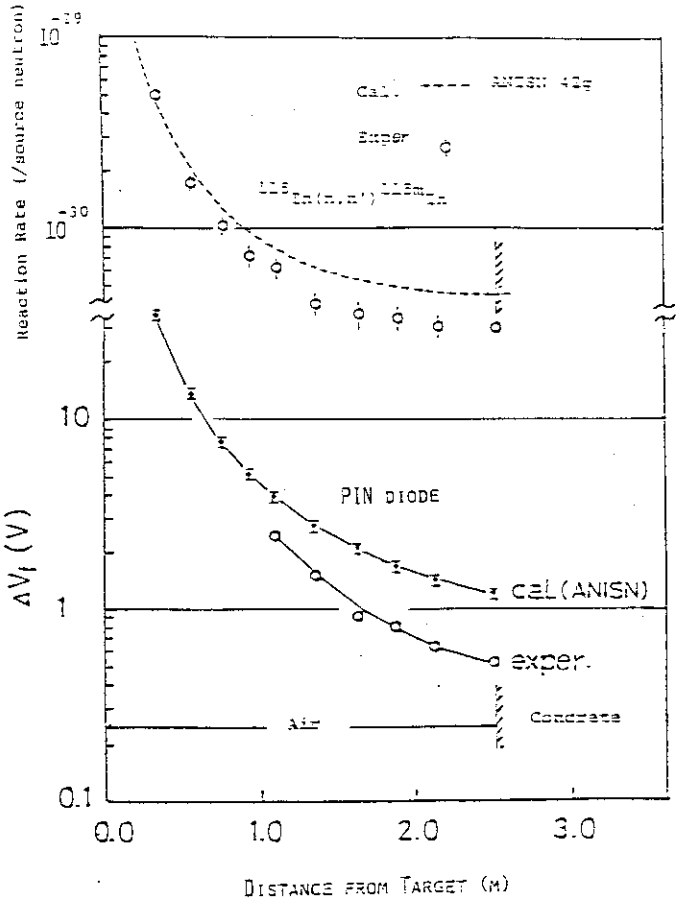

Fig.4.4.2
Integral response of PIN diode in the target room. The reaction-rate distribution of $^{115}In(n,n')^{115m}In$ is shown for the comparison.

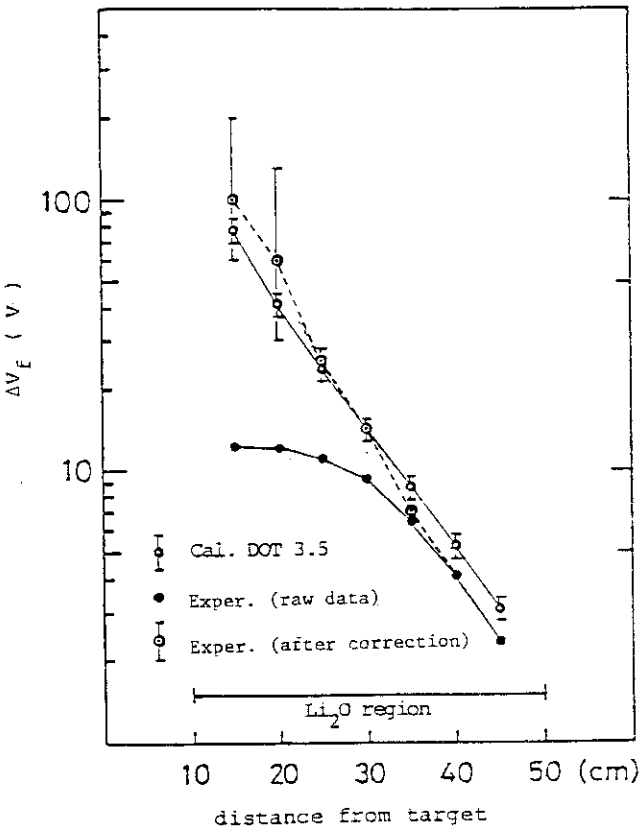

Fig.4.4.3
Integral response distribution of PIN diode in the Li_2O slab assembly

4.5 A Method for Tritium Production-Rate Measurement by Li_2O Pellets

H. Maekawa, K. Tsuda and Y. Ikeda

As the tritium production-rate is one of the important items in the simulated fusion reactor blanket experiment, several methods were proposed to measure it. Lithium-oxide is a promising candidate for the blanket material as the tritium breeder due to high lithium atom density and hence is adopted in a fusion experimental reactor design at JAERI.

Therefore we developed a new method using a sintered Li_2O pellet. This method has following advantages:

i) Chemical composition of pellet is just the same as the experimental blanket assembly.

ii) Sintered Li_2O pellet is fairly stable and easy to handle.

iii) Atomic density of Li per unit volume is highest among lithium compounds.

iv) Chemical treatment of pellet is very simple to make a liquid scintillation sample.

Chemical treatment of Li_2O pellet

i) Put the irradiated Li_2O pellet (12 mmϕ x 2 mm, ~ 0.35 g) in a 20 ml Teflon vial and add 6 ml of water. The vial is closed and wait until the pellet is dissolved completely. It takes about two days at the normal room temperature.

$$Li_2O + H_2O \longrightarrow 2LiOH$$

Then the tritium trapped in Li_2O pellet transfers to the solution.

ii) Add 0.85 ml of fluoric acid (46.5 w/o). The vial is closed and wait for 2 ~ 3 hours until the solution is cool down.

$$LiOH + HF \longrightarrow LiF \downarrow + H_2O$$

iii) The vial is centrifugated to deposit the salt of LiF completely.

iv) Add 10 ml liquid scintillator (Aquazol-2) kept warm at 60°C. After then the solution becomes cloudy. The vial is closed.

v) Turn the vial upside down and shake it gently and carefully not to mix the LiF salt into the solution.

vi) Return the vial normal direction and let it settle down about 30 minutes. Then the solution becomes translucent gel and is ready for the sample to be measured by a liquid scintillator counting system.

In order to compare this method with the conventional method, the tritium production rates in a lithium blanket assembly were measured by both Li_2O and Li_2CO_3 pellets. Natural, enriched ^6Li and ^7Li pellets of Li_2O and Li_2CO_3 were manufactured from very high purity powder of Li_2CO_3. Total impurity in $^{N}Li_2CO_3$, $^6Li_2CO_3$ and $^7Li_2CO_3$ powder were less than 2.42, 175 and 93 ppm. Both Li_2O and Li_2CO_3 pellets were irradiated simultaneously in a lithium-oxide slab assembly at the distance of 10 and 20 cm from the front side along its central axis. (See 4.6) The size and weight of Li_2O and Li_2CO_3 pellets were 12 mmϕ x 2 mm, ~ 0.35 g, 13 mmϕ x 4 mm, ~ 0.85 g, respectively.

The results were summarized in Table 4.5.1. The experimental errors were 1 ~ 6 % for statistical one. The data of Li_2O agree well with those of Li_2CO_3 within the error. It was demonstrated that the liquid scintillation method using Li_2O pellet could be applied to the fusion blanket experiment.

Following items are the subject for a future study and in progress.

i) Evaluation of tritium that leaks from a pellet during the irradiation.

ii) Evaluation of tritium that is not left in the solution during chemical treatment.

iii) Effect of induced activity other than tritium.

Table 4.5.1 Comparison Between Li_2O and Li_2CO_3 Pellets

		Li_2O	Li_2CO_3	Li_2O / Li_2CO_3
10 cm	^7Li	4.555×10^{-29}	4.742×10^{-29}	0.961
	^6Li	1.469×10^{-28}	1.538×10^{-28}	0.955
	^{N}Li	5.588×10^{-29}	5.507×10^{-29}	1.015
20 cm	^7Li	1.377×10^{-29}	1.272×10^{-29}	1.083
	^6Li	8.346×10^{-29}	9.142×10^{-29}	0.913
	^{N}Li	1.878×10^{-29}	1.771×10^{-29}	1.060

* Unit : Tritium / Li atom · source neutron

4.6 Tritium Production-Rate Distribution in a 40 cm Li_2O Slab Assembly

H. Maekawa, K. Tsuda, T. Iguchi*, Y. Ikeda, Y. Oyama, T. Fukumoto and T. Nakamura

The size of Li_2O assembly was 31.5 cm in equivalent radius and 40.6 cm in thickness. The Li_2O bricks were made from Li_2O powder by cold pressing. Three types of blocks were made to sizes of 5.06 cm x 5.06 cm x 5.06 cm, 10.12 cm and 20.24 cm long. They were manufactured by sealing one, two and four bricks, respectively, in a 0.2 mm-thick stainless steel box. Density of Li_2O bricks was 75.5 % of the theoretical density. Lithium-oxide blocks were stacked to form a pancake cylinder in a frame composed by stacking thin-walled aluminum square tubes. The target was located at 10 cm from the front surface of the assembly on its central axis. An water-cooled 20 Ci Ti-T target was set at the end of 80° beam line in the large target room of the FNS. The deuteron beam energy and average beam current during the irradiation were 310 keV and 2 mA, respectively. The absolute neutron yield was estimated by counting the associated α-particles of the D-T reaction.

The tritium production-rate distributions along the central axis of the assembly were measured by the following three methods:

(1) Liquid scintillation counter method with Li_2O pellets. (See 4.5)

(2) Liquid scintillation counter method with Li_2CO_3 pellets.[1)]

(3) Self-irradiation method using LiF TLD.[2)]

In case of the third method, the result was not obtained because the TLDs were under self-irradiation. The size and weight of Li_2O and Li_2CO_3 pellets were 12 mmϕ x 2 mm, ~ 0.35 g and 13 mmϕ x 4 mm, ~ 0.85 g, respectively. Enriched ^6Li and ^7Li pellets of Li_2O and Li_2CO_3 were used to measure the reaction rate of $^6Li(n,\alpha)T$ and $^7Li(n,n'\alpha)T$, separately. The pellets were set at the small spaces between the Li_2O blocks along the central axis. Total neutron yields at the target were 5.18×10^{15} and 1.11×10^{16} for the irradiations of Li_2O and Li_2CO_3 pellets, respectively.

Preliminary analysis was carried out using the two-dimentional

* Faculty of Engineering, The University of Tokyo

transport code DOT3.5.[3] A 135-group cross section set used in the calculation was GICXFNS[4] obtained from ENDF/B-IV data file except the cross section of $^{7}Li(n,n'\alpha)T$. This cross section was taken from the data of P.G. Young evaluation.[5] The result of the Monte Carlo calculation was adopted as the input source neutron spectrum. (See 4.13.) The first collision source and P_5-S_{16} approximation were employed in this analysis.

The experimental results are shown in Fig. 4.6.1 with the calculated ones. The measured $^{6}Li(n,\alpha)T$ and $^{7}Li(n,n'\alpha)T$ reaction rates were estimated considering the atomic density of pellets. The systematic and statistical errors were ± 5.4 % and 1 ~ 15 %, respectively. The agreement for $^{7}Li(n,n'\alpha)T$ reaction is good within experimental error. For $^{6}Li(n,\alpha)T$ reaction, the distributions of experiment and calculation are resemble each other, however, there exist the differences of about 20 % in the absolute comparison. A simple survey calculation shows that the distribution of $^{6}Li(n,\alpha)T$ reaction rate near the surface of the target side is very sensitive to the source neutron spectrum below 1 MeV. Further investigations including the analysis by use of BERMUDA-2DN code[6] are in progress.

References

1) Dierckx R.: Nucl. Inst. Meth. 107, 397 (1973).
2) Maekawa H.: JAERI-M 6055 (1975) (in Japanese); UCRL-TRANS-11196 (1977).
3) Rhoades W. A. and Mynatt F. R.: ORNL/TM-4280 (1979).
4) Seki Y., et al.: JAERI-M 83-061 (1983).
5) Young P. G.: Trans. Am. Nucl. Soc., 39, 272 (1981).
6) Suzuki T. et al.: JAERI-M 82-190 (1982) (in Japanese); Sixth Int. Conf. on Radiation Shielding, May 16-20, 1983, Tokyo, Japan, 3b-3.

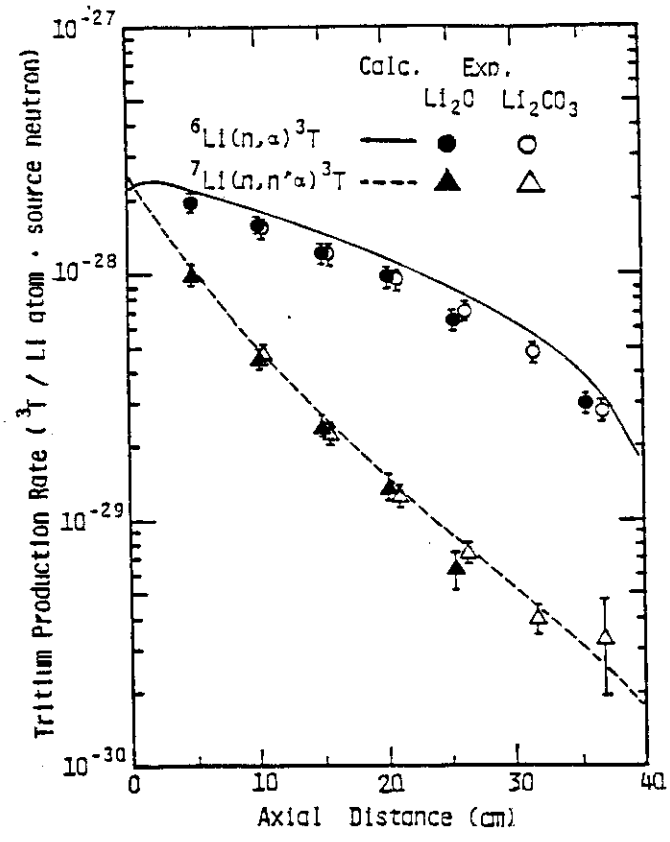

Fig. 4.6.1 Tritum production rate distribution in 40 cm Li_2O slab assembly

4.7 Reaction-Rate Distribution Measurement in a 40 cm Li_2O Slab Assembly by the Foil Activation Technique

Y. Ikeda, T. Fukumoto, H. Maekawa, Y. Oyama and T. Nakamura

As the integral experiment on fusion blanket neutronics, some reaction-rate distributions in a Li_2O slab assembly were measured by the foil activation technique. The size of the assembly was 31.5 cm in equivalent radius and 40.6 cm in thickness. Activation foils of Al, Ni, Nb, Zr and Au were set both inside and outside of the assembly. After an irradiation for 11.5 h by D-T neutrons the production rate of which was about 2 x 10^{11} n/sec, gamma-rays emitted from each produced activity were measured by using a 60 cm^3 Ge(Li) detector and reaction rates of $^{27}Al(n,\alpha)^{24}Na$, $^{58}Ni(n,2n)^{57}Ni$, $^{93}Nb(n,2n)^{92m}Nb$, $^{90}Zr(n,2n)^{89}Zr$, $^{197}Au(n,2n)^{196}Au$ and $^{197}Au(n,\gamma)^{198}Au$ were deduced by performing several corrections. Reaction-rates corresponding to the measured ones were calculated by the two-dimentional code, DOT3.5[1] and activation cross sections.[2),3)] The calculational conditions were the same as those in 4.6. In Fig. 4.7.1, reaction-rate distributions of $^{27}Al(n,\alpha)^{24}Na$ on the central and 20 cm off-central axes in the assembly are shown in comparison with the calculated ones. Concerning the distribution along the central axis, it can be seen that the calculation overestimated it slightly and the discrepancy increases as the distance from the front surface increases. In the cases of the 20 cm off-central axis, there is rather large overestimation near the front surface, but in the deeper region, the overestimation decreases. This may be caused by the angular distribution of the source neutron, which is strongly influenced by the target assembly structure, not taken into account in the calculations.

The distribution of $^{197}Au(n,\gamma)^{198}Au$ reaction rate is shown in Fig. 4.7.2. It can be seen that the calculation slightly overestimated it in the assembly. However, at both front and back surfaces, underestimations were observed and it may be due to room returned neutrons that were not considered in the calculation.

It is of interest to compare the results between the direct 14 MeV neutron component in the angle dependent leakage spectra and the high threshold reaction-rate distribution, such as $^{58}Ni(n,2n)^{57}Ni$. The

comparison was performed in a form of C/E. In Fig. 4.7.3, a comparison of C/E values between the leakage spectra and the $^{58}Ni(n,2n)^{57}Ni$ reaction rates is shown. It can be seen that as the angle becomes deeper, the C/E becomes larger. The tendencies of both C/E against to angles are similar each other. It can be said that the confidences of the independent measurements increase.

Further analysis will be performed by using the DOT3.5 code including the weighted angle dependent first collision source and by using other two-dimentional code, BERMUDA-2DN.[4)]

References

1) Rhoudes W. A. and Mynatt F. R.: "The DOT-3 Two Dimentional Discrete Ordinate Transport Code with Anisotropic Scattering," ORNL/TM-4280 (1979).
2) Kinsey R.: "ENDF/B Summary Documentation, BNL-NCS-17541 (ENDF-201), 3rd Edition (ENDF/B-V," available from the National Nuclear Center, Brookhaven Laboratory, Upton, N. Y. (July 1979).
3) Greenwood L. R.: "Extrapolated Neutron Activation Cross Sections for Dosimetry to 44 MeV," ANL/FPP/TM-115 (1978).
4) Suzuki T., et al.: "BERMUDA-2DN: A Two-Dimentional Neutron Transport Code," JAERI-M 82-190 (1982) (in Japanese).

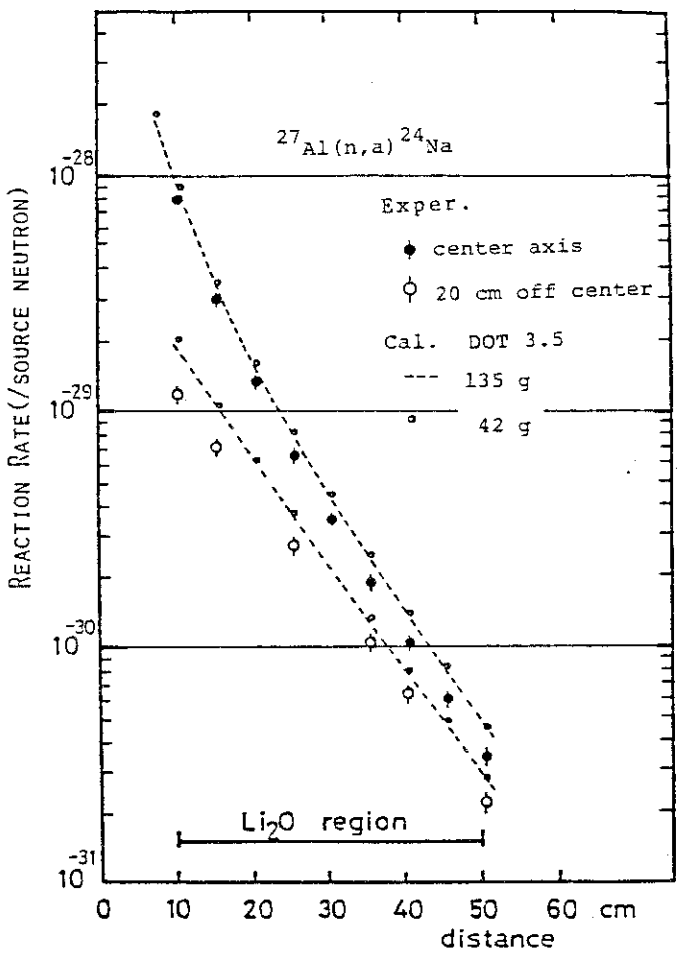

Fig.4.7.1
Reaction rate distribution of $^{27}Al(n,\alpha)^{24}Na$ in the Li_2O slab assembly

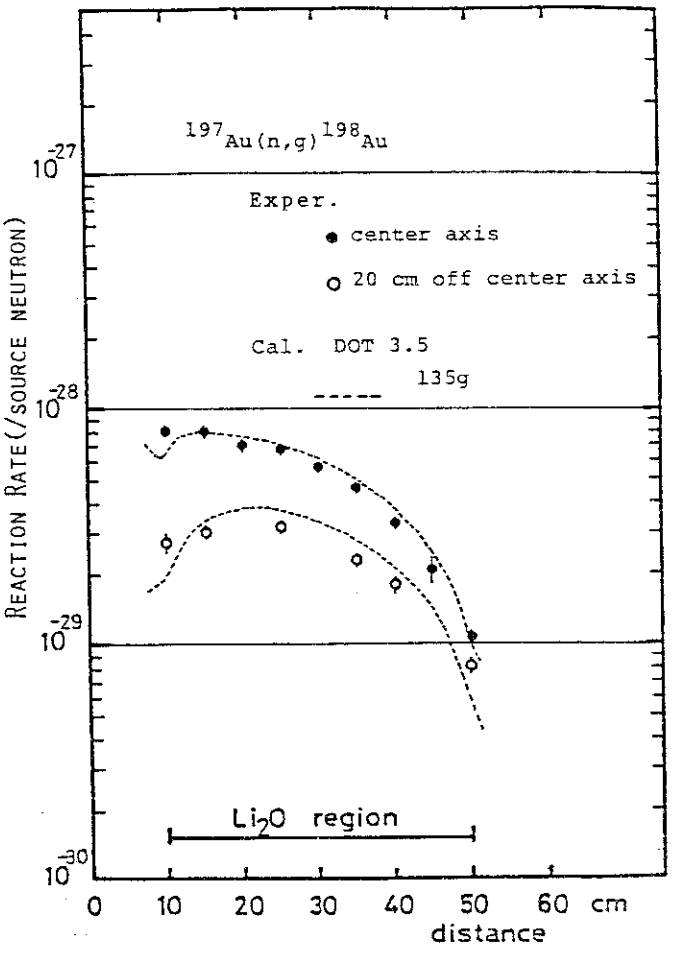

Fig.4.7.2
Reaction rate distribution of $^{197}Au(n,\gamma)^{198}Au$ in the Li_2O slab assembly

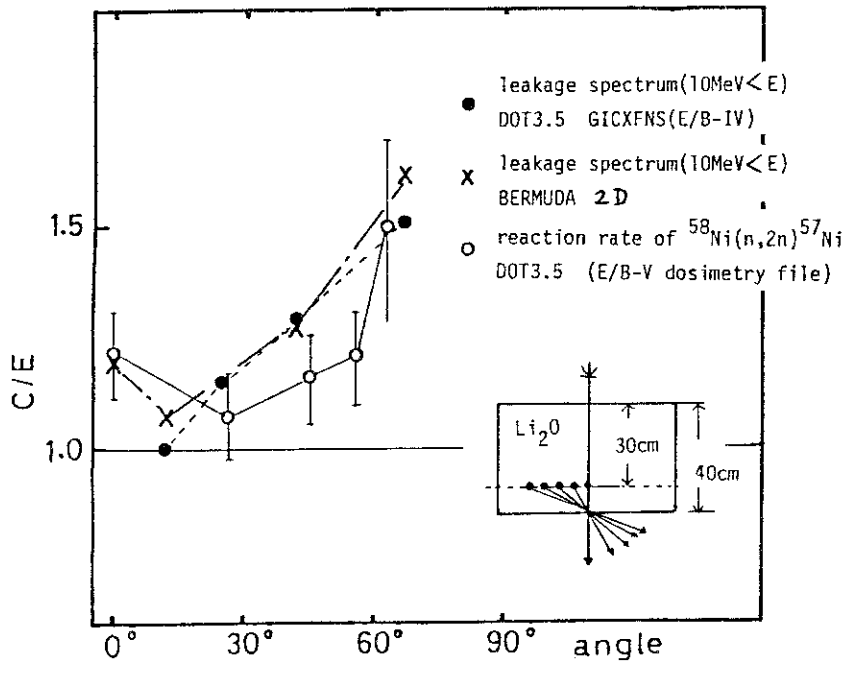

Fig. 4.7.3 Comparison of C/E of the direct 14 MeV neutron components

4.8 An Experimental Study of Induced Activity in the Type 316 Stainless Steel by D-T Neutron Fields

Y. Ikeda, Y. Seki, H. Maekawa, Y. Oyama and T. Nakamura

The induced activity in the structural materials of a D-T fusion reactor by 14 MeV neutrons is very important in terms of the following; (a) gamma-ray dose estimation for personnel access after reactor shutdown, (b) decay-heat after shutdown, (c) production of long-lived radioactive wastes. A code system THIDA has been developed in JAERI[1] for the calculation of exposure dose rate around a fusion device. It has been applied in the optimization of shielding in term of the personnel access and in the shielding design of INTOR.

Although there had been need for comprehensive comparison between predicted activation calculation and measurement to check the code system, experimental data for activation was limited.

Therefore, the activation and transmutation process in a type of 316 stainless steel (SS316) were examined by irradiation experiments using the intense 14 MeV neutron source FNS in order to verify the THIDA code system including its nuclear data library. The samples of SS316 were placed in three different well defined neutron irradiation fields. One sample was positioned at 10 cm from the target. There was no structural materials or assembly around the sample to avoid the perturbation of the neutron field. The second and the third samples were placed in the lithium oxide pseudo-spherical blanket assembly with a graphite reflector. One was located at 12.6 cm from the target and the other was at 22.6 cm, just at the boundary of Li_2O and C region. Samples were irradiated by 14 MeV neutrons with the source intensity of about 2.1×10^{11} n/sec. After irradiations, spectra of gamma-ray emitted from each sample were successively measured by using a 60 cm^3 Ge(Li) detector following cooling times from 10 min to about a month and each gamma-ray spectrum and relative dose were compared with those calculated by THIDA. A typical comparison of gamma-ray spectra is shown in Fig. 4.8.1. In this case, the sample was irradiated in the direct neutron field and measured after 6.9 hr cooling time. It is clearly seen that the dominant gamma-ray intensity is due to the decay of ^{56}Mn (2.579 hr) and its value comes to above 90 % of the total. In Table

4.8.1, C/E values of the total gamma-ray intensity and its relative dose are tabulated. In most cases, the calculated gamma-ray intensity and dose agree with measured ones within ± 15 %. The agreements are surprisingly good as regards requirements of the nuclear design in this stage, i.e., uncertainties of a factor or two should be acceptable.

Further investigations should be needed to confirm the validity of the THIDA code system concerning with long-lived activities in SS316 and with activities in different kinds of materials.

Reference

1) Iida H. and Igarashi M., " THIDA-Code System for Calculation of The Exposure Dose Rate Around a Fusion Device," JAERI-M 8019, (1978),

Table 4.8.1 C/E of total gamma-ray intensity and relative dose

ID. No	γ-ray	dose
SS16B1	0.967 ± 0.031	0.977 ± 0.031
SS16B2	0.956 ± 0.030	0.922 ± 0.029
SS16B3	0.931 ± 0.029	0.928 ± 0.029
SS16B4	1.076 ± 0.033	1.041 ± 0.032
S23U11	0.908 ± 0.036	0.886 ± 0.035
S23U12	1.137 ± 0.045	1.145 ± 0.046
S23U13	1.011 ± 0.031	1.022 ± 0.032
S23U31	1.236 ± 0.042	1.195 ± 0.041
S23U32	1.158 ± 0.037	1.072 ± 0.034
S23U33	1.034 ± 0.032	1.035 ± 0.032

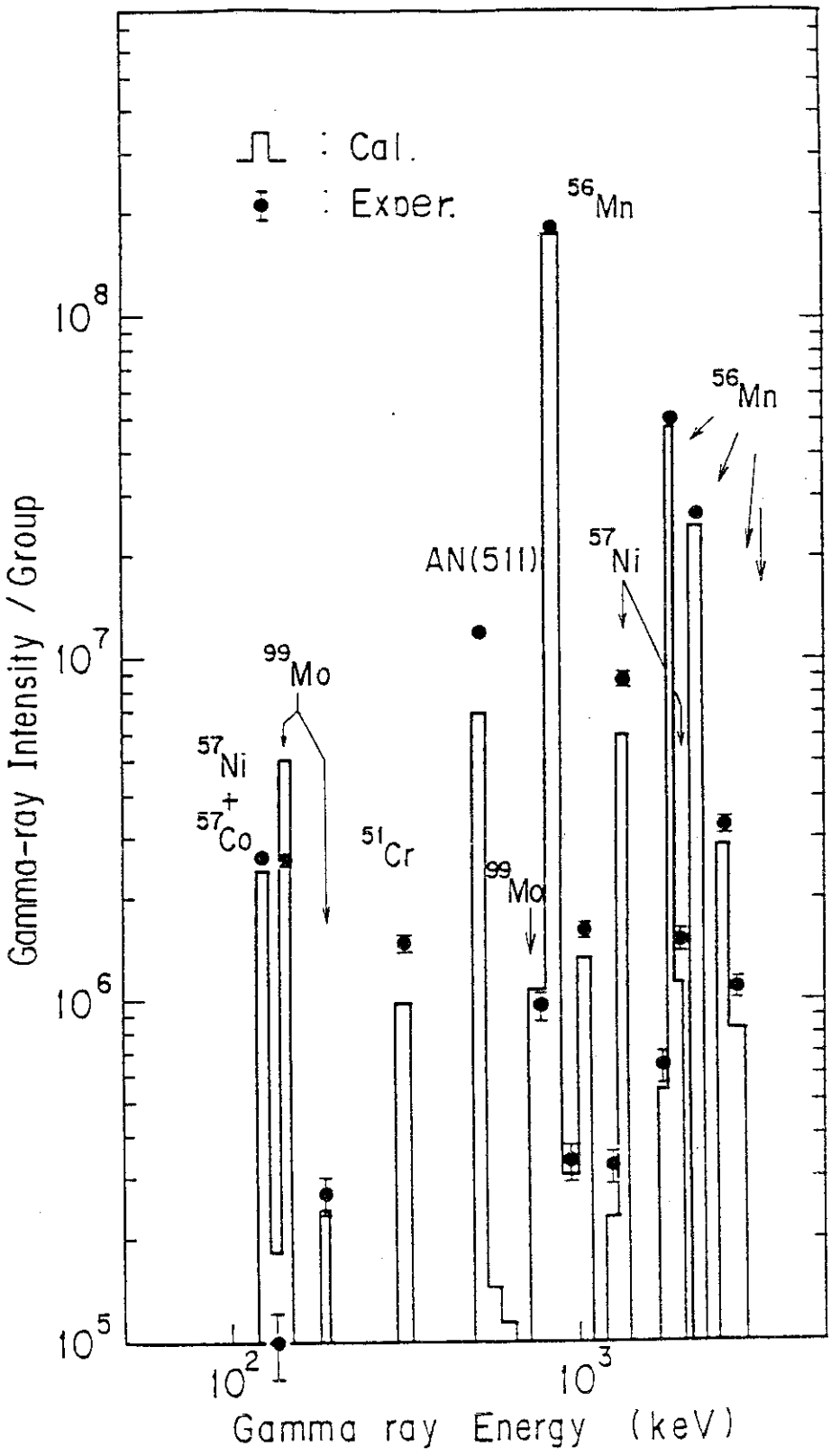

Fig. 4.8.1 Comparison of the gamma-ray spectra between the calculation and the measurement in the case of 6.7 hr cooling time. The irradiation position was at 10 cm from the target .

4.9 Measurement of Angle-Dependent Neutron Spectra from Lithium-Oxide Slab Assemblies by the Time-of-Flight Method

Y. Oyama and H. Maekawa

In the nuclear design of a D-T fusion reactor blanket, the tritium breeding ratio and the nuclear heating rate should be accurately predicted since they are essential to the overall design of a fusion reactor. The anisotropic scattering of neutrons with nuclei in the blanket material at high energy is emphasized by directivity of the neutron current from the core plasma to the blanket region. Thus the angular dependence of secondary neutrons plays an important role in the calculation, especially in the fusion neutronics. From this point of view, it is said that the reliability of the neutron transport calculations has not been verified enough.

Angle-dependent neutron spectra leaking from lithium-oxide assemblies were measured to provide the systematic benchmark data. The assemblies were made to a cylindrical slab to realize an appropriate calculational model. (Fig. 4.9.1) The measured area of angular fluxes were well-defined by a long neutron collimator.[1)]

The experimental configulation is shown in Fig. 4.9.2. The thicknesses of the assembly were 5.06, 20.24 and 40.48 cm. And the angles of 0, 12.2, 24.9, 41.8 and 66.8 degrees were selected out of the symmetrical S_{16} angular quadrature sets by the pre-analysis.[2)] The source neutrons of 15 MeV were produced in the interactions of 350 keV deuterons with 4 mg/cm^2 of Ti-T target. The measurement were carried out by using the time-of-flight (TOF) method with an NE213 liquid scintillator and the two-bias method.[3)]

The measured angle-dependent neutron flux, which was just equivalent to the angular flux given by a transport calculation, was defined by the following;

$$\Phi(r=0,\ z=20+\ell,\ \Omega,\ E_n) = \frac{C(E_n)}{\varepsilon(E_n)\cdot\Delta\Omega\cdot A_s\cdot S_n\cdot T(E_n)}$$

$$[\mathrm{n/sr\cdot cm^2\cdot unit\ lethargy\cdot source\ neutron}]\ ,$$

where

$\Phi(r=0,\ z=20+\ell,\ \Omega,\ E_n)$: angular flux per unit area for the neutrons of energy E_n and angle Ω at $(r=0,\ z=20+\ell)$,

$C(E_n)$: counts per unit lethargy for the neutrons of energy E_n,
$\varepsilon(E_n)$: detector efficiency for the neutrons of energy E_n,
ℓ : thickness of the slab assembly,
$\Delta\Omega$: solid angle subtended by the detector to the point on the surface of assembly ($\equiv A_d/L^2$),
A_d : counting area of the detector,
L : neutron flight path,
A_s : effective measured area defined by the detector-collimator system on the plane perpendicular to the collimator axis at the assembly surface ($r=0$, $z=20+\ell$),
S_n : source neutron yield obtained by the alpha monitor,
$T(E_n)$: attenuation due to air in the flight path.

The overall systematic errors of the obtained flux were estimated to be within + 5 % for the energy scale and - 2 ~ + 6 % for the quantity of flux. (Table 4.9.1) The results of experiment are to be published in JAERI-M report including graphs and numerical tables.

References

1) Oyama Y. et al.: JAERI-M 82-114 p.157 (1982).
2) Fukumoto T. et al.: private communication.
3) Oyama Y. et al.: JAERI-M 82-114 p.153 (1982).

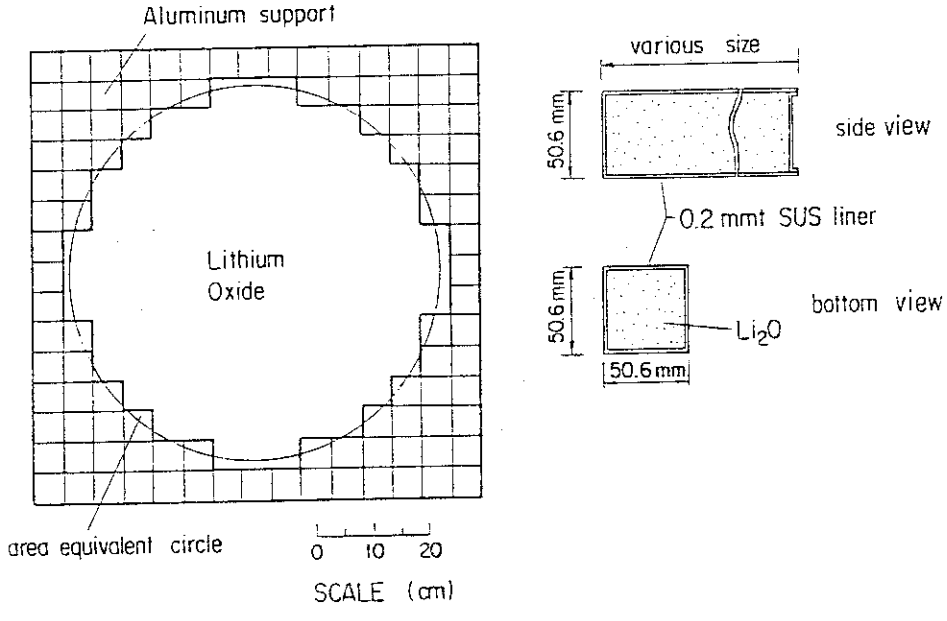

Fig.4.9.1 Pseudo-cylindrical Li_2O assembly and Li_2O block

Table 4.9.1 Uncertainty of experimental resalts

Energy Resolution

item	Assembly 5 cm	20 cm	40 cm
time resolution		±2 %	
emission time spread	±1 %	±3 %	±5 %

Energy Scale

item	Assembly 5 cm	20 cm	40 cm
time zero	+1 %	+3 %	+5 %

Flux

item	random	systematic
$\epsilon(E_n)\cdot S_n\cdot\Delta\Omega$	± 3 ∿ 5 %	< + 2 % *
A_s	± 0.5 %	< ± 2 %
$C(E_n)$	± 1 ∿ 20 %	< + 1 %
$T(E_n)$		negligible
density of Li_2O $		< + 1 %
overall	± 3 ∿ 20 %	−2 ∿ +6 %

* excluding the error due to the absolute source neutrons that is cancelled by using the experimental source in the calculation.

$ This error is not appropriate to include in the experimental value but it should be considered in the calculational flux.

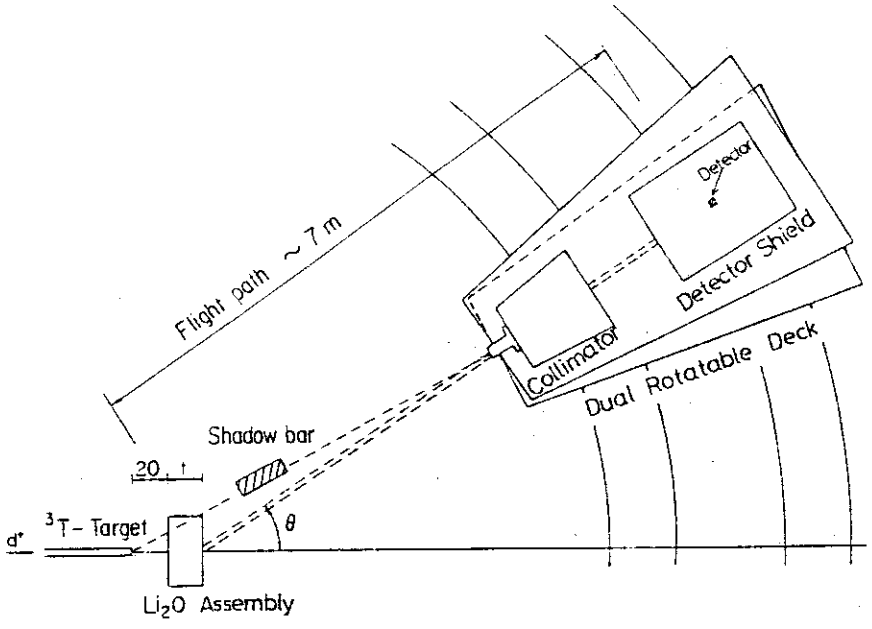

Fig.4.9.2 Experimental configulation

4.10 Analysis of Time-of-Flight Experiment on Lithium-Oxide Slab Assemblies by DOT3.5

Y. Oyama, S. Yamaguchi and H. Maekawa

The angle-dependent spectra of neutrons leaking from lighium-oxide slab assemblies were measured as a benchmark experiment. (See 4.9) In this work, the calculational analysis of the experiment was carried out. The purpose of the analysis was as follows:

(1) To examine the procedure for making comparison with the experimental results.

(2) To compare the results calculated by DOT3.5[1] with the experimental ones.

(3) To test the effect of cross section change of $^{7}Li(n,n'\alpha)T$ reaction taken from a new evaluation by P. G. Young.[2]

The calculational code was the two dimensional transport code DOT3.5. The measured source spectrum was used as input source and a first collision source (FCS) method was adopted. The group cross section set was GICXFNS[3] processed from ENDF/B-IV and V by the NJOY code.

The radial distribution of the calculated angular flux on the rear surface of assembly was investigated. The calculational flux was averaged with respect to the azimuthal angle and radial distance from the central axis over the area of 10 cm in diameter. (Fig. 4.10.1) The ratios of the angular flux at central position to the radial averaged flux are shown in Fig. 4.10.2. The averaged angular flux was reduced to be about 5 % compared with the flux at the center.

A typical result of 20 cm-thick assembly is shown in Fig. 4.10.3. The calculated spectra agree well with the experimental ones considering the absolute comparison. There exist, however, some differences partially. The cross section change of ^{7}Li affected spectral shapes little, but in the case of energy integrated comparison, the tendency was contrary to the experimental results. This result suggests that the elastic cross section of ^{7}Li should be re-evaluated. These results are to be published in JAERI-M report in detail.

References

1) Rhoades W. A., Mynatt, F. R.: ORNL/TM-4280 (1973).

2) Young P. G.: Trans. Am. Nucl. Soc., 39, 272 (1981).

3) Seki Y., et al.: JAERI-M 83-190 (1983).

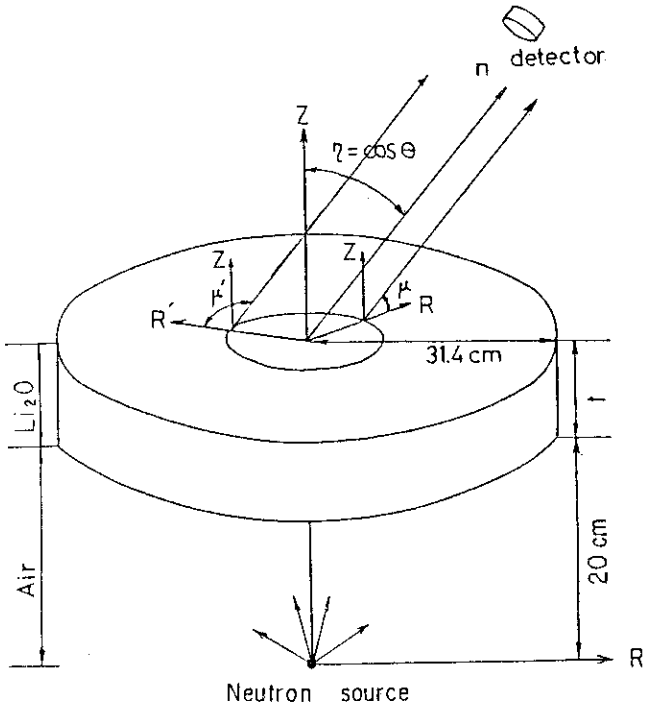

$$\langle\phi\rangle_{\mu} = \frac{\sum^{\mu} \phi(\eta,\mu)\omega_{\mu}}{\sum^{\mu} \omega_{\mu}}$$

$$\langle\phi\rangle_{\mu\cdot R} = \frac{\sum^{r} \langle\phi\rangle_{r} 2\pi r \Delta r}{\sum^{r} 2\pi r \Delta r}$$

Fig.4.10.1 The procedure of averaging the calculated flux to compare with the experimental one.

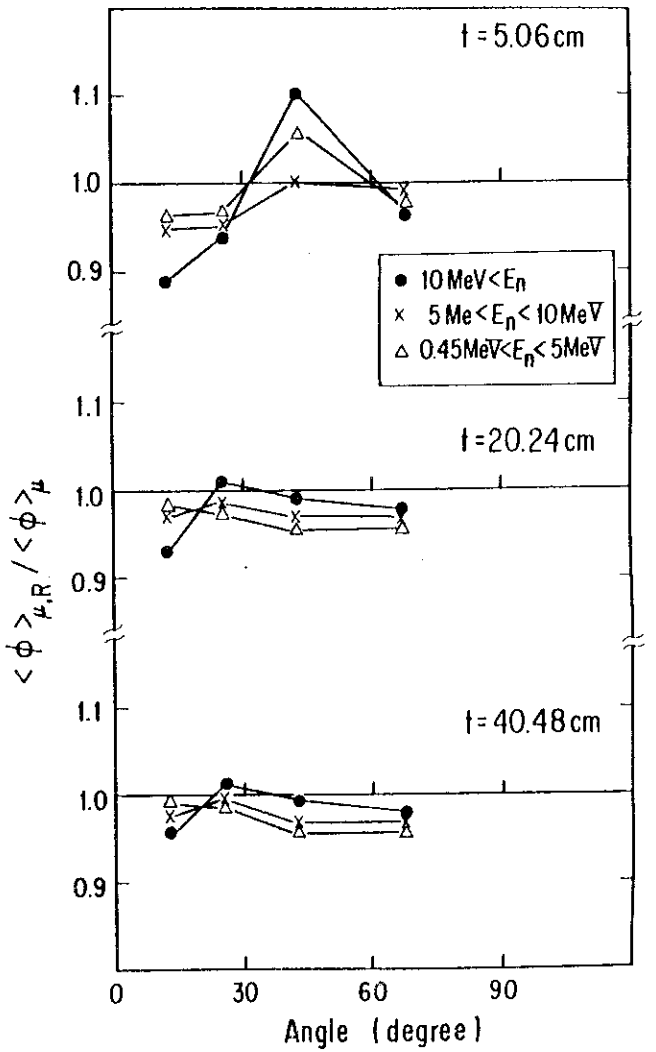

Fig.4.10.2 The effect of radial distribution of the angular flux.

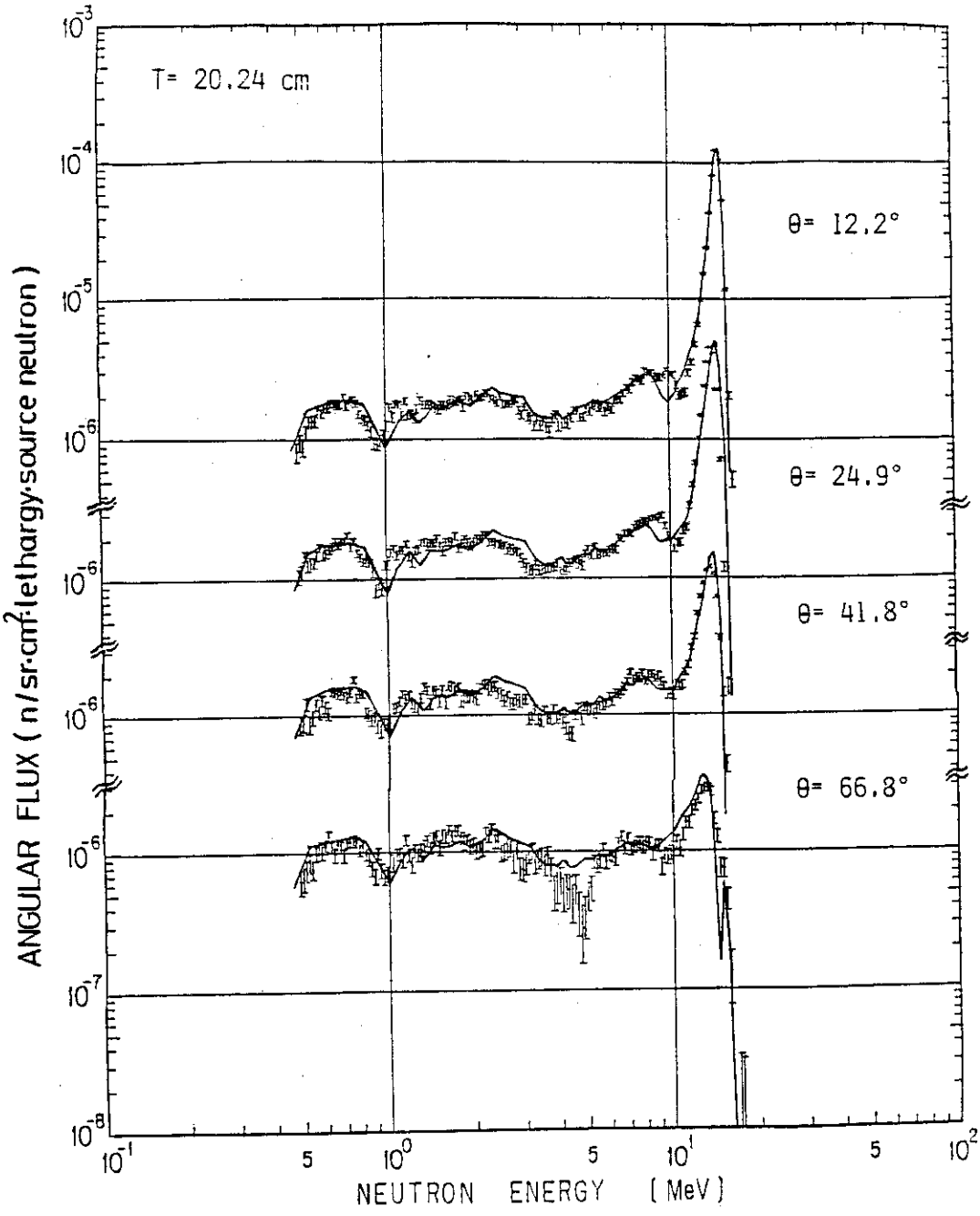

Fig.4.10.3 The typical comparison between the calculated and measured spectra.
The solid lines show the calculational results by DOT3.5.

4.11 Pre-Analysis on a Fusion Blanket Neutronics Experiment Utilizing an Experimental Hole of FNS Target Room #2

T. Fukumoto, T. Nakamura and Y. Seki

An integral experiment program on fusion neutronics has been proposed to obtain design-oriented data for a breeding blanket by utilizing intense 14 MeV neutrons and a modeled blanket module located in an experimental hole at the target room #2 of the FNS facility.(Fig. 4.11.1) A series of pre-analysis has been carried out on the basic system to examine feasibility of the program. The objectives of the present analysis are 1) to estimate the effects of the finite radial-dimension of the module and the incident neutron spectrum on the tritium production characteristics in the module and 2) hence, to examine how well the FNS module concept can approximate the neutronic property of the fusion reactor blanket.

The following items have been studied in this pre-analysis:

i) The radius of Li_2O module system at A of Fig. 4.11.1 was varied in steps from as-built 32.5 cm up to fictious 1 m, and tritium production rate (TPR) distributions were calculated and compared to see the influences of neutron leakage and inflow on the module. As an example TPR distributions of ^6Li and ^7Li in the radial direction of the module at the axial position of 290 cm from the target is shown in Fig. 4.11.2.

ii) The radial TPR distributions of a simplified fusion reactor blanket with and without first wall layer of 2 cm were calculated for comparison with the calculated TPR distribution along the central axis of the FNS module in order to examine the degree of approximation of the experiment. The results are shown in Fig. 4.11.3.

iii) A parametric calculation was carried out for the purpose of clarifing the effect of the spectral shape of input neutrons on the medium, i.e. Li_2O. TPR distribution in a infinite Li_2O slab of 80 cm thickness was calculated for the unit intensity source neutron beam of mono energy corresponding to each of the energy group in the cross section set GICX40[1] which was used in the present pre-analysis. Representative distributions are given in Fig. 4.11.4.

As the results of this pre-analysis, the following conclusions have been derived.

i) The radial size of the module is not large enough to be free from the boundary effect. The influence of neutron leakage from the Li_2O region affects the TPR on the central axis, especially for ^6Li, but the difference from the large system is within the range of correction with good accuracy. On the other hand, the effect of neutron inflow to the Li_2O region from the concrete region does not affect it.

ii) There is some difference in the spectral shape of incident neutron between the experimental system and the fusion blanket model. And the TPR distribution near the front face is sensitive to the spectrum of scattered, i.e., slowed down neutrons. Appropriate spectrum tailoring might be needed in the experimental arrangement and a correction by means of data and method will be required to some extent.

iii) Notwithstanding the fact mentioned above, it has been found that the simulation by the module represents fairly well the neutronic characteristics of fusion reactor blanket as a whole.

References

1) Seki Y. and Iida H.: "Coupled 42-group Neutron and 21-Group Gamma Ray Cross Section Set for Fusion Reactor Calculations," JAERI-M8818 (1980).

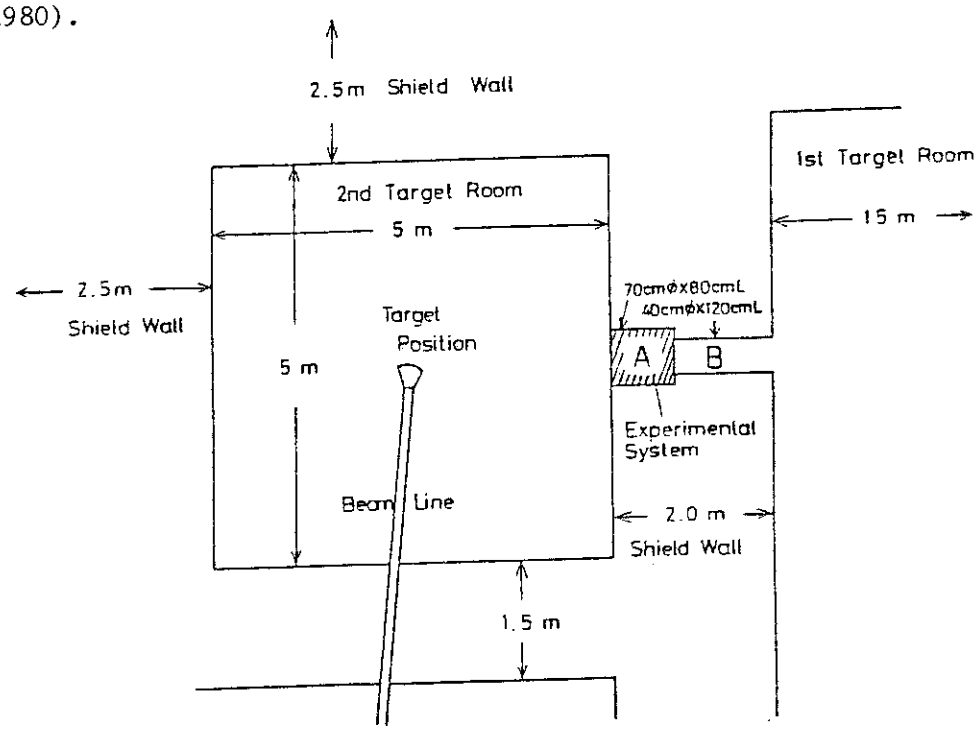

Fig.4.11.1 Experimental Arrangement

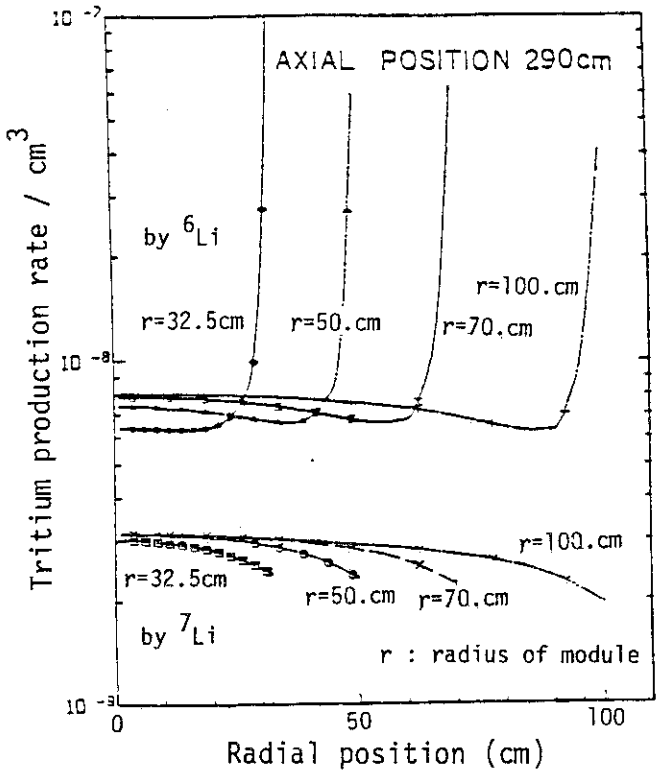

Fig.4.11.2 TPR distributions in the radial direction of the module

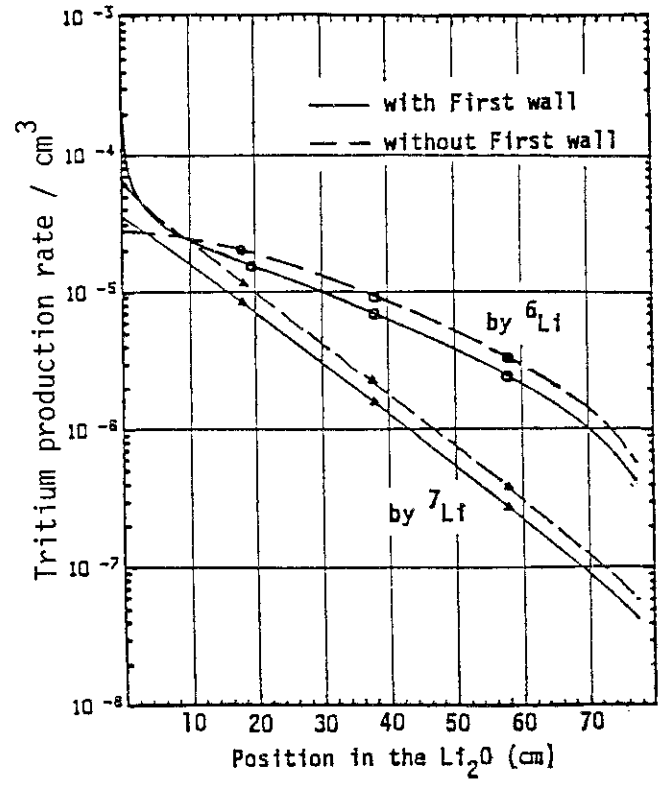

Fig.4.11.3(a) The radial TPR distributions of a simplified fusion reactor blanket model with and without first wall

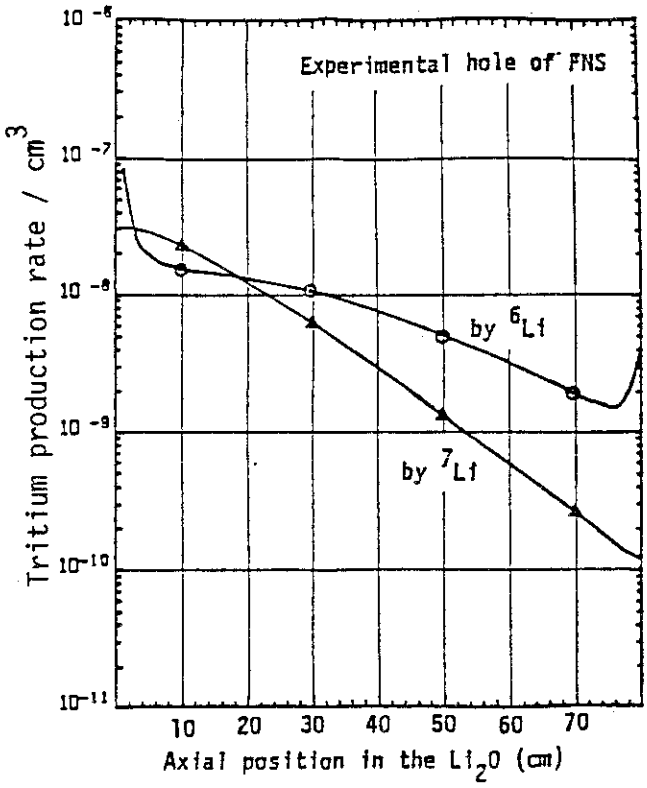

Fig.4.11.3(b) TPR distributions along the central axis of the FNS module

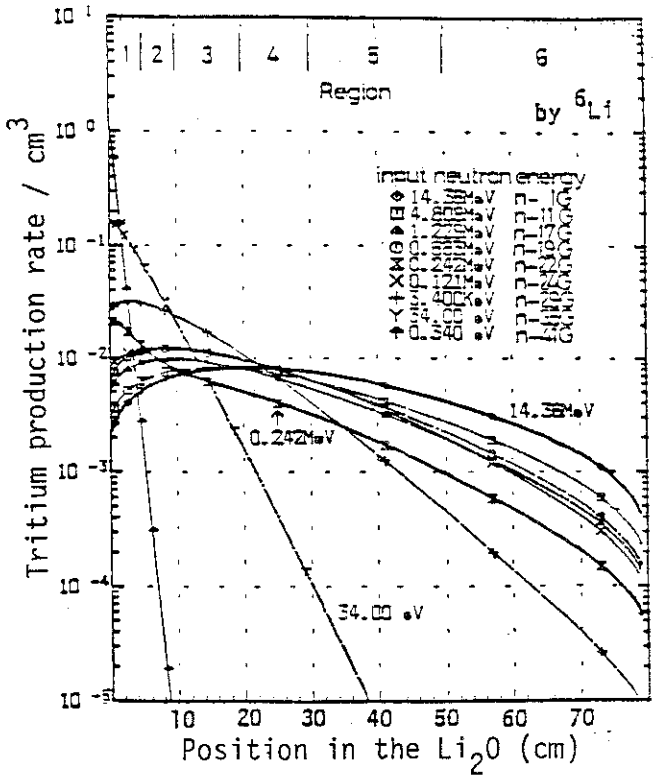

Fig.4.11.4 TPR distributions for nuit neutron sources corresponding to selected energy groups of GICX40 set

4.12 Calculation of Absolute Fission-Rate Distributions Measured in the Graphite Reflected Lithium Oxide Blanket Assembly[1)]

Y. Seki, H. Kawasaki*, H. Maekawa, Y. Oyama, Y. Ikeda and T. Nakamura

The fission-rate distributions of ^{232}Th, ^{238}U, ^{237}Np and ^{235}U have been measured in a pseudo-spherical graphite reflected lithium oxide (Li_2O-C) assembly in 1978.[2)] The 14 MeV neutrons were generated at the center of the assembly by the D-T reaction with a 300 kV Cockcroft-Walton type accelerator called PNS-A. The fission rates were calculated using the newly evaluated nuclide densities[3)] and current nuclear data.

Neutron transport in the Li_2O-C assembly was calculated using the one-dimensional discrete ordinates transport code ANISN[4)] with the P_5-S_{64} approximation. The assembly was modelled as a multi-layered sphere with fine mesh interval of about 0.5 cm in the Li_2O and graphite regions.

Neutron group cross sections for the 8 nuclides which constitute the Li_2O-C assembly were processed from the evaluated nuclear data files. For the nuclides other than ^{12}C and ^{7}Li, the nuclear data in ENDF/B-IV were used. For ^{12}C, the data in ENDF/B-V standard cross section library[5)] were used. As for ^{7}Li, the nuclear data in ENDF/B-IV was used with the following modification. The $^{7}Li(n,n'\alpha)T$ reaction cross section in the original ENDF/B-IV was replaced by the one recently evaluated by P. G. Young.[6)] In order to preserve the total cross section of ^{7}Li, the elastic cross section was also changed to compensate for the change introduced by the replacement of the $^{7}Li(n,n'\alpha)T$ reaction.

The 135-group neutron cross sections were processed from the above nuclear data using the NJOY code.[7)] The cross sections were made for the infinite dilution and at 300°K. Constant flux weighting was used to derive group cross sections from point wise data. In order to calculate the fission rates, the 135-group fission cross sections of ^{232}Th, ^{238}U, ^{237}Np and ^{235}U were also calculated using NJOY under the same calculational condition. In addition to the 135-group neutron cross

---

* Century Research Center Corporation Ltd.

sections, the 100-group cross sections prepared for the preliminary analysis[2] was also used with some modifications to calculate the fission rates.

As a result, the calculated and measured fission rates mostly agreed within the estimated experimental error. The agreement is particularly good in the Li_2O region indicating the validity of the calculated neutron spectra in the region. The calculation underestimates the ^{232}Th fission rate in the graphite region as shown in Fig. 4.12.1. The calculation overestimates the ^{235}U fission rate by about 15% in the graphite region near the Li_2O region. (Fig. 4.12.2)

References

1) Seki Y. et al.: JAERI-M 28-114 (1983).
2) Maekawa H. et al.: J. Nucl. Sci. Technol., 16[5], 377 (1979).
3) Maekawa H., Seki Y.: J. Nucl. Sci. Technol., 19[9], 771 (1982).
4) Engle W. W. Jr.: K-1693, Computing Technology Center, Union Carbide Corporation (1967).
5) Fu C. Y., Perey F. G.: "New Evaluation of C for Version V, MAT 1306," Oak Ridge National Laboratory (1979).
6) Young P. G.: Trans. Am. Nucl. Soc., Vol.39, 272 (1981).
7) MacFarlane R. E. et al.: LA-7584-M (ENDF-272) (1978).

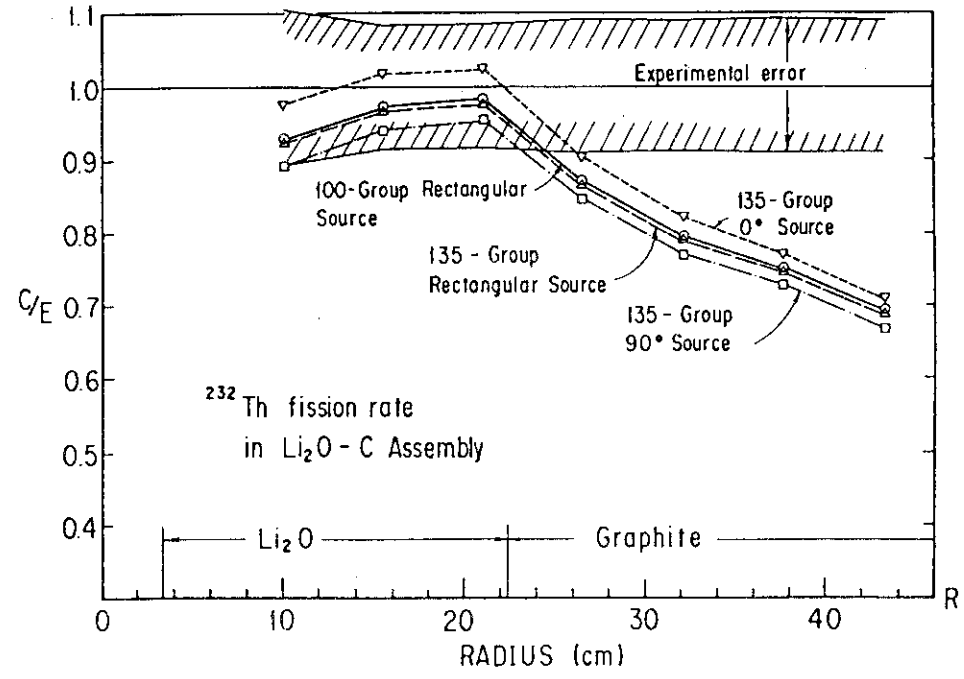

Fig. 4.12.1 Ratio of calculated to experimental C/E values of ^{232}Th fission rate in Li_2O-C Assembly

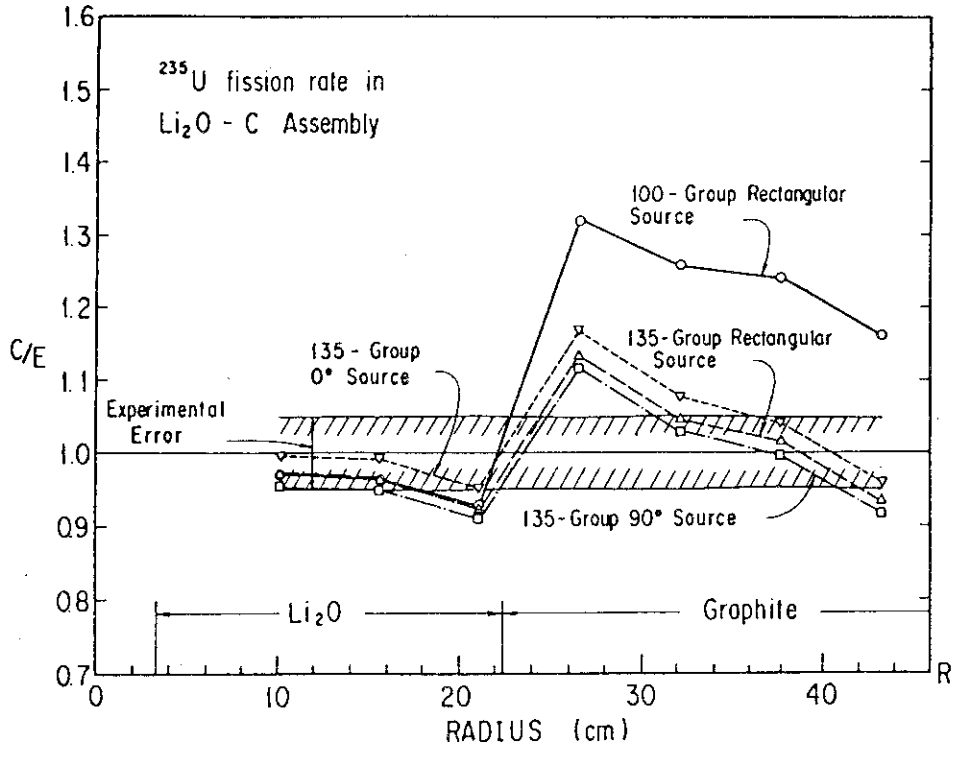

Fig. 4.12.2 Ratio of calculated to experimental C/E values of ^{235}U fission rate in Li_2O-C Assembly

4.13 Monte Carlo Calculations of the Source Characteristics of the FNS Water Cooled Type Tritium Target[1)]

Y. Seki, Y. Oyama, T. Ikeda, S. Tanaka, H. Maekawa, T. Nakamura and H. Kawasaki*

The source characteristics of a water cooled target of the FNS have been calculated using a three dimensional Monte Carlo method.

The Monte Carlo radiation transport code MORSE-GG[2)] was used to calculate the neutron transport and secondary gamma-ray emission and transport in the target assembly. Macroscopic cross sections for the copper backing, stainless steel structure and cooling water, in the form of 28-group neutron and 7-group gamma ray (28n-7γ) coupled cross section, were used in the calculations. The 28n-7γ cross sections have been derived by collapsing the 135n-21γ cross sections with the flux weight obtained by the one dimensional ANISN calculation,[3)] using a spherical model of the target assembly. The 135n-21γ coupled cross sections have been processed from the ENDF/B-IV nuclear data file by the NJOY code system[4)] and the GAMLEG-JR code.[5)]

The results of the calculations were compared with the measured ones[6)] and the following conclusions have been obtained.

(1) Good agreement was obtained in the calculated and measured angular distributions of the activation reaction rates of $^{27}Al(n,\alpha)^{24}Na$ and $^{56}Fe(n,p)^{56}Mn$.

(2) The angular distribution of neutrons measured with the time-of-flight method was in reasonable agreement with the calculated one when the systematic errors in the measurement and the difference in detector configurations for the calculation and measurement are considered.

(3) Fairly good agreements between measurement and calculation have been obtained for the neutron energy spectra in the forward direction to the beam line as shown in Fig. 4.13.1. As regards the neutron spectra at other angles, some discrepancies in the shape of the source peak and the calculational overestimation of the

---

* Century Research Center Corp. Ltd.

neutrons below 1.7 MeV were observed. (See Fig. 4.13.2) The calculational overestimate is partly attributed to the fact that the portion of the target assembly seen by the detector used in the measurement is different from that used in the calculation. The discrepancy in the shape of the source peak is caused by the inappropriate pulse shaping in accelerator operation.

(4) The largest discrepancy has been observed between the measured and calculated spectra of neutron induced gamma rays in the target assembly. Although the gamma-ray production cross section data is speculated to be the cause of this discrepancy, further investigation is required.

References

1) Seki Y., et al.: To be published in J. Nucl. Sci. Technol.
2) Straker E. A., et al.: ORNL-4585 (1970).
3) Engle W. W., Jr.: K-1693, Computing Technology Center, Union Carbide Corporation (1967).
4) MacFarlane R. E., et al.: LA-9303-M, Vol. I and II (ENDF-324), (1982).
5) Miyasaka S., et al.: JAERI-M 6936 (1977).
6) Ikeda Y., et al.: JAERI-M 82-114, 165 (1982) also Ikeda, Y., et al.: To be published as JAERI-M Report.

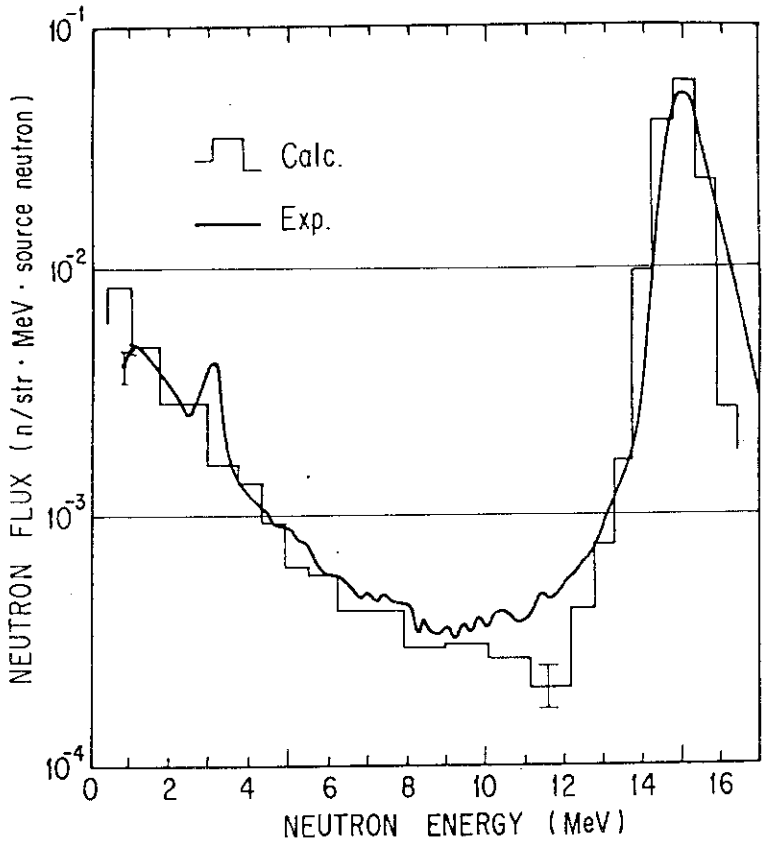

Fig. 4.13.1 Calculated and measured source neutron spectra at 0° to the deuteron beam

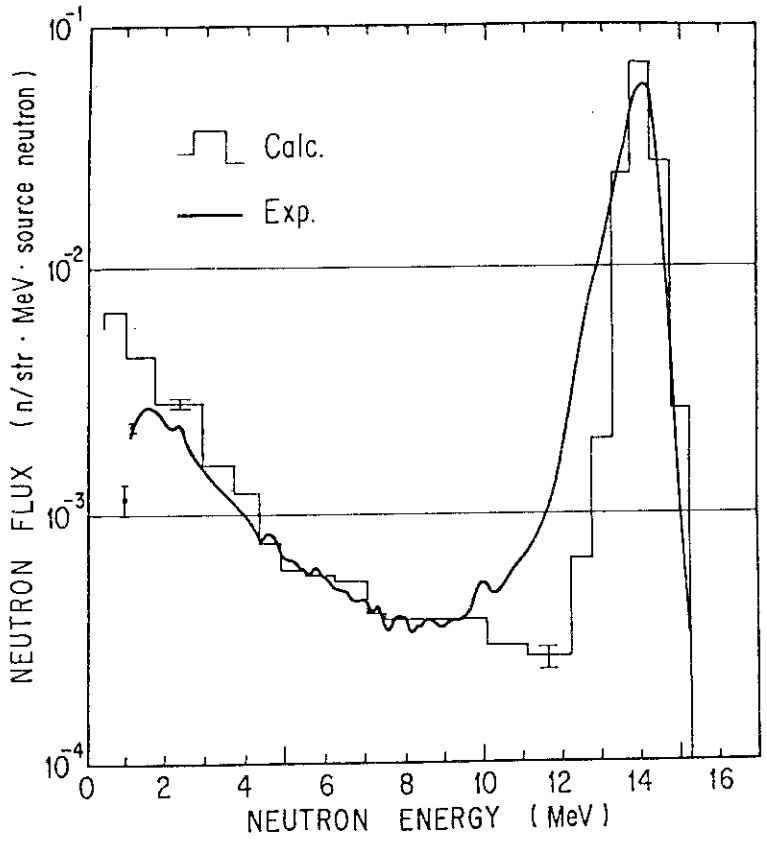

Fig. 4.13.2 Calculated and measured source neutron spectra at 90° to the deuteron beam

4.14 A Calculation of Anisotropy Factor for Determination of D-T Neutron Yield by the Associated Particle Method

S. Yamaguchi, Y. Oyama and H. Maekawa

As the neutron yield monitor in the FNS, the associated α-particle method is adopted. The absolute total neutron yield Y_n is given by the relation;

$$Y_n = \frac{4\pi}{\Delta\Omega_\alpha} C_\alpha R_\alpha(E_d, \theta_\alpha) \quad , \tag{1}$$

where C_α is the α count, $\Delta\Omega_\alpha(\theta_\alpha)$ the solid angle subtended by the α counter, R_α the anisotropy factor, E_d the incident deuteron energy, θ_α the angle at which the α detector is placed to the incident deuteron beam. (See Fig. 4.14.1)

The expression for the anisotropy factor is derived as follows;[1)]

$$R_\alpha(E_d, \theta_\alpha) = \frac{\int_0^{E_d} (\frac{d\sigma}{d\omega'}) / (\frac{dE}{dx})_{Ti\text{-}T} \, n_T(x(E))dE}{\int_0^{E_d} (\frac{d\sigma}{d\omega'}) / (\frac{dE}{dx})_{Ti\text{-}T} \, (\frac{d\omega'}{d\omega})_\theta n_T(x(E))dE} \quad , \tag{2}$$

where $(d\sigma/d\omega')$ is the differential cross section of D-T reaction in the center-of-mass system,[2)]

$(dE/dx)_{Ti\text{-}T}$ the stopping power of deuteron in a Ti-T target,

$(d\omega'/d\omega)_\theta$ the solid angle conversion factor from the center-of-mass system to the laboratory system,

$n_T(x(E))$ the tritium distribution with depth in a Ti-T target.

To determine the neutron yield accurately, it is necessary to estimate the value of the anisotropy factor correctly. Calculations herein were carried out to examine the uncertainty of anisotropy factor R_α.

The effect of difference between old stopping power data[1)] and recent Ziegler's one[3)] on the anisotropy factor was examined. Calculation shows that there is only a 0.3 % change in $R_\alpha(E_d$=400 keV, θ_α=179.1°) in spite of a 30 % change in the stopping power.

The relativistic effect was examined. It was proved that the change in R_α was only 0.2 % when the nonrelativistic kinematics was replaced by the relativistic one to calculate the solid angle conversion factor.

The tritium distribution with depth in the target was assumed constant in the absence of any other information. It is necessary to consider the tritium depletion by bombardment of deuteron beam. Experiments[4] show that the depletion is most severe at the end of the range of deuterons. Then calculations were done for a model shown in Fig. 4.14.2. This model was determined considering the result of Ref. 4). The calculated results are summarized in Table 4.14.1. They show that the tritium depletion reduces the value of $R_\alpha(E_d$=400 keV, θ_α=179.1°) about 3 %.

From these calculations, it is concluded that the anisotropy factor has uncertainty of about 3 % mainly due to the tritium depletion caused by the bombardment of deuteron beam.

References

1) Benveniste J. and Zengen J.: UCRL-4266 (1954).
2) Liskien H. and Paulsen A.: Nuclear Data Tables 11, 569 (1973).
3) Andersen H. H. and Ziegler J. F.: "The Stopping Power and Ranges of Ions in Matter Vol. 3," ed. Ziegler J. F., Pergamon, New York (1977).
4) Davis J. C. and Anderson J. D.: J. Vac. Sci. Technol., 12 (1975).

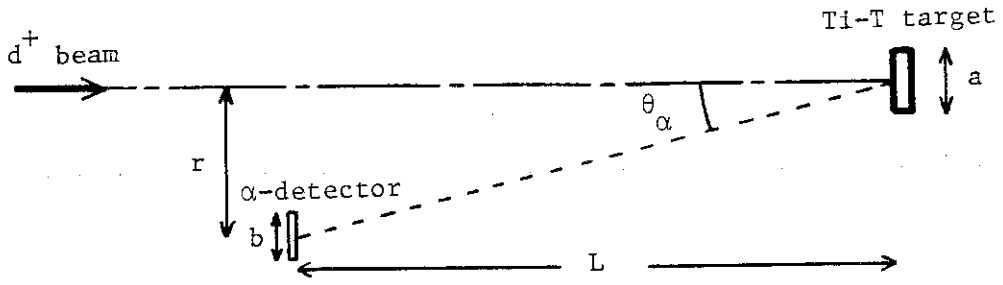

Fig. 4.14.1 Arrangement of Ti-T target and α-detector

(a=20±5, b=0.9835±0.0054, r=25±5, L=1578±1 (mm))

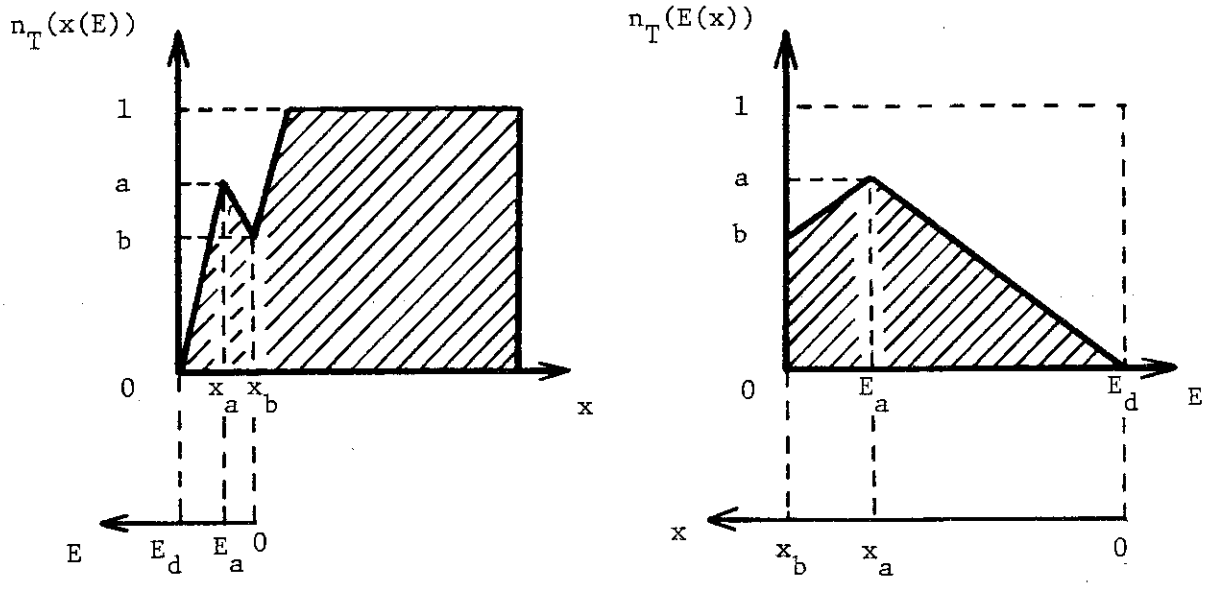

Fig. 4.14.2 A model of tritium depth profile

(E_d=400 keV, x_b=1.6 mg/cm^2, x_a=1.0 mg/cm^2, E_a=100 keV)

5. Shielding

5.1 Shielding Experiments for a Shielding Safety Evaluation Code System of Spent Fuel Transport Cask

S. Tanaka, A. Yamaji*, M. Adachi++, Y. Sakamoto+, J. Katakura+, Y. Naito+ and T. Yamahara+++

Shielding experiments of spent fuel transport casks were carried out according to the experimental plan to confirm the reliability of a shielding safety evaluation code system. The purpose of this experiment is to obtain the data which are available for examining the reliability of a shielding calculation code system and nuclear data libraries. The whole experimental plan is composed of three items concerning the PWR and the BWR spent fuels, that is

1) the experiments to assess the gamma-ray and neutron source intensity of the spent fuel,
2) the experiments to confirm the modeling technique of the source geometry composed of spent fuel assemnlies, and
3) the experiments to evaluate overall shielding calculations of the spent fuel transport cask in a three-dimensional geometry.

Two kinds of experiment have been already performed for PWR spent fuel assemblies according to the plan.

One[1] is the experiment on the item 1) and 2), in which three spent fuel assemblies of the PWR with the burn-up of 8400 MWD/t, 18000 MWD/t and 36000 MWD/t were used. Distributions of gamma-ray dose rate, fission rates of $^{235}U(n,f)$ and $^{232}Th(n,f)$ reactions around each assembly in the water pool were measured. Similar measurement was made for a combination of the three fuel assemblies arranged in a L-shape. Through these experiments, it was found that the neutron intensity is dependent strongly on the burn-up of fuel assemblies. The multiplication of neutrons was also observed for a combination of the three spent fuel assemblies.

---

* Ship Research Institute
+ Department of Nuclear Safety Evaluation , JAERI
++ Department of Research Reactor Operation, JAERI
+++ Department of Reactor Fuel Examination , JAERI

The other[2] is the experiment on the item 3). The NH-25 spent fuel transport cask was used, in which a fuel assemby of 36000 MWD/t burn-up used for the earlier experiment was contained. Measurements of the distributions outside the cask placed vertically were performed in detail for the gamma-ray dose rate, neutron dose equivalent rate, reaction rates of $^{3}He(n,p)$ and $^{235}U(n,f)$ reactions in an atomosphere. Energy spectra of gamma rays and fast neutrons were also measured at several positions outside the cask using a NE213 scintillation detector. Secondary gamma rays above the energy of a few MeV were observed clearly outside the cask. Furthrmore, distributions of gamma-ray dose rate and fission rates of $^{235}U(n,f)$ and $^{232}Th(n,f)$ reactions were measured inside the cask set in the water pool. The attenuation of gamma-ray dose rate was also measured in the lid of the cask.

Figure 5.1.1 show a vertical cross-sectional view of the NH-25 transport cask containing a PWR spent fuel assembly. Figure 5.1.2 is an example of the measurements of gamma-ray dose rate and neutron dose equivalent rates around the cask.

References

1) Tanaka S. et al. : "Experiments for the Assessment on Source Geometry of PWR Spent Fuel Assembly," JAERI-M 82-202 (1982).
2) Tanaka S. et al. : "Shielding Experiment of a Spent Fuel Transport Cask for a PWR Spent Fuel Assembly," JAERI-M 82-201 (1982).

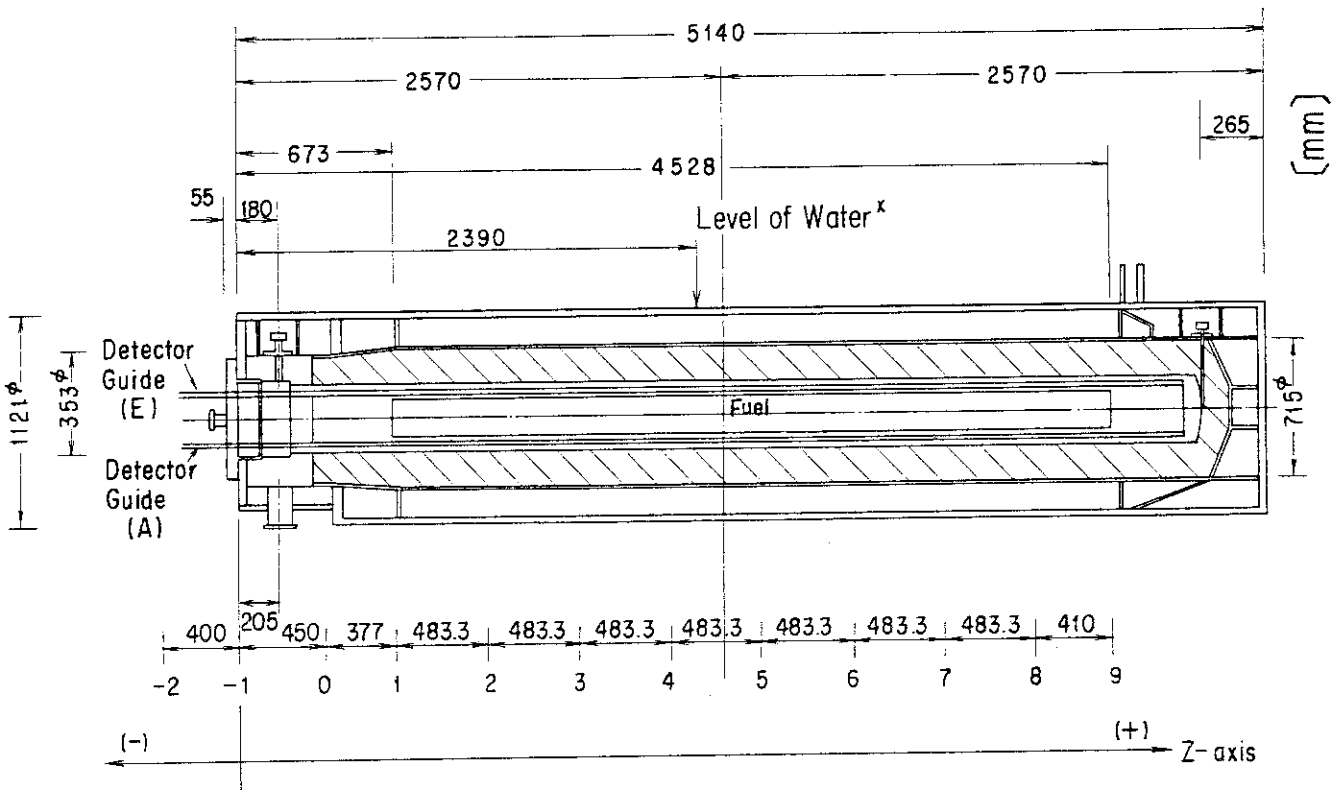

Fig.5.1.1 A cross sectional view of the NH-25 transport cask containing a PWR fuel assembly

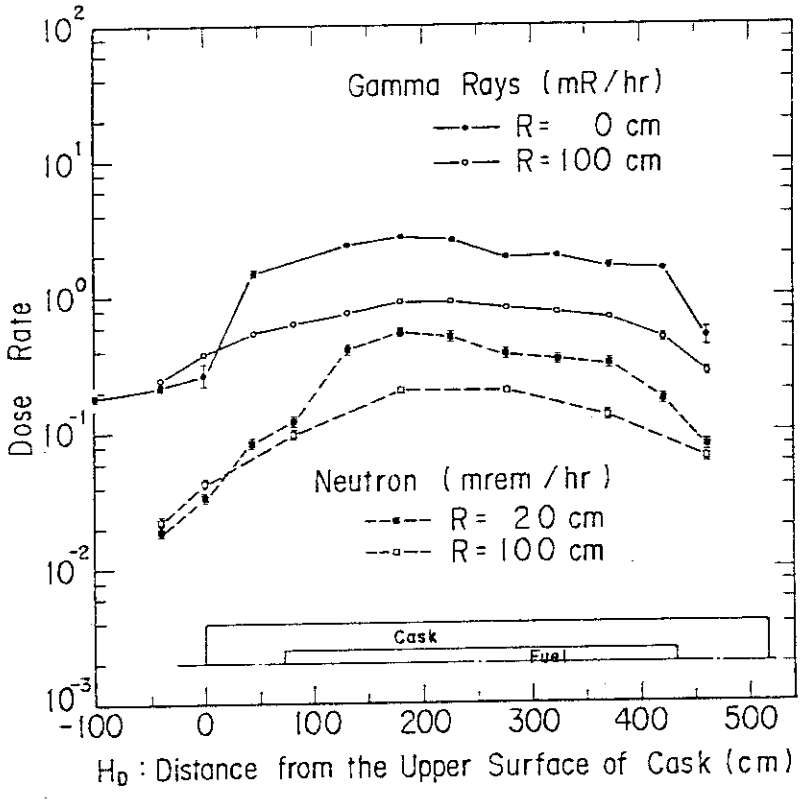

Fig.5.1.2 Distribution of gamma-ray and neutron dose rates around the cask

5.2 A Study on Direct Integration Method for Solving Neutron Transport Equation in Three-Dimensional Geometry

N. Sasamoto

A numerical method was established for solving neutron transport problems in the three-dimensional (X,Y,Z) geometry[1),2)] based on the method of direct integration of the transport equation.[3)] Several new techniques have been implemented into the method to make it well adopted to practical neutron transport calculations in the three-dimensional geometry. Use of a functional approximation for spatial distribution of the source term with a combination of linear and exponential functions enables one to perform calculations with coarse spatial mesh intervals keeping the results accurate. In addition, a technique for evaluating the scattering source based on an estimated spectral shape in each material region allows use of coarse energy mesh intervals without reducing calculational accuracy as compared with the calculation using fine meshes.

Theoretical analysis of the error in the direct integration method was made, on a basis of the theory by Lee and Vaidyanathan.[4)] As a result, it was revealed that the original method with a source term representation by a linear or an exponential function has a leading error of Δ^3 (Δ denotes a spatial mesh interval), which is the same order as that of the diamond difference scheme in the Sn method. In order to improve the mathematical error, we introduced in the present study a scheme with the source distribution approximated by a quadratic function, which is found to have a leading error of the order of Δ^4.

Based on the present method, the neutron transport code in the three-dimensional (X,Y,Z) geometry, PALLAS-XYZ, was developed. Validity of the present method was confirmed by calculating the following three neutron transport problems (Problems I, II and III).

Problem I is the pool critical assembly (PCA) benchmark experiments made at the Oak Ridge National Laboratory. The calculated neutron fluences greater than 0.1 and 1.0 MeV, the dpa (displacement per atom), and the reaction rates of fast neutron threshold reactions were compared with experiments. The comparison shows that the PALLAS-XYZ calculations were seen to agree with the experiment on reaction rate with a maximum

deviation of 30 %, and to agree well with the experiment in the integral fluxes and the dpa, within the range of experimental error.[5]

Problem II is an experiment of neutron streaming through an annular duct, performed at the swimming pool-type reactor JRR-4 (JAERI).[6] Comparisons were made of the PALLAS-XYZ calculated $^{58}Ni(n,p)$ reaction rate distribution along the annular duct, with the experiment and with the three-dimensional Sn code ENSEMBLE calculation by an approximation of S4/P1.[7] As a result, the PALLAS-XYZ calculation was found to somewhat overestimate the experiment at the duct mouth and underestimate it in the vicinity of its exit, whereas the ENSEMBLE calculation shows a more rapid decrease within the annular duct than the PALLAS one.

Problem III is to estimate the detailed neutron fluence in the reactor pressure vessel of a typical 1000 MWe class PWR power reactor with a vessel inner radius of 220.28 cm.[8] Neutron transport calculations were made for various models of a 1000 MWe class PWR with PALLAS codes in combined (X,Y,Z) + (R,θ), (R,θ) and (R,Z) geometries to obtain azimuthal variation for the integral fluxes above 1.0 and 0.1 MeV, and dpa. We obtained an azimuthal peaking factor of about 2.7 at 40° in the integral fluxes above 1.0 and 0.1 MeV, and the dpa at the inner surface of the pressure vessel. Furthermore, it was pointed out that the transport calculation in the (X,Y,Z) geometry is a standard tool for evaluating the angular flux leaking from the (X,Y,Z) geometrical core, from which the neutron fluxes are determined in terms of absolute value at various positions outside the core.

References

1) Sasamoto N.: "A Study on Direct Integration Method for Solving Neutron Transport Equation in Three-Dimensional Geometry," JAERI-M 82-167 (1982).
2) Sasamoto N. and Takeuchi K.: Nucl. Sci. Eng., 80, 554 (1982).
3) Takeuchi K. and Sasamoto N.: Nucl. Sci. Eng., 80, 536 (1982).
4) Lee S. M. and Vaidyanathan R.: Nucl. Sci. Eng., 76, 1 (1980).
5) McElroy W. N., et al.: "LWR Pressure Vessel Surveillance Dosimetry Improvement Program: PCA Experiments and Blind Test," NUREG/CR-1861 (HEDL-TME 80-87, R5), Hanford Engineering Development Laboratory (1981).
6) Miura T., Takeuchi K. and Fuse T.: "Measurement and Calculation of

Radiation Streaming Through Annular Ducts," Report of Ship Research Institute, 16, 6 (1979) (in Japanese).

7) Nishimura T., Tada K., Yokobori., and Sugawara A.: J. Nucl. Sci. Technol., 17, 539 (1980).

8) Takeuchi K. and Sasamoto N.: to be published in Nucl. Technol.

5.3 Development of the BERMUDA Code System

T. Suzuki, A. Hasegawa, T. Mori and T. Ise

Since 1979 the development work of the transport code system BERMUDA has been carried out in the Shielding Laboratory to analyze blanket neutronics experiments performed with the Fusion Neutronics Source (FNS), and to establish an accurate and efficient shielding analysis system for fusion and fission reactors.

In 1980, developed was a one-dimensional neutron transport code BERMUDA-1DN (renamed from PALLAS-TS[1]) for plane and spherical geometries, and then in March of 1982, a two-dimensional (r,z) neutron transport code BERMUDA-2DN was completed.[2] The BERMUDA-2DN was satisfactorily verified in 1982 through the benchmark test using the measured leakage spectra from Li_2O slab assemblies at Fusion Reactor Physics Laboratory.[2),3)]

In March of 1983, a three-dimensional (x,y,z) neutron transport code BERMUDA-3DN has been programed in FORTRAN source program, though being debugged now. As for gamma-ray transport code, a one-dimensional code BERMUDA-1DG commences to be programed. In addition, a one-dimensional adjoint neutron transport code BERMUDA-1DNA is going to be developed.

The present status and the future prospects of code development are summarized as follows:

(1) First period (1979 - 1984)

geometry	(i)	1-dim.	slab(z), sphere(r)	(1D)
	(ii)	2-dim.	cylinder(r,z)	(2D)
	(iii)	3-dim.	rectangular(x,y,z)	(3D)
problem	(a)	neutron transport		(N)
	(b)	gamma-ray transport		(G)
	(c)	neutron transport (adjoint)		(NA)

	1D	2D	3D
N	○	○	⬡
G	□	△	△
NA	□	△	△

○ : developed (-1DN, -2DN)
⬡ : under development (-3DN)
□ : going to be developed (-1DG, -1DNA)
△ : comparatively simple (combination of the upper and the left)

(2) Second period (1984－1989)

(i) treatment of various geometries such as infinite cylinder (r), (r,θ), slab (x,y), sphere (r,θ), cylinder (r,θ,z), finite elements, torus, bent duct streaming, etc.

(ii) anisotropic treatment of (n,n'α) in continuum level, (n,2n), etc.

(iii) Bremsstrahlung effect, photon-electron cascade process (into heat conversion coefficients).

The BERMUDA calculation model differs from that of the Sn method in the following points:

(a) The Legendre polynomial expansion is not used in dealing with anisotropy of scattering. For elastic and inelastic (discrete levels) scatterings, the code uses a numerical integration of the double-differential cross section based on the kinematics of neutron-nucleus collision, i.e., the correlation between scattering angle and ratio of energies before and after a collision.

(b) The transport equation to obtain the spatial distribution of angular flux is integrated at each spatial mesh point along each direction of discrete ordinates (Direct Integration Method). Thus the angular flux is determined on each mesh point instead of mid-point over the mesh interval.

In addition, the differences of model between the BERMUDA code and the PALLAS code series by Takeuchi may be summarized as follows:

(c) The PALLAS calculates the angular flux distribution at energy mesh point without consideration of group width, so that it does not need the iteration technique. While the BERMUDA uses the usual

conception of the group theory, so that the code employs the iteration technique for the scattering source from the self group. Moreover, the angular flux values are renormalized at each iteration stage by neutron balance within the group, over the whole spatial region.

(d) The double-differential cross sections are used for the inelastic scattering of discrete levels as well as the elastic scattering.

(e) For the sake of adoption of the group theory, σ_s $(\vec{\Omega}' \to \vec{\Omega},\ E' \to E)$ is doubly integrated with respect to both E' and E. Accordingly the concept for boundaries of group energy and of discrete angular region on the unit sphere has become very clear.

The calculational procedures for solving the time-independent transport equation and for obtaining the group-angle scattering matrices are described in detail in Refs.1) and 2).

References

1) Suzuki T., Ishiguro Y., Matsui Y.: "PALLAS-TS: A One-Dimensional Neutron Transport Code for Analyzing Fusion Blanket Neutronics," JAERI-M 9492 (1981) (in Japanese).

2) Suzuki T., et al.: "BERMUDA-2DN: A Two-Dimensional Neutron Transport Code," JAERI-M 82-190 (1982) (in Japanese); Sixth International Conference on Radiation Shielding, 3b-2, Tokyo, May 1983.

3) Maekawa H., et al.: "Measurements of Angular Flux on Surface of Li_2O Slab Assemblies and Their Analysis by a Direct Integration Transport Code BERMUDA," ANS Fifth Topical Meeting on the Technology of Fusion Energy, (Poster Session), Knoxville, Tenn., April, 1983.

5.4 Streaming Profile of D-T Neutrons Through a Large Straight Duct

Y. Oyama, T. Nakamura and T. Fukumoto

A streaming experiment was carried out by using the straight duct which was a part of the experimental port placed in the shield wall separating the two target rooms at FNS.[1] This experiment provides the data to examine data and methods in a large diameter penetration problem with a length-to-diameter ratio (L/D) of 2.95. The axis of the duct has an angle of 80° relative to the direction of deuteron beam and the distance between the target center and the exit of the port is 4.5 m. (Fig. 5.4.1)

The spatial distribution of fast neutron dose was measured by a 14 mm-diameter spherical NE213 liquid scintillator mounted on a small-size photomultiplier. The efficiency curve of the detector was obtained by the Monte Carlo code SPMONT, corresponding to the discrimination level of pulse height. To determine the sectional shapes, the detector traverses across the streaming beam were performed at 25, 75 and 125 cm behind the exit of the duct in the vertical direction as is shown in Fig. 5.4.2. The detector counts in a period of traverse were stored successively in a time bin of 1024 channel multiscaler after the neutron-gamma discrimination. The source intensity was monitored by two Th-232 fission counters calibrated by using the associated particle method. Fast neutron spectra were also measured by a 4.65 cm-diameter by 4.80 cm-height NE213 scintillator. The measured points were selected as representatives of the streaming beam center, the boundary and the tail for each traverse.

The transversal neutron dose distributions measured by the small NE213 detector are given in Fig. 5.4.3 for the distance of 25, 75 and 125 cm from the exit of the port with the results of the calculation by the two dimensional transport code DOT3.5. The streaming beam had a well-defined edge and a hump was observed just outside the edge, which moved outward as the measuring line departed from the port exit. In Fig. 5.4.4, the spectra measured at the locations given in Fig. 5.4.2 are shown in the same relative arrangement as the calculated ones. The relative shape of the spectra showed fairly good agreement between the measurement and the calculation except for the neutrons lower than 10 MeV on the center axis.

Reference

1) Nakamura T., et al.: 6th Int. Conf. Radiation Shielding, Tokyo, May 16-20 (1983).

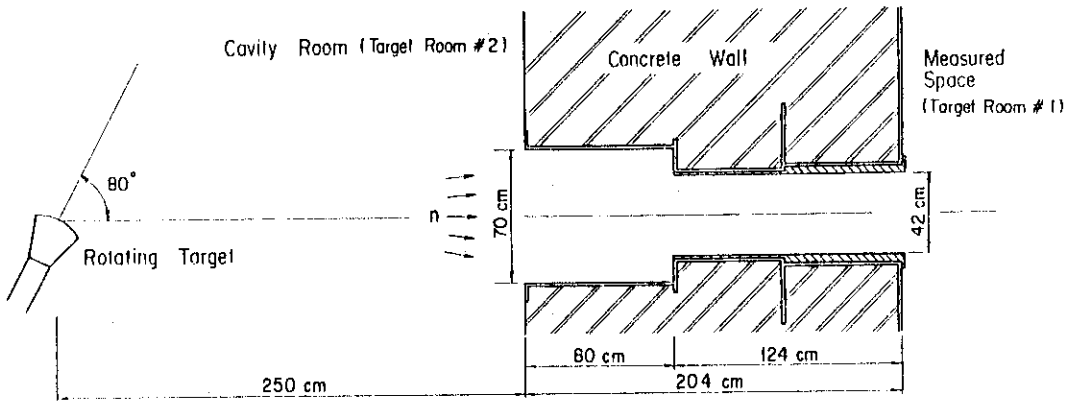

Fig.5.4.1 Horizontal section of the experimental port between target room #1 and target room #2

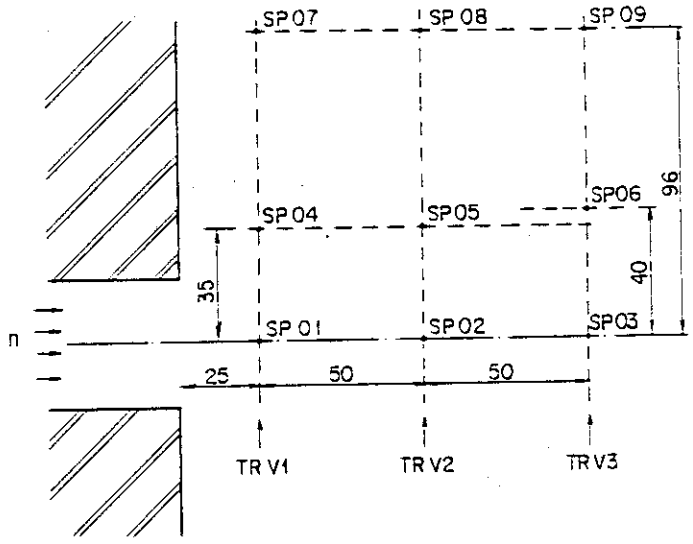

Fig.5.4.2 Detector traverse lines and locations for the beam profile and spectrum measurements

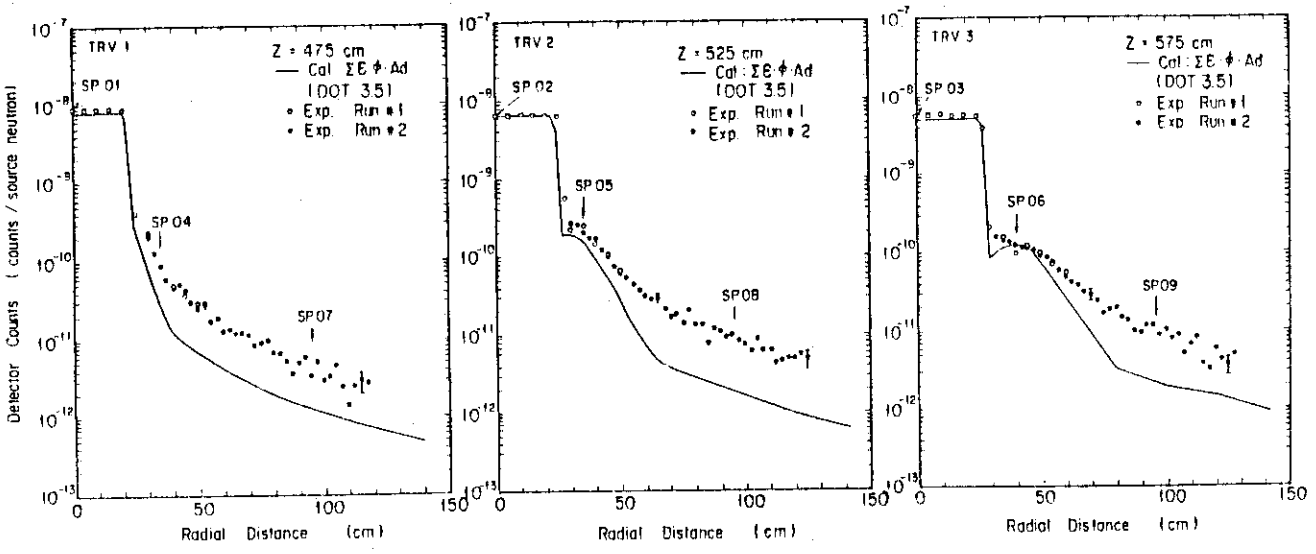

Fig.5.4.3 Fast neutron dose distributions across the streaming beam at the distances of 25, 75 and 125 cm from the port exit

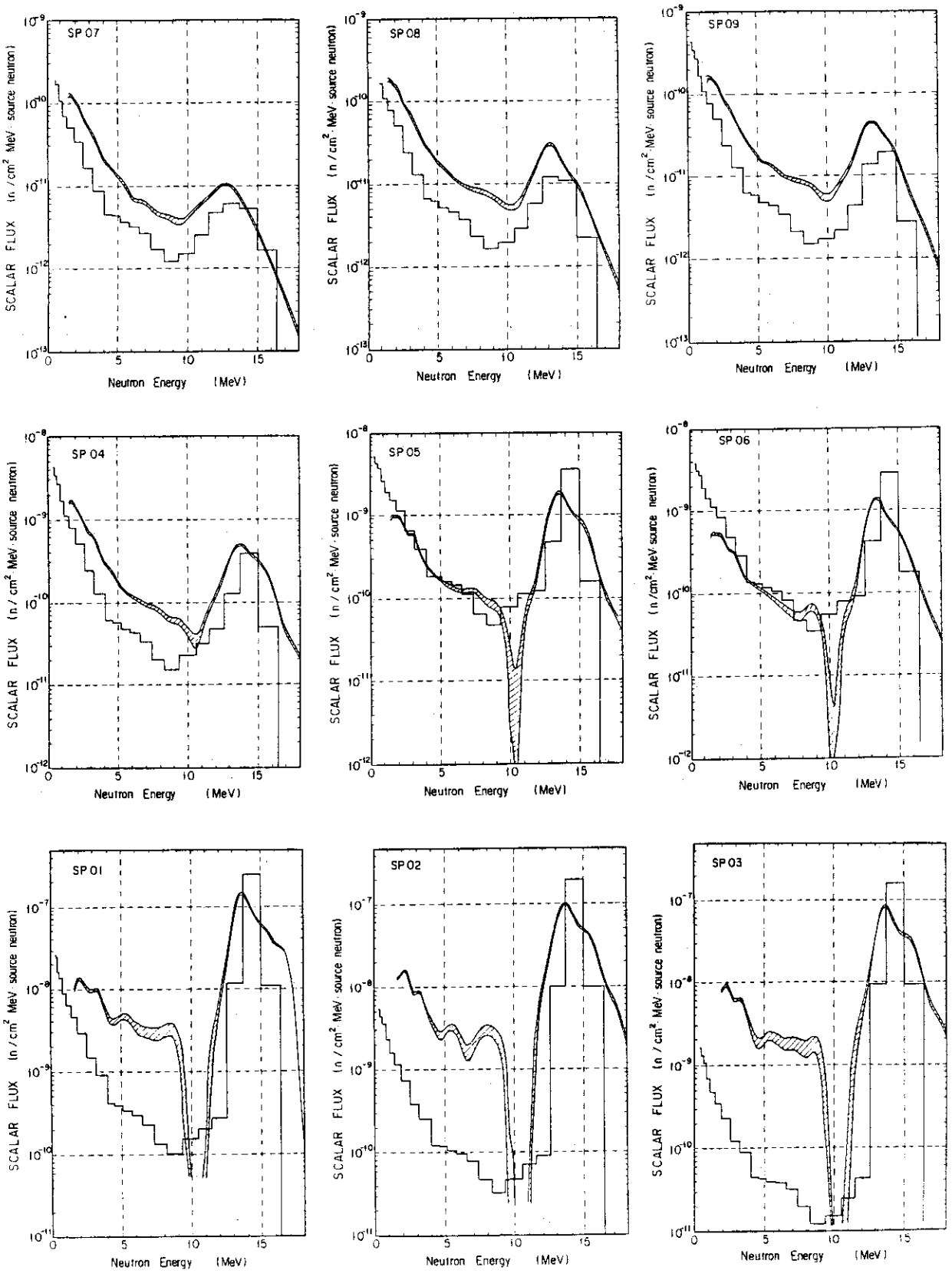

Fig.5.4.4 Fast neutron energy spectra at nine locations on the streaming beam axis and in the shade

5.5 A Fast Neutron Streaming Experiment at the Small-Diameter Long Holes on the Rotatable Shield Plug

T. Nakamura, Y. Oyama and S. Yamaguchi

A large experimental port and a plug to fit it are prepared in the 2 m thick shield wall separating the target room #1 and the work room of the FNS facility. The port is located at 5.5 m from the target position of the 80° beam line in the direction of 90° to deuteron beam. The central axis of the port and plug is set off by 5.52 cm in horizontal and 22.08 cm in vertical directions relative to the exact 90° line drawn from the target center. The plug has a 20 cm diameter hole for time-of-flight experiment and fourteen parallel holes of 3.6 cm in diameter for neutron beam experiment, the lining of the hole being of 0.3 cm mild steel and the rest of the plug filled with non-shrinking ordinary concrete. The plug can rotate in the port so as to change the location of each hole relative to the target position according to the experimental requirements. Thus, an array of the small holes were simulated by the superposition of the different rotating angles as shown in Fig. 5.5.1.

Axial distributions in the set of six selected holes were measured by using the same small NE213 detector as described in 5.4. The angles of the incident neutrons to the central axis of each hole were 0°, 0.6°, 1.2°, 2.3°, 3.5° and 5.8° at the hole mouth, respectively. During the measurement in a hole, the other holes were plugged with shielding tampers so as to avoid the possible interference. The streaming profiles were measured at the exits of the 0° hole and the nearest two in the same way as described in 5.4. The length to diameter ratio (L/D) was 56.

The systematic change in the fast neutron dose distributions of the group of holes is given in Fig. 5.5.2. Near the mouth, the number of neutrons in each hole was about the same. In the #1 hole, the counts decreased and approached to $1/r^2$ curve assymptotically as the detector moves deep into the hole, r being the distance between the target and the detector. For oblique neutron incidence, the curve departed from that of #1 on the way and fell rapidly at a constant slope in semi-log scale, i.e., exponentially. The larger was the angle, the sooner it started to droop. The 1/10 length of the slope was about 30 cm. The streaming profiles of the neutron at the exits of the #1 and next two holes are shown in Fig. 5.5.3.

The fast neutron spectra were measured by the small spherical NE213 scintillator at eight points on the axis of the 0° hole to examine the spectral change as a function of the distance from the hole mouth. The neutron-gamma ray discrimination and the unfolding of the pulse height distribution were just the same as the case of the 5 cm-diameter by 5 cm-high NE213 scintillator except that the response functions were newly calculated by the SPMONT code.

The fast neutron spectra measured inside and outside of the #1 hole showed systematic change corresponding to the axial traverse. To make the comparison simple, the unfolded spectrum at each location was integrated in four energy ranges. Table 5.5.1 shows the fraction of the neutron counts in each energy band as a function of position in the hole. The spectra at 100 cm and therefrom show small difference indicating the neutrons measured are directly from the target or slight-angle scattered ones with no appriciable energy change. The low energy component of 7 ~ 9 % is considered to be due to the scattered neutrons at the target assembly itself. The negative value in 7.4 ~ 10.0 MeV range is caused by unfolding procedure.

Table 5.5.1 Fast neutron energy spectra bunched in four energy ranges at the various locations along the axis of the #1 hole

Distance from the Hole Mouth (cm)	Neutron Energy Range (Mev)			
	2.4 - 5.0	5.0 - 7.4	7.4 - 10.0	10.0 - 16.0
- 40	0.240	0.066	0.006	0.689
0	0.222	0.071	0.005	0.703
20	0.118	0.063	0.008	0.810
40	0.090	0.044	- 0.010	0.876
60	0.067	0.035	- 0.015	0.913
100	0.064	0.028	- 0.011	0.920
180	0.063	0.031	- 0.018	0.923
240	0.061	0.028	- 0.018	0.930

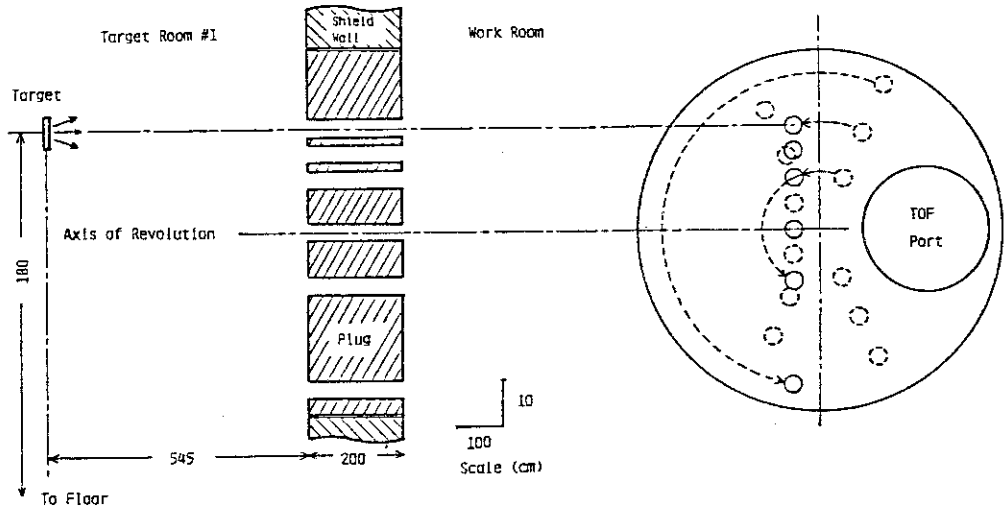

Fig. 5.5.1 Arrangement of small-diameter experimental holes on the rotatable shield plug

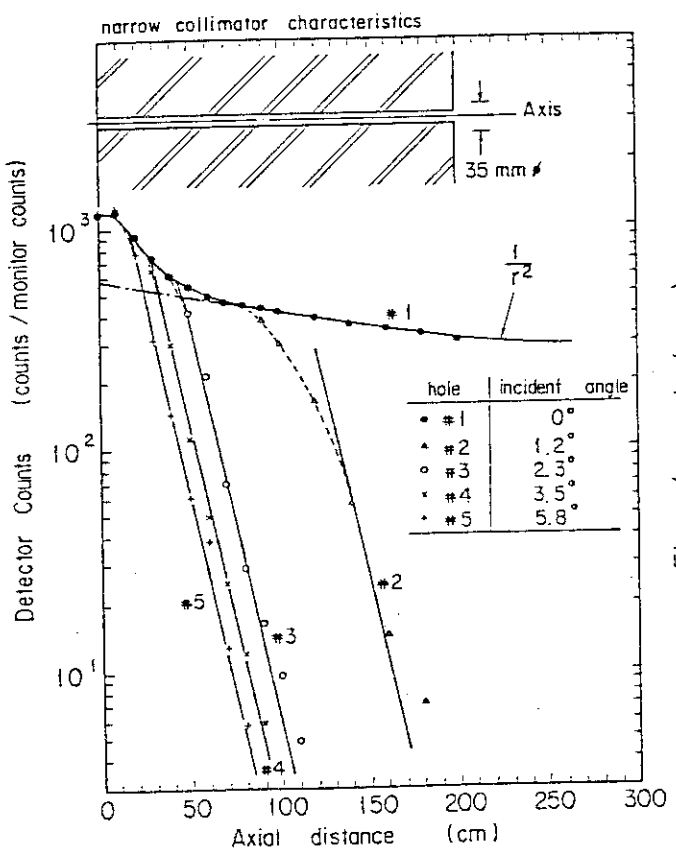

Fig. 5.5.2 Axial fast neutron dose distributions in the small-diameter long experimental on the shield plug

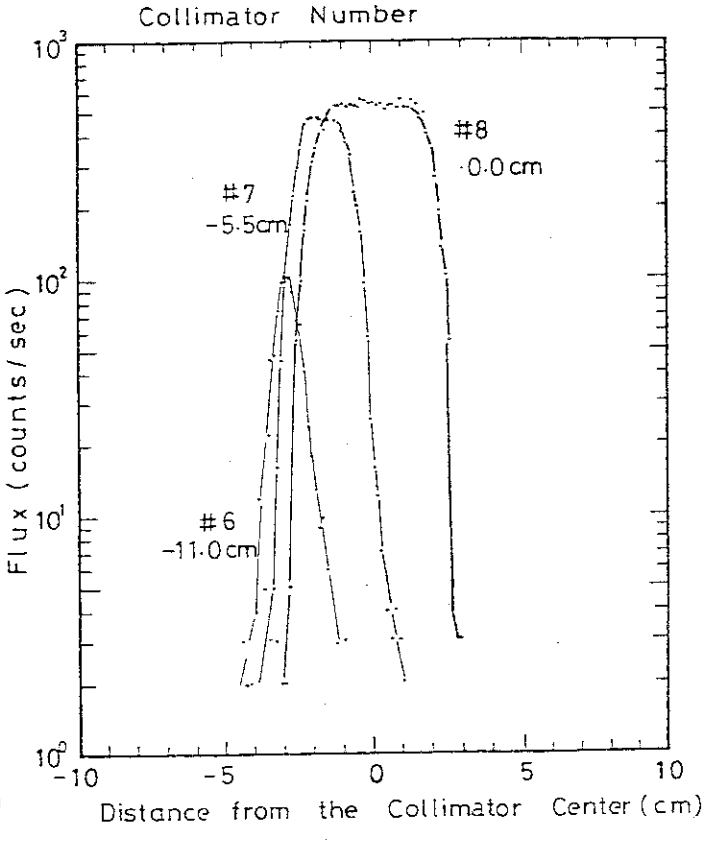

Fig. 5.5.3 Streaming beam profiles of the small-diameter long holes

5.6 Monte Carlo Analysis of a Streaming Experiment of D-T Neutron and Secondary Gamma Rays Through a Concrete Bent Duct[1)]

Y. Seki, S. Tanaka, Y. Oyama, N. Sasamoto, H. Kawasaki*,
Y. Ikeda, H. Maekawa and T. Nakamura

A benchmark D-T neutron streaming experiment[2)] was analyzed using a three dimensional Monte Carlo method. The streaming experiment examined the behavior of D-T neutrons and secondary gamma rays in a concrete bent duct constructed as a personnel access way in the Fusion Neutronics Source Facility (FNS). (Fig. 5.6.1)

The Monte Carlo calculations were carried out by the MORSE-GG code[3)] using a fairly accurate representation of the FNS target room and the concrete duct structure. The cross section set used in the calculations is a 28-group neutron and 7-group gamma-ray (28n-7γ) coupled cross section set collapsed from the 135n-21γ coupled cross section set GICXFNS[4)] which has been processed from the ENDF/B-IV nuclear data file using the NJOY code.[5)] In the Monte Carlo calculation, source neutrons were generated from the D-T target using the neutron energy spectrum obtained by another Monte Carlo calculation[6)] which was in good agreement with the measured spectrum.[7)]

The calculated and measured fast neutron spectra in the duct agreed mostly within the statistical errors as shown in Fig. 5.6.2. The calculation of the fast neutron dose equivalent also showed a good agreement with the measurement. Thus the data and method employed in the present analysis are shown to be valid for estimating the fast neutron streaming through a large duct in a concrete structure.

The calculation slightly overestimated the neutron dose equivalent and some agreement has been obtained between the calculated and measured thermal neutron flux. Although the gamma-ray energy spectra were in good agreement, the distribution of calculated gamma-ray exposure dose differed from the measured data.

---

* Century Research Center Corporation Ltd.

References

1) Seki Y., et al.: Sixth Int. Conf. on Radiation Shielding, Tokyo, Japan, May 16-20 (1983), 6b-6.
2) Tanaka S., et al.: JAERI-M 82-130 (1982).
3) Straker E. A., et al.: ORNL-4585 (1970).
4) Seki Y., et al.: JAERI-M 83-061 (1983).
5) MacFarlane R. E., et al.: LA-9303-M, Vol I and II (ENDF-324), (1982).
6) Seki Y., et al.: To be published in J. Nucl. Sci. Technol.
7) Ikeda Y., et al.: To be published as JAERI-M Report.

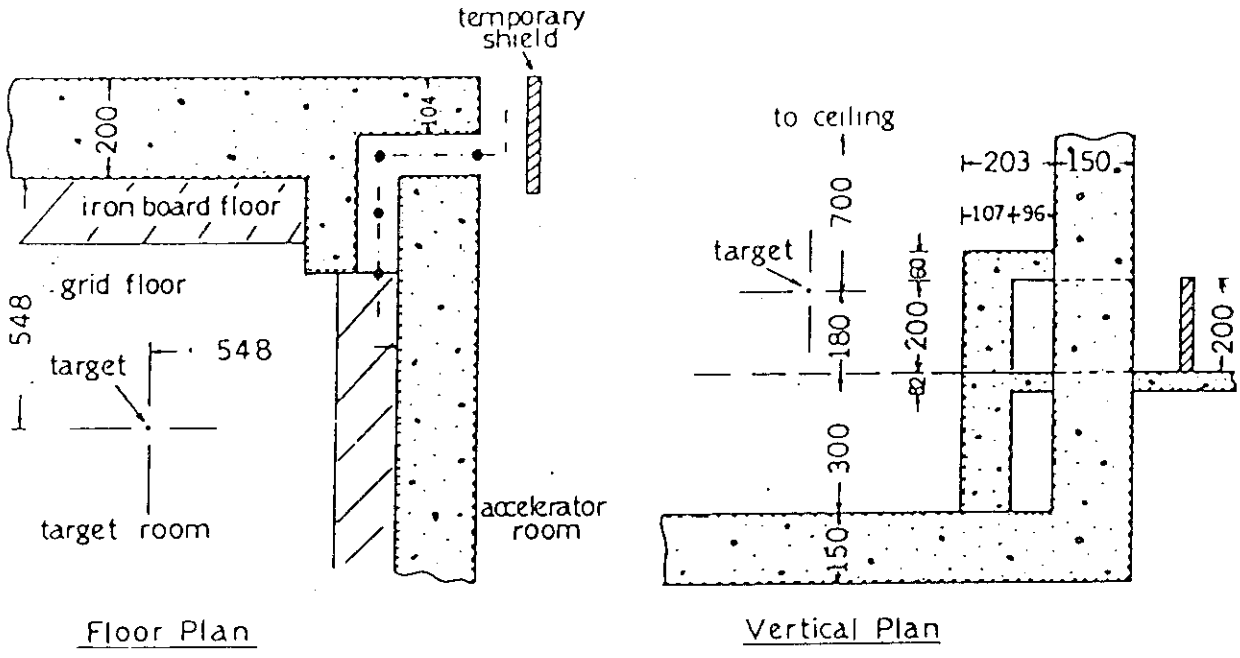

Fig. 5.6.1 Layout of the streaming duct (personnel access way)

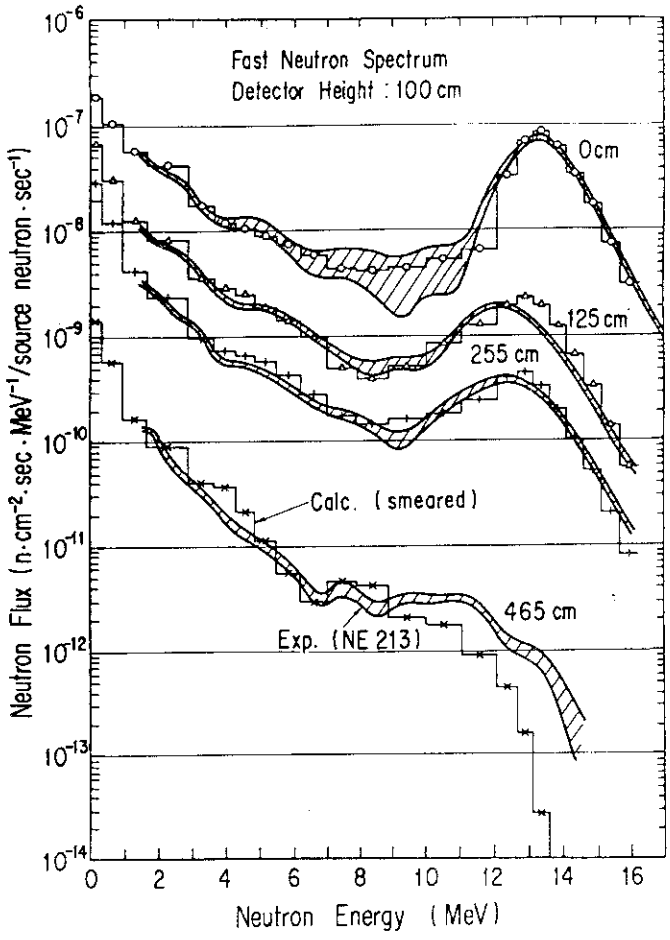

Fig. 5.6.2 Calculated and measured fast neutron spectra at 4 locations in the duct

6. Reactor and Nuclear Instrumentation

6.1 Development of an In-Vessel Water Level Gauge for LWR's

K. Ara and N. Wakayama

The in-vessel water level gauge, in principle, is based on the measurement of the temperature distribution on the surface of a long sheathed heater-pin which is partially immersed in water. Instead of adopting the measurement with many thermocouples, a binary-coded thermocouple array consisting of differential thermocouple trains (DTCT's) is settled on or in the sheath of a heater-pin to give a binary output related to the water level. Thus, this new-type of water level gauge was named BICOTH (BInary-COded Thermocouple-array with Heater).

Figure 6.1.1 illustrates the fundamental configuration and the operating characteristic of BICOTH. Here, four DTCT's are settled inside the heater-pin sheath to detect the water level. That is, (a) the measuring range is divided into ten sections, (b) a different number based on a binary gray code is assigned to each section, and (c) the binary-coded thermocouple array composed of four DTCT's has each DTCT's pairs of differential hot-junctions arranged in order to generate one digit of four-digit binary number assigned to each section; thus, (d) the output signals of the DTCT's correspond to the binary numbers assigned to each section where the water surface exists. In other words, the BICOTH is able to generate the binary number which indicates the section where the water surface exists.

After feasibility tests of the method with a prototype BICOTH, two types of in-vessel BICOTH were fabricated. One was a heater-pin type in which five DTCT's were settled in the heater-pin sheath to identify twenty-three different water-levels in the range of 2.6 m, (Figure 6.1.2). The other was a flexible-wires type, consisting of five metal-sheathed DTCT's with a diameter of 1.6 mm and with heater wires installed inside with each DTCT, (Figure 6.1.3). The performance of each type was examined under the conditions of cold water and high-temperature, high-pressure water, and encouraging results were obtained. Figures 6.1.4 and 6.1.5 show their static characteristics.

Reference

Ara k., Wakayama N., Kobayashi k.: NUREG/CP-0027, Vol. 3, pp. 1667-1680 (1982).

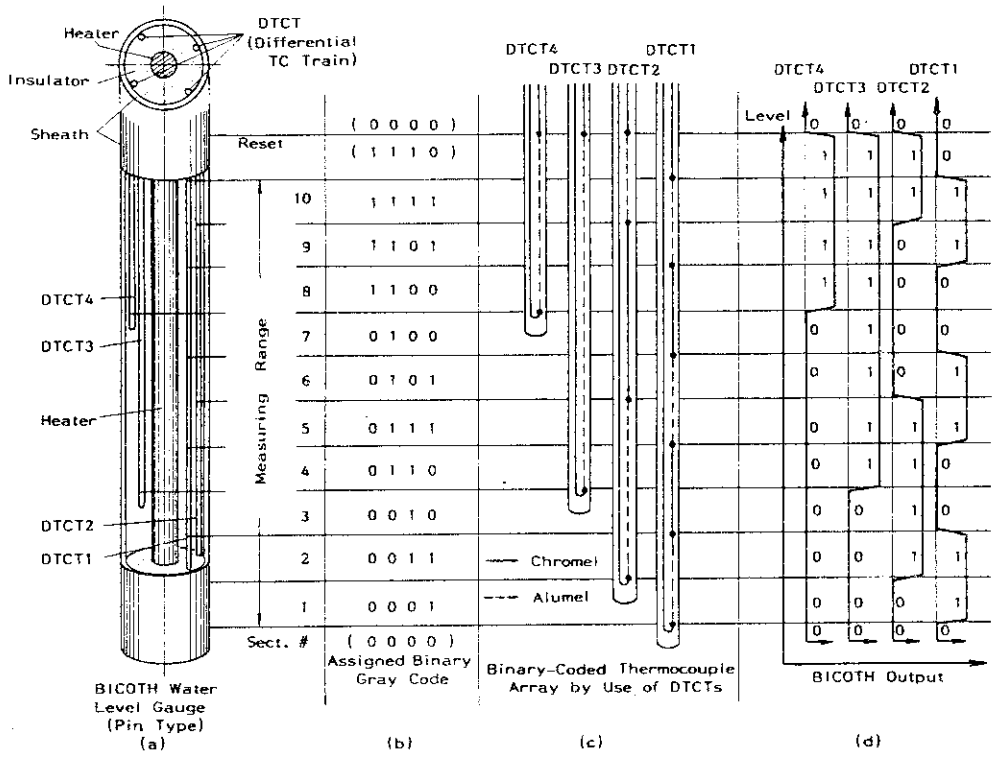

Fig.6.1.1 Fundamental configuration and operating characteristic of BICOTH

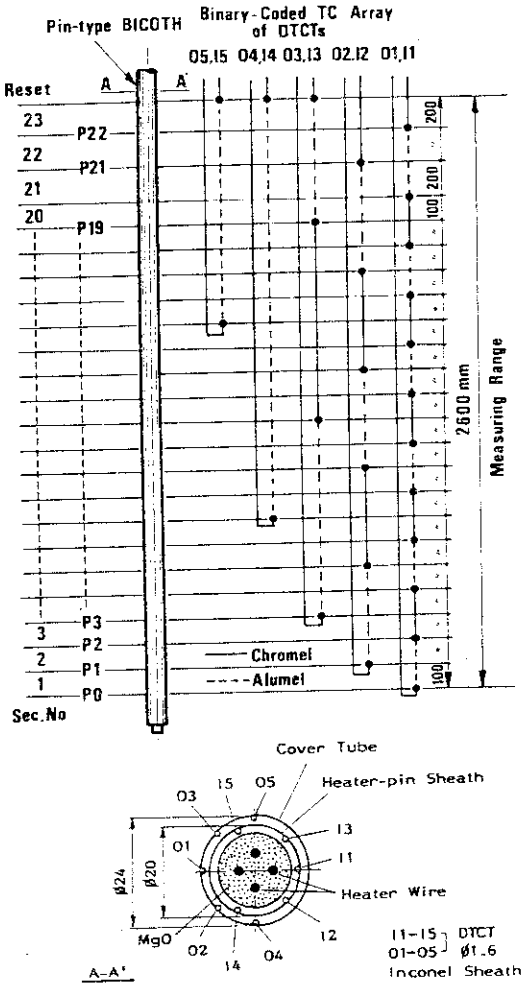

Fig.6.1.2 Heater-pin type BICOTH

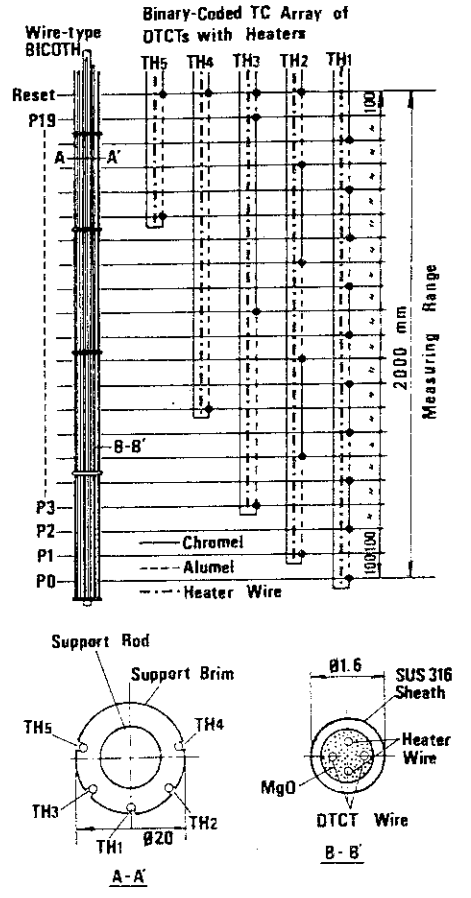

Fig.6.1.3 Flexible-wires type BICOTH

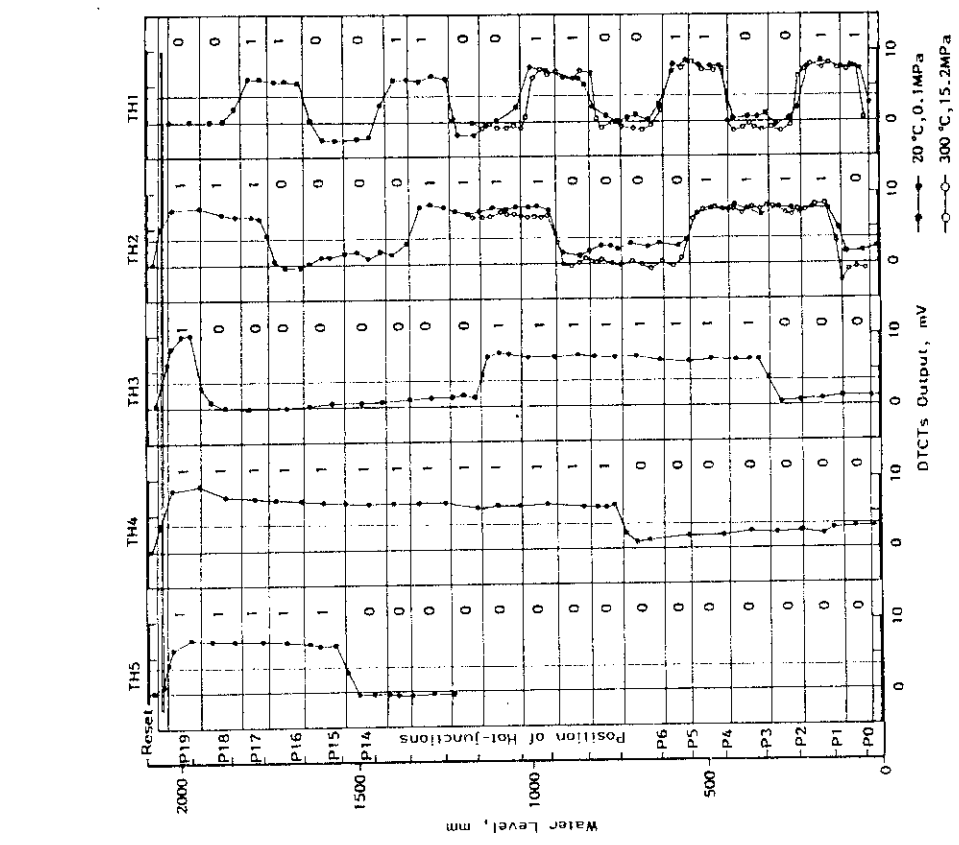

Fig.6.1.5 Static characteristic of flexible-wires type BICOTH

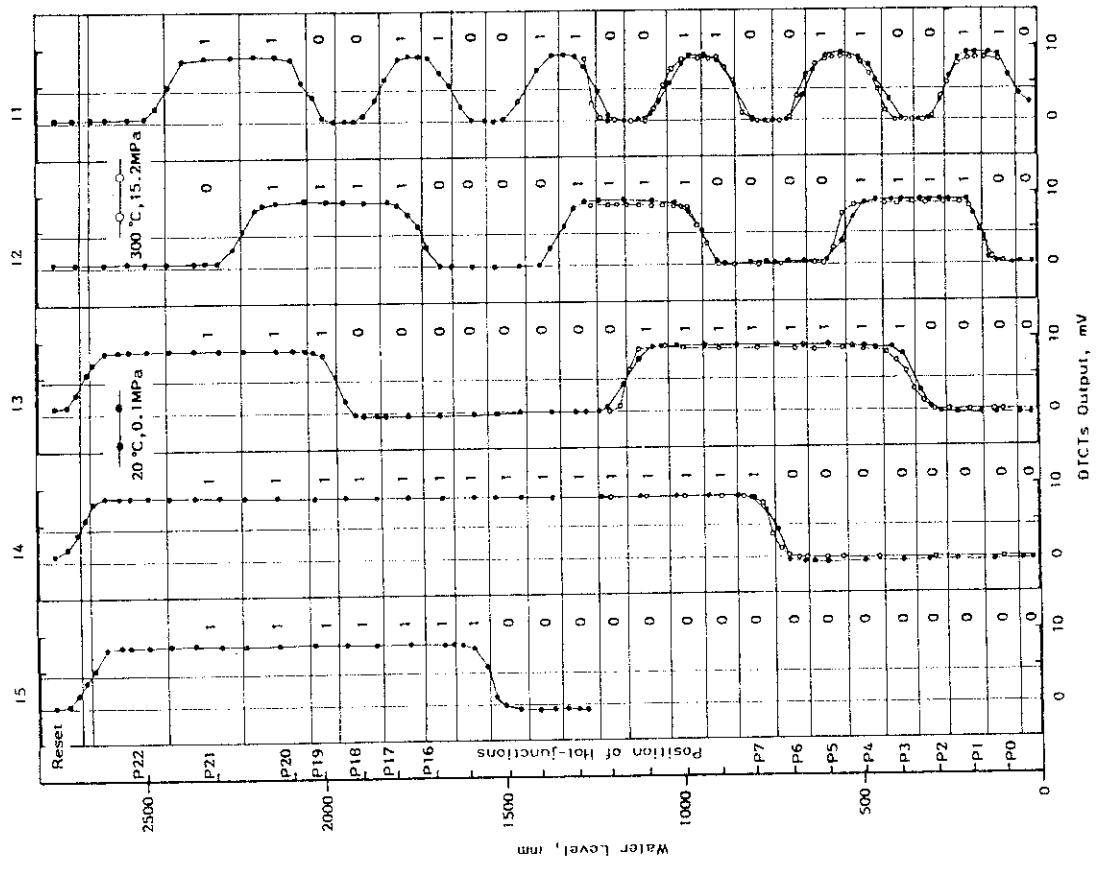

Fig.6.1.4 Static characteristic of heater-pin type BICOTH

6.2 Development of Fuel Failure Detection Method for the Coated Particle Fuels of VHTR

H. Terada, M. Katagiri, N. Wakayama, H. Yoshida, H. Ohtsu[+], H. Ohkawa[+], T. Niibo[+] and H. Itoh[+]

Coated particle fuels (CPF's) in a HTGR release fission products(FP) little by little to the primary coolant even during the normal operation. Therefore, the radiation background level due to the FP-nuclides in the primary coolant becomes rather higher than those in the conventional type reactors using metal cladding fuels. Moreover, the background level changes considerably depending on the normal change of the reactor state, i.e., fuel temperature, neutron flux, burn-up rate and the other factors. These facts make it extremely difficult to detect the small increase of the FP-level due to the fuel failure of the CPF's.

In the development of the high sensitive fuel failure detection(FFD) method for the VHTR, following ideas should be effective. Those are

1) monitoring of short-life FP-nucldes selectively to eliminate the high level of the background due to long-life FP-nuclides, and
2) diagnosis using state equations with the concentrations of FP-nuclides in the primary ccolant in order to distinguish the slight change of the background level, caused by CPF failures, from the normal change depending on the reactor operation.

In order to realize the above ideas, the experiments were carried out using an irradiation rig which can supply sample gas containing FP-nuclides swept from CPF-specimens under irradiating in the JMTR. Figure 6.2.1 shows the block diagram of the FFD experimental equipments. In the experiment, it was studied to detect selectively shorter life FP-nuclides under conditions of changing the travelling-time of the sample gas between the detector and the CPF-specimens in the reactor core. Figure 6.2.2 shows the ratio of Xe-138 and Kr-88 versus the travelling time measured in the No. 57 and 58 operations of the JMTR. The ratios change reasonably along with a calculated curve. It is made clear from this result that selective detection of the shorter life FP-nuclides from among long-life FP-nuclides is possible by controlling of the travelling time of the sampling gas.

The experimets will be performed to establish the state equations using the FFD experimental equipments in the next step.

+ Irradiation Division II, Department of JMTR Project

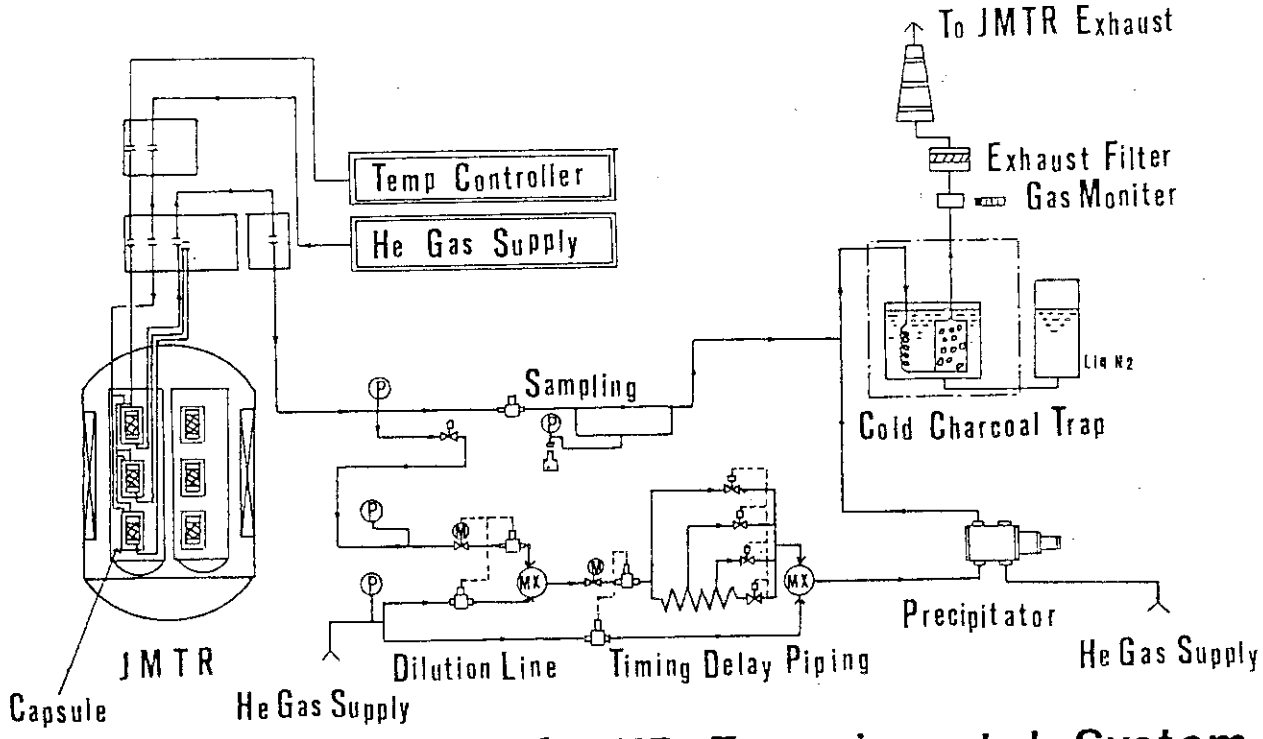

Fig.6.2.1 **Flow Diagram of FFD Experimental System**

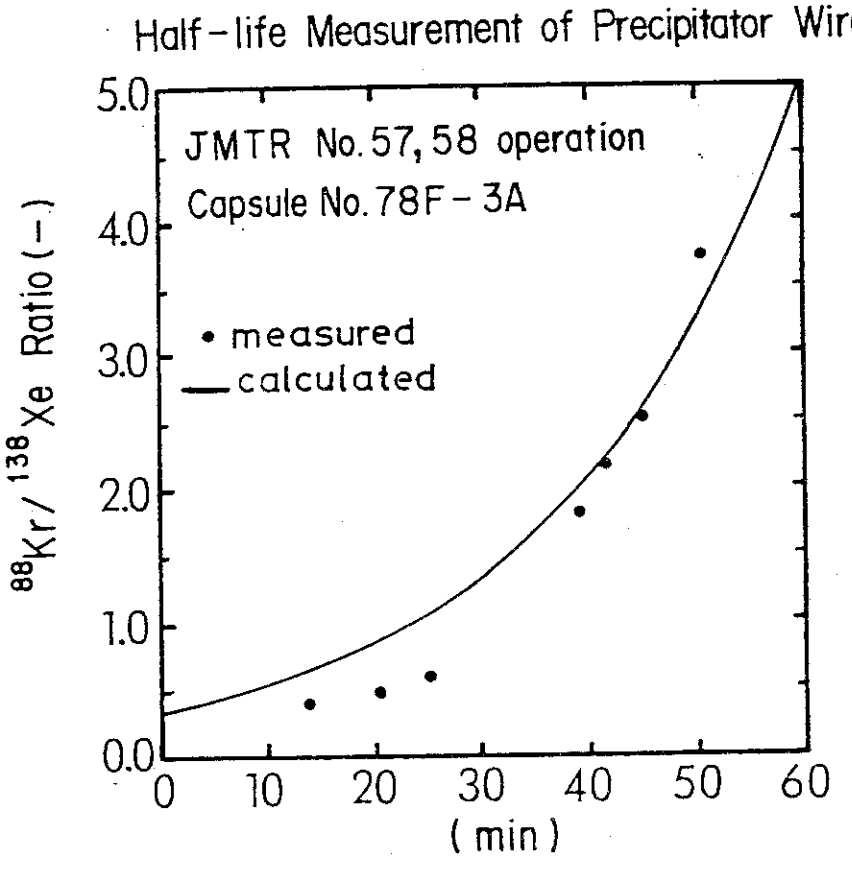

Fig.6.2.2 Travelling time of FP-nuclides from the reactor core to the precipitator

6.3 Development of Cable Insulators and Cables for LMFBR Instrumentation

T. Kakuta, K. Ara and N. Wakayama

Several mineral-insulated cables were developed in order to be used in high-temperature and high-radiation environments around the primary circuits of LMFBR. Their performances were tested under simulated reactor conditions.

An improved-type of 600 V power cable, FML-600P where organic sheath was made of Polyolefin, as shown in Fig. 6.3.1, was gamma-irradiated up to 5×10^9 R. The cable showed good electrical performances, and good compatibility between sheath and other structure materials was confirmed. The results are shown in Fig. 6.3.2.

The structure of tri-axial cables, type 79-01 and 79-03, are shown in Fig. 6.3.3. They were tested under simulated accident conditions. The cables were heated up to 360°C twice and then maintend at 270°C for 100 hours. In this test, D.C. 1000 V was supplied to the cables for observation of transmission characteristics and other electrical performances. Cables showed all excellent performances. Further, their dielectric breakdown strength was examined after tests and enough strength was recorded. It was concluded that the cables could demonstrate the whole of their cable functions even under FBR-accident conditions. The results are shown in Fig. 6.3.4.

The reformed N-type connectors, were fabricated and connected with the SiO_2-insulated metal sheathed tri-axial cables, RR-TRIAX-50, are shown in Fig. 6.3.5. They have been developed for nuclear instrumentation. Their total performances were examined from an applicative point of view. Test results showed their excellent performances, including electrical characteristics, B.P.N. chracteristics, and insulation resistances, up to the temperature of 550°C. The results are shown in Fig. 6.3.6.

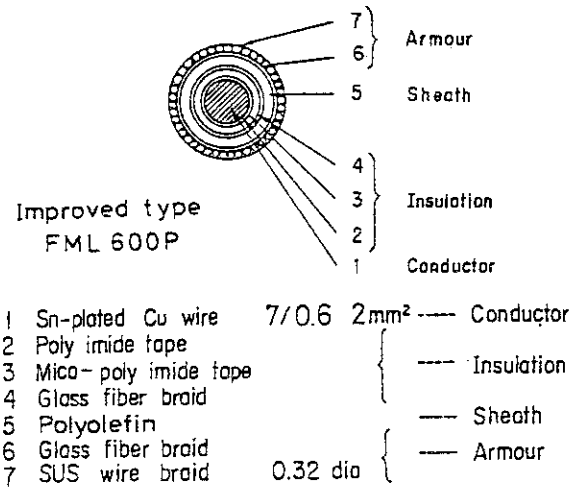

1	Sn-plated Cu wire	7/0.6 2mm²	Conductor
2	Poly imide tape		Insulation
3	Mica-poly imide tape		
4	Glass fiber braid		
5	Polyolefin		Sheath
6	Glass fiber braid	0.32 dia	Armour
7	SUS wire braid		

Fig. 6.3.1 Improved-type FML-600P cable

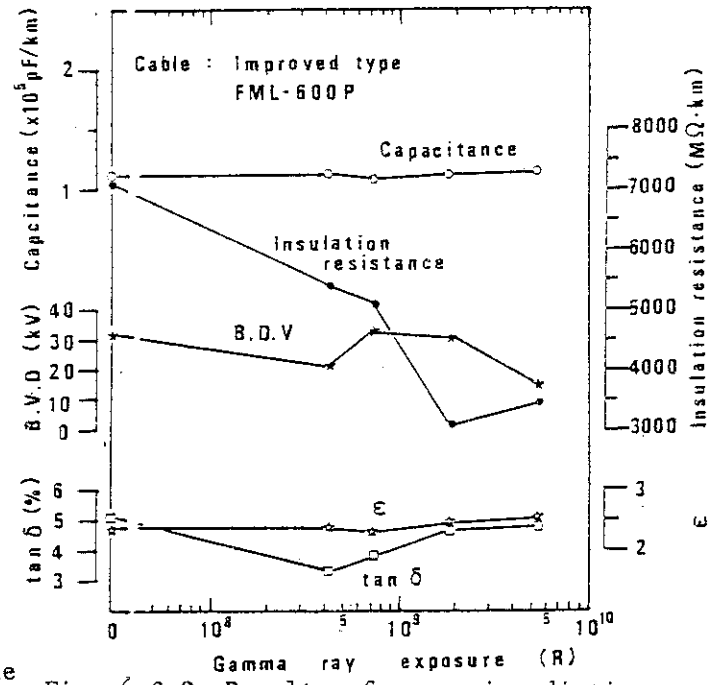

Fig. 6.3.2 Results of gamma-irradiation test for FML-600P

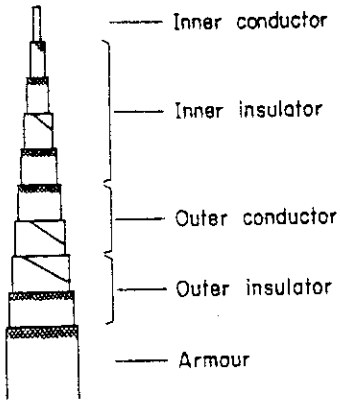

	Materials			Size
	79－01	79－02	79－03	
Inner conductor	Poly imide enamelled Ag-plated Cu wire		Ag-plated Cu wire	0.9 mm Dia.
Inner insulator	Glass fiber winding and braid (Poly imide impregnate) / (Non impregnate) Glass fiber tape Glass fiber braid			5.0mm O.D. 2.0mm Thick.
Outer conductor	Ag-plated Cu wire braid Ag-plated Cu tape			0.14mm Dia. 0.1 mm Thick.
Outer insulator	Glass fiber tape Glass fiber braid			0.4mm Thick.
Armour	SUS wire braid			0.32mm Dia.
Diameter	—	—	—	8 mm O.D.
Weight	150 kg/km	140 kg/km	140 kg/km	—

Fig. 6.3.3 Structure of tri-axial cables

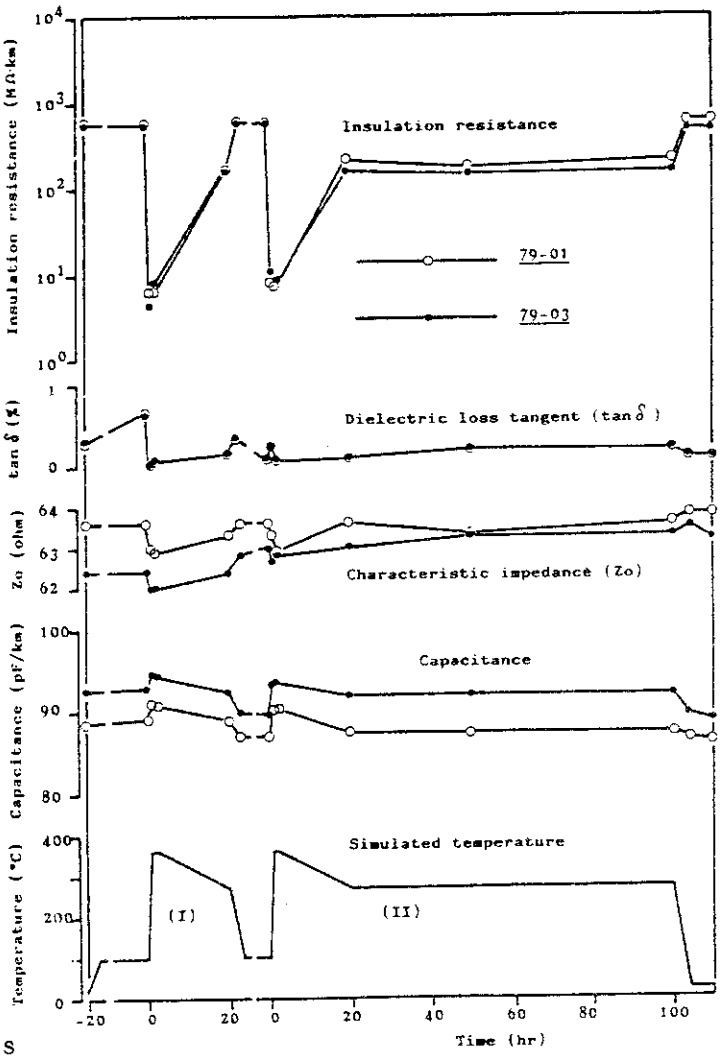

Fig. 6.3.4 Results of simulated accident test for tri-axial cables

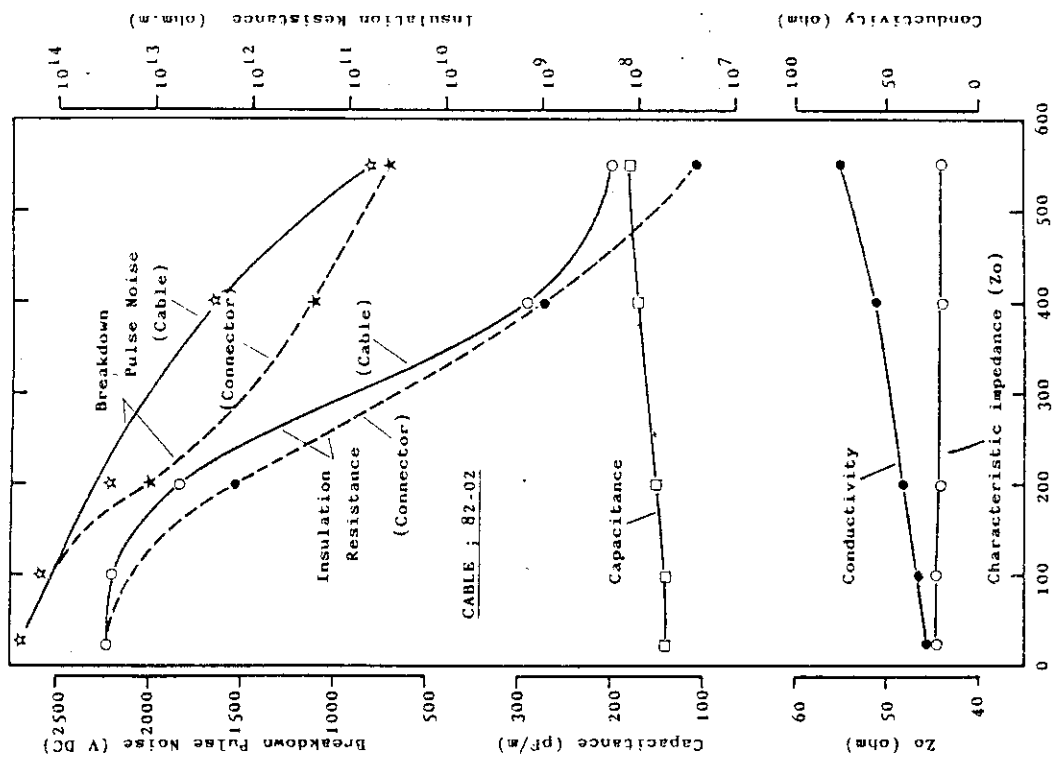

Fig. 6.3.6 Results of high-temperature test for RR-TRIAX-50

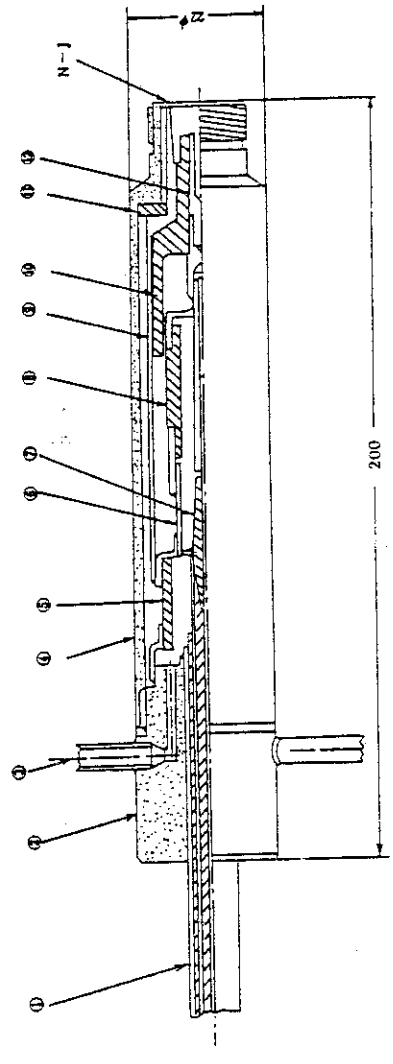

No	PARTS	MATERIAL	REMARKS
1	M.I Cable	RR-TRIAX-50	
2	Body	SUS-304	
3	N, tip off	SUS-304	
4	Body shell	SUS-304	
5	Outer seal	Ceramic, Kovar	
6	Sleeve	SUS-304	

No	PARTS	MATERIAL	REMARKS
7	Sleeve	Ceramic	
8	Inner seal	Ceramic, Ni	
9	Outer cond.	Brass	Ag-plate
10	Spacer	Ceramic	
11	Outer spacer	Ceramic	
12	Inner contact	Brass	Ag-plate

TRIAX-N-J Hermetic type

Fig. 6.3.5 Combined type "N" connector for SiO_2-insulated cable

6.4 Development and Test of Cover-Gas On-Line Gamma-Ray Monitor (V)

E. Sakai

A cover-gas monitor test facility CGMTF was dismantled in March 1983, which had been operated at JRR-3 nuclear reactor since April 1979 for testing various fuel failure detection systems for liquid metal cooled fast breeder reactor development taking advantage of helium cover-gas which contained rare-gas fission products (Kr-85m, 87, 88, Xe-133, 135m, 135, 138, Rb-88 and Cs-138 of the order of 10^{-3} μCi/cm^3) and Ar-41 of the order of 10^{-2} μCi/cm^3. The fuel failure detection systems tested were an on-line Ge(Li) gamma-ray spectrometer system combined with three types of chambers (100cm^3 cover-gas chamber, 100cm^3 room temperature charcoal chamber and 10cm^3 cooled charcoal chamber), a proportional counter type precipitator system and a membrane type fission product separator/concentrator system. One who feels interest in the test results should refer to the reports 1) to 5).

The results obtained on these systems, especially the results on an evaluation of the fuel failure detection sensitivities of the on-line Ge(Li) gamma-ray spectrometer system with 10cm^3 cooled charcoal chamber contributes very much to the designing and the safety evaluation for the fuel failure detection system of the prototype fast breeder reactor "MONJU" under construction.

The on-line Ge(Li) gamma-ray spectrometer system will be moved to the experimental fast breeder reactor "JOYO" for actual cover-gas monitoring. One problem in JOYO is the limited space for setting and servicing the Ge(Li) detector which requires a maintenance-free Ge detector. The present status of the development of high-purity Ge detectors cooled with closed-cycle cryogenic refrigerators, and the problems and counterplans are indicated.[6] The main problems are the effect of vibration and the maintenance of vacuum; we reduced the former using bellows[7] and already finished a continuous operation for two months. The prospects for completion of this technique seem to be bright.

References

1) Sakai E. and Kubo K.: "Development and Test of Cover-Gas On-Line Gamma-Ray Monitor (I)," SJ 250 79-06 (March 1979) (in Japanese).

2) Sakai E., Kubo K. and Yoshida H.: "Development and Test of Cover-Gas On-Line Gamma-Ray Monitor (II)," SJ 250 80-27 (June 1980) (in Japanese).

3) Sakai E., Kubo K. and Yoshida H.: "Development and Test of Cover-Gas On-Line Gamma-Ray Monitor (III)," SJ 250 81-07 (March 1981) (in Japanese).

4) Sakai E., Kubo K. and Yoshida H.: "Development and Test of Cover-Gas On-Line Gamma-Ray Monitor (IV)," SJ 250 82-17 (June 1982) (in Japanese).

5) Sakai E., Miyazawa T. and Sekiguchi N.: "Summary of In-Pile Loop Experiments Related to the Development of the Fuel Failure Detection Systems for LMFBR's in Japan," KfK 3203 IWGFR/38, p.147 (June 1982).

6) Sakai E.: "Development and Test of Cover-Gas On-Line Gamma-Ray Monitor (V)," PNC SJ 950 83-01 (March 1983) (in Japanese).

7) Sakai E. Murakami Y. and Nakatani H.: "Performance of a High-Purity Ge Gamma-Ray Spectrometer System Using a Closed Cycle Cryogenic Refrigerator," IEEE Trans. Nucl. Sci., NS-29, No. 1, p.760 (1982).

6.5 Gamma Irradiation Effects in Optical Fibers

T. Kakuta and K. Sanada*

Introduction

The data concerning the radiation damage of the optical fibers have been reported in several papers. Among them there are peculiar phenomena such as photobleaching effects, radiation induced hardening, these mechanism have been uncertainly explained at present. This paper describes light power and dose rate dependece on photobleaching effects of optical fibers in radiation environment. Radiation induced loss in optical fibers are produced when the electrons and holes released by the radiation are occupied pre-existing traps such as oxgen vacancy, etc. It can be considered that kind and amount of pre-exiting traps in the core depend on the composition of core glass, fabrication methods and conditions etc. Therefore, photobleaching effects in optical fibers fabricated by different methods and conditions were investigated at several bleaching light intensities and gamma-radiation dose rates.

As a result, it has been found that characteristics of optical fibers in the radiation environment are strongly related to the fabrication methods and conditions.

Experiment

The induced losses during and after steady state ^{60}Co gamma irradiation were continuously measured by using LED (0.85μm). The intensity of the bleaching light travelling in the fiber was varied from 0.14μW - 14μW, as measured at the out put end. Fig. 6.5.1 shows the schematic diagram of experimental systems. The exposed fiber length at the different dose rates was 100m and dose rates were varied from 5×10^3 to 5×10^4 R/hr. Table 6.5.1 shows characteristics of fibers used for experiment. Pure silica glasses are made by various method such as Plasma, OVD, VAD and MCVD. Low OH content fibers provided by Plasma and MCVD were selected for this experiment. The fibers studied were 50μm core and 125μm o.d. step-index with /SiO/BO/F cladding and covered with 400μm silicone and 0.9mm nylon.

*Fujikura Ltd.

Light Power Dependence of Photobleaching Effects

Radiation induced loss increase and recovery curves obtained at different light powers are shown in Fig. 6.5.2(a)-(c) for fiber-A, fiberb-B and fiber-C. From these curves, it has been found that radiation induced loss curves of fiber-B and fiber-C made by Plasma method are significantly influenced by the light intensities compared with fiber-A provided by the MCVD method. Fiber-B has much higher radiation tolerance than fiber-C having loss peak around 0.6μm in a state of unexposed fiber. The difference of radiation tolerance is seen to be fabrication condition-dependent such as reaction temperature, oxgen gas flow rate, and so on. From the recovery curves, it has been clarified that decay rates become larger with incleasing light intensity travelling in the fiber.

Dose Rate Dependence of Photobleaching Effects

Radiation induced loss increase curves obtained at different dose rates when bleaching power is kept constant are shown in Fig. 6.5.3(a)-(b). From these figures it has been found that the shapes of loss increase curves are strongly affected by the fabrication conditions. The radiation induced loss of fiber-C increase with increasing total dose, where as the induced curves of fiber-B saturate with increasing total dose. In the case of the same dose, radiation induced losses of fibers become larger with increasing dose rate.

Conclusion

We have studied the bleaching power and gamma-radiation dose rate dependence of the photobleaching effects in optical fibers fabricated by different methods and conditions.

As a result, it has been found that characteristics of optical fibers in the radiation environment are very much related to the fabrication methods and conditions.

Refferences

1) Titchmarsh, J. G. : Electron. Lett., 1979, 15, p.111
2) G. H. Sigel, et al. : proc. IEEE, 68, p.1236 (1980)

Table 6.5.1 Characteristics of fibers

TNo	ΔN (%)	OH (ppm)	Loss at 0.85 μm (dB/Km)	Fabrication Method	Loss peak around 0.6μm
A	0.7	1	2.1	MCVD	—
B	0.8	15	2.4	Plasma	—
C	0.9	10	3.5	Plasma	100 dB/km

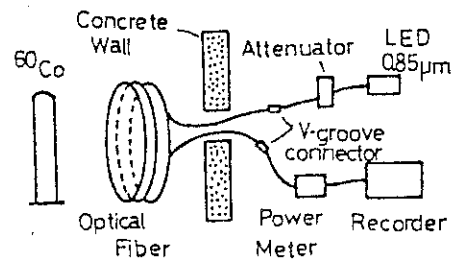

Fig. 6.5.1 Measuring diagram

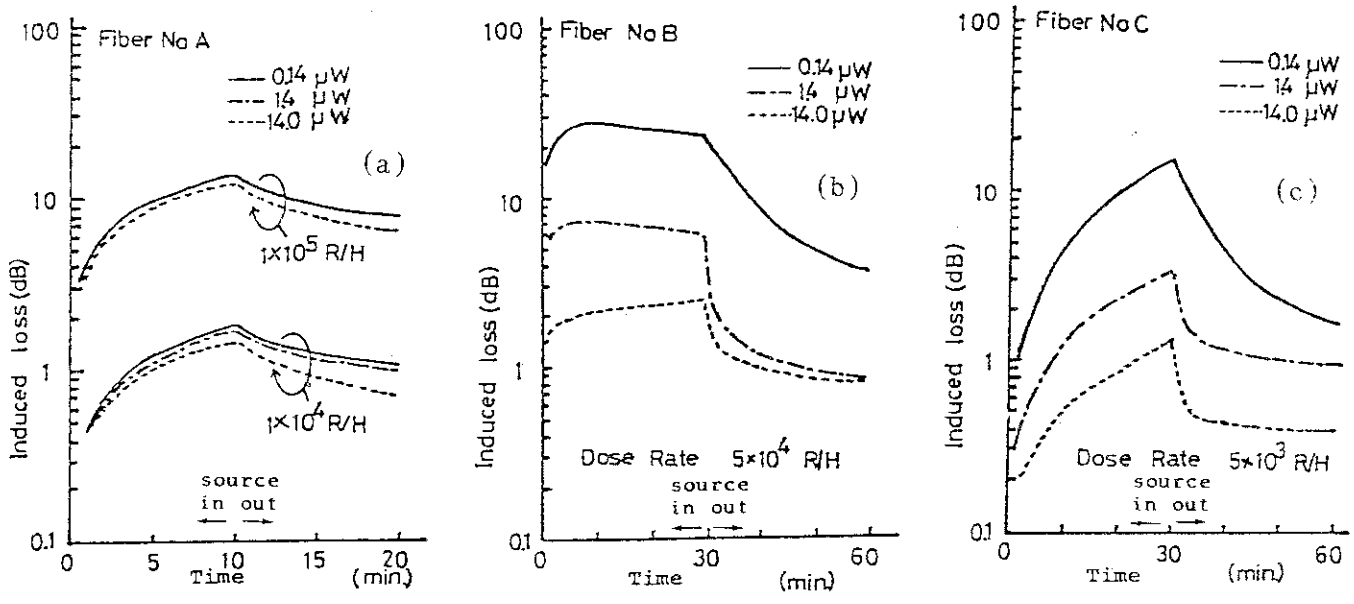

Fig. 6.5.2 Light power dependence of photobleaching effects

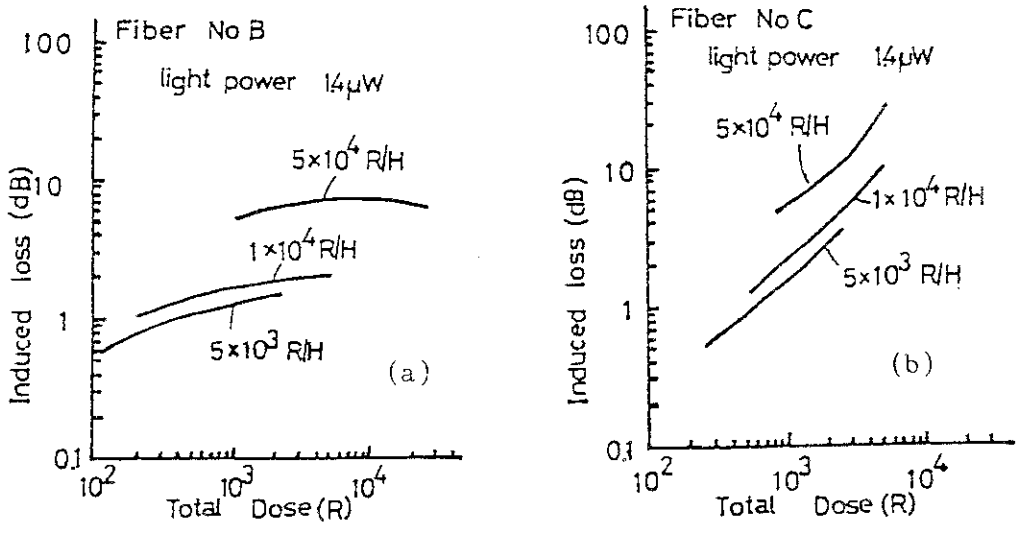

Fig. 6.5.3 Dose rate dependence of photobleaching effects

6.6 Improvement of a Closed-Cycle Cryogenic Refrigerator-Cooled High-Purity Germanium Gamma-Ray Detector System

E. Sakai, M. Nagai,* T. Nagasawa,* T. Takagi,* S. Ishikawa* and H. Nakatani*

Our previous results on the performance of a closed-cycle cryogenic refrigerator-cooled high-purity germanium detector system was reported in Reference 1 in which the effect of the vibration noises of the cold head on the achievable energy resolution was reduced by using two bellows for supporting the detector crystal. One problem of this system was inability of maintaining the vacuum in the chamber longer than 3 days probably due to the degassing from the inside wall of the chamber.

A newly-designed chamber shown in Fig. 6.6.1 was made. A long stainless steel tube fixed on the left-hand plate supports the detector crystal situated in the right-hand chamber. The results obtained from this chamber are summarized in Table 6.6.1 in which the FWHM energy resolutions for 60 keV, 122 keV and 1333 keV gamma-rays are listed with two different high-purity germanium detectors. The $50mm^2$ x 5mm detector gave a good energy resolution of 2.0 keV FWHM for 1333 keV gamma-rays although 1.3 keV FWHM for 60 keV gamma-rays showed a considerable effect of the vibration noises. The $400mm^2$ x 15mm detector gave 1.4 keV and 2.4 keV FWHM's for 60 keV and 1333 keV gamma-rays, respectively, and the effect of the vibration was larger than that for the $50mm^2$ x 5mm detector. This difference was probably caused by the different conditions of the vibration systems due to the different weights of the two detector crystals.[2)]

This new chamber was continuously operated for two months without any vacuum trouble. Molecular sieve and an ion pump will be used in the future experiments to ensure one year continuous operation.

References

1) Sakai E., Murakami Y. and Nakatani H.: "Performance of a High-Purity Ge Gamma-ray Spectrometer System Using a Closed-Cycle Cryogenic

* Summer visitors from Faculty of Engineering, Toyama University, 1-1, Nakagawasonomachi, Takaoka 933, Japan.

Refrigerator," *IEEE Trans. Nucl. Sci.*, NS-29, No. 1, pp. 760-763 (1982).

2) Sakai E., Hayashi Y.* Usui S.* and Nakatani H.*: "Cooling of High-Purity Germanium Detector with a Cryogenic Refrigerator," *The 37th Annual Meeting of Physical Society of Japan*, 2pSH14 (October 2, 1982, Sapporo, Japan).

Table 6.6.1 Energy resolutions obtained from high-purity Ge detector cooled by a closed-cycle cryogenic refrigerator

hpGe detector = APTEC 05005B (50mm^{2}x5mmt) -600V 77.6K
Cryogenic refrigerator = Cryosystem,Inc. LTC-21
Preamplifier = CI 970C (cooled FET)
Main amplifier = CI 2010 SYM HI

1982/8/22

Shaping time(us)	60keV gamma-ray FWHM(keV)	60keV gamma-ray FWIM(keV)	122keV gamma-ray FWHM(keV)	122keV gamma-ray FWIM(keV)	1333keV gamma-ray FWHM(keV)	1333keV gamma-ray FWIM(keV)
0.25	1.779	3.555	1.790	3.342	1.940	4.895
1	1.225	2.316	1.313	2.357	1.943	3.833
2	1.371	2.560	1.494	2.617	(2.864)	(4.809)
4	1.699	3.153	2.025	2.999	2.104	5.033
8	1.986	3.915	2.218	4.429	2.626	5.381

hpGe detector = APTEC CP4015S (22.8mm dia.x15mmt, 6.12cm^3)
-2000V 77.5K

1982/8/28

0.25	1.877	3.582	2.137	4.044	9.578	21.721
1	1.359	2.736	1.376	2.731	2.610	4.894
2	1.439	3.380	1.420	3.020	2.348	4.448
4	1.944	6.848	1.839	4.721	2.576	4.737
8	3.132	9.116	3.062	7.837	3.138	7.804

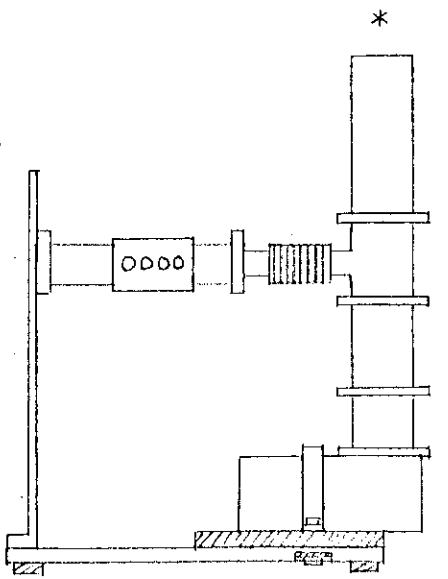

MT 16-93 - 106

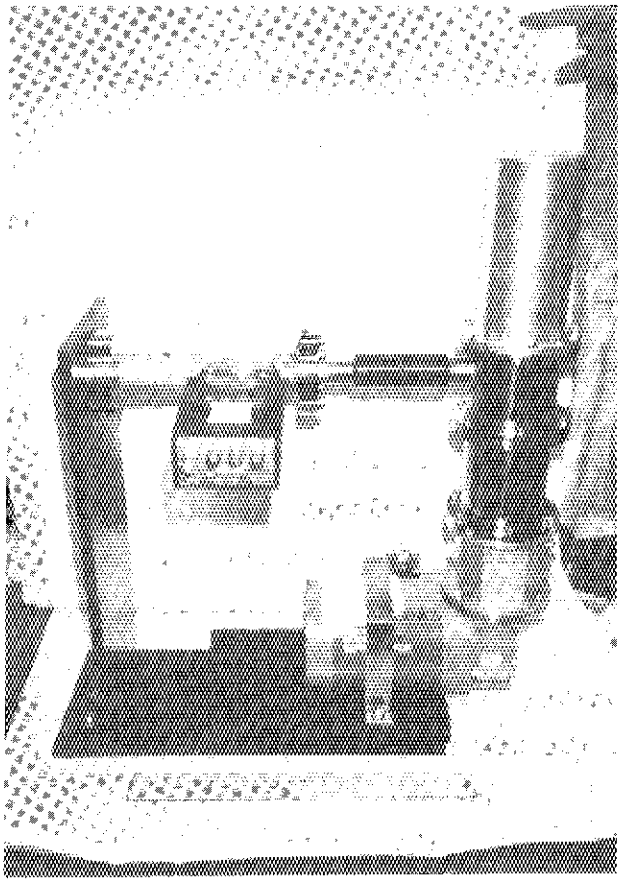

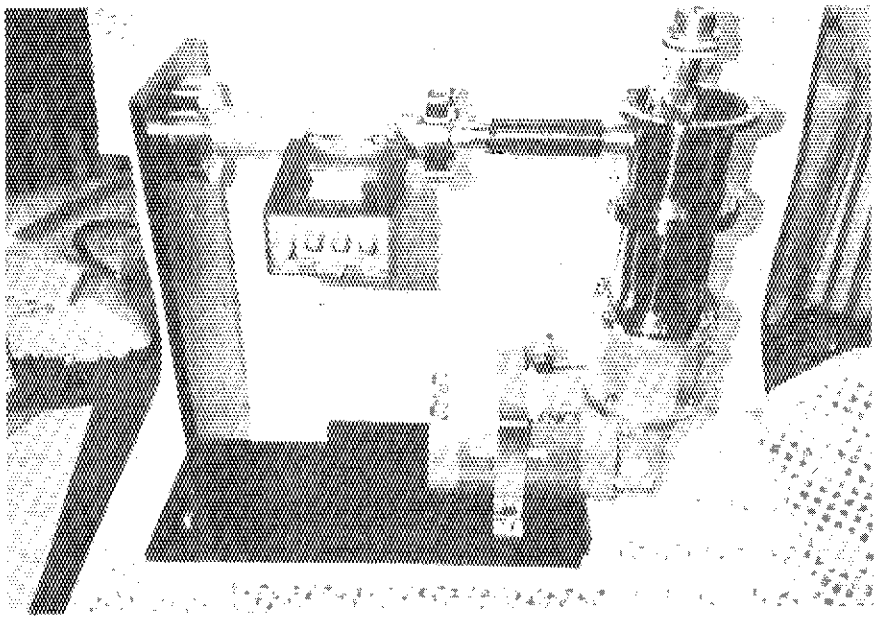

Fig.6.6.1 A newly-designed chamber for high-purity germanium detector cooling by closed-cycle cryogenic refrigerator

6.7 Development of Room Temperature Semiconductor Radiation Detectors

E. sakai, T. Takagi*, T. Nagasawa*, M. Nagai*, S. Ishikawa*
and H. Nakatani*

(I) Performance Test of Small Oxide-Passivated p-n Junction Type Silicon Detectors

Recently, an oxide passivation technique combined with photoengraving and ion implantation was successfully applied to fabricate silicon detectors of leakage currents less than 1 nA/(cm^2·100μm) and give 1.5 keV FWHM energy resolution for 122 keV gamma-rays at room temperature.[1] Fuji Electric Research and Development, Ltd. (FERD) also applied the oxide passivation technique to manufacture diffused p-n junction type silicon detectors of small size which exhibited leakage currents less than 1 nA at room temperature.[2] Their detector construction is shown in Fig. 6.7.1 and the starting materials were 10 - 30 kΩ·cm p-type crystals supplied by Komatsu Electronic Metals Co. The 8 μm thick n^+-layer of 1 mm diameter and the 3 μm p^+-layer were made by diffusing P and B at 1200°C. The crystal was 3.6 x 3.6 mm^2 x 140 μm and encapsulated in a TO-5 can with a 20 μm thick aluminum foil window.

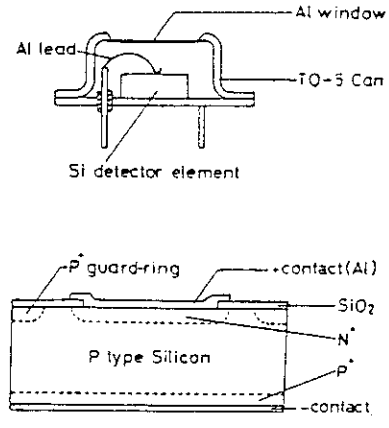

Fig.6.7.1 Construction of oxide-passivated p-n junction type silicon detector made by Fuji Electric R & D

We measured the performance of the four detectors supplied by FERD at room temperature, dry-ice temperature (-80°C) and liquid nitrogen temperature (-196°C). The leakage currents at 40V bias at room temperature, -80°C and -196°C were 0.5 nA, 1 pA and 50 fA, respectively. The capacitance was 1 pF at 40 V bias. The FWHM energy resolutions for 60 keV gamma-rays at 40 V bias were 1.5 keV, 1.0 keV and 1.0 keV, respectively, at room temperature, -80°C and

* Summer visitors from Faculty of Engineering, Toyama University, 1-1, Nakagawasonomachi, Takaoka 933, Japan

-196°C when a room temperature DC-coupled preamplifier was used. These results at room temperature confirm the reported performance of this type of the detectors[2] although Reference 2 did not describe the performance at -80°C and -196°C. We feel that this particular type of the detectors have limited application due to their too small sensitive volume. We require the detectors of much larger sensitive volume, at least 1 cm^2 x 1 mm from the view point of ordinary X-ray spectrometry.

(II) Development od GaSe Radiation Detectors

Only one report[3] was published in 1974 on the use of GaSe as a radiation detector material. In order to test the possibility of this material as a room temperature radiation detector, we evaporated gold or aluminum of 9 mm^2 onto 50 to 100 μm thick cleaved plates of GaSe grown by the Bridgman method to make Au-GaSe-Au and Au-GaSa-Al. The measurement of current vs. bias voltage characteristics revealed the material resistivities of (2 - 4) x 10^7 Ω·cm, but no formation of the necessary rectifying surface-barrier. We will test newly-grown crystals again in the next fiscal year.

References

1) Kemmer J., Burger P., Henck R. and Heijne E.: "Performance and Applications of Passivated Ion-Implanted Silicon Detectors," *IEEE Trans. Nucl. Sci.*, NS-19, No. 1, pp. 733-737 (1982).

2) Yabe M., Sato N., Kamijo H., Takechi T. and Shiraishi F.: "A Silicon X- and Gamma-Ray Detector for Room Temperature and Low Voltage Operation," *Nuc.. Instr. and Methods*, 193, pp. 63-67 (1982).

3) Manfredotti C., Murri R. and Vasanelli L.: "GaSe as Nuclear Particle Detector,"*Nucl. Instr. and Methods*, 115, pp. 349-353 (1974).

6.8 Uncertainty in Peak Area Evaluation

H. Gotoh and K. Teranishi*

When we evaluate the area of a peak well-resolved in a gamma-ray pulse height distribution, we usually do it by drawing a base-line underneath the peak. As the base-line, a straight line, a step function-type base-line or a cubic line are selected. To increase the stability of the base-line, plural channels of data at the both sides of the peak are used for the base-line determination. Although the uncertainty of the base-line is usually derived on the assumptions that the base-line is represented by the given function and that the count of each channel obeys the law of Poisson statistics, the satisfaction of the assumptions is not clear apriori. When we use plural channels of data more than necessary, the excess number of degree of freedom can be used to test the assumptions. If the result of the testing is 'rejection', the intervals of background regions should be changed, the shape of base-line should be changed, or the overall uncertainty of the peak area should be increased.

Fig. 6.8.1 is a pulse height distribution of the 586 keV peak of ^{152}Eu. The net peak area is about 7,800 counts. We intend to evaluate the area of the peak applying a step function-type base-line with a step at the center of the peak. We set the lower background region for the determination of the height of the left step to the 21 channels, 2,310 through 2,330 channels, and the higher background region for the right step to the 21 channels, 2,360 through 2,380 channels, both rather arbitrarily.

At this sort of statistics, the results of the χ^2-squares tests are 'acceptance' for both background regions, and the base-line is drawn as shown in Fig. 6.8.1. The uncertainties of the heights of both wings of the base-line are determined only by the statistics of counts and the area of the peak is obtained as 7,844 ±293 (1 σ) counts by the method described previously.[1)]

Reference

1) H. Gotoh and K. Teranishi: JAERI-M 82-114 (1982), p.117-119

* Hitachi Ibaraki Technical College, Hitachi Ltd.

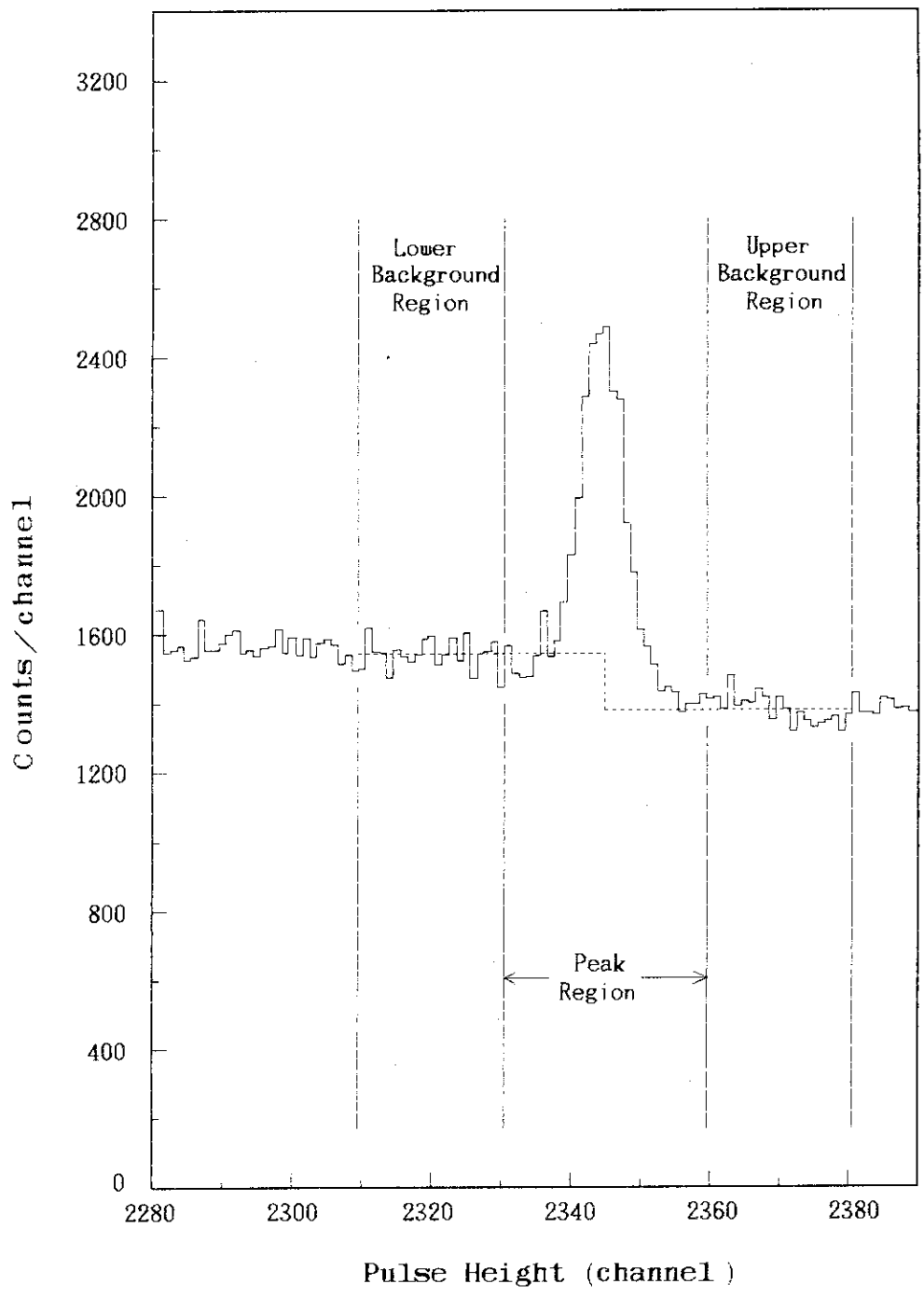

Fig.6.8.1 Pulse height distribution of 586keV peak of ^{152}Eu

6.9 Induced Radioactivities in Silicon and Germanium Irradiated with Various High-Energy Heavy Ions

E.Sakai

Semiconductor detectors are known to be sensitive to radiation damage which can be annealed by heating at high temperature. In the case of high-energy heavy ion detection with semiconductor detectors, fusion reactions are expected in the semiconductor materials to increase background counting rates due to long-life radioactivities produced. These radioactivities can not be annealed by heating. We have measured gamma-ray spectra from silicon and germanium irradiated with various high-energy heavy ions accelerated by JAERI 20 MeV Tandem accelerator to obtain radioactivities and production cross sections of residual radionuclides. The cross sections were obtained from observed radioactivities and the numbers of atoms of silicon or germanium in the heavy ion ranges. Figures 6.9.1 and 2 show the gamma-ray pulse height distributions obtained from silicon and germanium irradiated by 150 MeV $^{35}Cl^{9+}$ ions, respectively. Table 6.9.1 shows some of the results obtained.

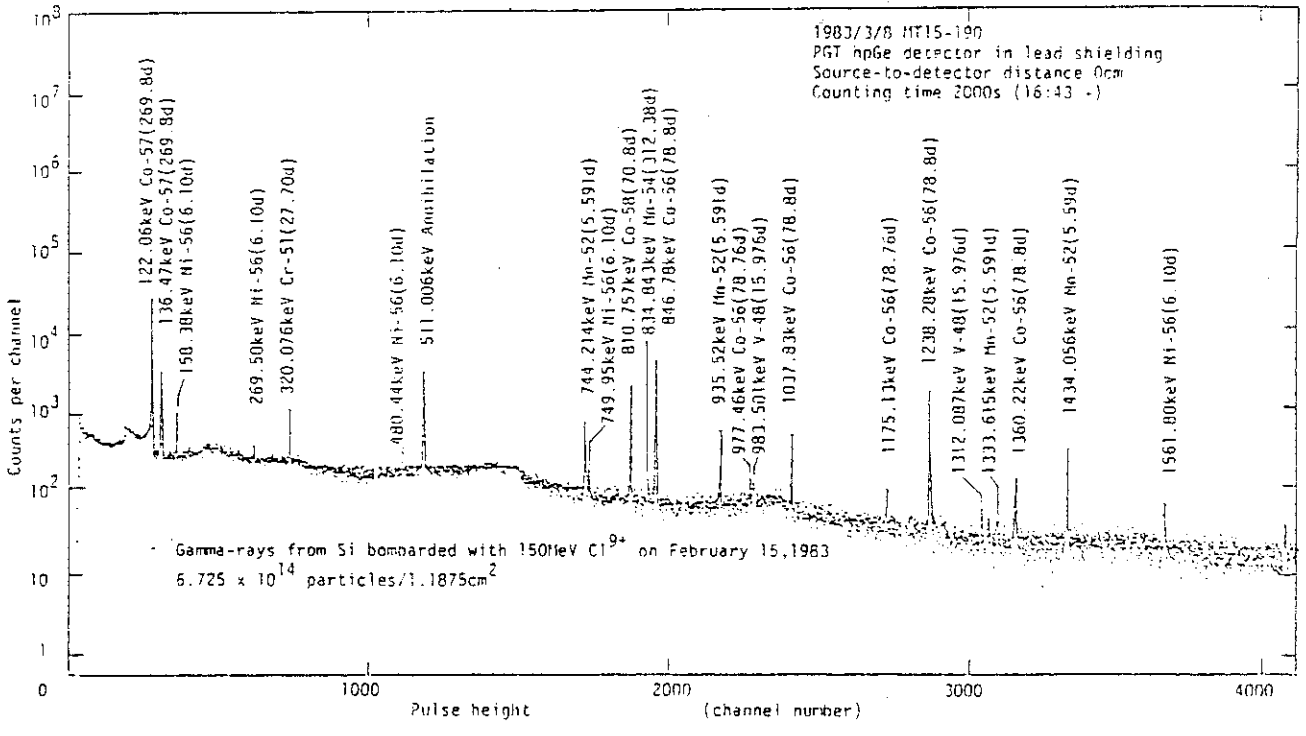

Fig.6.9.1 Gamma-ray pulse height distribution obtained from silicon irradiated by 150MeV Cl^{9+} ions.

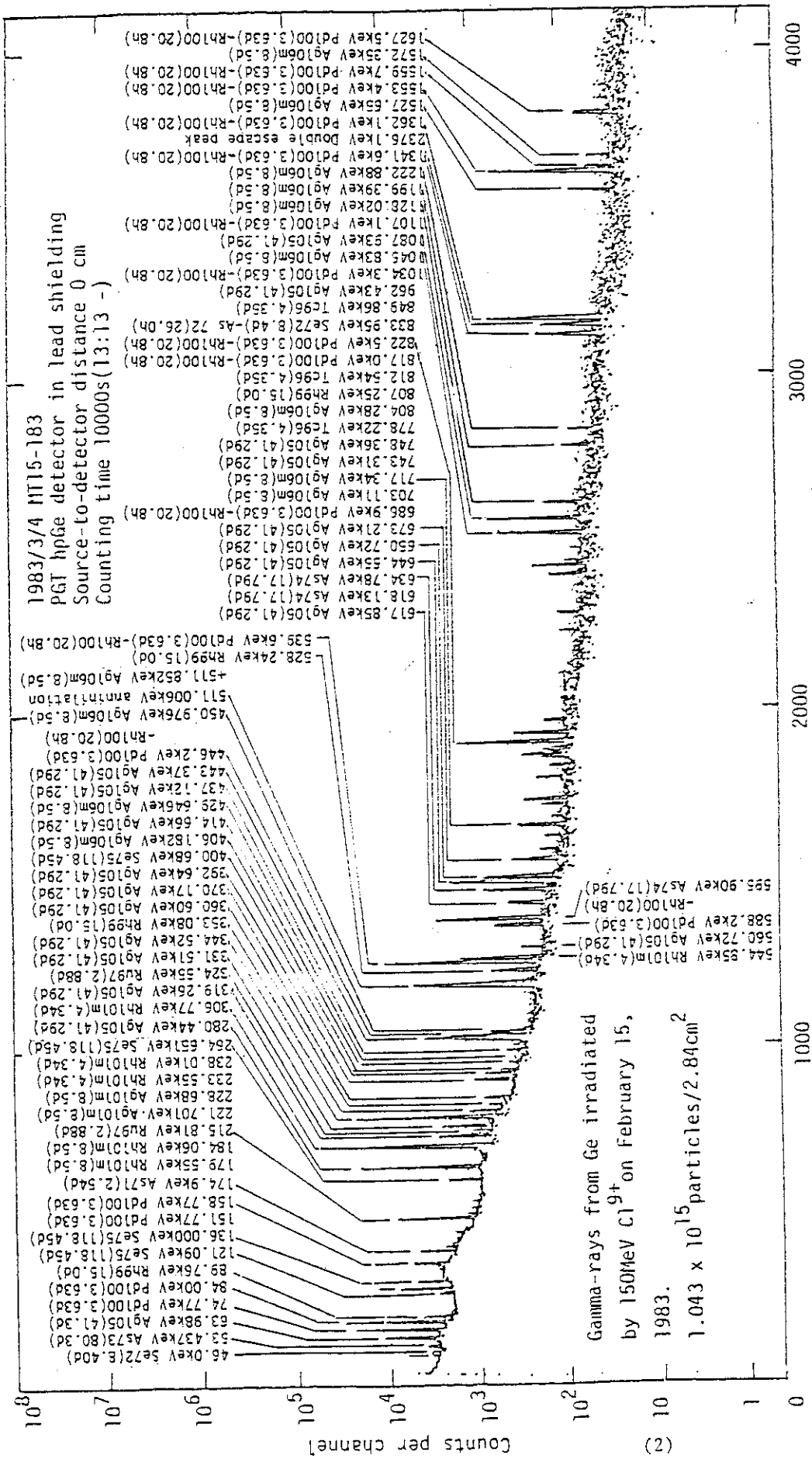

Fig.6.9.2 Gamma-ray pulse height distribution obtained from germanium irradiated by 150MeV Cl^{9+} ions.

Table 6.9.1 Residual radioactive nuclides, their radioactivities, numbers of atoms and production cross sections found in silicon and germanium irradiated by high-energy heavy ions

Heavy ions	Number of particles	Irradiated material	Residual nuclide	Radioactivity(uCi)	Number of atoms	Cross section(mb)
100MeV $^{16}_{8}O^{6+}$	3.52E15 /1.42cm^2	Si	Na-22(2.6y)	1.8E-4	7.9E8	0.46
			Be-7(53.3d)	2.85E-3	7.0E8	0.41
100MeV $^{16}_{8}O^{9+}$	7.17E15 /2.90cm^2	Ge	As-73(80.3d)	4.1E-2	1.5E10	8.2
			Se-75(118.45d)	3.1E-2	1.7E10	9.3
			Rb-83(86.2d)	4.2E-1	1.66E11	89.9
			Rb-84(32.9d)	3.2E-1	3.4E10	18.3
			Sr-82(25.0d)	9.3E-1	1.1E10	5.8
			Sr-85(64.85d)	1.45E-1	1.45E11	78.3
			Y-88(106.61d)	6.0E-2	2.9E10	15.9
			Zr-88(83.4d)	5.3E-2	2.0E10	0.9
150MeV $^{35}_{17}Cl^{9+}$	6.73E14 /1.19cm^2	Si	V-48(15.976d)	6.0E-4	4.4E8	2.9
			Cr-51(27.70d)	1.5E-2	1.9E9	12.4
			Mn-52(5.591d)	2.9E-2	7.5E8	5.0
			Mn-54(312.38d)			
			Co-56(78.8d)	1.8E-2	4.6E9	30.5
			Ni-56(6.10d)	4.0E-3	7.7E7	0.5
			Co-57(269.8d)	1.4E-2	1.2E10	77.1
			Co-58(70.8d)	8.6E-3	2.0E9	12.9
150MeV $^{35}_{17}Cl^{9+}$	1.04E15 /2.84cm^2	Ge	As-71(2.54d)	4.82E-2	5.6E8	4.14
			Se-72(8.40d)	1.7E-3	4.7E7	0.34
			As-73(80.30d)	2.4E-3	6.2E8	4.6
			As-74(17.79d)	4.8E-3	2.7E8	2.0
			Se-75(118.45d)	5.1E-4	1.95E8	1.4
			Tc-96(4.35d)	8.2E-4	1.14E7	0.08
			Ru-97(2.88d)	8.14E-2	7.5E8	5.5
			Rh-99(15.0d)	1.3E-3	6.1E7	0.45
			Pd-100(3.63d)			
			Rh-101m(4.34d)	8.4E-2	1.2E9	8.5
			Ag-105(41.29d)	1.9E-2	2.5E9	18.1
			Ag-106m(8.5d)	2.4E-3	6.5E7	0.47
150MeV $^{58}_{28}Ni^{9+}$		Si	Co-56(78.76d)	2.4E-3	8.6E8	
			Co-57(271.65d)	2.2E-4	2.8E8	
			Rb-83(86.2d)	0.78	4.5E10	
			Sr-85(64.85d)	1.25E-2	5.4E9	
150MeV $^{58}_{28}Ni^{9+}$	3.67E14 /3.14cm^2	Ge	None			
80MeV $^{127}_{53}I^{7+}$	2.93E14 /3.14cm^2	Si	None			

6.10 Least Squares Method for Instrumentation

M. Haruyama, H. Gotoh and H. Yagi

Nowadays many instruments are assisted by mini-computers or personal computers. And if we beforehand prepare proper least squares routines for such small computers, we shall be able to get final results without using a large computer and save time and labor for excess data handling. So, we made a program to prepare procedures of least squares method for instrumentation.

We can not put a general purpose least squares routine into a small computer, because it will require a large computer memory and take a long computing time. Our set of least squares routines should be composed of several routines suited for the kinds of problems. We classified the least squares problems by the type of conditions encountered in instrumentation and obtained Table 6.10.1. Each routine will be built of some kinds of modules of common use.

Some of routines have been programmed into mini-computers for pulse height analysis and data plotting and personal computers for computed tomography.

Table 6.10.1 Classification of Least Squares Problems

<table>
<tr><th>Type #</th><th>measure-ment</th><th colspan="3">Classification</th></tr>
<tr><td>1</td><td rowspan="2">direct measure-ment</td><td colspan="3">Unconstraint</td></tr>
<tr><td>2</td><td colspan="3">Constraint</td></tr>
<tr><td>3</td><td rowspan="6">indirect measure-ment</td><td rowspan="2">a transformation matrix is unitary</td><td colspan="2">linear</td></tr>
<tr><td>4</td><td colspan="2">non-linear</td></tr>
<tr><td>5</td><td rowspan="4">a transformation matrix is non-unitary</td><td rowspan="2">a transformed weight matrix is regular</td><td>linear</td></tr>
<tr><td>6</td><td>non-linear</td></tr>
<tr><td>7</td><td rowspan="2">a transformed weight matrix is irregular</td><td>linear</td></tr>
<tr><td>8</td><td>non-linear</td></tr>
<tr><td colspan="5">Application of the law of error propagation</td></tr>
</table>

7. Reactor Control and Diagnosis

7.1 Eigenvalue Programs in Plant Dynamics and Control

J.Shimazaki

In the field of plant dynamics and control, there are many problems which are transfered to an eigenvalue problem and solved by its own methods. These problems arise from stability evaluation of an objective plant, modal analysis and modal control, calculation of optimal state-feedback control, and reduction methods of dimension of a large-scale dynamical system. The QR method[1)2)] is one of the most powerful ones to calculate all the eigenvalues of a general matrix. However, only a few eigenvalues are sufficient to analyze the plant dynamics and control[3)]. For example, there usually exist only a few modes of poor stability in plant dynamics.

In order to analyze these modes the power method for solving eigenvalue problems is applied after some modifications. The basic procedure of the method is to calculate first a maximum absolute eigenvalue and the corresponding eigenvector of a matrix, and then the remaining eigenvalues are calculated by the eigenvalue deflation method. The main improvement is that the power method has been made applicable to the cases of both nearly equal eigenvalues and confluent ones. Figure 7.1.1 shows the flow chart of the main program for the improved power method. The effectiveness of the improved method was shown with some examples of different kinds of eigenvalues which were calculated using computer code based on this method.

In addition, the deflation method, which removes the calculated eigenvalue from the matrix and reduces the dimension of the matrix, was presented in comparison with the ordinary deflation method.

References

1) Wilkinson J.H., Reinsch C.: "Linear Algebra," Springer-Verlag (1971).
2) Fujimura T., Tsutsui T.: "EISPACK-J: Subprogram Package for Solving Eigenvalue Problems," JAERI-M 8253 (1979) [in Japanese].
3) Shimazaki J.: "An Improved Power Method for Solving Eigenvalue Problems in Plant Dynamics and Control," JAERI-M 82-083 (1982) [in Japanese].

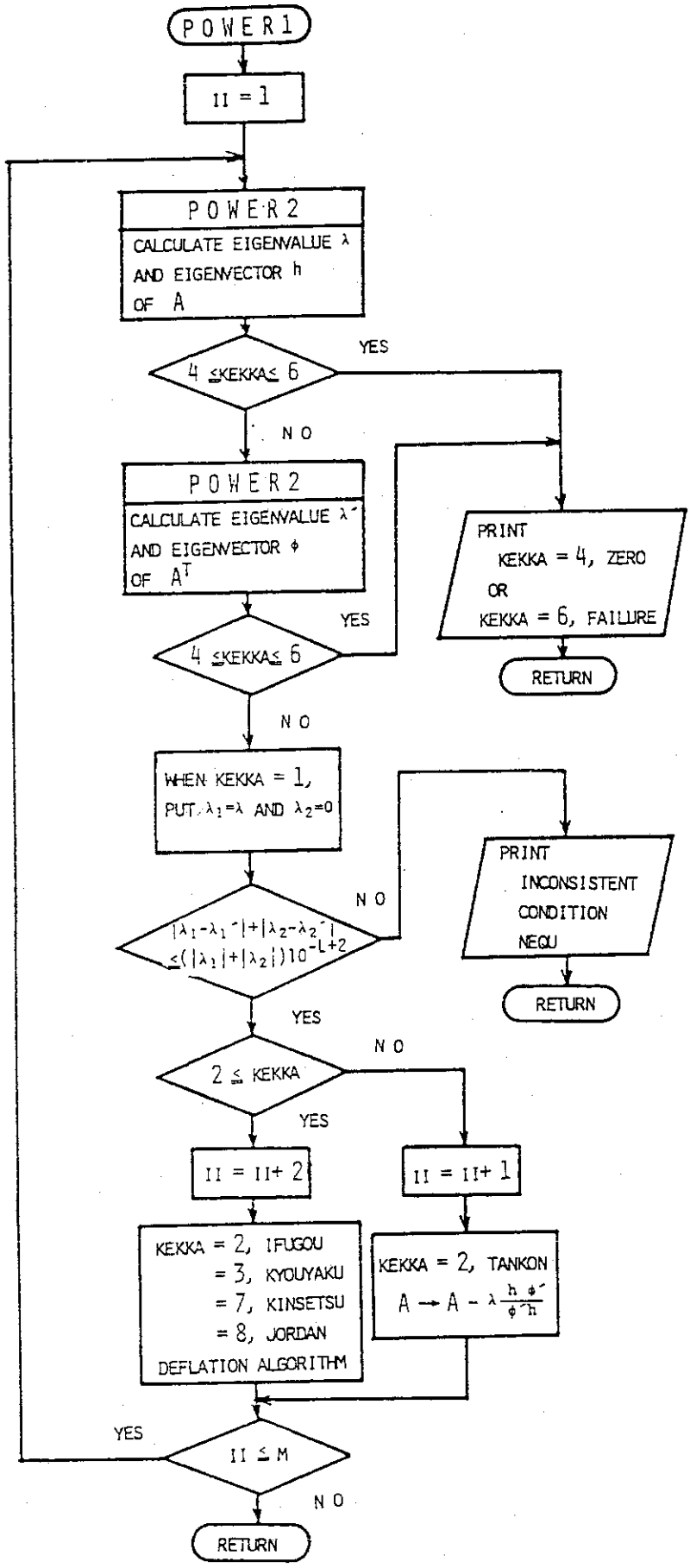

Fig.7.1.1 Flow chart of main program for improved power method

7.2 Dynamics Simulation Algorithm in the CAD System for Control System Design and Evaluation

J.Shimazaki, H.Usui and Y.Shinohara

A CAD (Computer Aided Design) system for control system design and evaluation (Version 1) has been developed[1]. This system has good characteristics in the method of describing dynamic model, dynamic simulation, interactive design system and data management.

As for the dynamic simulation, the time interval can be chosen so as to evaluate the transient within 2000 time steps, because the discrete model with a relatively large time interval is made by the Padé approximation method newly developed[2]. This dynamic simulation requires a short computing time and a small number of memory in which many simulation resuls are stored. The dynamic simulation is executed by the use of four files prepared for the subsystem, the control system and the total connection. The results of simulation stored in a file are used for graphic display to evaluate the response curves to various types of disturbance.

The CAD system was extended and revised to accept a control system model describing transfer functions and to simulate the transient with a large time interval. The CAD system is designed in the form of state-space representation for the effective dynamic simulation of a large scale system. Therefore the transfer function model is reformed into a state-space representation (observe canonical form) and then the discrete model is automatically generated in the revised CAD system. The minimalized dimensional realization and multidimensinal transfer function will be discussed in the future. In the dynamic simulation there exists a problem of time delay between subsystems in the case of a very large time interval chosen. Ordinarily, this problem does not occur because the subsystem has a sufficient time delay in its dynamics and the time delay between them is negligible. The iteration scheme shown in Figure 7.2.1 was developed to solve the problem. This iteration was usually convergent within several times.

References

1) Shimazaki J., Shinohara Y.: "A CAD System for Control System Design and Evaluation (Version 1)," JAERI-M 82-180 (1982) [in Japanese].

2) Shimazaki J.: "On Error Evaluation of Padé Approximants to exp(z)," Trans. SICE, Vol.19,No.2,p.197 (1982) [in Japanese].

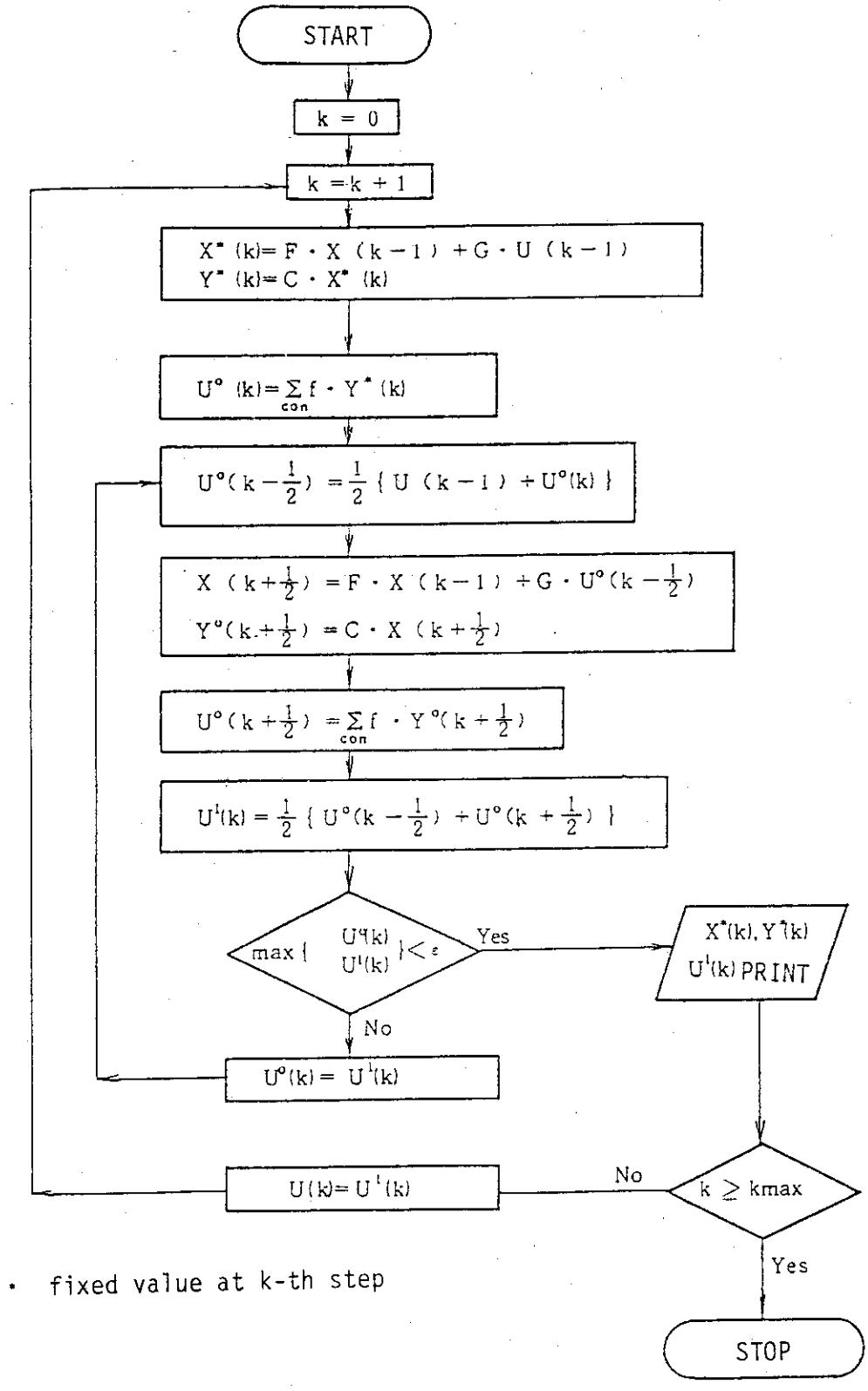

• fixed value at k-th step

Fig.7.2.1 Flow chart of iterative calculation in dynamic simulation on the CAD system

7.3 Development of Computer Code STAR-II for Dynamics Analysis and Diagnosis of Nuclear Reactor Systems

K. Hayashi, R. Oguma and K. Watanabe

The STAR-II, a computer code for dynamics analysis and diagnosis of nuclear reactor systems based on reactor noise analysis, has been developed as a HYSHARE-600 version of the original code STAR[1] which had been developed for PACER-600 computer system and published in 1981.

This code, as well as STAR, has been designed for a hybrid computer which is advantageous for handling of reactor noise data in analog form. In addition, this code includes all programs necessary for the analysis work from data acquisition through display of graphs, and main part of the analysis work can be performed using a user terminal.

This code permits system dynamics analysis in both time and frequency domain based on multivariate autoregressive (AR) modeling using the Yule-Walker (YW) method[2] or the least squares (LS) method and also spectral analysis by the Blackman-Tukey method or the fast fourier transform method which is mainly used for checking the validity of identified AR model. Furthermore, nonlinear system analysis programs using higher order spectrum are prepared in this code. Various diagnostic studies are also possible by combined use of these programs.

The main addition and modification adopted in STAR-II are as follows.

(1) Addition of a new algorithm for identification of the AR model
The LS method using the Householder transformation[3]

(2) Addition of the method for nonlinear system analysis :
Higher order spectral analysis
1) Bispectral analysis ..... Bispectra
..... Bicoherence
2) Criss spectral analysis .... Criss spectra
.... Criss coherence

(3) Modification of the method for dynamics analysis of system with feedback :
Signal transmition path analysis[4]
1) Global analysis ... Noise contribution ratio
... Signal contribution ratio

2) Local analysis .... Noise source power spectra
.... Extended partial coherence
.... Partial noise contribution ratio

So far some part of this code had been completed, that is, data acquisition, a part of preprocessing, data file utility, identification of the univariate AR model using the YW method, the Burg's method and the LS method and its applications.

References

1) Hayashi K., Oguma R. and Watanabe K.: "Computer Code - STAR : Statistical Analysis of Random Data - for Dynamics Analysis and Diagnosis of Nuclear Reactor Systems," JAERI-M 9761 (1981) (in Japanese).
2) Akaike H. and Nakagawa T.: "Statistical Analysis and Control of Dynamics Systems," Saiensu-sha (1971) (in Japanese).
3) Kitagawa G. and Akaike H. : Ann. Inst. Statist. Math., 30 (1978) Part B, 351-363
4) Oguma R.: "A New Method for Coherence Analysis of Systems with Feedback Effect Based on Autoregressive Modeling," JAERI-M 9756 (1981) (in Japanese).

7.4 Experimental Study of Boiling Detection

Y. Fujii, K. Hayashi, Y. Shinohara

In order to study the methods of detecting coolant boiling in the core of a nuclear reactor using neutronic and acoustic signals, a small water boiling loop has been constructed and installed at a light water critical assembly. An electrically heated in-core test section of the loop was inserted in the center of the core. A similar electrically heated out-of-pile test section with a transparent outer tube was also constructed in order to correlate the boiling regimes with acoustic signal patterns by visual inspection.

The boiling experiment was conducted with various combinations of heater power, flowrate and inlet water temperature. The neutronic signals were obtained from two CIC's which were located close to the core at opposite sides across the core. Three accelerometers were mounted on the test section tube; one on the inlet and two on the outlet side of the tube in order to obtain boiling acoustic signals.

An out-of-pile boiling experiment has also been conducted using a different type of heater and water tank in order to compare the acoustic noise characteristics between two cases.

The neutronic and acoustic noise signals were processed using an analyzer to obtain their power spectral density, correlaion and coherence functions. From this analysis, the following results were obtained.

(1) The nucleate boiling can be detected by observing the power spectral density functions of the acoustic signals but not by those of neutronic signals.

(2) The bulk boiling can be detected by observing the power spectral density functions of neutronic signals but less easily by those of acoustic signals because of their attenuation caused by large bubbles generated.

(3) Occurrence of boiling can be better confirmed by observing the coherence functions between the neutronic and acoustic signals.

Other methods of signal processing are also being applied with the aim of improving the detection sensitivity.

7.5 Study of Robotic Technologies for Nuclear Facilities

Y. Shinohara, H. Usui, Y. Fujii, S. Saito and A. Kumagai

Studies are being continued in order to develop advanced robotic remote handling systems for nuclear facility application.

In order to study the kinematic control of a multi-joint manipulator, a small manipulator with five degrees of freedom was purchased. Computer programs for controlling the movement of the manipulator to transfer objects have been developed using a high level computer language for robot control.

An experimental robotic remote handling system has also been constructed in order to study engineering problems such as control, communication, man-machine interface, etc., which are important for developing an advanced versatile robotic remote handling system.

The system can be divided into two parts: mobile work station and control station. The mobile work station consists of an electrically driven manipulator with seven degrees of freedom, a TV camera, a microphone, a servo- control unit, a sub-computer, two transmitters, etc., which are mounted on a crawler-type vehicle. The control station includes a main computer with its peripheral devices such as a CRT display terminal, disc drive, etc., a TV monitor, a master arm for the manipulator, a control panel with switches and buttons for manipulating the mobile station control.

Communication between the mobile work station and the control station is provided by two optical fibers or radio link.

All the system is controlled using the computer. The manipulator can be controlled in one of the following four modes; dial, master-slave, teach-and-playback and programmed control.

Development of computer programs for improved system control is now under way.

Reference

1) Shinohara, Y.: "Robot Technologies for Dismantling Reactor Facilities" Handbook of Automation and Robotization in Construction Works.(1982)

8. Development of Safequards Technology

8.1 A Near-Real-Time Materials Accountancy Model and its Preliminary Demonstration in Tokai Reprocessing Plant

K. Ikawa, H. Ihara, H. Nishimura, M. Tsutsumi* and T. Sawahata*

During the years from the spring of 1978 to May 1981 the governments of Japan, France and the United States of America mutually pursued a programme for the improvement of safeguards techniques as applied to spent fuel reprocessing facilities, with particular emphasis on the applicabilities of these techniques to the PNC Tokai facility. The International Atomic Energy Agency (IAEA) also participated in the programme, which was called by the acronym TASTEX for Tokai Advanced Safeguards Technology EXercise.

Among thirteen individual tasks (A∿M) of TASTEX programme, there was Task F for an investigation of the feasibility of applying to the PNC-Tokai Plant what has now come to be called near-real-time materials accountancy. Task F was carried out as a joint effort involving a number of persons of IAEA, Los Alamos National Laboratory (LANL), PNC, and JAERI. As the study progressed, the summary results have been presented before meetings of European Safeguards Research and Development Association (ESARDA), American Nuclear Society (ANS), Institute of Nuclear Materials Management (INMM), and the International Safeguards Symposium [1,2,3,4], and published, too (5,6). While the TASTEX programme was closed on May 1981, investigation of applicability of the n.r.t. accountancy system has been continued after that, and gave some valuable results particularly with regard to operational experiences of the field tests and analyses of sources of measurement bias.

Since the International Working Group on Reprocessing Plant Safeguards (IWG-RPS) recognized that the n.r.t. accountancy concept would have a significant potential for the improvement of IAEA safeguards, there has been considerable worldwide interest in it. A Consultants Working Group Meeting, sponsored by IAEA, on current technical status of n.r.t. materials accountancy was held on January 1982, and recommended to make more field exercises and demonstrations[7,8]. In those circumstances, PNC and JAERI have continued development work in this field.

The basic concept of an n.r.t. accountancy model proposed for PNC-Tokai reprocessing plant is described as follows:

(a) weekly in-process inventories would be taken of plutonium in the process MBA,

* Power Reactor and Nuclear Fuel Development Corporation

(b) measurements of both flow and inventory would be carried out either by conventional chemical methods or by instrumental (NDA) methods,
(c) all measurements would be completed, and the resulting MUF would be determined and evaluated, within a period of about two or three days after the in-process inventory, and
(d) evaluation of MUF data would be based on statistical techniques which utilize sequences of short term material balances.

The n.r.t. material balance equation is solved weekly using dynamic estimate of in-process physical inventory. Some or all of the data used in the n.r.t. material balance are determined using procedures designed to give rapid but not necessarily highly precise results. The in-process physical inventory includes all significant inventory quantities, but several minor process holdup quantities are knowingly omitted. Thus during initial startup operations MUF includes this unmeasured in-process inventory. Under steady-state conditions, only the fluctuations in this in-process inventory appear in MUF.

Analysis of materials accounting data for possible loss or diversion is one of the major functions of the n.r.t. accountancy system. Decision analysis, which combines techniques from estimation theory and system analysis, is well suited for statistical treatment of the imperfect n.r.t. material balance data that become available sequentially in time.

Effectiveness of the proposed n.r.t. accountancy model was evaluated by means of simulation techniques. The result showed that weekly material balances covering the entire process MBA could provide sufficient information to satisfy IAEA guidelines for small or medium-sized facilities. Applicability of the model to the actual plant has been evaluated by a series of field tests which covered four campaigns. In addition to the materials accountancy data, many valuable operational data with regard to additional locations for an in-process physical inventory, the time needed for an in-process inventory, etc., have been obtained. A CUMUF (cumulative MUF) chart of the resulting MUF data in the C-1 and C-2 campaigns clearly showed that there had been a measurement bias across the process MBA. This chart gave a dramatic picture of the power of the n.r.t. accountancy concept by showing the nature of this bias, which was not clearly shown in the conventional materials accountancy data.

The result of the field tests in the C-1 and C-2 campaigns triggered an operator's investigation on the bias problem. A special team was organized in Tokai Reprocessing Plant to resolve it. Two sources of bias

were identified and corrected, but it has been understood that on the basis of the available data these two biases should have accounted for only a part of the total observed bias. After these corrections the 81-2 campaign data were collected and found to be biassed positively. Change in the direction of the bias should be another problem, which suggests there may be another source of error that could not be accounted for by the two corrections identified in fact. The result of the investigation on the bias problem was reported elsewhere[9].

The study of five years since 1978 has shown that it might be feasible to apply near- real-time materials accountancy to the PNC Tokai Reprocessing Plant, that doing so could fulfill IAEA objectives in terms of detection timeliness and sensitivity, and that by such a system impacts on normal operations could be minimized. The next step of the development work of the near-real-time materials accountancy system in the PNC-Tokai Reprocessing Plant is to make a full demonstration of the system including Agency verification activities. It is planned to start as one of the projects of the Japan Support Programme for Agency Safeguards (JASPAS).

References

(1) Lovett J.E., et al.: Proc. ESARDA First Annual Symposium (1979).

(2) Ikawa K., et al.: Report of the Kiawah Island Topical Meeting, NBS Special Publication 582, 730 (1980).

(3) Ikawa K., et al.: Proc. INMM 22nd Annual Meeting, 390 (1981).

(4) Ikawa K., et al.: "A Near-Real-Time Materials Accountancy Model and its Preliminary Demonstration in Tokai Reprocessing Plant," Nuclear Safeguards Technology 1982, Vol.I, 499, IAEA-SM-260/136 (1983).

(5) Lovett J.E., et al.: "Application of the Basic Concepts of Dynamic Materials Accountancy to the Tokai Spent Fuel Reprocessing Facility - A Feasibility Study," IAEA STR-94 (1980); JAERI-M-9186 (1980).

(6) TASTEX: Tokai Advanced Safeguards Technology Exercise, IAEA Technical Reports Series 213 (1982).

(7) Department of Safeguards, IAEA: "Current Status of Near-Real-Time Materials Accountancy," IAEA STR 108 (1982).

(8) Lovett J.E., et al.: "Near-Real Time Materials Accountancy, A Technical Status Report," Nuclear Safeguards Technology 1982, Vol.I, 487, IAEA-SM-260/145 (1983).

(9) Tsutsumi M., et al.:"Result of Material Accountancy and Control and an Evaluation for MUF at the Tokai Reprocessing Plant," Nuclear Safeguards Technology 1982, Vol.II, 433, IAEA-SM-260/118 (1983).

8.2 Preliminary Evaluation of Near-Real-Time Materials Accountancy Models in a Large-Scale Reprocessing Plant

K. Ikawa, H. Ihara and H. Nishimura

A study of the feasibility of applying the concept of near-real-time materials accountancy (n.r.t. accountancy) to large scale spent fuel reprocessing facilities has been investigated using the Allied-General Nuclear Services Fuel Reprocessing Plant at Barnwell (BNFP) (1500 ton Heavy Metal/year) as the reference facility. This study has been carried out basing on the experience obtained in the study of the n.r.t. accountancy system using the existing Tokai Reprocessing Plant under the TASTEX (Tokai Advanced Safeguards Technology Exercise) programme[1,2,3]. Although a similar study had been performed at Los Alamos National Laboratory[4,5], this study has been carried out for the following two specific purposes:

(i) to investigate the feasibility of applying the ten-day-detection-time model, which was developed for a medium sized reprocessing plant under the TASTEX programme, to a large-scale reprocessing facility, and

(ii) to investigate the practical detection goals such as detection goal quantities as a function of significant quantities, detection times and probabilities related to detection capability and false alarm rates.

This study is at present at an early stage and has given us limited results which could not permit us to get clear-cut conclusions for the problems above mentioned.

In this study a near-real-time materials accountancy system is assumed in the plutonium purification process of the chemical separation process in order to evaluate its effectiveness from the view point of the materials accountancy for safeguards. At an early stage of this study, it was considered that the area to be covered by the n.r.t. accountancy should be the whole area of the chemical separation process. A simulation programme, DYSAS-R II, for such a purpose was developed. The result of test calculations indicated that a long-term simulation calculation of the whole material balance area requires very much computer time. Since the budget of this study was restricted, the time and space covered by a simulation programme had to be limited in shorter and smaller ones, i.e., four months and the plutonium purification process instead of the whole processes.

Main conditions of the n.r.t. accountancy are as follows:

(A) Sub-MBA structures: Two set of sub-MBA structures for the n.r.t. accountancy system were considered. These sub-MBA's require additional measurement points to get near-real-time material balances in these areas.

(B) Material Balance Periods: Three cases for 8 hrs, 2 days, and 1 week (168 hrs), which correspond to "the ten-day-detection-time model" developed in TASTEX project, were assumed for the comparison purpose.

(C) Frequencies of Calibration of Analysis and Flow Meters: Two cases, for every 24 hrs and every week were assumed.

(D) Measurement Accuracies of n.r.t. accounting: A set of data of measurement accuracies were assumed.

The results of simulation runs for diversion sensitivity analyses are summarized as follows:

Capability to Detect Abrupt Diversions

(1) In all cases simulated, the abrupt diversion can be detected before the total plutonium amount diverted does not exceed 8 kg.

(2) So long as the results of simulations up to now are evaluated, the following is suggested; An n.r.t. accountancy model of a single n.r.t. MBA for the whole plutonium purification process with a weekly in-process inventory, i.e., weekly material balance, may meet IAEA provisional criteria for detecting the abrupt diversion of 8 kg of plutonium.

(3) However, if the weekly material balance is adopted, there may be possibility that an order of 7 kg of plutonium could be diverted without detection, because the number of alarms may be so small and their level of significance may be so low that an inspector may not decide that the diversion has occurred.

(4) If the chemical separation process is divided into two separate parallel lines, however, longer (than 7 days) material balance period may be sufficient to counteract the abrupt diversion strategy.

Capability to Detect Protracted Diversions

(1) In case of the 8 hr-material balance period, the diversion of the minimum diversion rate, i.e., 8 kg Pu per year, could be detected at 3.5 months after the diversion was initiated. The total plutonium amount diverted did not exceed 2.3 kg when detected.

(2) In case of the 2 day-material balance period, the n.r.t. accountancy

model of the MBA model 1 could detect the diversion of the rate of 52 kg Pu per year at 36 days after the initiation of diversion, and the total plutonium amount diverted was restricted to 5.2 kg. If the MBA model 2 was adopted instead of the model 1, the diversion of the same rate could be detected at 3.8 months after its initiation, and the total amount at detection was restricted to 16.4 kg.

(3) In case of the weekly material balance, the diversion of the rate of 52 kg Pu per year could be detected at 4 months later, and the total amount diverted was restricted to 17 kg.

Evaluation of the Results of Simulations

(1) The time covered by the simulation runs is too short to bring a clear-cut conclusion on the capability to detect the protracted diversion. Longer simulations (6 months - 1 year) are desirable.

(2) The capability of the n.r.t. accountancy should be evaluated for the case that the plant consists of two parallel process lines, taking correlations between the two lines into consideration.

(3) The capability should also be evaluated when the n.r.t. accountancy system is extended to cover the whole chemical separation process. Correlations between two material balances of the dissolution-coseparation process and the succeeding plutonium purification process could be effectively utilized for safeguards purpose.

The study of the feasibility of applying the n.r.t. accountancy system to safeguarding large-scale reprocessing plants is still at an early stage. Quantitative evaluations of the capability of attaining detection goals by the n.r.t. accountancy system have just been started in Japan. From the study performed up to now several useful suggestions were obtained, and they can be utilized in the future study.

References

1. TASTEX: Tokai Advanced Safeguards Technology Exercise, IAEA Technical Reports Series 213 (1982).
2. Ikawa K., et al.: "Study of the Application of Near-Real-Time Materials Accountancy to Safeguards for Reprocessing Facilities," to be published as a JAERI-M report.
3. Lovett J.E., et al.: IAEA STR-94 (1980); JAERI-M-9186 (1980).
4. Hakkila E.A., et al.: LA-6881, Vol. I, II (1977)
5. Hakkila E.A., et al.: LA-8042 (1980)

8.3 Simulation Study of Safeguarding Uranium Enrichment Facility

K. Ikawa and Y. Hisamatsu*

The most concern with the uranium enrichment facility from the viewpoint of safeguards is the production of high enriched uranium without declaration. In the Hexapartite Project, technology holders accepted for IAEA inspectorate to access to the cascade hole of their centrifuge enrichment plants for the purpose of detection of such HEU production. Such an access will be done without announcement to the operator but the frequency of accesses is limited to some value depending on the plant characteristics and conceivable diversion scenarios. The safeguards approach of this type has now become to be called as "Limited Frequency Unannounced Access (LFUA)" approach.

The most concern of operators with LFUA approach is the possible leakage of sensitive information of the enrichment technology through inspection activities. Therefore operators desire to limit the frequency of access to the minimum, while the inspectorate wishes to make sufficient access to get his objective and quantitative conclusions. A sort of optimization will be needed to solve this problem and the reliable method for such an optimization must be developed as soon as possible. A key factor which may be used in such optimization will be the time to produce a significant quantity of HEU by modifying the cascade configuration. Another factor is the type of modifications as have been considered in the Hexapartite project.

To get information of these factors from the actual plant seems impossible for us. Therefore we have, again as in the case of reprocessing plant, developed a computer simulation system, and simulation runs have been done to simulate a lot of HEU production scenarios. The results showed, however, that there are still minor problems to be solved with regard to mathematical treatment of the time dependent behaviour of the material flows in cascades. Nevertheless, the simulation system has proved itself effective as a tool for designing LFUA safeguards approach for enrichment facilities.

---

* Century Research Center Co.

8.4 Simulation Study of Safeguarding MOX Fuel Fabrication Facilities

K. Ikawa, H. Ihara and Y. Hisamatsu*

A large scale mixed oxide (MOX) fuel fabrication facility is a sensitive facility from the view point of the international safeguards, because it usually contains a great amount of plutonium which could be used to produce nuclear explosive devices. Designing of materials accountancy system in such a facility is very important and should be made in parallel with the facility design in order to incorporate it into the facility design itself. As described in the previous sections (8.1, 8.2), it is convenient for such design to use simulation technology. Therefore we have developed computer simulation systems using Westinghous Anderson MOX Plant as a reference model plant. One of the simulation systems is DYSAS-M, which can simulate material flows in the plant in detail. A brief description of the simulation system will be made in Section 8.7.

Using these simulation systems, a feasibility study of applying the concept of near-real-time materials accountancy for safeguarding a MOX facility has been made since 1980. This study is, however, at present at an early stage and has given us limited results which could not permit us to draw a clear-cut conclusion for the effectiveness and the practicality of applying n.r.t.accountancy to the model MOX plant.

The model plant produces 100,000 LWR fuel rods of 2.0 kg MOX (PuO_2 :4 %, UO_2 :96 %) , or 200 MT MO_2/year, with 60% load factor. Feeds of the plant are 194 MT UO_2/year and 8 MT PuO_2/year.

Diversion scenarios assumed in the present study are abrupt diversion of the rate of 8 kg Pu/week and protracted uniform diversion of the rate of 8 kg Pu/year, 16 kg Pu/year, 24 kg Pu/year, 32 kg Pu/year and 52 kg Pu/year. In order to counter these diversion scenarios, the process area were assumed to be divided into four sub-material balance areas, the 1st sub-MBA includes PuO_2 blending and bulk storage areas, 2nd sub-MBA includes MO_2 powder blending and MO_2 storage areas, 3rd sub-MBA includes MO_2 pelletizing and inspection area, green pellet conveyer(storage), pellet sintering area and sintered pellet storage and inspection area, and the 4th sub-MBA includes pellet grinding area and pellet inspection and storage area. In these four sub-MBA's , n.r.t. accountancy systems are assumed to

* Century Research Center Co.

be adopted. Material balance periods assumed are 8 and 24 hours and 4 days. Calibrations are assumed to be made at every 24 hours both for bulk measurement systems and analytical systems. Each of simulation calculations covered four weeks.

The results are summarized as follows:

(1) Standard deviation of MUF-D is ranged between 1.01 to 1.03 kg Pu without depending on the assumed material balance periods and diversion scenarios. This is because of the very large amount of inventory in comparison with the amount of flow.

(2) The n.r.t. materials accountancy models assumed have a capability to detect abrupt diversion without depending on the length of their material balance periods.

(3) The n.r.t.materials accountancy models assumed could detect protracted diversion of the rate of 16 kg Pu/year with 8 hour-material-balance period, that of 32 kg Pu/year with 24-hour-material-balance period, and that of 52 kg Pu/year with 4-day-material-balance period.

(4) Protracted diversion of the rate of 8 kg Pu/year, which is the present IAEA detection goal, could not be detected by the assumed n.r.t. accountancy models within the simulated period, i,e., four weeks.

(5) Simulation of longer period is needed before drawing any conclusion about the capability of detection for 8 kg Pu protracted diversion.

8.5 Development of a Dynamic Material Flow Simulation Code for Reprocessing Facilities : DYSAS-R.II

H. Ihara, K. Ikawa, H. Nishimura, H. Sakuragi* and M. Ido**

In the Task-F of TASTEX projects[1], which started in 1978 and ended in 1981, a material flow simulation code DYSAS-R was developed to provide fundamental data for construction of a concept of Near-Real Time Materials Accountancy and for evaluation of its effectiveness, and the code successfully contributed the objective as an important tool for a quantitative study. Enlarging the function of DYSAS-R in such manner that the code is not restricted to a specific reprocessing plant and that the simulation is possible for the plant of an arbitrary capacity, if desired, with a different combination of processes, a new version of the code, DYSAS-R.II, has been developed. The code uses the GASP IV simulation language[2] just like other flow simulation codes developed in the Safeguards Technology Laboratory, JAERI. Using this code, it is possible to simulate the flow of nuclear materials in a continuous process of the reprocessing plant as well as in a batch process or in a mixed process of these. In addition, DYSAS-R.II has the following characteristics:

- Simulation of the plant may be restricted to a specific process, e.g., Pu purification process or co-dicontamination process.
- A simulation is possible for the flow of an isotope, e.g., Pu239, U235 or U238 instead of Pu or U.
- The code has a variable-dimensional array for the variables and a module to each type of processes. Because of these features, the code has a capability to simulate a mini-plant which consists of some selected number of processes, if desired, with an additional process or without some original processes only by changing the input data. It is also possible to select an arbitrary number of materials for simulation purpose. If a new process not registered in the code should be added to the plant, modification of the code can easily be done by adding a new routine for this process without changing other part of the code.
- The code has two options for the solvent extraction process; one is a simple model called 'functional box model'[3] in which the distribution of material concentration in the process is approximated as expressed by an

* Shikoku Electric Power Co.

** ISL Co. Ltd.

exponential function; the other is a model called 'SEPHIS model'[4] in which the chemical reaction among, and the distribution equilibrium of, the materials at the individual stage of the extraction process are handled accurately and the non-equilibrium state of the process is also handled properly although not exactly. Users can choose one of these models depending on their requirement to the quality of the simulation.

- If desired, an inventory in a pipe between two processes or in a small pot, and an elapsing time needed for the material to pass through the pipe can be taken into consideration in the simulation calculation.
- Flow vibration in the process is simulated using the standard random walk technique of the Monte Carlo method as follows:

(1) if the material flow exceeds a given value of upper or lower limit of vibration as the result of a random number generated, then the flow is controlled to return to the average value.

(2) the flow is determined by generating a random number within the limit of vibration which is established in proportion to the time length of the simulation calculation and to a given vibration width.

- As for the diversion, material reduction (or addition if the facility is misused) is supposed to take place at anywhere in the process area or at a place, where the product is transferred to the next storage area, with some amount of nuclear material being taken instantaneously at time t or a constant amount of material being taken continuously from time t1 to time t2 or with a combination of these extreme cases.

Fig. 8.5.1 gives an example of output from DYSAS-R.II, which shows a vibration of Pu inventories in the processes of the AGNS reprocessing plant as the result of the material flow simulation.

References

1) Ikawa K., et al.: "Study of the Application of Near-Real Time Materials Accountancy to Safeguards for Reprocessing Facilities," to be published as a JAERI-M report.

2) Pritsker A.: "The GASP IV Simulation Language," Wiley-Interscience (1974).

3) Hakkila E.A., et al.: "Coordinated Safeguards for Materials Management in a Fuel Reprocessing Plant," LA-6881 (1977).

4) Watson S.B., Rainey R.H.: "Modification of the SEPHIS Computer Code for Calculating the Purex Solvent Extraction System," ORNL-TM-5123 (1975).

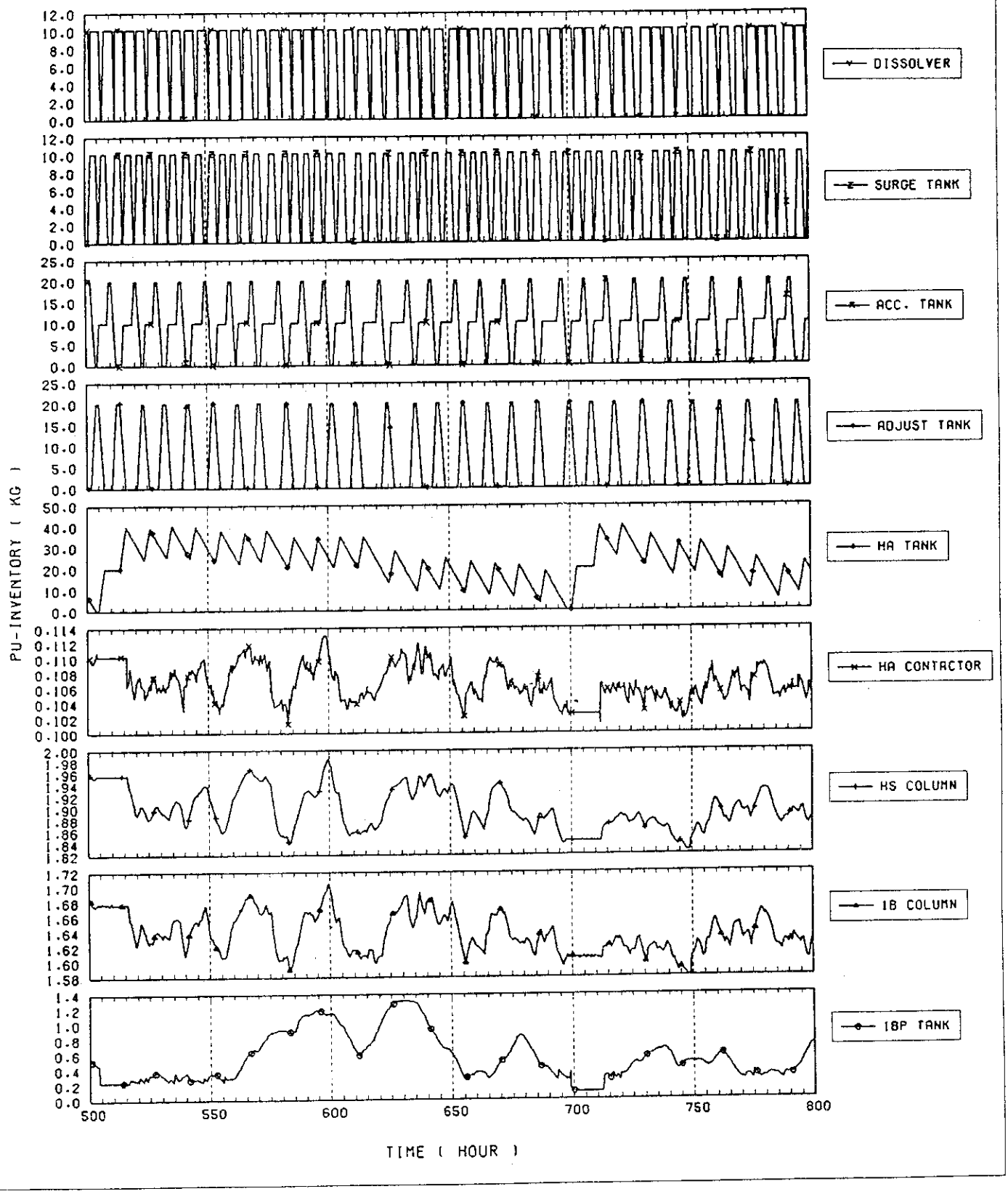

Fig.8.5.1 An example of output from DYSAS-R.II, which shows a vibration of Pu inventories in the processes of the AGNS reprocessing plant

8.6 Development of a Dynamic Material Flow Simulation Code for Pu Conversion Facilities : DYSAS-C

H. Ihara, T. Koyama*, K. Ikawa and H. Nishimura

In order to attain the timeliness goal in safeguarding Pu conversion facilities[1)2)], a near-real time materials accountancy (NRTA) system could be introduced into the facilities as an improved safeguards approach. Therefore it is important to analyze an applicability of such system to a Pu conversion plant. For this purpose a simulation technique can be used. A code, named DYSAS-C, to simulate dynamically a material flow and inventory in each process of the plant has been developed in order to prepare the fundamental data required for a quantitative evaluation on how the NRTA system works as an effective and efficient safeguards measures.

As a model plant, a facility in which Pu-U mixed nitrate solution is converted to the mixed oxide powder in order to prepare an input material for MOX fuel fabrication facilities was chosen. This facility is supposed to apply the microwave heating method to the dinitration process, which will be working in the PNC plant if the planned operation begins in Autumn, 1983. Also the model facility has a similar feature with the PNC plant, i.e., it receives plutonium nitrate and uranium nitrate solutions which are produced in a plant similar to the PNC Tokai reprocessing facility and mixes these solutions in a rate of 1:1 before proceeding to the dinitration and oxidation processes. The model Pu conversion plant is shown in Fig. 8.6.1.

DYSAS-C was written in FORTRAN-IV and it uses a subroutine package prepared by the GASP-IV simulation language[3)] for scheduling process events and integrating process variation. Each process was classified by its function and each group of processes was programmed as a module in the code. The model plant, in general, consists of processes with a continuous operation mode and processes with a batch operation mode. The batch operation was modelled as if the materials instantaneously transfer to the next process according to the schedule. On the other hand, flow of materials in the process under a continuous operation was supposed to fulfill the following continuous equations :

$$\frac{dM(t)}{dt} = \Sigma F_i(t)$$

---

* Visiting research engineer from ISL Co. Ltd.

and

$$\frac{dS(t)}{dt} = \Sigma C_i(t) \cdot F_i(t)$$

where M(t) is an amount of bulk material in a process at time t, S(t) is a quantity of SNM in the process at the time t, $F_i(t)$ is a mass flow rate of bulk material in i-th input or output stream at the time t, and $C_i(t)$ is a concentration of SNM in the i-th stream at the time t. These equations are solved under proper initial conditions and process constraints, and the results give a dynamical behavior to each process. A material balance is calculated for each process as well as for all processes in a given time step based on the material flow and inventory in the process. This balance data is stored on a file together with its components as the true status value at the time and used as an input data to the measurement simulation code. Characteristics of DYSAS-C are summarized as follows:

(1) it is flexible to a change of processes because any combination of the processes is realized by giving a proper input data to the code.

(2) it is responsive to a change of process capacity of the plant by changing the status data and the scheduling data at each process.

(3) it has a capability to simulate a diversion of nuclear material (or a misuse of the plant: an artificial addition of nuclear material to the process) in an abrupt or protracted mode or an mixed mode of these.

References

1) Dayem H.A., et al.: "Coordinated Safeguards for Materials Management in a Nitrate-to-Oxide Conversion Facility," LA-7011 (1978).

2) Dayem H.A., et al.: "Coordinated Safeguards for Materials Management in a Uranium-Plutonium Nitrate-to-Oxide Coconversion Facility: Corpecal," LA-7521 (1979).

3) Pritsker A.: "The GASP-IV Simulation Language," Wiley-Interscience (1974).

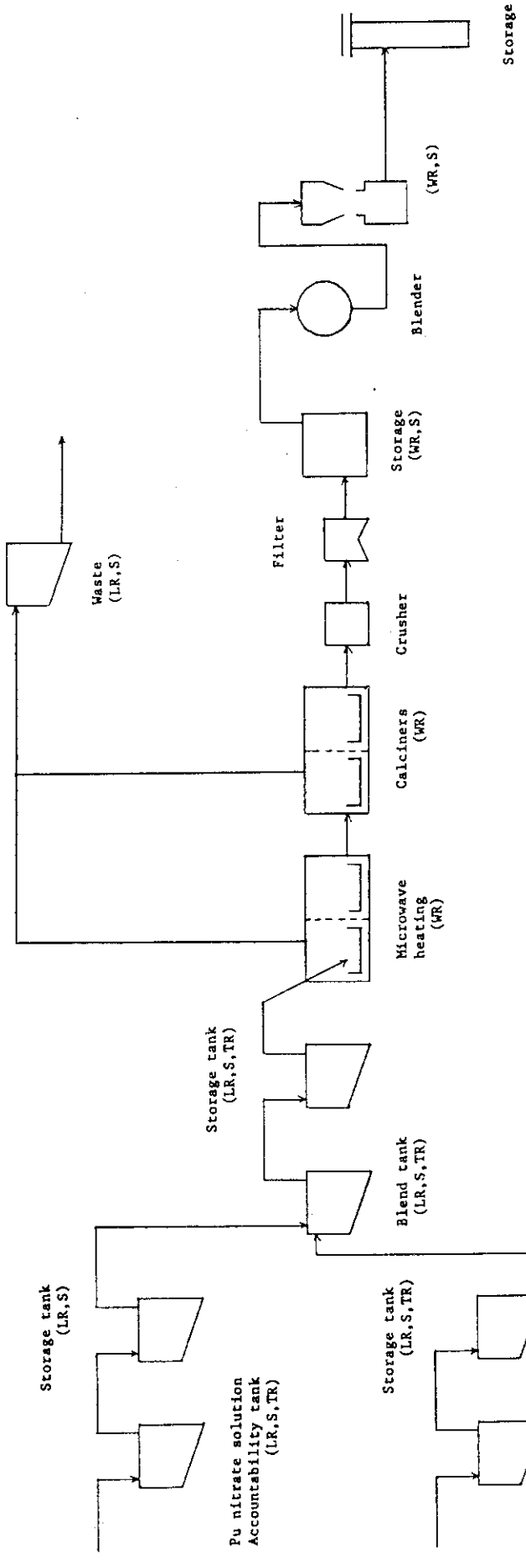

Fig. 8.6.1 Model Pu Conversion Plant Process Flow

8.7 Development of a Dynamic Material Flow Simulation Code for MOX Fuel Fabrication Facilities : DYSAS-M

H. Ihara, K. Ikawa, H. Nishimura and Y. Hisamatsu*

In order to evaluate a design of the Near-Real Time Materials Accountancy in a MOX fuel fabrication facility, a code named DYSAS-M has been developed to simulate quantitatively the amount of flow and holdup in each processes of the facility.

As a model facility, the Anderson plant of Westinghouse[1)2)] which produces 100,000 fuel rods (containing 2 kg MO_2 for each rod) for LWR's (Pu: 4 w%) by processing annually 200 t MO_2 was chosen. The code handles such nuclear materials as PuO_2, UO_2 and MO_2 which have various physical forms, e.g., powder in bulk, in a can or in a container, pellets or rods, etc. The base line of the model mixed-oxide plant is composed of the following processes; PuO_2 receiving, storage and unloading; PuO_2 powder blending and storage; MO_2 powder blending and storage; MO_2 pelletizing and inspection; green pellet storage; pellet sintering, storage and inspection; pellet grinding, inspection and storage; fuel rod loading, inspection and storage; and clean scrap recover system. A block diagram of the base line of the plant is shown in Fig. 8.7.1.

DYSAS-M provides a capability to simulate the plant under operation by generating a time dependent event using the Monte Carlo simulation method. Every particular unit process receives events of the material flow and inventory according to the schedule which is prepared by a controller routine written in the GASP IV simulation language[3)]. The material balance equation of the n-th period is given as follows,

$$MB_n = XM_{n-1} + HU_{n-1} + DV_{n-1} + BI_n - XM_n - HU_n - DV_n - BO_n - SM_n - WM_n - AS_n - DIV_n$$

where MB is a true material balance and should be 0, XM is an in-process inventory, HU a holdup, DV losses, BI an input batch, BO an output batch, SM a scrap, WM wastes, AS samples taken for analyses, and DIV is a material diverted.

Event data obtained by a simulated operation of the plant are stored in a disk file for further use in the measurement simulation code SIMAC.

References

1) USAEC Docket No. 70-1432 (1973).

2) Shipley J.P., et al., LA-6536 (1977).

3) Pritsker A.:"The GASP IV Simulation Language," Wiley-Interscience(1974).

* Century Research Center Co.

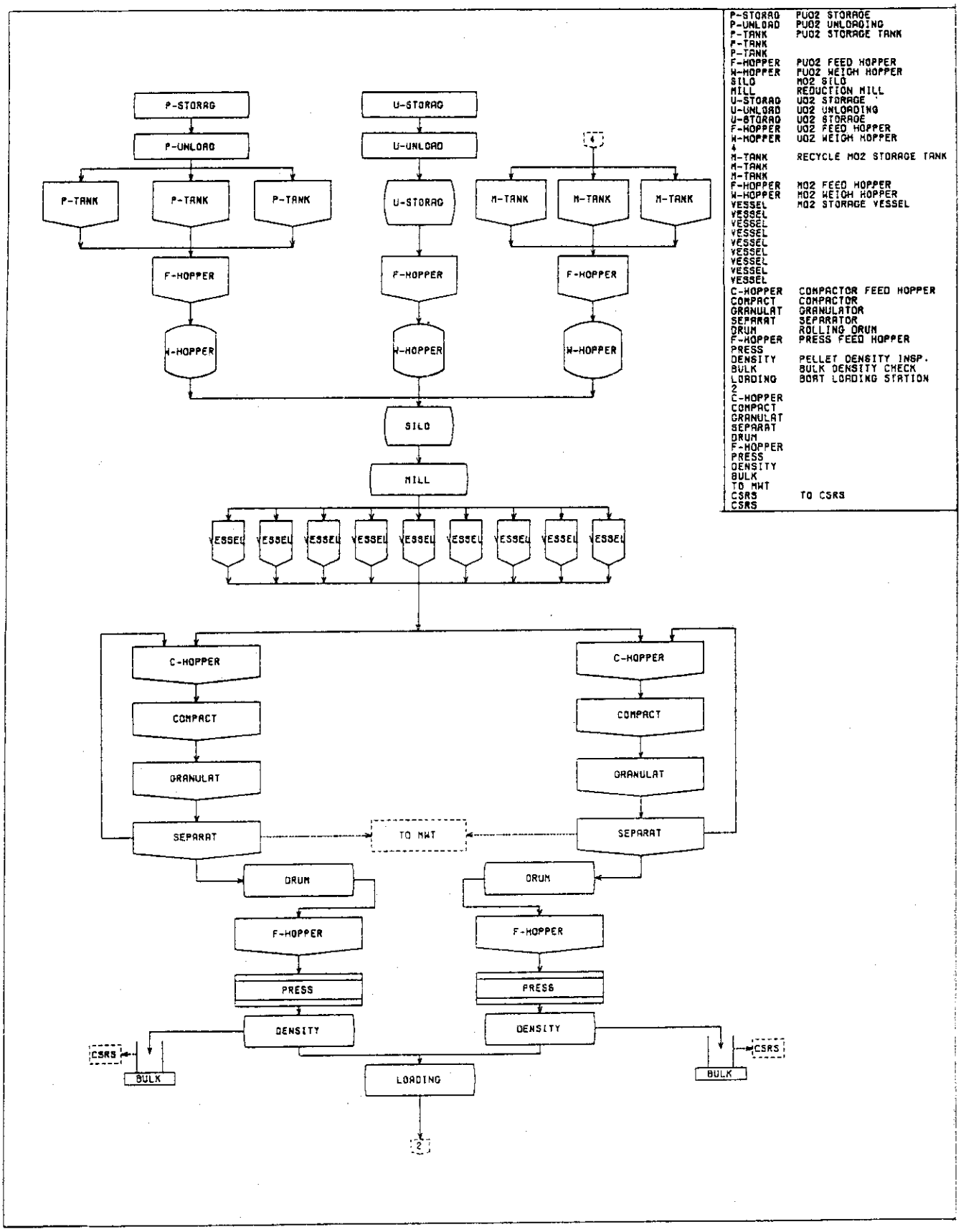

Fig.8.7.1 Base process line in the model mixed-oxide fuel fabrication plant

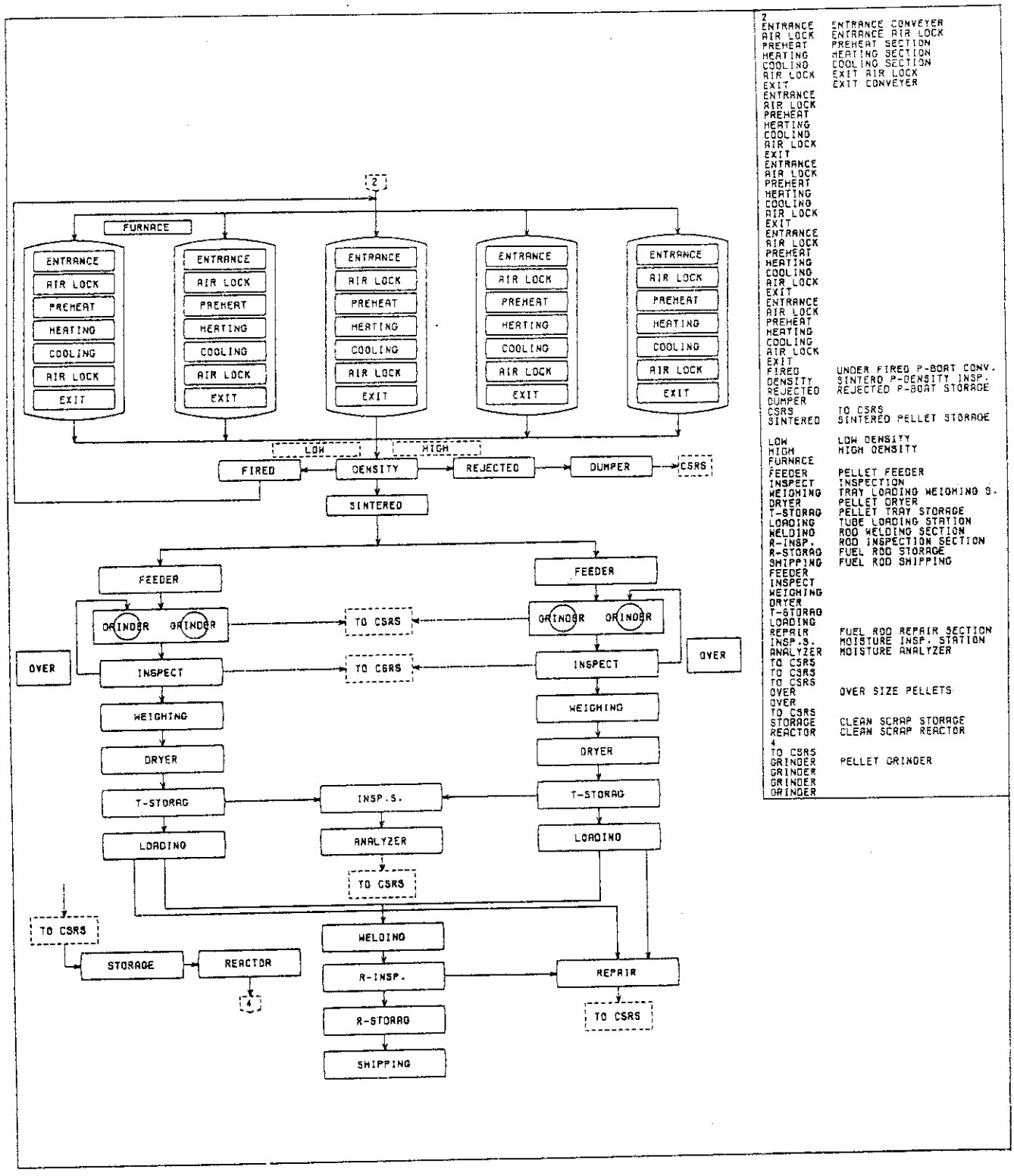

Fig.8.7.1 (Continued)

8.8 Development of a Dynamic Material Flow Simulation Code for Centrifuge Enrichment Facilities : DYSAS-E

H. Ihara, K. Ikawa, H. Nishimura and Y. Hisamatsu*

In order to study an application of the near-real time (n.r.t.) materials accountancy concept to safeguarding centrifuge enrichment facilities, a code, named DYSAS-E, has been developed as a tool for simulation of material flow and inventory in each process of the facility.

This code uses the GASP IV simulation language for simulation purpose and has six function modules for a group of processes of the facility. These are:

(1) TANKDD model: Input and output materials are transferred batch-wise.
(2) TANKDC model: Input material is supplied batch-wise but output material is transferred continuously to the following process.
(3) TANKCD model: Input material is supplied continuously but output material is transferred batch-wise.
(4) TANKCC model: Input and output materials are transferred continuously.
(5) Square cascade model[1], and
(6) Ideal cascade model[1].

Combining these function modules, the code is able to simulate any type of facilities. A dynamical material behavior in the cascade[2] can be simulated as well as its static behavior by solving a differential equation for the material at each stage of the cascade using the Runge-Kutta method. This differential equation was introduced under the following assumptions:

(a) Flow rate is not changing.
(b) Rate of the inventory at each stage to the flow of enriched material (up-stream) is constant.
(c) Inventory of the material is mostly localized in the high pressure side of the centrifuge and its concentration is represented by the material concentration in the flow of depleted material (down-stream).
(d) No gas leaks from processes in all stages of the cascade.

Since it is difficult to acquire a detailed information on the centrifuge enrichment plant, the code provides the data needed for simulation by making a cascade model and by calculating the number of

* Century Research Center Co.

stages in each section, e.g., enriching and stripping, and the characteristics of this model, based on such input data as separation factor, head separation factor (square cascade only), material composition in feed, product and tail stream, reflux ratio (square cascade), and feed flow ratio. Tanks and pipes are supposed to be the places where a removal of nuclear material might take place. It is not possible, however, to simulate a diversion of nuclear material from the cascade in the present version of the code, although it is possible to analyze such a diversion scenario as enriching the fissile uranium isotope into a given percentage of enrichment by supplying a part of nuclear material from the product pipe in the cascade to a clandestine cascade as a feed. The code has a function of restart for the simulation covering a long period of time, i.e., interrupting the simulation calculation at any time and starting again the calculation from that time consecutively.

References

1) Ikawa K.: "Feasibility Study on the Application of the Basic Concepts of Dynamic Materials Accountancy to a Uranium Enrichment Facility Using Centrifuge Process (I)," JAERI-M 9173 (1980) (in Japanese).

2) Naruse Y., Yoshida H.: "Separation of Gases by Porous Membrane Method," JAERI-M 7858 (1978) (in Japanese).

8.9 Development of a Simulation Code for Safeguards Measurements and Accountancy : SIMAC

H. Ihara, K. Ikawa, H. Nishimura, H. Sakuragi* and M. Ido**

In order to simulate safeguards measurements and accounting procedures, a Monte Carlo computer code SIMAC has been developed.

A model of measurement errors and their propagation is that of J.L. Jaech's[1)2)]. Using the flow simulation data generated in advance by a material flow simulation code, e.g., DYSAS-R.II, DYSAS-C, DYSAS-M and DYSAS-E, the code, SIMAC, simulates the measurements of nuclear material in a facility including analyses of samples taken in the key measurement points, which are carried out both by the operator for accountancy purpose and by the inspector for verification purpose.

In SIMAC, only the multiplicative model is adopted to express a measured value with precision and accuracy (errors are not of absolute values but of relative ones). In general a measurement error is assumed to consist of three components,

(a) a random error which affects only a single member of a set of measurements,

(b) a short-term systematic error which affects some, but not all, members of the set of measurements, and

(c) a long-term systematic error which affects all members of the set of measurements.

For these error components, further assumptions are imposed:

(i) Each error component has a characteristic of unbiased random variable, which means that the error component has a normal distribution with a mean value of zero and a given standard deviation and that, if any known measurement biases exist, the data are to be appropriately corrected.

(ii) Error components are uncorrelated with one another, which means that the covariances between two error components are to be zero.

In a simulation process, a random number is generated for each measurement to determine its random error component. As for the short-term systematic error, a new random number is generated only when a set of conditions are different from the previous ones, e.g., when a calibration has been done. On the contrary in case of the long-term systematic error, a

* Shikoku Electric Power Co.

** ISL Co. Ltd.

random number is generated at the beginning of the simulation, and it is used throughout that simulation without any change.

Using such error model, and taking into consideration a sampling error, net weight of an item and its element factor and isotope factor are calculated mathematically. Then, the amount of element or isotope and its variance are calculated combining these values.

In SIMAC, a run covers the whole period of time to be simulated for the generation of measurement data. Based on these generated data, MUFs and a CUMUF are calculated as well as their standard deviations, taking into account the propagation of systematic errors correctly. At present, SIMAC has a modified version for each type of facility. Some versions have a special procedure for sampling for the generation of inspector's measurement data. In case of reprocessing facilities, however, such procedure is not necessary because inspectors take all batches for measurements due to the size of batches. In case of the version for MOX fuel fabrication facilities, such plant specific feature as a structure of sub-MBAs is taken into consideration. For enrichment plants, it might be required to add to the code the additive model for the expression of measurements because inventory of gaseous material has to be handled properly, although such model is not built in at the moment.

References

1) Jaech J.L.: "Statistical Method in Nuclear Material Control," TID-26298, Exxon Nuclear Company (1973).

2) Hakkila E.A., et al.: "Coordinated Safeguards for Materials Management in a Fuel Reprocessing Plant," LA-6881 Vol.1 (1977).

8.10 Development of Safeguards Data Analysis Codes : SADAC and SPTPLT

H. Ihara, K. Ikawa, H. Nishimura, M. Ido* and H. Sakuragi**

Analysis of accountancy data for the purpose of the timely detection of a possible nuclear material loss or diversion is one of the major functions of material management and accountancy system. SADAC (Safeguards Data Analysis Code) and SPTPLT (Safeguards Probability Test Plotting Code) have been developed for this aim[1]. SADAC has a capability of detecting both a short-term loss, or abrupt diversion, and a long-term loss, or protracted diversion, and SPTPLT has a capability of displaying and plotting the results of the analyses. The decision analysis, which is applied to the accountancy data in SADAC, has the following main targets :

(a) detection of the event(s) that SNM has been lost or diverted,

(b) estimation of the amount lost or diverted, and

(c) determination of the significance of the estimates.

Normally SADAC handles the data generated by SIMAC, and the results of the decision analyses, e.g., sequential decisions, are graphically given in a form of alarm sequence chart by SPTPLT.

The present version of SADAC includes the following analysis methods:

1) LEMUF: a test based on the Limit of Error of MUF ($\pm 2\,\sigma_{MUF}$).

2) CUMUF: a test based on the CUmulative sum of MUFs.

3) UDT : Uniform Diversion Test based on an average loss estimated by Kalman filter.

4) Wilcoxon Rank sum test :
one of non-parametric tests, where the Rank sum which is a sum of ranks of material balances is analyzed. This test is used if the measurement error statistics are unknown or non-Gaussian.

5) SVT : Sequential Variance Test, which is based on the observation that a variance of material balances is to be larger than that expected from measurement error causes if a loss (or gain) occurs.

6) SMBT : Smoothed Materials Balance Test, which uses two Kalman filters, i.e., one is for running forward in time to estimate the beginning inventory and the other is for running backward in time to estimate the final inventory.

---

* ISL Co. Ltd.

** Shikoku Electric Power Co.

Decision tests examine all possible, contiguous subsequences of available material balance data at several levels of significance. Results of the decision tests are given in an alarm sequence chart, on which the alarm sequences are displayed graphically specifying to each of them its length, time of occurrence and level of significance, in a manner of pattern recognition. A summary of the results and their trends is obtainable from this device. By the help of SPTPLT, these results can be printed on a paper using NLP or can be displayed in a colour figure on the screen of D-SCAN.

Fig. 8.10.1 gives a result of the tests, where the upper side of the figure relates to a case of no diversion and, on the other hand, the lower side gives a case of uniform diversion. The farthest left graphs show a Shwart chart of material balances. Second from the left gives a CUMUF chart and the center case is an alarm sequence chart obtained by CUMUF tests. Second from the right gives a chart of average losses estimated by Kalman filter and the farthest right shows an alarm sequence chart based on the average losses.

Reference

1) Ikawa K., Ihara H., Nishimura H., Hirata M., Sakuragi H., Ido M., Sawahata T., Tsutsumi M., Iwanaga M., Suyama N., Lovett J.E.: "Final Report of TASTEX Task-F: Study of the Application of Near-Real Time Materials Accountancy to Safeguards for Reprocessing Facilities," to be published as a JAERI report.

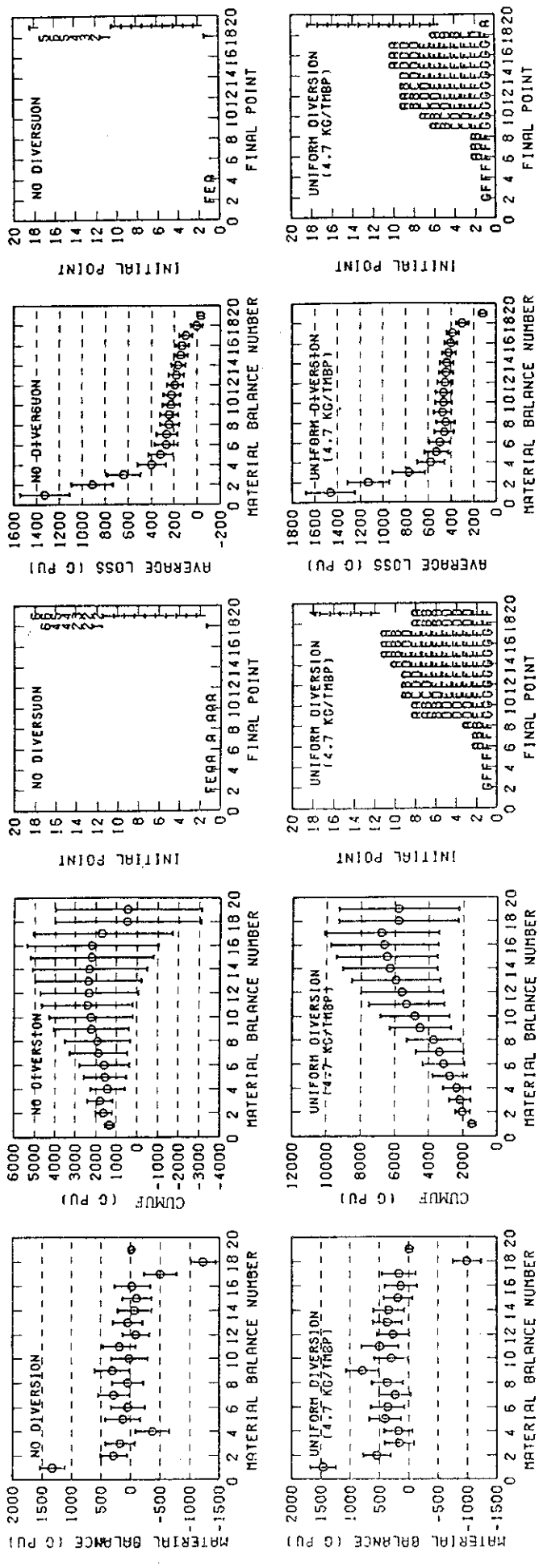

Fig.8.10.1 An example of output from SADAC and SPTPLT, showing a Shwart chart, a CUMUF chart, an alarm sequence chart of CUMUF tests, an average loss chart and an alarm sequence chart of average loss tests from left to right

8.11 Investigation of a Sample Plan for Safeguards Verification Activities

H. Nishimura, K. Ikawa, M. Hirata, S. Asai* and K. Hirose*

The Japanese Government has maintained a State system of accounting for, and control of, nuclear materials, SSAC, for nearly five years - since December 1977 - under the NPT safeguards agreement between the International Atomic Energy Agency and Japan. This system has a verification function operated by the national authority as well as the measuring, recording and reporting functions kept by the operators of various kinds of facilities as one of the fundamental elements of SSAC.

Experience gained during this period has shown that some problems remain to be solved concerning the design and implementation of the present safeguards system. The Japanese Government organized a working group to solve these problems. The authors have been involved in this working group, and have reviewed the present theoretical model of MUF analysis together with the theory of the sampling plan. The authors recommended the Government to improve both of them, and presented a method able to reduce sample sizes for variables measurements[1].

They improved this method and deduced a generalized theory for attribute-variables sample sizes as an optimization process of the inspector minimizing the non-detection probability, and of the diverter maximizing it by manipulating the relevant parameters[2].

The method is based on the assumption that the mixed attribute-variables sampling method should be maintained as a fundamental tool for verification. The main point of the method is to receive a maximum capability of detecting anomalies from both attribute and variables measurements using two statistics, which would be statistically independent from each other because one statistic consists mainly of systematic error, the other consists of random error and these two kind of errors are considered to be independent from each other. At the same time in the new theory, the attribute measurement and the variables measurement should complementarily cover a whole defect region in measuring an item, i.e., the detection power of attribute tests is to be extended to a smaller defect region and the paired data analyses are to be carried out over the attribute measurements as well as for the variables test. As a result of

* Science and Technology Agency

such procedure, the capability of detecting anomalies can be increased enormously especially in a medium defect region.

Although a full application test of this method is under way, the preliminary result shows a possibility of considerable benefits to both operators and inspectors[3].

The authors also investigated on what and how the verification procedure should be if the proposed method is adopted in the safeguards verification activities[1)2)]. As a result, they found that it is essential to the newly developed sample theory to estimate a more realistic measurement error standard deviation based on the historical paired data and that the quality of attribute measurements should be controlled strictly so as to benefit from the proposed model. Although additional statistical tests are required to analyze attribute data, however, these additional procedures would not require much effort.

References

1) "The first report issued by the Materials Accountancy Analysis Working Group of the Council for Investigation of Safeguards Technology," Materials Accountancy Analysis Working Group (1982) (in Japanese).

2) Nishimura H., et al.: "Investigation of a Sample Plan for Safeguards Verification Activities," Nuclear Safeguards Technology 1982, Vol.II, 317, IAEA-SM-260/71 (1983).

3) Nishimura H., Kikuchi I.: "Design Study of an improved Safeguards Verification Procedure using Non-Destructive Assay Techniques," Advisory Group Meeting on Evaluation of the Quality of NDA Measurement Data, E16 (1982).

8.12 Enrichment Measurement of FCA Uranium Fuels with SAM-2

H. Gotoh and R. Kurokawa*

We once experienced that the enrichment values of FCA uranium fuels taken with SAM-2 show fluctuations larger than expected from counting statistics. Then we studied a precise calculation scheme for deriving the enrichment values from the SAM-2 data.[1] The present authors newly took data on standard uranium pellets to study the excess uncertainties in the enrichment values of FCA fuels.

Table 8.12.1 shows an example of data taken on standard pellets. The enrichments of pellets tested were of five kinds ranging from 1.996 to 3.38t weight %. Each five kinds were measured five times. The sequence of measurement was randomized. Five pellets of equal enrichment were counted at the same time to obtain adequate counting rates. An expression, $ET = aC_1 - bC_2$, was fitted to the data, where E, T, C_1 and C_2 are the nominal enrichment, the counting time, the counts of channel 1 and 2, respectively, a and b being the coefficients to be determined. The values of $a = 5.5232 \times 10^{-3}$ and $b = 4.8287 \times 10^{-3}$ were obtained. The fifth column is the enrichment values recalculated using these coefficients. The seventh column is the ratio of the difference between the measured enrichment and the nominal enrichment to the nominal enrichment. The fluctuations of the results are ascertained by the χ^2 test to be within the range expected from the Poisson statistics of counts.

Table 8.12.2 shows an example of data taken previously on FCA uranium fuels. The content of the table is obtained via the same procedures as those used for Table 8.12.1. The χ^2 test shows the fluctuation of the result is out of the range expected from the Poisson statistics of counts. The fact that the relative deviation of lower enrichment show systematically positive values seems to indicate that an expression with a constant term will improve the fitting. The analysis is now in progress.

Reference

1) H. Gotoh: JAERI-M 9672 (1981), p.123-124

* Nuclear Material Control Center

Table 8.12.1 Measured data on standard uranium pellets with SAM-2

#	nominal enrich-ment (%)	count-ing time (min)	channel 1 (counts)	channel 2 (counts)	measured enrich-ment (%)	relative deviation
1	1.996	10	16104	14605	1.8493	-0.0735
2	2.598	10	17418	14624	2.5660	-0.0123
3	2.678	10	17372	14418	2.6400	-0.0142
4	2.678	10	17453	14419	2.6842	0.0023
5	3.268	10	18621	14740	3.1745	-0.0286
6	2.598	10	17482	14342	2.7374	0.0537
7	2.598	10	17611	14453	2.7551	0.0605
8	3.386	10	18978	14916	3.2868	-0.0293
9	1.996	10	16407	14502	2.0664	0.0353
10	1.996	10	16287	14500	2.0011	0.0025
11	3.386	10	19323	14998	3.4378	0.0153
12	3.268	10	18665	14654	3.2403	-0.0085
13	3.386	10	19047	14863	3.3505	-0.0105
14	2.678	10	17279	14546	2.5269	-0.0564
15	3.386	10	19010	14909	3.3079	-0.0231
16	3.268	10	18617	14583	3.2481	-0.0061
17	1.996	10	16226	14529	1.9534	-0.0213
18	3.268	10	18615	14509	3.2827	0.0045
19	2.598	10	17406	14514	2.6124	0.0056
20	3.268	10	18737	14494	3.3573	0.0273
21	1.996	10	16491	14421	2.1519	0.0781
22	2.678	10	17562	14543	2.6846	0.0025
23	2.598	10	17579	14637	2.6487	0.0195
24	2.678	10	17532	14497	2.6902	0.0046
25	3.386	10	19107	14881	3.3750	-0.0033

Table 8.12.2 Measured data on FCA uranium fuels with SAM-2

#	nominal enrich-ment (%)	count-ing time (sec)	channel 1 (counts)	channel 2 (counts)	measured enrich-ment (%)	relative deviation
1	92.87	120	61214	13529	92.8314	-0.0004
2	92.94	120	63174	15637	91.4756	-0.0158
3	92.82	120	61964	14718	91.3245	-0.0161
4	92.94	120	56598	10024	92.2525	-0.0074
5	92.79	120	55814	9192	92.7659	-0.0003
6	93.00	120	60692	13447	91.9535	-0.0113
7	92.99	120	63196	15284	92.4338	-0.0060
8	92.95	120	56712	9587	93.6198	0.0072
9	92.82	120	65378	17241	91.9317	-0.0096
10	92.82	120	60703	13360	92.2013	-0.0067
11	92.99	120	59136	12284	91.7106	-0.0138
12	93.01	120	53635	7410	92.8220	-0.0020
13	92.85	120	64548	16396	92.3826	-0.0050
14	92.86	120	65093	17090	91.7269	-0.0122
15	92.84	120	65718	17060	93.1092	0.0029
16	92.94	120	48045	3073	92.3599	-0.0062
17	19.93	300	31426	5659	20.3929	0.0232
18	19.93	300	37505	10200	20.7753	0.0424
19	19.93	300	31862	5808	20.6030	0.0338
20	19.93	300	39234	11826	20.5383	0.0305
21	19.93	300	33453	7060	20.6374	0.0355
22	19.93	300	31319	5523	20.4442	0.0258

8.13 Resin-Bead Technique for Uranium and Plutonium Determination

N. Shinohara, S. Okazaki, S. Tamura, H. Okashita and T. Komori

"Resin-bead" method originally developed in ORNL[1,2] and NBS[3] is a novel technique to determine mass-spectrometrically a nanogram amount of uranium and plutonium adsorbed on an ion-exchange resin bead. From the viewpoint of safeguards, this technique is of interest to the IAEA because of simplicity of separation of uranium and plutonium from fission products, of convenience of transportation by reducing the amount of nuclear and radioactive materials in the inspection samples, and, finally, of popularity of high sensitivity mass spectrometer in the nuclear arena.

Recently the IAEA initiated an interlaboratory comparison programme aiming to establish the resin bead method as a means of safeguards implementation, and the JAERI has participated in the programme along with the PNC and the NMCC from Japan. The first round-robin samples prepared by the IAEA using the NBS reference standard materials have been distributed on December 1982 to examine and adjust the individual instruments.

While the loading method of the bead on the filament of mass spectrometer was recommended to be in use of colloidal graphite as adhesive agent, we have adopted 10% glycerol solution instead of the colloidal graphite. After establishment of measurement procedures by manual operation, an automatic control programme of the instrument (VG Isomass 54E-38) was written in the Hewlett-Packard BASIC of the instrument computer following the manual procedures thus established.

The round-robin samples were measured by both manual and automatic operations. The results seemed reasonable in consideration of the NBS reference values and dispatched to the IAEA. The second round-robin samples which must be blind will be distributed in the fiscal year of 1983.

References

1) Walker R.L., Eby R.E., Pritchard C.A., Carter J.A.: Anal. Lett., 7, p.563 (1974).

2) Walker R.L., Pritchard C.A., Carter J.A., Smith D.H.: ORNL/TM-5505 (1976).

3) Barnes I.L., Sappenfield K.M., Shields W.R.: "Recent Developments in Mass Spectroscopy," Univ. of Tokyo Press (1970).

8.14 Development of Isotope Correlation Techniques

H. Okashita, Y. Nakahara and H. Umezawa

Measurements of nuclear material input to a reprocessing plant, in particular of plutonium, are of great importance from the viewpoint of safeguards, since it is the starting point of plutonium accountancy based on direct measurements.

Isotope correlation techniques have been studied to verify input accountability measurements at a reprocessing plant. On the basis of a historical data bank, correlation between plutonium-to-uranium ratio and isotopic variables was derived as a function of burnup. The burnup was determined from the isotopic ratios of uranium and plutonium, too. Data treatment was therefore made in an iterative manner (Fig. 1). The isotopic variables were defined to cover a wide spectrum of isotopes of uranium and plutonium. The isotope correlation techniques evaluated important parameters such as the fuel burnup, the most probable ratio of plutonium to uranium, and the amounts of uranium and plutonium in reprocessing batches in connection with fresh fuel fabrication data. In addition, the most probable values of isotope abundance of plutonium and uranium could be estimated from the plutonium-to-uranium ratio determined, being compared with the reported data for verification.

A pocket-computer-based system was developed to enable inspectors to collect and evaluate data in a timely fashion at the input accountability measurement point by the isotope correlation techniques[1]. The device is supported by battery power and completely independent of the operator's system. The software of the system was written in BASIC. The data input can be stored in a cassette tape and transferred into a higher level computer (Fig. 2). The correlations used for the analysis were given as a form of analytical function. Coefficients for the function were provided relevant to the type of reactor and the initial enrichment of fuel.

Correlation between the plutonium-to-uranium ratio and the isotopic data has been studied by several workers in consideration of sensitivity, linearity and neutron spectral effects[2-6]. However, it would be a risk if a particular isotope was regarded as the only parameter to be correlated with the plutonium-to-uranium ratio, because isotopic data generated from routine measurements are often less credible, especially for minor isotopes. The proposed procedure in the present work takes into

consideration all available isotopic data which provide complementary information.

Experience gained so far at the Tokai Reprocessing Plant has shown that cumulative results (Fig. 3) over a campaign composed of a number of dissolution batches agreed well with shipper's values as well as with measured product masses[7]. Although differences between the masses obtained by the isotope correlation techniques and those measured by the reprocessor scattered more than five percent in batch-by-batch comparison due to incomplete transfer of the solution from dissolver and intermediate vessels, relative random errors associated with the cumulative masses of uranium and plutonium were small enough for one to look for a possible systematic bias. Detection of a 1-2% systematic difference would be practicable, when verification by the present method was applied to a whole campaign comprising several tens of batches.

To reinforce the isotope correlation techniques as real effective measures for safeguards at reprocessing plants, on-site applicability should be demonstrated. The procedures developed in the present work would be easily operated by safeguards inspectors with the software provided in a small portable computer and would enable them effectively to collect the data and to verify them in a timely fashion. Moreover, successive accumulation of the data measured by the safeguards authority as well as by the reprocessor and other laboratories should be continued to elaborate the correlations. Effectiveness and confidence of the isotope correlation techniques will increase with increasing data base.

References

1) Umezawa H., Nakahara Y.: "Isotope Correlation Techniques for Verifying Input Accountability Measurements at a Reprocessing Plant," Nuclear Safeguards Technology 1982, 1, 473-484, IAEA-SM-260/72 (1983).
2) Christensen D.E., et al.: "Development of Isotope Safeguards Techniques - Summary," ACDA/ST-277-1 (1974).
3) Wellum R.,et al.:Proc.ESARDA Symp.Isotope Correlation-Stresa 1978, p.55.
4) Napier B.A., Timmerman C.L.: ibid., p.67.
5) Umezawa H., Okashita H., Matsuura S.: ibid., p.97.
6) Bouchard J., Darrouzet M., Robin M.: ibid., p.225.
7) TASTEX : Tokai Advanced Safeguards Technology Exercise, IAEA Technical Report No. 213, IAEA, Vienna, "Task-K", p.177 (1982).

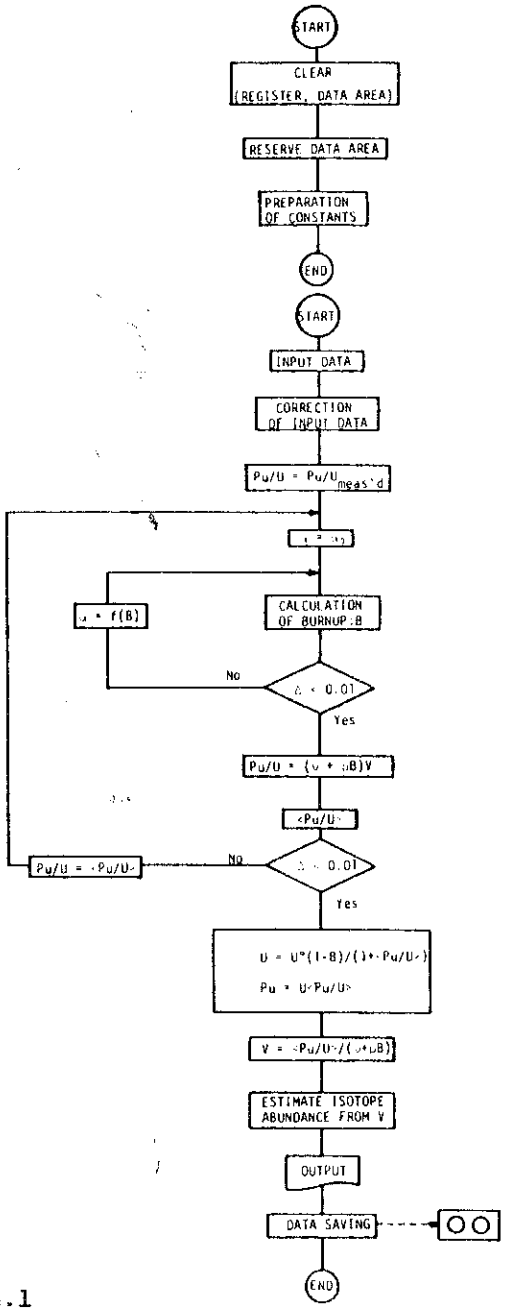

Fig.8.14.1

Flow chart of the ICT analysis system using a Sharp PC-1500 pocket computer.

```
 ICT PROG. START  110114.3553

BATCH SERIAL NO. =  21

---- DATA INPUT ---->

A$:CAMPAIGN NAME = C1
B$:BATCH NAME    = FUJI-047
C$:REACTOR TYPE  = B

A:FINAL U CONCENT(G/L) = 186.36
B:FINAL U-234(W/O) = 0.018
C:FINAL U-235(W/O) = 1.553
D:FINAL U-236(W/O) = 0.19
E:FINAL U-238(W/O) = 98.239

F:FINAL PU CONCENT(G/L) = 0.852
G:FINAL PU-238(W/O) = 0.392
H:FINAL PU-239(W/O) = 75.19
I:FINAL PU-240(W/O) = 17.219
J:FINAL PU-241(W/O) = 6.117
K:FINAL PU-242(W/O) = 1.082

L:DATE OF PU MEAS.     = 800507
M:DATE OF DECAY NORM.  = 790831

N:TOTAL SOLN VOL(L) = 2379.37
O:HEEL SOLN VOL(L)  = 9.59

P:SHIPPERS U(G)  = 379316
Q:INIT. U-234(G) = 73.25
R:INIT. U-235(G) = 9637.6
S:INIT. U-236(G) = 0
T:INIT. U-238(G) = 377598

IF FAILED DATA INPUT, CORRECT:e.g.F=X
X; SO ON:THEN <CONT>.


--- CORRECTED DATA ---

U CONCENT(G/L) = 1.7284E 02
U-234(W/O) = 1.8047E-02
U-235(W/O) = 1.5571E 00
U-236(W/O) = 1.8923E-01
U-238(W/O) = 9.8235E 01

PU CONCENT(G/L) = 8.1697E-01
PU-238(W/O) = 3.9682E-01
PU-239(W/O) = 7.4885E 01
PU-240(W/O) = 1.7078E 01
PU-241(W/O) = 6.5728E 00
PU-242(W/O) = 1.0665E 00
```

Fig.8.14.2 *Output of the input data and corrected data of a given reprocessing batch from the Sharp PC-1500 system.*

```
MEASURED   PU/U = 4.5621E-03
CALCULATED PU/U = 4.5623E-03
BURNUP  IN FIMA = 1.1121E-02

CAMPAIGN NAME = C1        BATCH NAME = FUJI-047        BATCH SERIAL NO. = 21

    ICT(A)*  REP(C)*   D*100-A CUM.ICT(F)  CUM.REP(H)  H+F(I)   I*100-F
    REA(B)   C-B(E)    E*100-B CUM.REA(G)     (G)        H+G(J)   J*100-G
      (G)      (G)       (%)      (G)                    (G)       (%)

UT  3.812E 85 4.415E 85 6.826E 01 1.588E 01 7.310E 06 7.883E 06-2.278E 05-3.185E 00
     3.783E 85          6.218E 01 1.639E 01 7.305E 06          -2.223E 05-3.043E 00
U4  9.856E-01 1.800E-02-8.876E-01-9.881E 01 9.135E 04 1.172E 03-9.817E 04-9.871E 01
U5  1.515E 00 1.553E 00 3.830E-02 2.528E 00 1.847E 05 1.818E 05-2.765E 03-2.642E 00
U8  1.818E-01 1.839E-01 0.100E-03 4.454E 00 1.159E 04 1.208E 04 4.965E 02 4.283E 00
U8  9.738E 01 9.823E 01 8.412E-01 8.637E-01 2.102E 06 6.958E 05-1.345E 04-1.894E 00
PT  1.748E 03 2.817E 03 2.769E 02 1.598E 01 3.185E 04 3.115E 04-2.837E 02-2.289E 00
PF  1.418E 03 1.640E 03 2.302E 02 1.632E 01 2.583E 04 2.528E 04-6.293E 02-2.437E 00
P8  2.237E-01 3.921E-01 1.683E-01 7.524E 01 8.513E 01 1.887E 02 5.656E 00 5.945E 00
P3  2.498E 01 2.519E 01 2.966E-01 3.961E-01 2.498E 04 2.351E 04-5.706E 02-2.369E 00
P8  1.767E 01 1.721E 01-4.646E-01-2.628E 00 5.589E 03 5.494E 03-9.432E 01-1.688E 00
P1  6.117E 00 6.114E 00-2.506E-03-4.185E-02 1.751E 03 1.632E 03-5.907E 01-3.372E 00
P2  1.078E 00 1.081E 00 2.138E-03 1.982E-01 3.385E 02 3.530E 02 1.453E 01 4.293E 00
                    *) FIGURES FOR ISOTOPES ARE GIVEN IN (W/O).

READY CASSETTE, KEY-IN <CONT>.


*** END OF ICT PROG. ***
```

Fig.8.14.3 *Output of results of the ICT analysis of a given batch from the Sharp PC-1500 system.*

8.15 Development and Performance of the Personnel Portal Monitor for the Fast Critical Facility FCA

T. Mukaiyama, H. Ogawa, Y. Yokota and H. Kuroi

At FCA, a personnel portal monitor has been developed[1,2] to support international safeguards and to stimulate the reduction of inspection frequency. This portal monitor represents the first unattended equipment of this kind being proposed for use in an international safeguards role. As may be expected, a very comprehensive evaluation of the system is required.

To Evaluate the performance of the portal monitor, IAEA and JAERI/FCA agreed to conduct field tests. The Phase I field test was conducted in 1980 to evaluate the system features and performance factors. Several system modifications were agreed upon during the Phase I test and later completed in 1981.

Phase II Field Test of Portal Monitor

Phase II field test for the FCA portal monitor was conducted during the period of April to August 18th, 1982, jointly by JAERI/FCA and IAEA. Phase II test was the long-term test of the portal monitor under actual operating conditions as practical as possible. Emphasis is placed on accumulation of the data on the metal detection capability, false alarm rates, etc. During the Phase II test, the Agency inspector visited the facility periodically, reviewed printed data and verified video tapes.

A team which consisted of staff of IAEA and staff of JAERI/FCA analyzed a pile of raw data at the end of five-month field test period at FCA. The team concluded that the system false alarm rate over the whole test period was 0.4% of total passages. The result of Phase II test was reported at the IAEA safeguards symposium in Vienna, November, 1982.

Modification of Portal Monitor

FCA Portal Monitor was modified after the Phase II field test. The modifications are as follows;

1) Automatic door-lock-up feature of the portal monitor upon metal detection was changed so as to use the auto-door only for controlling traffic through the portal monitor.

2) Every signal and sign which may reveal the state-of-health of portal monitor healthiness have been taken away so that the operator now has no chance to perceive the system malfunction.

Future Plan for Development

Data analysis and long-term experience with the use of the portal monitor brought some further requirements on additional system modifications and more tests. Consequently, the portal monitor will be redesigned after tests to incorporate several significant improvements, namely microprocessor control and modular system construction. These refinements aim to improve the Agency's safeguards performance in the field in providing high quality man-machine interface with a computer and presenting the possibility of establishing a good regular maintenance and repair programme based on exchange of modules.

References

1) Mukaiyama T., Kuroi H., Vodrazka P., Matolcsy A.: "Development and Performance of the Advanced Containment and Surveillance System at the Fast Critical Facility FCA," Nuclear Safeguards Technology 1982 (Proc. Symp. Vienna, 1982), IAEA-SM-260/121 (1983).

2) Mukaiyama T., Kuroi H.: "The Expected Performance and Benefits of an Advanced Containment and Surveillance System at the Fast Critical Facility FCA of JAERI," Proc. 22nd Annual Meeting INMM, San Francisco, p.20 (1981).

8.16 Development of RECOVER and TRANSEAVER Systems

H. Kuroi and R. Yoshihara

1. RECOVER System

The RECOVER (Remote Continual Verification) project started in 1979 with an aim to demonstrate an advanced safeguards measures for a timely collection of alarm signals from containment/surveillance (C/S) devices installed in strategic facilities, under the participation of IAEA, Japan, the United States of America, and other five countries.

An on-site multiplexer (OSM) was installed in the fast critical assembly FCA with four monitoring units (MUs) for periodically interrogating the status of C/S devices, i.e., the Portal Monitor (two MUs), a surveillance camera and a fiber optic seal.

A three-week test with a frequent interrogation was carried out in 1980 and a six-month test was completed in 1982 under a reduced rate of calling. For up-grading the system, a new capability to transmit alpha-numerical data was developed by IAEA in 1981 and JAERI cooperated with IAEA to demonstrate this feature in FCA in May 1982. The OSM was replaced by a modified one and a test for transmission of alpha-numerical data was successfully carried out between Tokai and Vienna via a commercial telephone line. The result of this test was reported before the 5-th RECOVER participants' coordination meeting, June 1982, Vienna.

As the results of these tests, the RECOVER concept has been proved to be feasible. In order to implement the system as one of the IAEA safeguards measures, however, further field tests are needed to gather much information for evaluating the effectiveness and efficiency of the system, while the development of new sensors and the improvement of interfaces between sensors and the system are required.

The RECOVER system is so powerful to verify the status of C/S devices remotely and timely, so that the function of the system could be used for the State system of accountancy and control with much enhanced capability. For this purpose, an attempt to expand the RECOVER function for domestic use was initiated in 1982 under a research contract between Science and Technology Agency and JAERI, based on a preliminary investigation carried out in 1981 on the concept of extended RECOVER system.

In 1982, a conceptual design of the JAEMS (JAERI type Monitoring System) has been completed on the following items:

1) System analysis which deals with communication media, safeguards data processing, and related cost estimates, etc.
2) Central verification unit for timely summary information on the entire system, and OSM for receiving data from monitoring units and for retaining the data for transmission to the command console.
3) Communication protocol which handles data transmission rates, prioritization of calls and communication system secrecy.

As another major task, the following modifications have been done on the RECOVER Remote Verification Unit (RVU) for Regional Use (RRVU) which was transferred from ACDA to JAERI based on a research agreement between ACDA and JAERI:

1) Alpha-numerical data treatment function was added.
2) Display function was changed so as to include strategic facilities in Japan for regional use.
3) Basic data transmission rate over telephone lines was changed from 300 baud to 2400 baud.
4) Communication protocol between RRVU and RVU was improved so as to avoid possible conflict between them.
5) Hardcopy function was added.

The following RECOVER equipments were transferred from ACDA to JAERI as a loan basis, conforming to the JAERI-ACDA Research Agreement; 4 sets of modem, 1 set of RVU, 5 sets of MU, 1 set of OSM and 1 set of DTE. Full set of RECOVER documentation was also transferred from ACDA to JAERI.
Using these equipments, a communication test will start in 1983 and the result will be reflected to the design and development of JAEMS.

2. TRANSEAVER System

A concept of the TRANSEAVER (Transport-over-sea-Verification) system which handles status information of the C/S measures installed in a moving facility on the sea has been developed extending the idea of RECOVER system which, on the other hand, treats with the C/S status information generated in a facility on land.

The conceptual design was carried out in 1981. Fig. 8.16.1 shows the concept of the system. In 1982, a further study was carried out, especially on a method to collect the data generated by the system.

TRANSEAVER

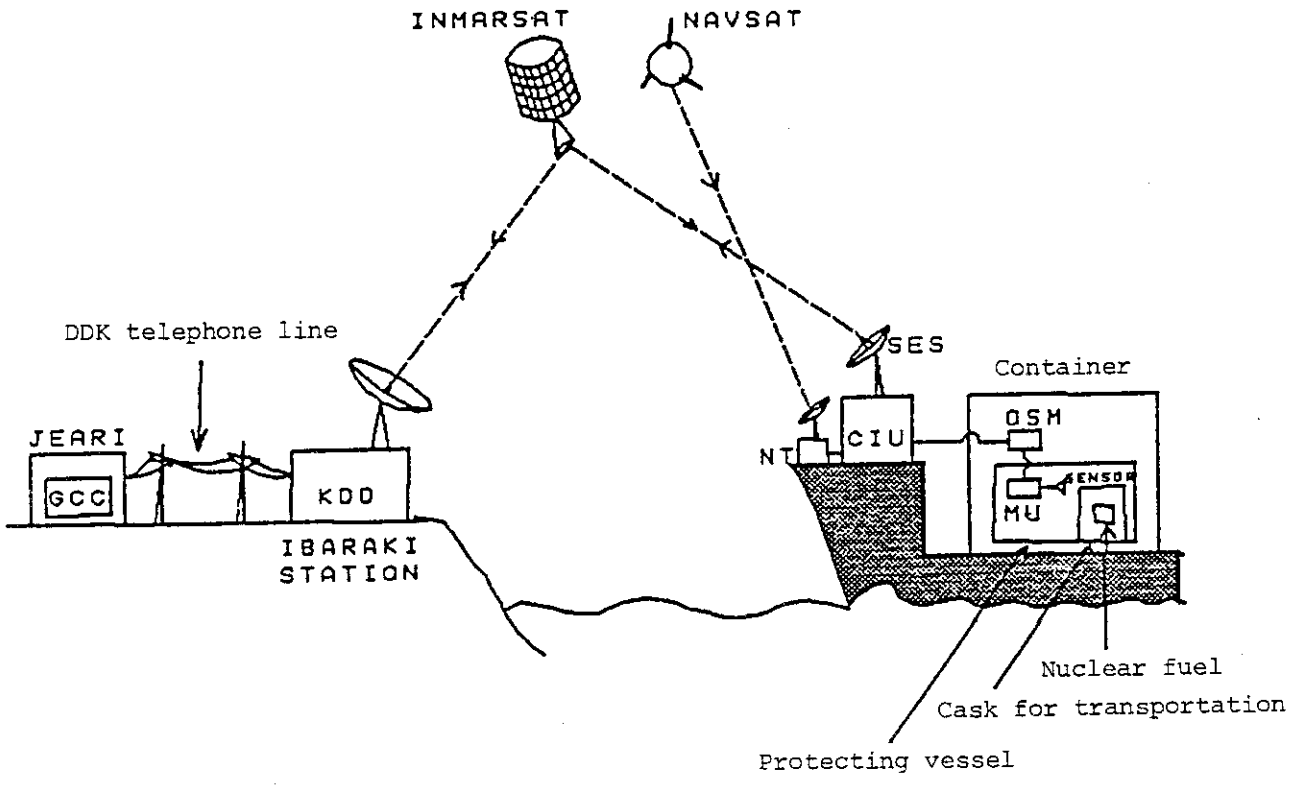

Fig. 8.16.1 Concept of the TRANSEAVER system

8.17 Development of Fiber Optic Seals

H. Kuroi and R. Yoshihara

Seal is one of the important safeguards measures to be applied for the international safeguards as well as for the national safeguards. At present the seals used in the fields are restricted to those, e.g. paper seals and metal seals, which neither have an in-situ verification capability nor a remote verification function. These features are vital to improve the safeguards effectiveness and efficiency, so that the efforts to develop a new seal have been spent in many countries.

A fiber optic seal is one of the best candidates to provide these features. In order to develop a reliable seal with high security, easy to interrogate its integrity on site, and verifiable of its status remotely and automatically, a new project for the seal development using fiber optic cables and a sophisticated electronic device was initiated in 1982 under a research contract between Science and Technology Agency and JAERI, based on a preliminary work in 1981 of surveying the development efforts spent so far in each country.

For an efficient seal development to be carried out in JAERI, a discussion was held with IAEA technical staffs on the subject. As the result, it was agreed that the major contribution both to the IAEA safeguards and to the national safeguards on this seal technique development should be to develop an auto-verification function for the seal using an optical pattern recognition technique. Based on this guideline, a conceptual design of the seal has been completed. A new JAERI seal would have such characteristics as;

1) Modular type design with remote verification capability as well as in-situ verification function, which economically fulfills a variety of requirements to the seals used in various facility circumstances.
2) Remote verification module, which is an improved type of electronic seal.
3) On-site verification module, which is designed to have an optical pattern recognition function.

A possibility to apply Charge Coupled Device, CCD, to the seal for optical pattern identification was investigated, and a conceptual design of the coupling device between a fiber optic end and the CCD was completed. For further study one Cobra seal was transferred from IAEA to JAERI.

8.18 Progress of the JASPAS Projects

H. Kuroi, H. Umezawa, K. Ikawa, H. Nishimura, T. Mukaiyama, H. Ihara, R. Yoshihara and Y. Nakahara

The Japan Support Programme for Agency Safeguards (JASPAS) was established on 5 November 1981 between the Government of Japan and the International Atomic Energy Agency for assisting the technical development of the Agency safeguards system with initial nine projects including the three projects (JA-1, JD-3 and JD-4: see below) which JAERI has carried out as the executing institution. JAERI's two other projects (JB-1 and JB-2) commenced on July 1982 as additional projects to JASPAS.

Followings are the summary of activities in 1982 for each project.

Project JA-1: Remote Continual Verification System (RECOVER)

The objective of this project is to develop a comprehensive secured communication system for remote continual verification of relevant safeguards and security status of nuclear material by upgrading and expanding the current RECOVER capability.

In 1981 only some preparatory works were carried out, but full scale activities commenced in this year on two main areas: Design Study of JAEMS (JAERI type Monitoring System) system and Modification of RECOVER Remote Verification Unit (RVU) for Regional Use (RRVU). Detailed description on these items are given in 8.16 of this annual report.

Another important aspect of JASPAS is to exchange technical information among experts concerned, to attain an efficient performance of the project. For this purpose, (1) one IAEA technical staff was invited to Japan for installation and initial test of the data terminal equipment, (2) one JAERI research staff visited the IAEA headquarters to discuss general concept of regional RECOVER use and future application of RECOVER technologies for the IAEA safeguards, and (3) two JAERI research staff visited ACDA for arranging RECOVER hardware and documentation transfer from ACDA to JAERI.

Project JB-1: Development of Quick Safeguards Data Collection and Evaluation Procedures

The objective of this project is to develop methods and procedures for safeguards data evaluation and corresponding software, and to assist inspectorate in quick data evaluation.

As a preparatory work, several meetings were held between staffs of

the safeguards technology laboratory, JAERI and IAEA specialists in order to investigate the present practices of safeguards data collection and evaluation and to indicate the problem areas. With regard to the specific problems of the Tokai reprocessing plant, the discussion showed that the following improvements are desirable because they could significantly reduce the time intervals between the collection of safeguards data at facility and the production of a preliminary result of evaluation, increasing the reliability of SSAC;

1) Making use of computers, including NDA microprocessors, in a coordinated manner between IAEA and Japan for data collection, data transfer and data processing with a common package of software in order to avoid data elements to be missed and to realize a rapid dispatch of the data to the evaluation teams stationed in the IAEA headquarters.

2) Utilizing the software system developed by JAERI for the reprocessing plant for the above purpose as a first step.

3) Developing and implementing a faster method of resolving outlier differences between PNC/NMCC and PNC/IAEA together with a quick method of reporting back the result to headquarters data evaluation teams.

In order to provide a common basis for data analysis between IAEA and Japan, INSPECT and DHATO which are currently used in IAEA were transferred from IAEA to JAERI with documents on the statistics recently developed.

Project JB-2: Isotope Correlation Technique for Safeguards Data Evaluation

The objective of this project is to demonstrate capability and performance of isotope correlation techniques in the view point of safeguards implementation, particularly for a reprocessing plant, and to establish an enough data base for the isotope correlation techniques.

In 1982, data evaluation procedures were developed to verify input measurement data of nuclear materials in a reprocessing plant by the isotope correlation techniques. A software system was prepared in BASIC to be operated with a pocketable computer, SHARP PC 1500, that could be easily brought into the spot. Performance and capability of the system were tested with some real campaign data of the PNC reprocessing plant.

The procedures and the software system were demonstrated, provided to the Agency, and examined in a meeting of the Agency's staffs and JAERI's experts on November 1982 at the Agency's headquarters. In that meeting future perspective was also discussed to develop a whole system for data evaluation of reprocessing safeguards. It was recognized that the isotope correlation would be an important part of verifying the input measurements

and perhaps the input-output analysis of the process area, too. More information is given in 8.14 of this annual report.

Project JD-3 : Containment/Surveillance Measures Incorporated with a Portal Monitor

The objective of this project is to develop the personnel portal monitor to be installed at the reactor building doorway and to develop the penetration monitor to secure the containment integrity of FCA reactor building.

In 1982, the works on this project has been done in three main areas, i.e Phase II field test of portal monitor, Modification of portal monitor, and Design of surveillance system and penetration monitoring system. These works are described in detail in the paper 8.15 of this annual report. As for the technical information exchange, (1) one JAERI research staff visited IAEA headquarters in Vienna for discussing the Phase II test plan, (2) one IAEA technical staff was invited to Japan to participate the phase II field test at FCA during the concentrated test period for ten days, and (3) one JAERI research staff visited Sandia National Laboratories to discuss intrusion detection technique to be used for FCA reactor building penetration monitoring system. As an equipment transfer, one VTR was sent to IAEA for the recorded video tape of the FCA portal monitor to be reviewed at the IAEA headquarters.

Project JD-4 : Auto-Identification Fiberoptic Seal

The objective of this project is to provide high security of seals, together with the convenience to use and cost-effectiveness of in-situ/remote monitoring, by developing a new fiber optic seal designed to incorporate the experience gained in other fiber optic seal design efforts sponsored by other countries.

With an aim to develop an auto-verification function for the seal using an optical pattern recognition technique, a conceptual design of the seal has been completed with a modular type design concept, i.e. remote verification module and on-site verification module. Application of Charge Coupled Device, CCD, for optical pattern identification of fiber optic seal was investigated. More information is given in 8.17 of this annual report.

For technical information exchange, one JAERI research staff visited the IAEA headquarters in Vienna to discuss the workplan of this project and one IAEA technical staff was invited to Japan for discussing on basic concept of new fiber optic seal and application of the CCD for optical pattern verification.

9. Committees' Activities

9.1 Committee on Reactor Physics

T. Asaoka

During this one year period, the Committee on Reactor Physics held the meetings 2 times in relation to the NEA Committee on Reactor Physics (NEACRP). For the Sixth International Conference on Radiation Shielding (ICRS) held on May 16-20, 1983, the Japanese Organizing Committee has been set up in April in order to prepare and manage the conference.

The Committee on Reactor Physics held the 42nd meeting in August to make preparation mainly for the 25th meeting of the NEACRP. Discussions were made on the draft of the review paper[1] on research activities of reactor physics in Japan for the period from October 1981 to September 1982. In addition, 10 technical papers were discussed for contributing to the topics of the meeting:

A-525; A Study on a Nuclear Criticality Safety Evaluation Technique (Y. Naito, J. Katakura, M. Yokota),

A-527; Evaluation of Computational Models for Spallation and Fission Reactions Used in an Accelerator Breeding and Transmutation Analysis Code (Y. Nakahara),

A-513; Homogenization Method of Pin Rods in ZPPR-10A Assembly (T. Takeda, K. Tanimoto, T. Yamamoto),

A-519; Analysis of Fuel Slumping Experiment on FCA Assembly VIII-2 (M. Nakano, H. Tsunoda),

A-520; Effect of Cell Calculation Model on the Analysis of Fuel Slumping Experiment (E. Wachi, T. Takeda, T. Sekiya),

A-532; Iterative Solution of the DFEM Algorithm of the Three Dimensional Neutron Transport Problems (T. Fujimura, Y. Nakahara, M. Matsumura),

A-536; Measurements of Gamma-Ray Energy Release Rates Following East-Neutron Fissions of U-238, Th-232 and Natural Uranium (M. Akiyama, S. An),

A-545; On the Reactivity Scale for Large LMFBR Cores (H. Nakamura, N. Tsuji),

L-260; A Study on the Potential Safety Advantage of Large Heterogeneous LMFBRs (K. Suzuki et al.),

A-556; A Study on Shielding Calculation Technique Using the Albedo-S_N Method (M. Kawai, J. Itoh).

The 43rd meeting of the Committee was held in October to review the 25th meeting of NEACRP where 47 technical papers were presented in connection with the following topics:

Validation of criticality methods, especially in geometries appropriate to reprocessing plant,

Rating distribution and reactivity effects of Gd poisons in thermal reactors,

Out-of-pile production of fissile materials,

Calculational methods for evaluating control rod worth in FBRs and their validation,

Reactor physics modelling of distorted cores,

3-D transport solutions for reactor calculations with emphasis on acceleration techniques, including those use in diffusion codes,

Beta and gamma heat measurements for fast and thermal reactors, particularly for Pu-239,

Sub-criticality reactivity monitoring in out-of-pile configurations (reactivity monitoring by noise and pulsed neutron methods, non-destructive testing of burn-up and isotope correlation),

Intercomparison of reaction rate measurements in fast reactors,

Delayed neutron data and reactivity scales, beta-eff data, and central reactivity worth discrepancies,

Heterogeneous cores (new physics related information).

In addition, discussions were extended to the following 3 NEA specialists' meetings planned by the NEACRP:

Specialists' meeting on the intercomparison of calculations for the pinplate cell heterogeneity benchmark (June 21-23, 1983, in Winfrith, U. K.),

Specialists' meeting on in-core instrumentation and the assessment of reactor nuclear and thermal/hydraulic performance (October 10-13, 1983, in Halden, Norway),

Specialists' meeting on reactor noise - SMORN-IV (October 1984, in Dijon, France).

Reference

1) Asaoka T., Shirakata K.: "Reactor Physics Activities in Japan (Oct. 1981 - Sept. 1982)," NEACRP-L-258 (Japan) (1982).

9.2 Subcommittees on Reactor Physics

T. Asaoka, Y. Ishiguro, T. Nakamura and T. Suzuki

The Subcommittees on Reactor System, Fusion Reactor and Shielding held the meetings 3, 4 and 2 times, respectively, to discuss topics of relevant to each field during this one year period.

The Subcommittee on Reactor System held the 8th meeting in June to discuss the activity plan in this fiscal year, the status of various types of LWR's with high conversion rates, and the result of burn-up calculations for the NEACRP LMFBR benchmark problem and the BWR benchmark problem with adjacent Gd poisoned fuel rods. In the 9th meeting held in August, discussions were made on the fuel management analysis for Fugen by using LAYMON and POLESTAR computer codes, as well as technical papers to be presented in the 25th meeting of the NEA Committee on Reactor Physics (NEACRP). Furthermore, the Subcommittee held the 10th meeting in February 1983 to review 4 papers related to the control rod calculation methods for LMFBR's and one paper dealing with the burn-up calculation for a BWR lattice with Gd poisoned fuel rods, which were presented at the 25th NEACRP meeting.

The Subcommittee on Fusion Reactor held the 8th meeting in July for the discussion of the activity plan in this fiscal year and to review TOF experiments for Li_2O plate systems performed by using FNS and neutron multiplication experiments with Pb carried out using OKTAVIAN in Osaka University. In the 9th meeting held in October, discussions were made on the measurement of leakage neutron spectra from slabs of various materials at OKTAVIAN, in addition to the review on blanket neutronics studies in the US and in the East European countries. In the 10th meeting held in December, preparations were made on the Japan-Us workshop to plan the cooperative research on fusion blanket neutronics and shielding. The results of the workshop were reviewed at the 11th meeting, in addition to the discussion on the methods and data to be used for analyzing JAERI-USDOE cooperative blanket neutronics experiments to be performed at FNS.

The Subcommittee on Shielding held the 14th meeting in July to decide to continue the Subcommittee's activity with 2 working groups (WG's), the sensitivity and uncertainty analysis WG and the shielding analysis method WG. In addition, discussions were made on the results

of NEACRP LMFBR and PWR shielding benchmark calculations to clarify reasons for large discrepancies of Japanese results from others. The reason for the LMFBR results was clarified to be due to the treatment of Na resonance valley at the 15th meeting of the Subcommittee held in March 1983, where also the review was carried out on the paper dealing with the adjustment of neutron multigroup cross sections presented in the 25th NEACRP meeting.

9.3 Japanese Organizing Committee for the Sixth ICRS

T. Asaoka, T. Suzuki and S. Kikuchi

The Japanese Organizing Committee for the Sixth International Conference on Radiation Shielding (ICRS) and its Technical Planning Committee held the meetings 3 and 5 times, respectively, to make preparations for the Sixth ICRS to be held on May 16-20, 1983, in Tokyo.

The Organizing Committee held the 1st meeting in June to review the first information sheet and the call-for-paper prepared by the Preparatory Committee set up in the last fiscal year. In addition, discussions were made on the over-all plan of the conference and the budget. On the other hand, the Technical Planning Committee held the 1st meeting also in June to discuss possible invited papers and candidates for session co-chairmen from Japan, as well as the over-all technical plan of the conference. At the 2nd meeting held in July, the Technical Planning Committee discussed the 2nd information sheet, including the conference venue and the registration fee, in addition to the possible contributed papers from Japan. The Committee held the 3rd meeting in September to select Japanese papers to be presented in the conference and to discuss the notice for the manuscript preparation of the papers.

After the International Technical Program Committee held on September 20 and 21 at Karlsruhe, FR Germany, to select 150 papers out of 164 and to determine the preliminary program schedule and candidates for session chairmen and co-chairmen, the Technical Planning Committee held the 4th meeting in October to improve the preliminary program schedule and to select additional candidates for session co-chairmen from Japan. The 2nd meeting of the Organizing Committee was held in December to review the status of the conference preparation and to arrange the opening session and the closing session. Furthermore, in the 3rd meeting held in March 1983, discussions were made mainly on the budget, in addition to the review of the 3rd information sheet prepared through the discussion at the 5th meeting of the Technical Planning Committee held in January 1983.

The preparation of the Sixth ICRS has thus been proceeded smoothly to have a successful international meeting reviewing advances in shielding and radiation protection for fission, fusion and related facilities, with an emphasis on practical aspects of shielding design, requirements for nuclear data and occupational exposure problems in operating power reactors.

Publication List

1. Nuclear Data and Group Constants

(1) Takano H., Ishiguro Y.: "Production and Benchmark Tests of Fast Reactor Group Constant Set JFS-3-J2," JAERI-M 82-135 (1982).

(2) Takano H., Hasegawa A., Kaneko K.: "TIMS-PGG: A Code System for Producing Group Constants in Fast Neutron Energy Region," JAERI-M 82-072 (1982).

(3) Hasegawa A. and Narita T.: "Comparisons of Energy Dependent Point-Wise Cross-Section Generation Codes: RESEND, RESENDD, RECENT," JAERI-M 82-128 (1982).

2. Theoretical Methods and Code Development

(1) Nakagawa M., Inoue H.: "Double Heterogeneity Effect of Fuel Pin and Subassembly in a Fast Power Reactor," Nucl. Sci. Eng., 83, 214 (1983).

(2) Nakahara Y., Tsutsui T.: "NMTC/JAERI, A Simulation Code System for High Energy Nuclear Reactions and Nucleon-Meson Transport Process," JAERI-M 82-198 (1982).

(3) Mori T., et al.: "Measurement and Analysis of Neutron Spectrum in a Molybdenum Pile," J. Nucl. Sci. Technol. 19 (6), 427 (1982).

(4) Harada H., Higuchi K., Ishiguro M., Tsutsui T., Fujii M.: "Vectorization of Nuclear Codes on FACOM 230-75 APU Computer," JAERI-M 83-025, (1983) (in Japanese).

(5) Inoue S., Fujimura T., Tsutsui T., Nishida T.: "Mannual for JSSL (JAERI Scientific Subroutine Library) (3rd Edition)," JAERI-M 82-095 (1982) (in Japanese).

(6) Ishiguro M., Tsutsui T.: "Vector Processing of the Neutron Transport Codes," JAERI-M 82-199 (1982) (in Japanese).

(7) Nishida T., Izui K.: "Identification of Small Sample Point Defect Clusters by High Resolution Electron Microscopy," Proc. 5th Yamada Conf., Kyoto (1981).

(8) Fujimura T., Nakahara Y., Horikami K., Suzuki T.: "Development of Optimization Program Package and its Application," Proc. of 3rd Math. Prog. Symp., Oct. 20-21, 1982, Tokyo, Japan (in Japanese).

(9) Iijima S., et al.: "Evaluation of Symbiotic Energy System between Gas-Cooled Fast Breeder Reactor (GCFR) and Multi-Purpose Very High Temperature Reactor (VHTR) (II) - Nuclear Characteristics of Reference GCFR Core -," JAERI-M 82-182 (1982) (in Japanese).

(10) Yoshida H., et al.: "Evaluation of Symbiotic Energy System between Gas-Cooled Fast Breeder Reactor (GCFR) and Multi-Purpose Very High Temperature Reactor (VHTR) (III) - Reference GCFR Core Configuration and it's Thermo-Hydraulic Characteristics -," JAERI-M 82-183 (1982) (in Japanese).

(11) Iijima S., et al.: "Evaluation of Symbiotic Energy System between Gas-Cooled Fast Breeder Reactor (GCFR) and Multi-Purpose Very High Temperature Reactor (VHTR) (IV) - GCFR Trangient Analysis and Safety Performance Evaluation -," JAERI-M 82-184 (1982) (in Japanese).

(12) Ihara H.: "GPLP: General Purpose Line Plotting Programme," JAERI-M 82-197 (1982) (in Japanese).

3. Integral Experiment and Analysis

(1) Ōbu M., Koyama K., Kuroi H.: "Verification of Core-Fuel Inventory of a Fast Critical Facility by Monitoring Reactor Physics Parameters," JAERI-M 82-153 (1982).

(2) Akino F.: "Study on Thermal Neutron Spectra in Reactor Moderators by Time-of-Flight Method," JAERI-M 82-207 (1982) (in Japanese).

(3) Tsuchihashi K., Takano H., Horikami K., Ishiguro Y., Kaneko K., and Hara T.: "SRAC: JAERI Thermal Reactor Standard Code System for Reactor Design and Analysis," JAERI-1285 (1982).

(4) Tsuchihashi K. and Mori T.: "An Analysis of KUCA MEU Cores by the JAERI SRAC Code System," International meeting on research and test reactor core conversions from HEU to LEU fuels, BNL (1982).

(5) Gotoh Y.: "Study of Stochastic Reactor Kinetic Equation," Progress in nuclear energy, Vol. 9, 303 (1982).

4. Fusion Neutronics

(1) Nakamura N., Maekawa H.: "Blanket and Shielding Experiments in Fusion Neutronics Source (FNS)," 9th Int. Conf. on Plasma Physics and Controlled Nuclear Fusion Research, Baltimore, U.S.A., 1-8 Sep. 1982, IAEA-CN-41/0-4.

(2) Seki Y., et al.: "Calculation of Absolute Fission-Rate Distributions Measured in Graphite-Reflected Lithium Oxide Blanket Assembly," JAERI-M 83-061 (1983).

(3) Maekawa H., et al.: "Measurements of Angular Flux on Surface of Li_2O Slab Assemblies and Their Analysis by a Direct Integration Transport Code 'BERMUDA'," ANS 5th Topical Meeting on the Technology of Fusion Energy, Knoxville, Tennessee, April 26-28, 1983.

(4) Nakamura N., et al.: "Radiation Streaming Studies at the Fusion Neutronics Source (FNS) Facility," 6th Int. Conf. on Radiation Shielding, Tokyo, Japan, May 16-20 (1983), 6b-5.

(5) Seki Y., et al.: "Monte Carlo Analysis of a Streaming Experiment of D-T Neutron and Secondary Gamma Rays Through a Concrete Bent Duct," ibid, 6b-6.

5. Shielding

(1) Takeuchi K. and Sasamoto N.: "Fundamental Theory of the Direction Integration Method for Solving the Steady-State Integral Transport Equation for Radiation Shielding Calculation," Nucl. Sci. Eng., 80, 536-553 (1982).

(2) Sasamoto N. and Takeuchi K.: "Direct Integration Method for Solving the Neutron Transport Equation in Three-Dimensional Geometry," Nucl. Sci. Eng., 80, 554-569 (1982).

(3) Tanaka S., Oyama Y., Sasamoto N. and Nakamura T.: "A Benchmark Experiment on D-T Neutrons and Secondary Gamma Rays Streaming Through a Concrete Bent Duct," JAERI-M 82-130 (1982).

(4) Sasamoto N.: "A Study on Direct Integration Method for Solving Neutron Transport Equation in Three-Dimensional Geometry," JAERI-M 82-167 (1982).

(5) Suzuki T., Hasegawa A., Mori T. and Ise T.: "BERMUDA-2DN: A Two-Dimensional Neutron Transport Code," JAERI-M 82-190 (1982) (in Japanese).

(6) Tanaka S., Yamaji A., et al.: "Shielding Experiments for Evaluating a Shielding Safety Evaluation Code System to Spent Fuel Processing Facilities - (1) ―Shielding Experiment of a Spent Fuel Transport Cask for a PWR Spent Fuel Assembly―," JAERI-M 82-201 (1982) (in Japanese).

(7) Tanaka S., Yamaji A., et al.: "Shielding Experiments for Evaluating a Shielding Safety Evaluation Code System to Spent Fuel Processing Facilities - (2) ―Experiments for the Assessment on Source Geometry of PWR Spent Fuel Assemblies―," JAERI-M 82-202 (1982) (in Japanese).

(8) Sasamoto N., Iida H., et al.: "Investigation of Shielding Analysis Method for Fusion Reactors," JAERI-M 82-216 (1982) (in Japanese)

6. Reactor and Nuclear Instrumentation

(1) Wakayama N., et al.: "Development of Experimental VHTR Instrumentation," IAEA-IWGCR Specialists' Meeting on GCR Core and High-temperature Instrumentation, 15-17 June 1982.

(2) Ara K., Wakayama N. and Kobayashi K.: "Development of In-Vessel Water Level Gauge for Light Water Power Reactors," International Meeting on Thermal Nuclear Reactor Safety, 29 Aug. - 2 Sept. 1982.

(3) Ara K., Yamada M. and Hoshi T.: "Development of Differential Transformer for High-Temperature Use," (in Japanese), J. Soc. Instrument Control Eng., Vol. 22, No. 2, pp. 229-234 (1983).

(4) Kakuta T., et al.: "Gamma Irradiation Effects on Fiber Optics," (in Japanese) EIM-83-21, IEEJ, 1 March 1983.

(5) Sakai E., Miyazawa T., Sekiguchi N.: "Summary of In-Pile Loop Experiments Related to the Development of the Fuel Failure Detection System for LMFBR's in Japan," KfK 3203 IWGFR/38, pp. 147 - 152 (1982).

(6) Sakai E.: "Radiation Detection and Its Application," (in Japanese) Denki Hyoron (Electrical Review) Vo. 7 '83, pp. 632-637 (July 1982).

(7) Sakai E.: "High-Purity Germanium Detectors," (in Japanese) Isotopes News, No. 340, pp. 8-12 (October 1982).

(8) Sakai E., Usui S., Ohkado H., Hayashi Y., Nakatani H.: "Temperature Dependence of Thermal Neutron Detection Performance of BF_3 Proportional Counters," IEEE Transactions on Nuclear Science, Vol. NS-30, No. 1, pp. 802-805 (February 1983).

(9) Sakai E., Horinaka H., Sonomura H., Miyauchi T.: "A Preliminary Observation of $AgGaSe_2$ as a Nuclear Radiation Detector," Proceedings of 1982 Annual Meeting of Materials Research Society on Nuclear Radiation Detector Materials, Boston, November 1 - 2, 1982 (to be published).

(10) Sakai E.: "A Brief Survey on Progress and Trends in Nuclear Radiation Detectors (I) - Gas Counters and Liquid Detectors -," Radioisotopes, Vol. 32, pp. 135-142 (March 1983).

(11) Sakai E.: "A Brief Survey on Progress and Trends in Nuclear Radiation Detectors (II) - Solid Detectors -," Radioisotopes, Vol 32, pp. 179-185 (April 1983).

(12) Kimura I., Sakai E.: "Radiation Measurement Handbook," (Japanese translation of G. F. Knoll's book, "Radiation Detection and Measurement," John Wiley & Sons, Inc., N.Y., 1979), Nikkan Kogyo Shinbunsha, Tokyo (November 1982).

(13) Sakai E., Kubo K., Yoshida H.: "Development and Test of Cover-Gas On-Line Gamma-Ray Monitor (IV)," (in Japanese) PNC SJ 950 82-17

(June 1982).

(14) Sakai E.: "Development and Test of Cover-Gas On-Line Gamma-Ray Monitor (V)," (in Japanese) PNC SJ 950 83-01 (March 1983).

(15) Sakai E.: "Semiconductor Nuclear Radiation Detectors," (in Japanese), "Isotope Binran (Handbook of Isotopes)," 3rd Edition, Chapter 15.6, Maruzen Ltd., Tokyo (to be published in Fall, 1983).

(16) Sakurai K., Gotoh H., Yamamoto S., Kobayashi K. and Kimura I.: "Cross Section Measurement for ^{199}Hg (n,n') ^{199m}Hg Reaction from 0.78 to 6.3 MeV," J. Nucl. Sci. Eng., 19 (10) pp. 775-780 (1982).

(17) The Committee on Analytical Chemistry of Nuclear Fuels and Reactor Materials, JAERI: "A Committee Report on the State-of-art of Uranium Isotopes Enrichment Measurement Techniques," JAERI-M 82-051 (1982).

7. Reactor Control and Diagnosis

(1) Shimazaki J.: "An Improved Power Method for Solving Eigenvalue Problems in Plant Dynamics and Control," JAERI-M 82-083 (1982) (in Japanese).

(2) Shimazaki J., Shinohara Y.: "A CAD System for Control System Design and Evaluation (Version 1)," JAERI-M 82-180 (1982) (in Japanese).

(3) Shimazaki J.: "On Error Evaluation of Pade Approximants to exp(z)," Trans. SICE, Vol. 19, No. 2, pp. 179-181 (1982) (in Japanese).

(4) Shimazaki J.: "Approximation Formulae of Integral for Making a Discrete Time Model," Trans. SICE, Vol. 19, No. 2, pp. 182-184 (1983) (in Japanese).

(5) Shinohara Y.: "Robots Working under Special Environment," Japan Science and Technology, Vol. 23, No. 215, pp. 79-85, (1982).

(6) Shinohara Y.: "Needs and R&D Status of Robot Technology for Nuclear Installations," Seminar on the development of robots for nuclear application, Tokyo, (1982).

(7) Shinohara Y.: "Trends in Robotization of Inspection Systems," Seminar on automation of inspection systems in nuclear power plants, Tokyo, (1982).

(8) Shinohara Y.: "Images and Evolutive Stages of Robots," 1983 National Symposium on Atomic Energy, Tokyo, (1983).

(9) Shinohara Y.: "Robot Technologies for Dismantling Reactor Facilities," Handbook of Automation and Robotization in Construction Work, (1982).

8. Development of Safeguards Technology

(1) Kurihara H., Haginoya T., Natsume H., Hirata M., Kawashima Y.: "Present Status and Development of Japan's Safeguards System," Nuclear Power and its Fuel Cycle (Proc. Conf. Salzburg, 1977), 7, 503 (1977).

(2) Ikawa K., Hirata M., Nishimura H., Kurihara H., Aoe S., et al.: "A Study on Improvement of Material Accountability Verification Procedure," Proc. Int. Symp. on Nuclear Safeguards Technology 1978, Vienna, 1, 39-64, IAEA-SM-231/33 (1978).

(3) Umezawa H., Okashita H., Matsuura S.: Proc. ESARDA Symp. Isotope Correlation - Stresa 1978, p.97.

(4) Miyasaka S., Koreki S., Nishimura H., Ikawa K., Hirata M.: "Experience of Japan in Complying with IAEA Data Reporting Requirement," IAEA Safeguards Workshop Seminar (1978).

(5) Lovett J.E., Hirata M., Augustson R.H.: "Application of the Basic Concepts of Dynamic Materials Accountancy to the Tokai Spent Fuel Reprocessing Facility - a Feasibility Study," Proc. ESARDA First Annual Symposium of Safeguards and Nuclear Material Management, Brussels (1979).

(6) Ikawa K., Ihara H., Nishimura H., Hirata M., Sakuragi H., Iwanaga M., Suyama N., Matsumoto K.: "Study of the Application of Semi-Dynamic Material Control Concepts to Safeguarding Spent Fuel Reprocessing Plants," Report of the Kiawah Island Topical Meeting on Measurement Technology for Safeguards Materials Control, November 1979, NBS Special Publication 582, 730-739 (1980).

(7) Nishimura H., Ikawa K., Hirata M.: "A Code to Evaluate Inspection Data by Paired Comparison Method - NPT-JAPAN System II, Part II -," JAERI-M 9146 (1980).

(8) Ikawa K.: "Feasibility Study on the Application of the Basic Concepts of Dynamic Materials Accountancy to a Uranium Enrichment Facility Using Centrifuge Process (I)," JAERI-M 9173 (1980) (in Japanese).

(9) Lovett J.E., Hirata M., Ikawa K., Augustson R.H.: "Application of the Basic Concepts of Dynamic Materials Accountancy to the Tokai Spent Fuel Reprocessing Facility - A Feasibility Study," IAEA STR-94 (1980); JAERI-M 9186 (1980).

(10) Ikawa K., Nishimura H.: "Safeguards System Analysis (I)," JAERI-M 9197 (1980) (in Japanese).

(11) Ikawa K., Ihara H., Nishimura H., Hirata M., Ido M., Lovett J.E., Matsumoto K., Tsutsumi M., Sawahata T.: "An Integrated Near-Real-Time Materials Accountancy Safeguards System," Proc. INMM 22nd Annual Meeting, San Francisco, 390-401 (1981).

(12) Mukaiyama T., Kuroi H.: "The Expected Performance and Benefits of an Advanced Containment and Surveillance System at the Fast Critical Facility FCA of JAERI," Proc. INMM 22nd Annual Meeting, San Francisco, p.20 (1981).

(13) Hirata M., Natsume H., Nishimura H., et al.: "The First Report Issued by the Materials Accountancy Analysis Working Group of the Council for Investigation of Safeguards Technology," Materials Accountancy Analysis Working Group (1982) (in Japanese).

(14) Nishimura H., Kikuchi I.: "Design Study of an Improved Safeguards Verification Procedure Using Non-Destructive Assay Techniques," Advisory Group Meeting on Evaluation of the Quality of NDA Measurement Data, E16 (1982).

(15) Ikawa K., Ihara H., Nishimura H., Tsutsumi M., Sawahata T.: "A Near-Real-Time Materials Accountancy Model and its Preliminary Demonstration in Tokai Reprocessing Plant," Nuclear Safeguards Technology 1982, Vol. I, 499-512, IAEA-SM-260/136 (1983).

(16) Lovett J.E., Ikawa K., Shipley J.P., Sellinschegg D.: "Near-Real Time Materials Accountancy, A Technical Status Report," Nuclear Safeguards Technology 1982, Vol. I, 487-497, IAEA-SM-260/145 (1983).

(17) Nishimura H., Ikawa K., Hirata M., Asai S., Hirose K.: "Investigation of a Sample Plan for Safeguards Verification Activities," Nuclear Safeguards Technology 1982, Vol. II, 317-330, IAEA-SM-260/71 (1983).

(18) Mukaiyama T., Kuroi H., Vodrazka P., Matolcsy A.: "Development and Performance of the Advanced Containment and Surveillance System at the Fast Critical Facility FCA," Nuclear Safeguards Technology 1982 (Proc. Symp. Vienna, 1982), 391-404, IAEA-SM-260/121 (1983).

(19) Umezawa H., Nakahara Y.: "Isotope Correlation Techniques for Verifying Input Accountability Measurements at a Reprocessing Plant," Nuclear Safeguards Technology 1982, Vol. I, 473-484, IAEA-SM-260/72 (1983).

(20) Gupta D., Avenhaus R., Beedgen R., Bennett C.A., Berg R., Canty M.J., Hein H.J., Hough C.G., Ikawa K., Jaech J.L., Kluth M., Kuechle M., Leitner E., Lovett J., Mainka E., Markin J.T., Nishimura H., Sellinschegg D., Shipley J.P., Spannagel G., Voss F., Weh R., Wuerz H.: "International Workshop on the Near-Real-Time Accountancy Measure:

Overview Report," Nuclear Safeguards Technology 1982, Vol. I, 513-539, IAEA-SM-260/29 (1983).

(21) Nishimura H.: "Topics from IAEA International Safeguards Symposium," J. Atomic Energy Society of Japan, 25(3), 189 (1983) (in Japanese).

Author Index